

**UNIVERSIDADE FEDERAL DE SANTA CATARINA
PROGRAMA DE PÓS-GRADUAÇÃO EM ENGENHARIA MECÂNICA**

**EVALUATION OF THE ACOUSTICAL PERFORMANCE OF LOUVRE
BY IMPULSE RESPONSE ANALYSIS**

**TESE SUBMETIDA À UNIVERSIDADE FEDERAL DE SANTA
CATARINA PARA A OBTENÇÃO DO GRAU DE DOUTOR EM
ENGENHARIA MECÂNICA**

ELVIRA BARROS VIVEIROS DA SILVA

FLORIANÓPOLIS, ABRIL DE 1998

**EVALUATION OF THE ACOUSTICAL PERFORMANCE OF LOUVRE
BY IMPULSE RESPONSE ANALYSIS**

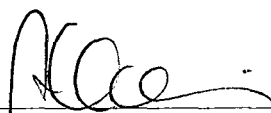
ELVIRA BARROS VIVEIROS DA SILVA

ESTA TESE FOI JULGADA ADEQUADA PARA OBTENÇÃO DO TÍTULO DE

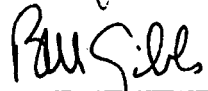
DOCTOR EM ENGENHARIA

**ESPECIALIDADE ENGENHARIA MECÂNICA, ÁREA DE CONCENTRAÇÃO:
VIBRAÇÕES E ACÚSTICA, E APROVADA EM SUA FORMA FINAL PELO
PROGRAMA DE PÓS-GRADUAÇÃO EM ENGENHARIA MECÂNICA**

BANCA EXAMINADORA:



**Abelardo Alves de Queiroz, Ph.D.
Coordenador do Curso**



**Barry Marshall Gibbs, Ph.D.
Orientador / Liverpool University**



**Samir Nagi Yoursi Gerges, Ph.D.
Orientador/UFSC**



Moysés Zindeluk, D.Sc.



Arcanjo Lenzi, Ph.D.



Miguel Aloysio Sattler, Ph.D.

*I wish I had understood earlier
that the true feeling of fulfilment in my life
would be found as much in moulding my sons' values
as in my professional success.*

*I would like to thank (and apologise to)
Frederico and Conrado,
who, despite the seemingly endless period of time to achieve it,
waited for me to finish this thesis.*

ACKNOWLEDGEMENTS

I would like to thank **Professor Frank Fahy**, at whose suggestion I carried out my research at the Acoustics Research Unit / Liverpool University. I could not have had a better place to work.

The challenge of doing a Ph.D. in England (with two young children) could never have been met successfully had I not had beside me:

Vilma M. dos Santos, who, warm and friendly, received me at her home while I was house hunting around Liverpool. It made the beginning much easier.

Gilcécia P. do Amaral e Silva, who was always ready to take my calls and sort out my whole life, even from Oxford.

Gary Seiffert, whose sense of humour would always turn my tears into laughter. This was even more important than his arranging whatever experimental set-up I worked with.

Max F. de Salis, for making us take a break from the rush of working hours and playing *Garota de Ipanema* on his guitar. He also helped me to find my way around Liverpool: from the cool restaurants to the trendy hairdresser and other invaluable tips.

Andy Moorhouse, to whom I turned many times and with whom I was relieved to learn that the acoustical laws were still valid (remember reciprocity?). He also became the adoptive father of Mixie (our hamster) when we left the UK.

Michael Stone, who loves Brazil in such a way that few of us do. We are both sure we were of the other's nationality in a previous life, and we wish we could swap passports now and again.

Bernard Berry, a busy person in charge of so many relevant posts, but always kind enough to spare some time, with words of enthusiasm, with a Ph.D. student.

My lovely neighbours in Alresford Road: **Peter, Norel, Philip and Anna**. They were essential to feeling I was at home at the end of the day.

Also: **Richard Lyon**, who generously shared all his information on open screens with me; **David Waddington**, who so kindly led me through the intensity measurements; **Hatem Ibrahim**, always with a spare cigarette to fuel my addiction; **Kenny Yap**, from the upper levels of mankind, ready

to deal with all my doubts about computer networks and worksheets; **Ning Qi**, who brought me some light to the darkness of *MatLab*; **John Goodchild**, whose classes were so pleasant to attend; **Sophie Maluski**, with whom I shared the difficulties of being a woman in the men's world of acoustics; **Tony White**, for giving me a hand every time I had a problem with cars, **Frank Carpenter**, for letting me work on his powerful computer, and the **Industrial Acoustics Company LTD**, for the supply of the louvre used.

I am also very grateful to Liverpool University, an institution thoughtful enough to have a special department to assist international students. **Ms. Sue Spencer**, in charge of us, was the person I turned to with all kinds of family problems: they were all sorted out. Also part of the team was **Ms. Kim Parkin**, whose support helped me in moments of distress.

John Green, my connection with the world outside acoustics, together with whom I had the pleasure to live unforgettable moments of pure British culture and who would be there (apart from some gaps...) to translate them to me.

On the other side of the Atlantic, the important Brazilians were:

Professor Samir N.Y. Gerges, who has encouraged me throughout my professional career in Acoustics, and has done so yet again.

Marco Nabuco and **Lia Kortchmar**, whose emails made me laugh in the lab. Unfortunately, I could not translate/explain them to the others - far too Brazilian...

Fundação Coordenação de Aperfeiçoamento de Pessoal de Nível Superior / **CAPES**, who gave me the financial support for my studies in England.

Lastly, the hardest task, to state the significance of having had **Professor Barry Gibbs** as my supervisor. I arrived in the UK expecting to have an appointment with my supervisor every other month. I could not be more wrong: all I had to do was to step into his office and ask if we could have a word. Inevitably, I would bring him a collection of doubts and have them replaced by brilliant ideas.

To be honest, it is almost easy to do a Ph.D. with a supervisor like him.

Many people have been named here all of whom were very important along the way. However, all efforts would have had no results if I had not had my mother beside me. It might sound expected, but these thanks go far beyond the usual cliché.

Even among those lucky enough to have a mum, not many will have one as supportive as mine. Furthermore, very few have a mum who is as expert in English, and fewer still have one who understands wave phenomena as well... Thanks, mum.

SUMMARY

An acoustic louvre is a building element that offers sound attenuation whilst allowing airflow through the aperture. A recent survey of manufacturers and suppliers of acoustic louvres in the UK revealed that the most commonly used method of measurement was the standard ISO 140, but that the results obtained overestimate the sound insulation. This is due to energy feedback through the aperture, containing the measured louvre, that gives rise to a strong coupling between the source and receiver chambers and makes correction for receiver room absorption problematical.

A more recent proposal measures the sound transmission through the louvre, from a reverberant to a free sound field. Measurement of the sound pressure field, external to a test chamber, with and without the louvre in the aperture, yields an insertion loss representative of field performance. However, the required test facilities can be expensive. Acoustic intensimetry measurements have been demonstrated also to be a more representative measure of the louvre performance, as laboratory and real sound field conditions are ideally the same. Nevertheless, special acoustic facilities and conditioned sound fields also are necessary.

Therefore, the acoustic performance of the device was investigated by an alternative method, which does not require large-scale acoustic facilities. Impulse analysis was considered a practical method to evaluate sound insulation, since the transmission loss coefficient of the device is obtained directly, without any correction for the acoustic field conditions in the test spaces. Furthermore, the instrumentation is simple and portable. It is relatively straightforward to set up a loudspeaker-louvre-microphone geometry that allows separation of the direct, diffracted and reflected components of the response time history. Each component then can be frequency analysed to obtain its contribution to the total insulation.

It was demonstrated that the main sound attenuation mechanisms of a louvre are impedance change in the louvre, constructive and destructive interference, and absorption. Therefore, the blade mass and geometry and gaps that compose the louvre, and the absorption material play an important role.

The sound transmission through louvres was measured in the frequency range 100 - 5 kHz and for incident angles between -60 degrees and +60 degrees. For the low frequency region (below 1 kHz), transmission loss was effectively independent of incident angle and displayed a monotonic increase with increase in frequency. Above 1 kHz, wave diffraction effects occur which are functions of louvre periodicity, incident angle, and wavelength. Different transmission paths through the slits cause destructive and constructive interference and the louvres are highly directional. It was observed that the angle of incidence parallel to the blade pitch gave the highest transmission coefficient and strongly influenced the angle averaged transmission loss.

To validate measurement, the sound transmission of the louvre was modelled in two ways. In the low frequency range, the behaviour is dictated by a mass layer effect, which is determined by the geometry of the louvre and air density. At mid- and high frequencies, Kirchhoff diffraction theory was used, which depends on the geometry of the set-up and louvre. The agreement between predicted and measured results was good. As the louvre behaviour could be described without taking into account the mass of the blades, it was deduced that this parameter is overvalued in the performance of the louvre. Some discrepancies between measured and predicted data are believed to be due to simplifications in the input data, such as for the blades sections, which were assumed rectangular, instead of curved.

To predict the field performance of the louvre in typical applications, i.e. on façades of industrial buildings, the reverberant to free measurement facility was numerically simulated by an image method. The reflection coefficient of the louvre and the transfer function across the blades were measured by the impulse response method to provide input data to the computer model. Results show that in real installations the insertion loss will vary less with frequency and angle of emission than indicated in impulse response measurement.

RESUMO

Venezianas acústicas são elementos de edificação que oferecem atenuação sonora ao mesmo tempo que permitem o fluxo de ar pela abertura. Recente pesquisa entre fabricantes e fornecedores de venezianas acústicas no Reino Unido revelou que o método de medição mais comumente usado era a norma ISO 140, mas que os resultados obtidos superestimam o isolamento sonoro. Isto é devido à realimentação de energia pela abertura que contém a veneziana em análise, que dá margem a um forte acoplamento entre as câmaras fonte e recepção e faz com que correções para a absorção da sala de recepção sejam problemáticas.

Uma proposta mais recente mede a transmissão sonora através da veneziana de campo reverberante para campo livre. Medições do campo de pressão sonora, externas a uma câmara de ensaio, com e sem a veneziana na abertura, levam à perda de inserção que é representativa do desempenho em campo. Porém, as instalações de teste exigidas podem ser caras. Medições de intensidade acústica também demonstraram ser uma medida mais representativa do desempenho da veneziana, já que condições de laboratório e de campo são idealmente as mesmas. Não obstante, instalações acústicas especiais e campos sonoros condicionados também são necessários.

O desempenho acústico do dispositivo foi investigado por um método alternativo que não requer amplas instalações acústicas. Análises impulsivas foram consideradas um método prático para avaliar o isolamento sonoro, já que o coeficiente de perda de transmissão do dispositivo é obtido diretamente, sem qualquer correção para as condições do campo acústico dos ambientes de teste. Além disso, a instrumentação é simples e portátil. É relativamente direta à montagem da geometria alto-falante/veneziana/microfone, que permite a separação dos componentes direto, difratado e refletido da resposta da história temporal. Cada componente pode ser, então, analisado em frequência para obter-se sua contribuição no isolamento total.

Foi demonstrado que os principais mecanismos de atenuação sonora de uma veneziana são a mudança de impedância na veneziana, interferência construtiva e destrutiva, e absorção. Então, a massa da lâmina, a geometria e vãos que compõem a veneziana e, também, o material de absorção desempenham um papel importante.

CONTENTS

Acknowledgements	iv
Summary	vii
Resumo	ix

Chapter 1 INTRODUCTION

1.1 Acoustic Louvres	2
1.2 Methods of Analysis of Open Screens	3
1.3 References	5

Chapter 2 METHODS OF MEASURING SOUND INSULATION

2.1 Terminology	7
2.1.1 Transmission Loss (TL)	7
2.1.2 Noise Reduction (NR)	8
2.1.3 Insertion Loss (IL)	9
2.2 Existing Methods	9
2.2.1 ISO 140 / BS 2750	9
2.2.2 BS 4718	12
2.2.3 Intensity	13
2.2.4 TL Using Reference Sound Source	14
2.2.5 HEVAC	16
2.3 Summary	17
2.4 References	18

Chapter 3 LOUVRE'S TRANSMISSION LOSS BY EXISTING METHODS

3.1 Introduction	21
3.2 Previous Research	22
3.3 Standard Method (ISO 140)	24
3.3.1 TL of Connecting Partitions	25
3.3.2 Reverberation Time Measurements	26
3.3.3 Transmission loss of the Aperture	26
3.3.4 Results	26
3.3.5 Reciprocity	27
3.4 Intensity Measurements	28
3.4.1 Principles of Measurement	28
3.4.2 Results	31
3.5 References	33

Chapter 4 IMPULSE RESPONSE ANALYSIS

4.1 Principle	43
---------------------	----

4.2	Maximum-Length Sequences (MLS)	44
4.2.1	Fast Hadamard Transform	45
4.2.2	Signal to Noise Ratio	46
4.2.3	Order of the Sequence	48
4.3	Measurement Method	48
4.3.1	Instrumentation	53
4.3.2	Temporal Window	54
4.3.3	Sources of Errors in MLS Analysis	54
4.3.4	Other Applications	56
4.4	References	57

Chapter 5 TRANSMISSION LOSS BY IMPULSE RESPONSE

5.1	Introduction	66
5.2	Preliminary Investigation of a Solid Screen	66
5.2.1	Normal Incidence	67
5.2.2	Oblique Incidence	68
5.3	Transmission Loss at Different Frequency Regions	69
5.3.1	Mechanisms of Attenuation	71
5.3.2	Frequency Dependency	72
5.3.3	Angular Dependency	72
5.4	Comparison to Other Methods	72
5.5	References	73

Chapter 6 SIMULATION OF TRANSMISSION THROUGH ACOUSTIC LOUVRE

6.1	Introduction	87
6.2	Wave Diffraction Model	87
6.2.1	Mathematical Foundation	88
6.3	Preliminary Simulation	90
6.4	Prediction Model for the Louvre	92
6.4.1	Low Frequency Range	93
6.4.2	Mid- and High- Frequency Range	94
6.4.3	Transfer-Function Measurements	94
6.5	Results	97
6.6	References	99

Chapter 7 ACOUSTIC MODELLING

7.1	Types of Modelling	112
7.1.1	Empirical Models	113
7.1.2	Modal Simulation	114
7.1.3	Geometrical and Energy Approaches	116
7.2	Insertion Loss Simulation by Image Methods	117
7.2.1	Introduction	118
7.2.2	Theory	119
7.2.3	General Model	121
7.2.4	Implementation of the Method	125
7.2.5	Preliminary Investigation	129

7.2.6	Simulation	132
7.2.7	Results	133
7.3	References	136

Chapter 8 REFLECTION FACTOR BY IMPULSE RESPONSE

8.1	Introduction	159
8.2	Principle of the Method	161
8.3	Direct Component	161
8.4	Analysis of Time Window	165
8.5	Absolute Error Due to Background Noise	166
8.6	Results	167
8.7	Application to the Image Method	168
8.8	References	169

Chapter 9 CONCLUSIONS

9.1	Introduction	181
9.2	Conclusions	182
9.3	Topics for Further Research	184

APPENDICES

	Photography of the Louvre	187
Appendix 1	Program Listing: Transmission Loss of a Solid Screen	190
Appendix 2	Program Listing: Transmission Loss of Louvre by Mass Layer Model	193
Appendix 3	Program Listing: Transmission Loss of Louvre by Diffraction Model	196
Appendix 4	Normal-Mode and Image Method Solutions for a Rectangular Enclosure of Rigid Walls	200
Appendix 5	Program Listing: Geometry for Reflection Coefficient Measurements	205
Appendix 6	Program Listing: Insertion Loss Simulation of HEVAC Test by Image Method	207
Appendix 7	Published Papers	216

CHAPTER 1 INTRODUCTION

- 1.1 Acoustic Louvres
- 1.2 Methods of Analysis of Open Screens
- 1.3 References

1.1 ACOUSTIC LOUVRES

The aim of the research reported in this thesis was to develop a method of predicting the field performance of acoustic louvres by means of data obtained by measurements which are simple both in terms of procedure and equipment and where specialist acoustic facilities are not required.

Louvres are common building elements used as either closure or partition elements when the closure is intended not to impede air flow, usually to the exterior. Louvres usually cover the whole aperture of a building, thus allowing natural ventilation, while preserving the privacy of internal areas and providing weather protection.

When used in Brazil and other tropical countries, louvres that have the function of avoiding or minimizing solar radiation into the room are known by the French expression "*brise soleil*". Those which reduce sound transmission are named "*acoustic Louvres*", a term which is commonly used in Europe and the USA but less so in Brazil (named "*venezianas acústicas*" in Portuguese).

Both *brise soleil* devices and acoustic louvres partially filter the external environment, the former reducing solar radiation and the latter reducing sound transmission, either as noise breakout or external noise breakin. Therefore, an acoustic louvre is used where noise control is required along with ventilation such as for enclosure of equipment that produces excessive noise, or for cooling tower inlet silencers. When used in façades, an acoustic louvre can be of significant dimension and become an important element in the aesthetic composition, similar to a *brise soleil*. There is no possibility of complete sound insulation when adequate airflow also is required. However, the sound insulation obtained, despite being low compared with equivalent solid screens, can be an important contribution to the control of industrial noise.

Acoustic louvres have yet to be fully exploited in Brazil. In fact, Brazilian architecture seems often to be dissociated from the environmental conditions and buildings do not give enough environmental protection for thermal and/or acoustic comfort. In a country where much of the climate is tropical and in which cities suffer some of the highest urban noise³⁷ levels in the world, incorporation of acoustic louvres in planning, and design or for remedial noise control therefore have important applications.

At present, acoustic louvres have been applied only for industrial noise control, such as in enclosures and are normally made to measure, rather than on large production scale. The design is rudimentary, involving little engineering scientific analysis, but relying heavily on the “practical” experience of the manufacturer or engineer. The result is that the design often matches the necessary airflow but a required sound insulation is seldom specified or achieved.

1.2 METHODS OF ANALYSIS OF OPEN SCREENS

At the present, a problem persists for evaluating low insertion loss devices, such as open screens. There is no simple engineering method of predicting louvre performance, and therefore measurement data will be required for the foreseeable future. However, no accepted method of measurement has yet been established.

Lyons [1] carried out a pilot survey of 45 manufacturers and suppliers of acoustic louvres in the UK. It was concluded that manufacturers do not have an agreed method of acoustically rating their products. The details of the survey are reproduced as follows:

- i) 66% of the companies giving feedback manufacture the louvres that they market.
- ii) Of these, 40% tested the louvre in accordance with ISO 140 [2] standard method of measurement or equivalent.
- iii) 13% used a national [3] standard method of test for silencers.
- iv) 1 tested louvres to the German [4] equivalent to ISO 140.
- v) 1 tested louvres to the American [5] equivalent to ISO 140.
- vi) 17% used an on site substitution measurement or other non-specific tests.
- vii) 30% performed no tests whatsoever.
- viii) Only 63% provided performance data on their louvres.
- ix) Only one company was currently considering optimizing their design.

It can be assumed that in Brazil the situation is not better. The process of quantifying the performance of products has only recently been introduced but is growing, mainly due to the modern attention given to Industrial Quality. However, financial considerations predominate as far as sound insulation assessment is concerned. The majority of measurements, if any, are

performed according to ISO 140 and this procedure requires expensive special facilities such as sound transmission suites.

There remains a need for a method of test and rating the sound insulation of acoustic louvres that does not require large-scale and expensive acoustic measurement facilities and where the data obtained are properly representative of performance in the installed condition.

The study begins by considering existing methods of measurement, presented in Chapter 2, with particular emphasis on the applicability of each method to open screens of low sound insulation.

In Chapter 3, the transmission loss of louvres is assessed by sound pressure and acoustic intensity measurement methods.

In Chapter 4, the principle of impulse measurement is introduced and the various fields of application presented. Maximum-length sequence (MLS) methods of acoustic excitation and acquisition are introduced and the system used to obtain the impulse response of systems, used throughout this work, is described.

The method is applied and validated in Chapter 5 in some preliminary investigations of thin solid panels. Different analyses of the time history lead to finite or infinite responses of the partitions, where the latter is obtained by means of processing the diffracted component also. The mechanism of sound transmission through louvres is investigated by analysis of the impulse response. The averaged overall performance is compared with the results obtained by standard (ISO 140) and acoustic intensity methods.

A theoretical approach used to predict the results for comparison with impulse measurement is presented in Chapter 6. The theoretical model is based on the mass layer effect for low frequencies and Kirchhoff's diffraction theory for mid- and high frequencies. The prediction model is modified by including the measured transfer function between the inlet and outlet apertures of the louvre. The predicted and measured far-field transmissions are then compared.

In Chapter 7, a procedure proposed by the Heating Ventilation and Air Conditioning

Manufacturers Association (HEVAC) [6] is shown to be the most representative of field performance. The HEVAC method is numerically simulated, using an image source approach, in order to relate the impulse response data to likely field performance.

Chapter 8 presents the method of impulse response measurement of absorption and reflection coefficients of acoustic louvres, which also are included in the image model numerical simulations. In this way, it is demonstrated that the field performance is obtained from impulse response measurement. Chapter 9 concludes the work done and suggests topics for further researches. In the appendices can be found the main program listings and the theory supporting the image method.

1.3 REFERENCES

- [1] Lyons R., *Building Elements of Low Sound Insertion Loss*, Ph.D. Thesis, University of Liverpool, (1993).
- [2] ISO 140:1978. *Methods of Measurement of Sound Insulation in Buildings and of Building Elements*. Parts 1 to 8.
- [3] BS 4718:1971. *Methods of Test for Silencers for Air Distribution Systems*.
- [4] DIN 52210/75. *Luft und Trittschalldämmung* (Tests in Building Acoustics: Airborne and Impact Sound Measurements Methods). German standard.
- [5] ASTM E90-75. *Standard Method for Laboratory Measurement of Airborne Sound Transmission Loss of Building Partitions*. American standard.
- [6] HEVAC Association Acoustics Group, *Guide Test Procedure for Acoustic Louvres, Issue 1*.

CHAPTER 2 METHODS OF MEASURING SOUND INSULATION

- 2.1 Terminology
- 2.2 Existing Methods
- 2.3 Summary
- 2.4 References

2.1 TERMINOLOGY

As seen in Chapter 1, the variety of methods and criteria to characterise and quantify sound insulation tends to lead to misinterpretation and confusion. This is particularly so when dealing with open screens. It will be seen that most methods of characterising sound insulation are not appropriate for low insertion loss devices such as louvres. In order to make perfectly clear the difference of results when using standard and alternative methods of assessing sound insulation, this chapter establishes the terminology of sound insulation and describes existing test methods.

2.1.1 Transmission Loss (TL)

Also known as Sound Reduction Index (SRI), the Transmission Loss of a partition is given by:

$$TL = 10 \log \left(\frac{W_i}{W_t} \right) \quad (2.1)$$

where W_i is the total power incident on the source side of the partition and W_t is the total power transmitted through the partition [1]. The ratio of sound powers, incident and transmitted, is the expression of transmission coefficient τ , therefore

$$TL = 10 \log \left(\frac{1}{\tau} \right) \quad (2.2)$$

TL depends on the frequency and the properties of the partition (and mounting conditions) only and is commonly obtained by measuring the level difference across the panel, as presented in ISO 140 (BS 2750) [2], according to:

$$TL = L_1 - L_2 + 10 \log \left(\frac{S}{S_s \bar{\alpha}} \right) \quad (2.3)$$

where L_1 and L_2 are the spatially averaged sound pressure levels in the source and receiving room, respectively, S is the area of the element or device, S_s and $\bar{\alpha}$ are the total surface area and the

average absorption, both in the receiving room. The measurements are normalised to eliminate these effects to give the TL, which is intrinsic to the element or device but also is a function of fixing conditions.

The measured data, obtained under laboratory conditions, may require modification in order to properly represent performance in real conditions. This is because, firstly, the method does not include the effect of flanking transmission. Secondly, the fixings in the real situation may not be the same as in the laboratory. Thirdly, although TL is independent of element area, the panel size can change the resonant frequencies. Lastly, the sound field in which laboratory measurements are performed, approximate ideal diffuse conditions, but this is hardly the case in practice.

2.1.2 Noise Reduction (NR)

Noise Reduction is the difference in sound pressure level across an element or device, $L_1 - L_2$ [3] and it is obtained from TL. For a reverberant receiving room, where $\bar{\alpha} < 0.2$.

$$NR = L_1 - L_2 = TL - 10 \log \left(\frac{S}{S_s \bar{\alpha}} \right) \quad (2.4)$$

For a non-reverberant receiving room,

$$NR = TL - 10 \log \left(\frac{1}{4} + \frac{S(1 - \bar{\alpha})}{S_s \bar{\alpha}} \right) \quad (2.5)$$

It must be observed that in equation (2.4) the terms of the right hand side are the same as those of the TL equation, but in equation (2.5) the sound pressure level on L_2 (the receiving side) is measured near the element surface.

Finally, for reverberant to free-field transmission, $\bar{\alpha} > 0.8$ and

$$NR = TL + 6dB \quad (2.6)$$

It is necessary to add 6 dB as a correction because the sound energy incident on the element on the room side is diffuse, whereas on the open side it is not [3].

2.1.3 Insertion Loss (IL)

If an element or device is inserted into the transmission path, the difference in sound level at the receiving point before and after the insertion is the IL, is given by:

$$IL = L_2 - L'_2 \quad (2.7)$$

where L_2 and L'_2 are the sound level pressure at the receiving point with and without the device, respectively.

2.2 EXISTING METHODS

The insulation performance of a partition or element can be evaluated in several ways. The methods, either standard or non-standard, are presented and their pertinence to open screens is discussed.

2.2.1 ISO 140 / BS 2750

The standard ISO 140 is equivalent to the British Standard BS 2750, and has been the main international standard for sound insulation measurements. Composed of several parts, only those concerning airborne sound of building elements, parts 1-3, and the amendment 1 of part 3, will be considered in this study.

The origins of standards on sound insulation in UK began with “The Housing Manual” [4] and appeared as part of the British Standard Code of Practice for Building, in the late 1940’s [5]. After a draft for discussion [6], a code for the standardisation of measurements of sound transmission was approved with some improvements by the Acoustics Standards Committee of the B.S.I. as British Standard 2750:1956. The code evolved into an ISO Recommendation and was replaced as a technical revision as ISO 140, parts 1 to 8, in 1978. In its second modification after

1956 part nine was added into BS 2750, and included those aspects of sound insulation. Since 1991 ISO and the European Committee for Standardization (CEN) have been revising building and room acoustics standards under a technical co-operation agreement [7]. New and revised international standards are to be adopted as European standards. ISO 140 has gone through a complete revision, Parts 10, 11 and 12 were added and its new version will be mandatory in the European countries. The main features of ISO 140:1995 and the revised specifications concerning the area of this study are as follows.

Part 1 - Requirements for Laboratory Test Facilities with Suppressed Flanking Transmission:

- i) Minimum room volume of 50 m^3 with at least 10% difference between room volumes.
- ii) Ratio of room dimensions is to be such as to avoid matching of standing waves.
- iii) The test opening is to be approximately 10 m^2 and the minimum shorter edge length 2.3 m, which can be less under special circumstances.
- iv) Source and receiver room must have diffuse field with the use of diffusing elements if necessary.
- v) Indirect sound transmission to be negligible compared with that through the test specimen.

The new version specifies that facilities with defined flanking transmission will no longer be allowed for standard measurements (as it has been in Germany, for instance). The volumes of the test rooms have been set to within a limit. Test openings are specified very strictly and mounting conditions are laid down in details.

Part 2 - Statement of Precision Requirements: the assessment of uncertainty in the measurements is dealt with in this item. Limits of confidence in the results are obtained by appraisal of their repeatability when source and microphone positions are changed. The comparison among inter-laboratorial results (reproducibility) rates the effects of systematic source of errors. This part of the standard will be revised in the future, after comparisons of measurements in accordance with other revised parts have become available.

Part 3 - Laboratory Measurements of Airborne Sound Insulation of Building Elements: gives measurements specifications, such as minimum number of microphone positions, microphones to

room boundaries distances and recommended positions for source. Among many revisions, the extension of the frequency range should be included in the next version. The European project “Intercomparison of Laboratory Measurements of Sound Insulation of Walls”, in which 21 countries take part, aims to obtain precise new data by application of the revised ISO 140-3, in order to revise ISO 140-2 [7]. To get improved reliability of sound insulation measurement results in the frequency range down to 50 Hz another European project is being carried out.

The measurement of transmission loss by the standard method, according to equation (2.3), can be considered in two parts: measurement of the noise reduction and the correction for absorption in the receiving room. The inadequacy of the method arises in the measurement of the latter if the element under test provides low insulation. The limitation is well understood [8,9,10,11,12], but is naturally avoided as normal building elements are likely to give high values of insulation. In reality, equation (2.3) is only true for components that offer a transmission loss greater than 15 dB. The general expression for transmission loss is given by:

$$TL = L_1 - L_2 + 10 \log \left(\frac{S}{S_s \bar{\alpha} + S\tau} \right) \quad (2.8)$$

Therefore, the assumption is that $S_s \bar{\alpha} \gg S\tau$ and the latter can be disregarded. The condition is fulfilled either for high values of TL, hardly achieved by open screens, or when the receiving room is highly absorbent, which would be incompatible with the requirement for diffuse field conditions.

The simplified expression for TL fails due to the energy feedback through the partition from the source into the receiver room. Due to the strong coupling between rooms, reverberation time measurement is problematical. For this reason, the procedure in ISO 140 is not recommended for any low transmission loss device (whether perforated or not), particularly at low frequencies. Mulholland [9] showed that when TL is less than 15 dB errors up to 5 dB could be expected. In an attempt to overcome the limitation, he investigated the use of the expression proposed by London [13] for low insulation partitions, which gives TL as:

$$TL = 10 \log \left[10^{\left(\frac{L_1 - L_2}{10} \right)} - 1 \right] + 10 \log \left(\frac{S}{S_s \bar{\alpha}} \right) \quad (2.9)$$

Equation (2.9) was found to be more accurate, although for elements of $TL < 10$ dB errors up to 2.5 dB were still detected.

Regarding the properties of the sound fields, certain discrepancies may occur at low frequency. Due to the presence of interference patterns, the sound level is higher near the walls than in the central region of a reverberation room [14]. The Waterhouse correction term is added to the source and receiver room pressure levels (see section 3.1.4).

The classical method of measurement of transmission loss is inconvenient, apart from its inadequacy when it comes to partitions of low insulation. It requires sophisticated and special facilities, such as a transmission suite, and involves two sets of measurements: one dealing with noise reduction and the other for the correction for absorption in the receiving room.

2.2.2 BS 4718

BS 4718 [15] is the British standard method of testing silencers for air distribution systems. Louvres and silencers are equivalent devices in the sense that both increase the attenuation (per metre run) by means of the increase of the perimeter/cross sectional area ratio due to the presence of absorption. In general terms, acoustic louvres provide greater airflow, whereas silencers have a better insulation performance.

As far as acoustic performance is concerned, the standard evaluates the silencer by two criteria. Firstly, its airborne sound attenuation analysed in one-third octave bands (static insertion loss). Secondly, the aerodynamic noise generated by airflow (regenerated noise).

The measurement of the static insertion loss uses a substitution method performed in-duct or into a diffuse field. The mean sound pressure level across a section of the duct is measured with the silencer in place, either in a diffuse receiving room or downstream of the silencer. The measurement is repeated with the silencer replaced by a section of straight ducting, the insertion loss given by the level differences.

Generated noise level can be measured either by a direct method, with the use of a reference sound

source, or by means of a substitution method. A fan provides the sound source and a flow of air through the silencer under test, which passes previously through a permanent silencer so as to supply a quiet airflow. In a diffuse receiving room, the mean sound pressure level at each microphone position is measured with and without the test silencer in place, but with equal airflow for both measurements. For the comparative method, an aerodynamic reference sound source is used.

Although used by some manufacturers to assess the performance of acoustic louvres, the standard states that the method should not be used to determine the performance of silencers designed to be installed to increase the sound insulation of a partition having a ventilation opening. The application of the standard for louvres and open screens is therefore not suitable.

2.2.3 Intensity

Intensity measurements are finding widespread application in acoustics, especially for determination of transmission loss of partitions [16,17,18,19,20,21,22,23]. An ISO working group has been working to standardise intensity measurement methods in the field of building acoustics and a new standard is under development, named Measurement of Airborne Sound Insulation using Sound Intensity. The measurement of TL by means of intensity has several advantages, such as:

- i) It gives the transmission loss directly without having to make corrections for the panel area and the absorption of the receiving room.
- ii) It eliminates the effect of flanking transmission.
- iii) Although the source room field must still be diffuse, there is no such restriction on the receiving room. Actually, the receiving room should be as non-diffuse as possible.
- iv) It makes possible the identification of the energy transmitted through different parts of a structure.

The incident sound power cannot be measured directly from sound intensity as this is zero in a diffuse field. However, the incident intensity I_i can be calculated from the measured spatially averaged sound pressure P_{rms}^2 in the source room from:

$$|I_i| = \frac{P_{rms}^2}{4\rho c} \quad (2.10)$$

where ρ is the density of air and c the speed of sound in air, so

$$L_{ii} \cong L_{ps} - 6 \quad (2.11)$$

The transmitted intensity $|I_t|$ is measured on the receiving side of the panel as the intensity vector component perpendicular to the panel surface. The sound transmission loss is then calculated from:

$$TL = L_{ps} - 6 - L_{it} \quad (2.12)$$

where L_{it} is the transmitted intensity level.

Although there are simplifications on the method, there is still the need of a reverberation room and controlled conditions for the receiving room. Chapter 3 presents the transmission loss of the louvre measured by a sound intensity method.

2.2.4 TL Using Reference Sound Source

The measurement of the equivalent absorption area in the receiving room required in ISO 140 can be obtained by two methods, as suggested in the standard:

- a) measuring the reverberation time T of the receiving room and calculating the absorption area from Sabine's formula:

$$A = \frac{0.16V}{T} \quad (2.13)$$

where V is the volume of the receiving room, or

b) using a reference sound source.

While the first method has been widely accepted and is common practice, the latter has been less popular. The steady-state measurement method, from a practical point of view, offers advantage because the same instruments used to measure noise reduction can be used to measure the room absorption correction. Only sound pressure level measurements are involved and the time consuming measurements of reverberation time are avoided. More importantly, the problem of maintaining diffuse conditions in a transient sound field is avoided.

The procedure to measure absorption using a reference sound source was laid down by Larsen [24], who compared what he called the “alternative” method with ISO 140. He demonstrated that transmission loss obtained using the standard method tends to give higher values than the reference sound source method.

In the alternative method the absorption in the receiving room is determined by exciting the receiving room by a reference sound source and measuring the sound pressure level resulting from it. From theory it is known that

$$A = S_s \bar{\alpha} = \frac{4\rho c W_R}{P_{2R}^2} \quad (2.14)$$

where W_R is the sound power emitted by the reference sound source and P_{2R}^2 is the mean sound pressure squared (averaged over the entire room).

By substituting equation (2.14) in (2.3), setting $\rho c = 400$ [Ns/m³] and introducing the reference values $W_0 = 10^{-12}$ [W], $P_0 = 20$ μ Pa and $S_0 = 1$ [m²] it is obtained:

$$\begin{aligned} TL &= L_1 - L_2 + 10 \log \frac{S}{S_0} - 10 \log \frac{W_R}{W_0} + 10 \log \left(\frac{P_{rms}}{P_0} \right)^2 - 10 \log \frac{4\rho c W_0}{S_0 P_0^2} \\ &= L_1 - L_2 + 10 \log \frac{S}{S_0} - L_{WR} + L_{2R} - 6 \end{aligned} \quad (2.15)$$

where $L_{WR} = 10 \log (W_R/W_0)$ and $L_{2R} = 10 \log (P_{2R}/P_0)^2$.

As in the case of the classical method, the Waterhouse correction term should be included for each of the sound pressure level measurements, i.e. one for the source room and two for the receiving room. However, the two sound pressure level measurements in the receiving room have opposite signs and therefore their correction terms are cancelled out, requiring only the correction term for the source room:

$$TL = L_1 + 10 \log \left(1 + \frac{\lambda S_1}{8V_1} \right) - L_2 + 10 \log \frac{S}{S_0} - L_{WR} + L_{2R} - 6 \quad (2.16)$$

Rearranging equation (2.16) leads to:

$$TL = L_1 + 10 \log \left(1 + \frac{\lambda S_1}{8V_1} \right) + 10 \log \frac{S}{S_0} - 6 - (L_2 + L_{WR} - L_{2R}) \quad (2.17)$$

Since L_2 and L_{2R} are the sound pressure levels in the receiving room when the transmitting room and the receiving room are excited respectively, it can be seen that the term $(L_2 + L_{WR} - L_{2R})$ is equal to the sound power level, L_{WR} , emitted into the receiving room by the wall under test (see equation (2.1)).

The method has the advantage of reducing the amount of instrumentation employed, as only sound pressures are involved, and avoids the assumption of diffuseness in a transient state.

2.2.5 HEVAC

In order to determine the static insertion loss of acoustic louvres or other louvre types which form part of a façade, the Acoustic Committee of the Heating Ventilating and Air Conditioning Manufacturers Association (HEVAC) proposed a more suitable method of measurement.

According to the new test proposed, the louvres should be installed in an outer wall of a test room of minimum volume 50 m^3 . The minimum room dimensions are 3.5 m for length, and 2.8 m for

width and height, with a recommended ratio of 5:4:3. The room interior walls, floor and ceiling should be acoustically hard, and the minimum and maximum louvre sizes are 1 m² and 2.4 m², respectively. Two sound sources generating broad band noise should be placed angled in relation to any wall, positioned in a non-symmetrical way, each facing into the nearest (diagonally opposite) corner of the test room. Measurements of sound pressure level are to be made at nine microphone positions at angles from 30⁰ to 150⁰ at 15⁰ intervals. Other requirements concerning minimum distances are: 0.5 m between any edge of the louvre and the adjoining walls, ceiling or floor; 1.5 m between louvre and the closest loudspeaker and raised 1 m above the floor level. The static insertion loss is given by the difference between the angle averaged sound pressure levels with and without the louvre. A directivity index of the louvre is calculated for each microphone position.

The determination of the insertion loss in a reverberant to free-field condition avoids the problem of coupling between rooms, as happens in ISO 140. It is also thought to be more representative of the field performance of the louvre, as it is tested in a condition that is likely to be representative of its habitual use as part of a façade. Another advantage is its ability to evaluate directivity. Although the method simplifies the necessity of a transmission suite, it still requires a large test facility.

2.3 SUMMARY

The terminology of sound insulation has been discussed and it has been demonstrated that the appropriate way to characterise the acoustic performance of acoustic louvres is by means of insertion loss (IL) rather than sound reduction index (SRI) or noise reduction (NR).

It also has been shown that existing standard recommended methods of measurement of sound insulation are inappropriate for acoustic louvres or any low insertion loss device. In addition, the test methods require large specialist facilities and are time consuming and expensive.

The proposal of HEVAC is more appropriate since it approximates more closely field performance conditions but also requires specialist acoustic facilities and controlled external conditions.

The same is true for methods involving acoustic intensimetry but they offer other advantages that

will be explored later in the thesis.

However, there remains a need for a test method that is properly representative of field performance, and does not require large specialist acoustic facilities. The principle of the method proposed in this thesis, impulse response analysis, is given in Chapter 3 as a prelude to a description of its use as a measurement method, in Chapter 4.

2.4 REFERENCES

- [1] Kinsler I.L. and Holmer C.I., *Interaction of Sound Waves with Solid Structures*, Chapter 11 of Noise and Vibration Control, Beranek L. L., McGraw-Hill, revised edition, (1988).
- [2] ISO 140 (BS 2750). *Methods of Measurement of Sound Insulation in Buildings and of Building Elements*. Part 1 to 12 (Revision 1994/1995).
- [3] Doelling N., Klepper D.L. and Beranek L.L., *Some Practical Acoustical Measurements*, Noise Reduction, McGraw-Hill, (1960).
- [4] Housing Manual, H.M.S.O, for the Ministries of Health and Works, London, (1944).
- [5] Allen W.A., *Party Walls with Improved Sound Reduction*, The Physical Society, Noise and Sound Transmission, (1949).
- [6] Parkin P.H., *Provisional Code for Field and Laboratory Measurements of Airborne and Impact Sound Insulation*, The Physical Society, Noise and Sound Transmission, (1949).
- [7] Hans G., *New International Standards for Building and Room Acoustics*, Appl. Acoustics, **52** (3/4), 185-196, (1997).
- [8] Mariner T., *Critique of the Reverberant Room Method of Measuring Airborne Sound Transmission Loss*, J. Acoust. Soc. Am., **33**(8), 1131-1139, (1961).
- [9] Mulholland K.A. and Parbrook H.D., *The Measurement of Sound Transmission Loss of Panels with Small Transmission Loss*, J. Sound Vib., **2**(4), 502-509, (1965).
- [10] Mulholland K.A. and Parbrook H.D., *The Measurement of Sound Transmission Loss*, J. Sound Vib., Letter to the editor, **5**(2), 391-394, (1967).
- [11] Bies D.A. and Pickles J. A., *The Measurement of the Transmission Loss of Low Noise Reduction Test Item*, Proc. Noise, Shock and Vib. Conf., 144-153, Melbourne, (1974).
- [12] Bies D.A. and Davies J.M., *An Investigation of the Measurement of Transmission Loss*, J. Sound Vib., **53**(2), 203-221, (1977).

- [13] London A., *Tentative Recommended Practise for Laboratory Measurements of Airborne Sound Transmission Loss of Buildings Floors and Walls*. (ASTM E 90-50T), J. Acoust. Soc. Am., **23**(6), 686-689, (1951).
- [14] Waterhouse R.V., *Interference Patterns in Reverberant Sound Fields*, J. Acoust. Soc. Am., **27**(2), 247-258, (1955).
- [15] BS 4718:1971. *Methods of Test for Silencers for Air Distribution Systems*.
- [16] Sullivan R.D. and Gibbs B.M., *Field Measurement of Sound Transmission Loss of Masonry Constructions by Acoustic Intensimetry*, Appl. Acoustics, **49**(3), 249-262, (1996).
- [17] Croker M.J., Raju P.K. and Forssen B., *Measurement of Transmission Loss of Panels by the Direct Determination of Transmitted Acoustic Intensity*, Noise Control Eng., **17**(1), 6-11, (1981).
- [18] Halliwell R.E. and Warnock A.C.C., *Sound Transmission Loss: Comparison of Conventional Techniques with Sound Intensity Techniques*, J. Acoust. Soc. Am., **77**(6), 2094-2103, (1985).
- [19] Fahy F.J., *Sound Intensity Measurements of Transmission Loss*, Proc. Inst. Acoustics, p. B5.1, (1982).
- [20] de Mey A. and Guy R.W., *Exploiting the Laboratory Measurements of Sound Transmission Loss by the Sound Intensity Techniques*, Appl. Acoust., **20**, 219-236, (1987).
- [21] van Zyl B.G., Erasmus P.J. and Anderson F., *On the Formulation of the Intensity Method for Determining Sound Reduction Indices*, Appl. Acoust., **22**, 213-228, (1987).
- [22] Cops A. and Minten M., *Comparative Study Between the Sound Intensity Method and the Conventional Two-Room Method to Calculate Sound Transmission Loss of Wall Construction*, Noise Control Eng., **2**, 104-111, (1984).
- [23] Guy R.W. and de Mey A., *Measurement of Sound Transmission Loss by Sound Intensity*, Canad. Acoust., **13**, 25-44, (1985).
- [24] Larsen H., *Power Based Measurements of Sound Insulation*, Measurement of Sound Absorption of Rooms Using a Reference Sound Source, Brüel & Kjær Technical Review, **4**, (1976).

**CHAPTER 3 LOUVRE'S TRANSMISSION LOSS BY EXISTING
METHODS**

- 3.1 Introduction
- 3.2 Previous Research
- 3.3 Standard Method (ISO 140)
- 3.4 Intensity Measurements
- 3.5 References

3.1 INTRODUCTION

Procedures have been reported in the literature where the required sound levels due to industrial machinery can be calculated in terms of acoustic louvre performance contained in manufacturer's technical literature [1]. However the noise control recommendations are likely to be based upon data performance that is not reliable.

It has been shown in Chapter 1 that there is a diversity of measuring methods adopted by manufacturers, therefore, the comparison of data is confusing and the data itself possibly arguable. Chapter 2 discussed the terminology of sound insulation and the confusions that sometimes result, and pointed out the inadequacy of ISO 140 when applied to open screens. Nevertheless, it was also seen from the survey that some manufacturers use the standard method to assess their products. Some manufacturers stated that good agreement was found when data measured in-situ by non-standard methods were compared with data measured by ISO 140.

In this chapter, the louvre transmission loss is measured, in third octave bands, by the standard method. However, it has been recognised, in Chapter 2, that measured transmission loss less than 15 dB must be treated with caution due to acoustic coupling between the transmission and reception rooms of a standard transmission suite.

Therefore, transmission loss was also measured by intensimetry, a method likely to be a measurement standard in the near future [2] and which is believed to be more representative of louvre performance when installed (again, see Chapter 2). The louvre evaluated in this work was manufactured by Industrial Acoustics Company, Inc. / IAC (UK), who kindly gave one product from their assembly line to the acoustics laboratory of Liverpool University. The louvre was 2.0m wide x 0.3m deep x 1.0m high. It consisted of steel on one side of the blades, as seen in Plate 1, and enclosed mineral wool covered by a perforated steel sheet on the other side, shown in Plate 2. The solid surface is for weathering and forms the external face of the louvre and the perforated inner face, over sound absorbing mineral fibre, was for sound insulation purposes. Plate 3 shows the louvre mounted in the aperture of the transmission suite.

3.2 PREVIOUS RESEARCH

Previous research on open screens can be divided into that concerned with the principle effects of transmission of slits and apertures and that concerned with practical devices such as louvres or barriers. The former is of interest in understanding the mechanisms involved with transmission loss of apertures and is discussed in detail in Chapter 5.

Gomperts [3] and Wilson and Soroka [4] determined the sound transmission loss through circular and slit-shaped apertures in a wall of finite thickness to predict the overall transmission loss of the wall. Mulholland and Parbrook [5] compared a number of theories for the sound transmission through thin circular apertures. Tanoiku and Konishi [6] compared the calculated noise reduction of a slit type barrier, using the line integral method, with that of a solid barrier, and showed that for a 3% opening there was negligible difference in noise reduction in the far field. This barrier offered a direct line of sight as did the regular slit screen (picket barrier) considered by Wassilieff [7]. Wassilieff shows that by careful selection of gap width significant improvement in attenuation at low frequencies is obtained when compared with solid barriers. This results from destructive interference of the sound passing through the gaps and around the barrier. The improved insertion loss occurs at certain frequencies and constructive interference at other frequencies will result in a reduced insertion loss.

Brittain and Salter investigated the noise reduction and insertion loss of acoustic louvres using a reverberant to semi-free field arrangement [8]. They were able to compare data with those of manufacturers, which were usually transmission loss data, determined in accordance with American standards. Below 1 kHz the noise reduction was 5-6 dB less than that given by the manufactures. However, the manufacturers A-weighted sound attenuation prediction at distances greater than 3 m from the façade compared favourably with measurements, and closer than this showed agreement with a theory of Rathe [9]. Differences between measurements and both theories were thought to be the result of near field effects.

Teplitzky [10] tested various types of metal and masonry louvre systems in accordance with American standards. Louvres of pure metallic blades and acoustical louvres were compared to field erected concrete grill screens with different layouts. Generally, all louvres provided relatively

little attenuation, in the range 2- 8 dB, at low frequencies, maximum values being obtained in the higher frequency range.

Louvres, originally designed as a lighting control system for highway tunnels, were investigated for acoustical purposes by Matsumoto [11]. Scale model measurements indicated that with absorption material the louvres could be more effective than solid barriers. A parametric survey was conducted on a newly designed roadway louvre and the influence of thickness, total absorption area and open area ratio of the blades evaluated by insertion loss measurements performed from reverberant to free sound fields. Results were A-weighted in respect to vehicle noise spectrum. Results showed that insertion losses greater than 25 dB can be achieved and proved that the parameters investigated play an important role in the acoustical performance of the louvre.

Lyons and Gibbs [12] investigated a novel type of open screen consisting of two rows of vertical pickets, having a sound absorption surface on one side. A parametric survey varying picket, gap, and cavity widths resulted in more than 100 screen configurations measured. Whilst recognising the problems of applying the standard method to such a low transmission loss device, the measurement survey still showed the usefulness of the measurements in identifying trends in performance. The results were consistent, and showed that these screens could be characterised in terms of three distinct frequency regions: low, mass layer controlled, high, diffraction, absorption and interference controlled, and a transition region. Empirical formulae were derived to give a model for predicting insulation performance with respect to these regions.

Chen [13] compared measurements with two-dimensional plane wave theory of transmission loss of rigid perforated screen. Experimental data was obtained in a special facility consisting of an anechoic chamber within a reverberation chamber, and intensity and sound pressure levels measured respectively and related to transmitted and incident sound power. The agreement between theory and measurement was reasonable at frequencies above 315 Hz. The study also revealed that transmission loss of a perforated screen is almost independent of the chosen material if all its dimensions are fixed.

3.3 STANDARD METHOD (ISO 140)

The facilities at the Acoustic Research Unit of Liverpool University are given in Table 3.1. It has a test aperture area of 3.5 m^2 , with minimum edge length of 1.6 m. This is less than that of 10 m^2 and 2.3 m, required by the standard. This theoretically implies that only measurements above 500 Hz would give reliable results. However, as the screen is open in form and of low transmission loss it was considered acceptable to treat this requirement as though dealing with windows where the size tested relates to the practical size used, and may be less than 2.3 m [14]. At present, the added Part 10 of ISO 140 deals specifically with sound insulation of small building elements [15]. The standard requires elements to be mounted centrally unless this is inconsistent with the practical application. The 2.0 m^2 louvre was placed flush with both faces in the aperture. The remaining surrounding area around the louvre was closed with a double leaf wooden partition, with absorption material inside.

TABLE 3.1 - Dimensions of Facilities and ISO 140 Requirements

Parameter	Receiver room	Source room	ISO 140 requirements
Volume (m^3)	122.00	74.00	50.00
Minimum vol. difference (%)	164.00	61.00	10.00
Area (m^2)	149.00	109.50	
Test area (m^2)	3.50	3.50	10.00
Minimum edge length (m)	1.66	1.66	2.30
Cut-off frequency (Hz): $M = 1$	200.00	250.00	
$M = 1/3$	100.00	160.00	

The cut-off frequency, f_c , which is the lowest frequency at which the reverberant sound field can be considered to be statistically reliable, was calculated according to [16]:

$$f_c = \sqrt{\frac{Mc^3T}{8.8\pi V}} \quad (3.1)$$

where T is reverberation time, V is the room volume, c is the speed of sound in air and M is the modal overlap index, a measure of mode spacing and overlap of the sound field. Schroeder [17] suggest a value of $M = 3$, giving the familiar Schroeder cut-off frequency, however, other researches have found that $M = 1/3$ gave good modal overlap and a value of unity was considered cautious [16]. Values of fc are given in Table 3.1 for the Liverpool facilities. For $M = 1/3$ the reverberant sound field was considered to be statistically reliable above 160 Hz in the source room and 100 Hz in the receiver room.

3.3.1 TL of Connecting Partitions

The structurally isolated rooms ensure flanking transmission is negligible and the transmission loss of the connecting wall should be much greater than that of the louvre. Therefore, previous to the louvre measurements the demountable partition around the louvre was tested for sound insulation. The louvre was covered on both sides with the same type of wooden panel used around it and absorption material introduced in the gaps in between blades. Figure 3.1 presents schematically the a) plan view and b) cross section of the arrangement.

The mean sound pressure levels in the source room were measured using a Brüel & Kjær 3923 Rotating Microphone Boom with a radius of 1.10 m and transverse time of 32". In the receiving room, the mean sound pressure level measurement was performed in the same manner as in the source room, this time the length of the arm of the rotating boom was reduced to 0.97 m due to the smaller dimensions of the room.

The standard requires reverberation time measurements to be evaluated according to ISO 354:1985 [18] (BS 3638:1987). A Brüel & Kjær 4417 Building Acoustics Analyser and Brüel & Kjær 3923 Rotating Microphone Boom with a radius of 1.10 m were used in the survey for both measurements of partition and louvre. The average reverberation time in the receiving room and transmission loss of the partition are presented in Figure 3.2 and 3.3, respectively, and the insulation offered was to be compared with that of the louvre.

3.3.2 Reverberation Time Measurements

The specific requirements of the standard were followed, as they were for the partition measurements. The repeatability test asks for six consecutive measurements of transmission loss and comparison of each consecutive pair. The difference between the two members of every pair is not to exceed the values given in ISO 140/2:1978 Annex A. Figure 3.4 presents the averaged reverberation time and the six individual curves.

3.3.3 Transmission Loss of the Aperture

The transmission loss of the open aperture had been measured in a previous research carried out in the laboratory [19]. It was assumed that a transmission loss of zero dB would be obtained thereby providing validation of the facility [20]. However, it became clear that such measurement exposed weakness in the standard method of test.

Results obtained by Lyons showed that the aperture presented TL values of up to 6 dB in the low frequency. This measurement phenomenon arises due to incorrect estimates of absorption in the receiving room ($S_s \bar{\alpha}$ in equation (2.7)). The problem is fairly well known [5,20,21,22,23] though not often approached as test elements usually offer a transmission loss of greater than 15 dB. The problem, as stated in Chapter 2, is energy feedback from the source into the receiver room that arises during the measurement of reverberation time, when the coupling between the reverberant rooms is strong. In his original work Buckingham [24] had intended that the panel transmission loss should be included in the total absorption of the room therefore being $S_s \bar{\alpha} + S_r$. This is found by measurement of the reverberation time and yields the transmission loss when used in equation (2.3). As seen in Chapter 2, it is normally assumed that $S_s \bar{\alpha} \gg S_r$ and this is valid for most cases except when the transmission loss is less than 15 dB, for instance, the louvre studied here.

3.3.4 Results

The accepted lower frequency of measurement of transmission loss by the time of this research was 100 Hz, although the revised version of ISO 140 [15] extends it down to 50 Hz. Certain

discrepancies in transmission loss measurements occur below the cut-off frequency, which may be defined as the frequency where the number of modes excited in an one third octave band will be less than 20 [25,26].

Low frequency differences are due, in part, to the increase in sound energy close to the surfaces of the receiving room, this being known as the Waterhouse effect [27]. This is the increased energy density at the wall boundaries of a room relative to the central portion of the room where the pressure is generally measured. The Waterhouse correction involves adding the following correction term

$$10 \log \left(1 + \frac{\lambda S}{8V} \right) \quad (3.2)$$

where S and V are surface area and volume respectively of each room. As each term will be opposite in sign and the room areas and volumes are similar the resulting correction will be negligible.

Figure 3.6 shows the measured values for transmission loss. The insulation performance presents the general trend of sound absorption materials, with greater values with increasing frequency up to a maximum, in the range of 1k to 2.5 kHz. As expected the louvre provides relatively little attenuation at the lower frequencies compared to the attenuation at higher frequencies. Data below 630 Hz, which present values less than 15 dB is considered not to be reliable due to effects of coupling between rooms. Also, at the low frequency region the aperture itself offers sound attenuation due to impedance change through the aperture. Therefore, the standard results overestimate the sound insulation of the louvre.

3.3.5 Reciprocity

A reciprocity test was also performed by taking measurements in both directions. Figure 3.6 shows reciprocal louvre transmission loss, where it is shown that when the large room was used as a source room the transmission loss is slightly lower than conventionally using a small source room. This result is consistent with those of Lyons [19], Halliwell and Warnock [26], and Guy [28], who, however, found later a trend that differ from that reported earlier [29]. As it might be

expected, the greatest differences were found in the frequency range below the cut-off frequency.

3.4 INTENSITY MEASUREMENTS

Sound intensity is not a modern acoustical concept, but it has recently found practical application in measurement driven by the advance in signal processing techniques. The foundation to the theory on intensimetry appeared in 1878 in Lord Rayleigh's principal work "The Theory of Sound" [30]. In the 20th century, important contributions were made by Olson [31] in 1931, Clapp and Firestone [32] in 1941, Bolt and Petrauskas [33], Baker [34], and Schultz in 1956, who proposed the first practical implementation of the intensity technique [35]. The 1970's saw application of the technique in the determination of sound power radiated by complex sources. Problems of adjustment and calibration were studied by Fahy [36,37] and Chung [38]. Rapid development of digital signal processing and Fast Fourier Transform (FFT) analysers resulted in improved speed and reliability of the method. Refer to Fahy [39] for a detailed review of work up to the late eighties.

In the field of building acoustics, an ISO working group has been established to develop a standard "Measurement of Airborne Sound Insulation Using Sound Intensity" [40]. While current standards give sound magnitude in the form of sound pressure level which is a measure of the variation about a static atmosphere pressure sound intensity gives the rate of transmitted energy in a specific direction, per unit area. Therefore, intensity measurements yield sound propagation paths from sources or from sound transmitted through screens, e.g. a louvre.

3.4.1 Principles of Measurement

Sound intensity can be defined as the average rate of flow of energy through a unit area normal to the direction of propagation [41]. Therefore, the following relation applies:

$$\frac{\text{energy}}{\text{area} \times \text{time}} = \frac{\text{force}}{\text{area}} \times \frac{\text{distance}}{\text{time}} = \text{pressure} \times \text{velocity} \quad (3.3)$$

The instantaneous acoustic intensity I_r , in a given direction r , is the product of the acoustic

pressure p and its corresponding particle velocity u in this direction [42]:

$$I_r = pu_r \quad (3.4)$$

As the instantaneous particle velocity is a vector quantity and pressure is a scalar quantity the product of the two quantities is another vector quantity.

The estimate of the acoustic intensity I_r , in the r direction, is the temporal average of the instantaneous acoustics. Therefore,

$$I_r = \overline{p(t)u_r(t)} \quad (3.5)$$

where the bar indicates time averaging.

In order to measure intensity, it is necessary to measure the two parameters, sound pressure and particle velocity. The measurement of sound pressure is now well established through the use of high quality condenser microphones. The direct measurement of particle velocity is not as simple, however, and is the main reason why intensity measurements have only become possible in the last decade.

The method of determining the intensity is based on the relation between acoustic pressures of two close microphones and the particle velocity, expressed by:

$$\rho \frac{\partial u_r}{\partial t} = -\frac{\partial p}{\partial x} \quad (3.6)$$

The particle velocity is determined from equation (3.6). Substituting it into equation (3.5) gives the acoustic intensity,

$$I_r(t) = -\frac{1}{\rho} p(t) \int \frac{\partial p(t)}{\partial x} dt \quad (3.7)$$

Using a finite difference approximation,

$$p(t) = \frac{1}{2} [p_1(t) + p_2(t)] \quad (3.8)$$

$$\frac{\partial p(t)}{\partial r} \cong \frac{p_2(t) - p_1(t)}{\Delta r}$$

and substituting into equation (3.7) gives

$$I_r = -\frac{1}{2\rho\Delta r} \overline{[p_1(t) + p_2(t)] \int [P_2(t) - p_1(t)] dt} \quad (3.9)$$

Equation (3.9) is the basis of modern sound intensity measurement systems.

For the determination of airborne transmission loss the incident and transmitted intensity levels are required, hence:

$$TL = L_{Ii} - L_{It} \quad (3.10)$$

where L_{Ii} is the incident intensity level and L_{It} is the transmitted intensity level. In a reverberant source room where the sound field is diffuse the incident intensity, I_i on the test panel is given by [43]:

$$I_i = \frac{P_{rms}^2}{4\rho c} \quad (3.11)$$

From equation (3.11) the following relationship between the incident intensity level L_{Ii} and the space averaged sound pressure level L_{ps} can be derived [44].

$$L_{Ii} \cong L_{ps} - 6 \text{ dB} \quad (3.12)$$

where L_{ps} is the source room space-average sound pressure level. The transmitted intensity is measured directly on the receiving side of the panel surface, and the transmission loss is obtained from:

$$TL = L_{ps} - L_{It} - 6 \text{ dB} \quad (3.13)$$

3.4.2 Results

The incident intensity was calculated from the mean sound pressure level in the source room, measured in the same way as for the standard method presented in section 3.3.

The transmitted sound intensity was measured directly using a Brüel & Kjær 3520 Sound Intensity Probe and Brüel & Kjær 2144 Analyser, using the face-to-face configuration with ½" microphone and 12 mm spacer. Calibration was by means of a Brüel & Kjaer 3541 calibration system.

Sound absorption material was introduced to the receiver room to ensure an acceptable reactivity index, i.e. the reverberant sound field of the receiving room is low enough not to exceed the capability of the probe to detect the sound intensity in a particular direction.

The spatial average sound intensity from the surface of the louvre was measured by continuous scan technique. Two sets of measurements were performed; sweeping the surface by hand horizontally and vertically with an averaging time of 3 minutes each. The probe was always held to the side and at arm's length to minimise the influence of the operator. The results with respect to the average transmitted intensities are shown in Figure 3.7 and the calculated transmission loss, using the average over the two directions, in Figure 3.8, together with ISO 140 result. The ISO measured values are higher than those of the intensity measurement throughout the frequency range, confirming the anticipation that ISO overestimates the louvre performance.

It can be argued that the difference is partially due to the interference-field in the source room, as discussed in section 3.1.4, and Waterhouse correction term should be taken into account [26,27,45,46]. Transmission Loss values obtained using intensity techniques may be underestimated if this is overlooked. As this is more significant at low frequencies it is believed to be partly responsible for the small though consistent discrepancies between conventional and sound intensity measurements [26,45]. The resulting expression is:

$$TL = L_{ps} - L_{lt} - 6 + 10 \log \left[1 + \frac{\lambda S_s}{8V_s} \right] \quad (3.14)$$

where S_s and V_s are surface area and volume respectively of the source room. Halliwell and Warnock argue that it is not correct to apply the Waterhouse correction to the source room measurements where the incident sound intensity only is required, though until further research work is done the correction is preferred over no correction at all [26]. Figure 3.9 shows the transmission loss as expressed in equation (3.14). An underestimation by intensity is not responsible for the difference, as the correction is not enough to match the results.

Various limitations are inherent to sound intensity measurements. Some of these error can be compensated for, such as phase mismatch, and the relative accuracy of results determined, whilst others such as sound reflections off the probe body must be accepted.

When dealing with solid screens, results have been shown to compare well with theory and conventional methods [16,46,47]. However, discrepancies exist at low frequencies as stated earlier and there are differences in the high frequency range thought to be due to finite difference error [26].

To summarise, it has been demonstrated that acoustic intensimetry is a more representative measure of louvre performance than the existing standard method since the laboratory sound field conditions ideally are the same as the real sound field conditions, i.e. diffuse to free-field. However, if low-noise free-field conditions exist on the 'external' side of the louvre, the intensimetry measurements do not offer significant advantages with respect to pressure measurement. In addition, large amounts of additional absorption must be installed in a receiver room if a standard transmission suite is to be modified to simulate reverberant to free-field transmission. This will be costly and time consuming.

Therefore, although intensimetry measurement results will be used for comparison, the remainder of the thesis will concentrate on the development of an impulse response technique since this approach promises a measurement method which does not require large acoustic facilities or extensive modification to large facilities.

3.5 REFERENCES

- [1] Sharland I., *Woods Practical Guide to Noise Control*, Woods of Colchester Limited, Salford, (1972).
- [2] ISO discussion document, *Measurement of Airborne Sound Insulation Using Sound Intensity*.
- [3] Gomperts M.C., *The Sound Insulation of Circular and Slit-Shaped Apertures*, *Acustica*, **14**, 1-9, (1964).
- [4] Wilson G.P. and Soroka W.W., *Approximation to the Diffraction of Sound in a Rigid Wall of Finite Thickness*, *J. Acoust. Soc. Am.*, **37**(2), 280-297, (1965).
- [5] Mulholland K.A. and Parbrook H.D., *The Measurement of Sound Transmission Loss of Panels with Small Transmission Loss*, *J. Sound Vib.*, **2**(4), 502-509, (1965).
- [6] Tanioku Y. Konishi K. and Maekawa Z., *Noise Reduction of a Slit-Type Barrier by Using Line Integral Method and Full Scale Model Measurement*, *Proc. InterNoise 1987*, 395-398.
- [7] Wassilieff C., *Improving the Noise Reduction of Picket Barriers*, *J. Acoust. Soc. Am.*, **84**(2), 645-650, (1988).
- [8] Brittain F.H. and Salter C.M., *Insertion Losses of Standard and Acoustic Louvres*, Paper delivered at the 85th Meeting of the Acoustical Society of America in Boston, (1973).
- [9] Rathe E.J., *Note on Two Common Problems of Sound Propagation*, *J. Sound Vib.*, **10**(3), 472-479, (1969).
- [10] Teplitzky A.M. and Carlson J.P., *Sound Transmission Loss of Ventilation Louvre*, *Sound Vib.*, 24-26, (1979).
- [11] Matsumoto K., Yamamoto K. and Yamashita M., *Noise Reduction by Absorptive Louvre*, *Proc. InterNoise 1991*, 509-512.
- [12] Lyons R. and Gibbs B.M., *Investigation of an Open Screen Acoustic Performance*, *Appl. Acoustics*, **49**(3), 263-282, (1996).
- [13] Chen K., *Study of the Acoustic Transmission Loss of a Rigid Perforated Screen*, *Appl. Acoustics*, **47**(4), 303-318, (1996).
- [14] ISO 140:1978. *Methods of Measurement of Sound Insulation in Buildings and of Building Elements*, Parts 1 to 8.
- [15] ISO 140. *Methods of Measurement of Sound Insulation in Buildings and of Building Elements*, Parts 1 to 12 (Revision 1994/1995).

- [16] Crocker M.J and Price A.J., *Noise and Noise Control*, vol.1, CRC Press, (1975).
- [17] Schroeder M.R., *Effect of Frequency and Space Averaging on the Transmission Response of Multimode Media*, J. Acoust. Soc. Am., **46**(2), (1969).
- [18] ISO 354:1985 (BS 3638:1987). *British Standard Method for Measurement of Sound Absorption in a Reverberant Room*.
- [19] Lyons R., *Building Elements of Low Insertion Loss*, Ph.D. Thesis, University of Liverpool, (1993).
- [20] Bies D.A. and Davies J.M., *An Investigation of the Measurement of Transmission Loss*, J. Sound Vib., **53**(2), 203-221, (1977).
- [21] Mariner T., *Critique of the Reverberant Room Method of Measuring Airborne Sound Transmission Loss*, J. Acoust. Soc. Am., **33**(8), 1131-1139, (1961).
- [22] Mulholland K.A. and Parbrook H.D., *The Measurement of Transmission Loss*, J. Sound Vib., **5**(2), Letter to the Editor, 391-394, (1967).
- [23] Bies D.A. and Pickles J.A., *The Measurement of the Transmission Loss of a Low Noise Reduction Test Item*, Proc. Noise, Shock & Vib. Conf., 144-153, (1974).
- [24] Buckingham E., *Theory and Interpretation of Experiments on the Transmission of Sound Through Walls*, Scientific papers of the bureau of standards, No.506, 20, 193-219, (1925).
- [25] Mulholland K.A. and Lyon R.H., *Sound Insulation at Low Frequencies*, J. Acoust. Soc. Am., **54**(4), 867-878, (1973).
- [26] Halliwell R.E. and Warnock A.C.C., *Sound Transmission Loss: Comparison of Conventional Techniques with Sound Intensity Techniques*, J. Acoust. Soc. Am., **77**(6), 2094-2103, (1985).
- [27] Waterhouse R.V., *Interference Patterns in Reverberant Sound Fields*, J. Acoust. Soc. Am., **27**(2), 247-258, (1955).
- [28] Guy R.W., De Mey A. and Sauer P., *The Effect of Some Physical Parameters upon the Laboratory Measurements of Sound Transmission Loss*, Appl. Acoust., **18**, 81-98, (1985).
- [29] Bhattacharya M.C. and Guy R.W., *The Influence of the Measuring Facility on the Measured Sound Insulating Property of a Panel*, Acustica, **26**, 344-347, (1972).
- [30] Rayleigh J.W.S., *The Theory of Sound*, Dover Publications, (1945).
- [31] Olson H.F., *Field-Type Acoustic Wattmeter*, J. Audio Eng. Soc., **22**, 321-328, (1974).
- [32] Clapp C.W. and Firestone F.A., *The Acoustic Wattmeter, an Instrument for Measuring Sound Energy Flow*, J. Acoust. Soc. Am., **13**, 124-136, (1941).

- [33] Bolt R.H. and Petrauskas A.A., *An Acoustic Impedance Meter for Rapid Field Measurements*, J. Acoust. Soc. Am., **15**, p 79, (1943).
- [34] Baker S., *Acoustic Intensity Meter*, J. Acoust. Soc. Am., **27**, 269-273, (1955).
- [35] Schultz T.J., *Acoustic Wattmeter*, J. Acoust. Soc. Am., **28**, 693-699, (1956).
- [36] Fahy F.J., *A Technique for Measuring Sound Intensity with a Sound Level Meter*, Noise Control Eng., **9**, 155-162, (1977).
- [37] Fahy F.J., *Measurement of Acoustic Intensity Using the Cross-Spectral Density of Two Microphone Signals*, J. Acoust. Soc. Am., **62**, 1057-1059, (1977).
- [38] Chung J.Y., *Cross-Spectral Method of Measuring Acoustic Intensity Without Error Caused by Instrument Phase Mismatch*, J. Acoust. Soc. Am., **64**, 1613-1616, (1978).
- [39] Fahy F.J., *Sound Intensity*, Elsevier Applied Science, New York, Chapter 2, (1989).
- [40] Goydke H., *New International Standards for Building and Room Acoustics*, Appl. Acoust., **52**(3/4), 185-196, (1997).
- [41] Kinsler L.E., Frey A.R., Coppens A.B. and Sanders J.V., *Fundamentals of Acoustics*, John Wiley & Sons, third edition, New York, (1982).
- [42] Gerges S.N.Y., *Ruído. Fundamentos e Controle*, Imprensa Universitária, Florianópolis, (1992).
- [43] Crocker M.J., Raju P.K. and Forssen B., *Measurement of Transmission Loss of Panels by the Direct Determination of Transmitted Acoustic Intensity*, Noise Control Eng., **17**, 6-11, (1981).
- [44] Fahy F.J., *Sound Intensity Measurement of Transmission Loss*, Proc. Inst. of Acoustics, B5.1-B5.4, (1982).
- [45] van Zyl B.G., Erasmus P.J. and Anderson F., *On the Formulation of the Intensity Method for Determining Sound Reduction Indices*, Appl. Acoust., **22**, 213-228, (1987).
- [46] Jonasson H.G., *Measurements of Sound Reduction Index with Intensity Technique - Nordtest Project 746-88*, Swedish National Testing and Research Institute, (1991).
- [47] Mintem M., Cops A. and Wijnants F., *The Sound Transmission Loss of a Single Panel Measured with the Two-Microphone and the Conventional Method - Comparison with the S.E.A. Model*, Appl. Acoust., **22**, 281-295, (1987).

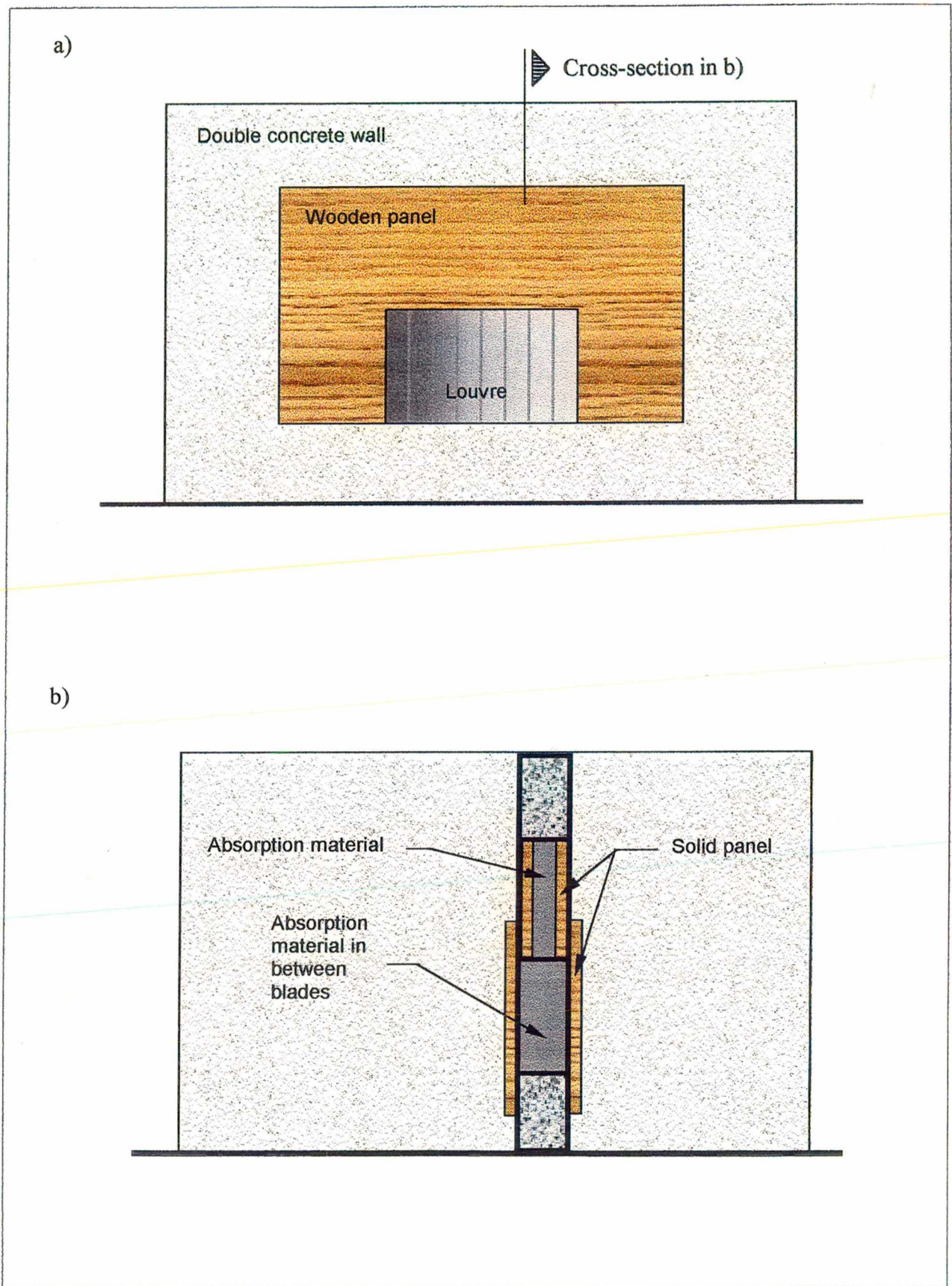


FIGURE 3.1 - Schematic a) layout and b) cross section of the arrangement for TL measurement of connecting partition in between chambers.

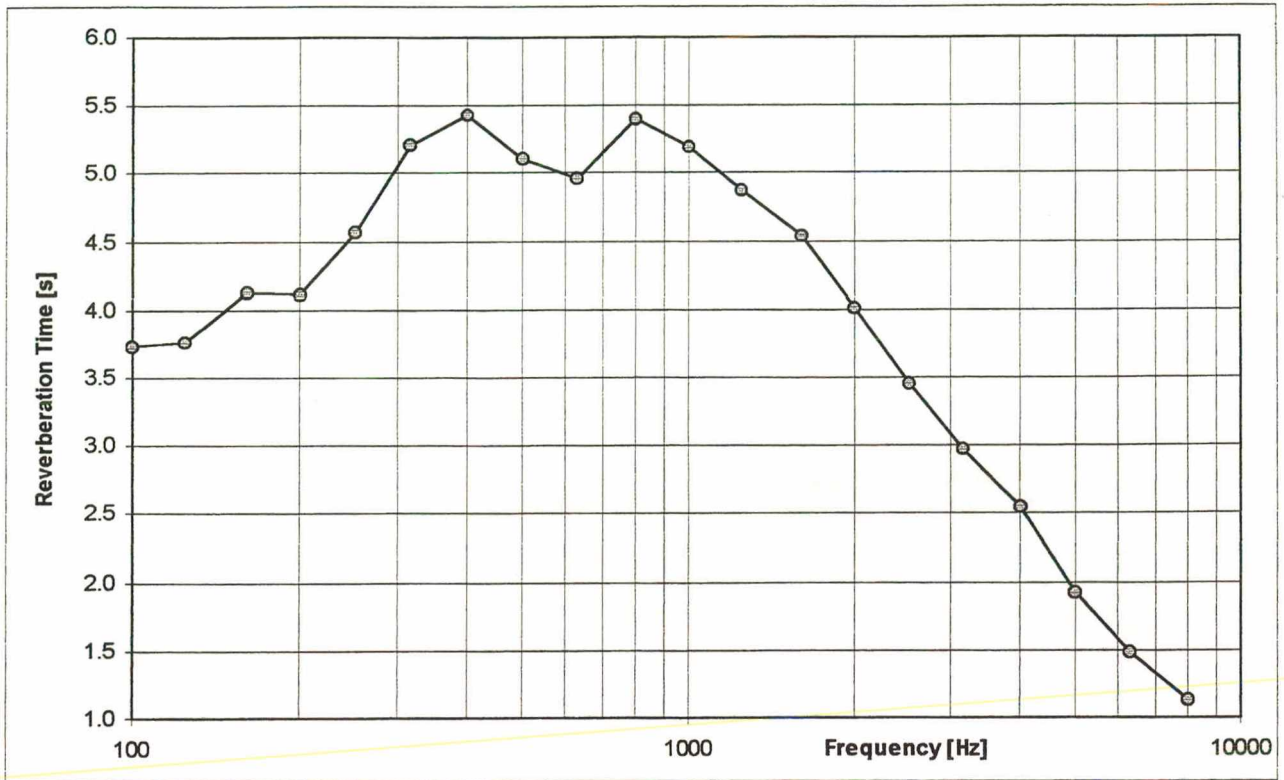


FIGURE 3.2 - Average reverberation time of receiving room with test area covered by wooden panel.

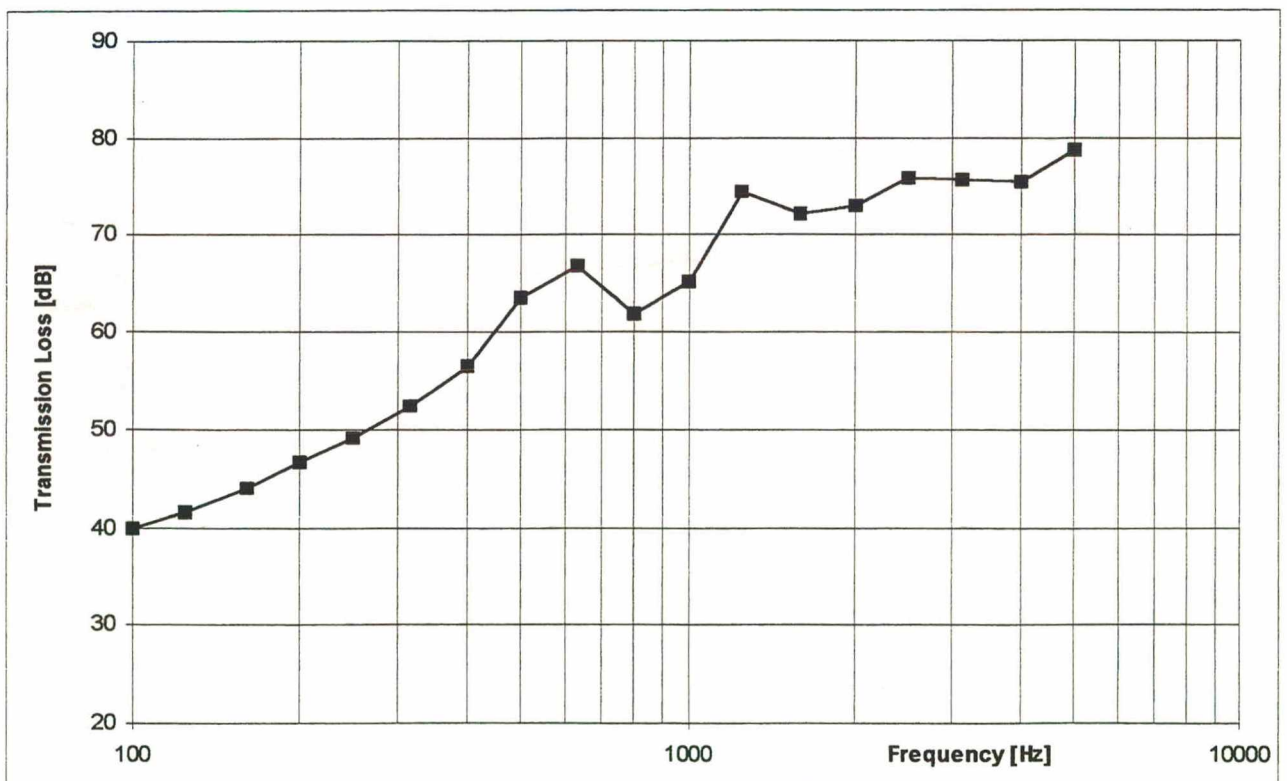


FIGURE 3.3 - Transmission loss of connecting partition with test area covered by wooden panel.

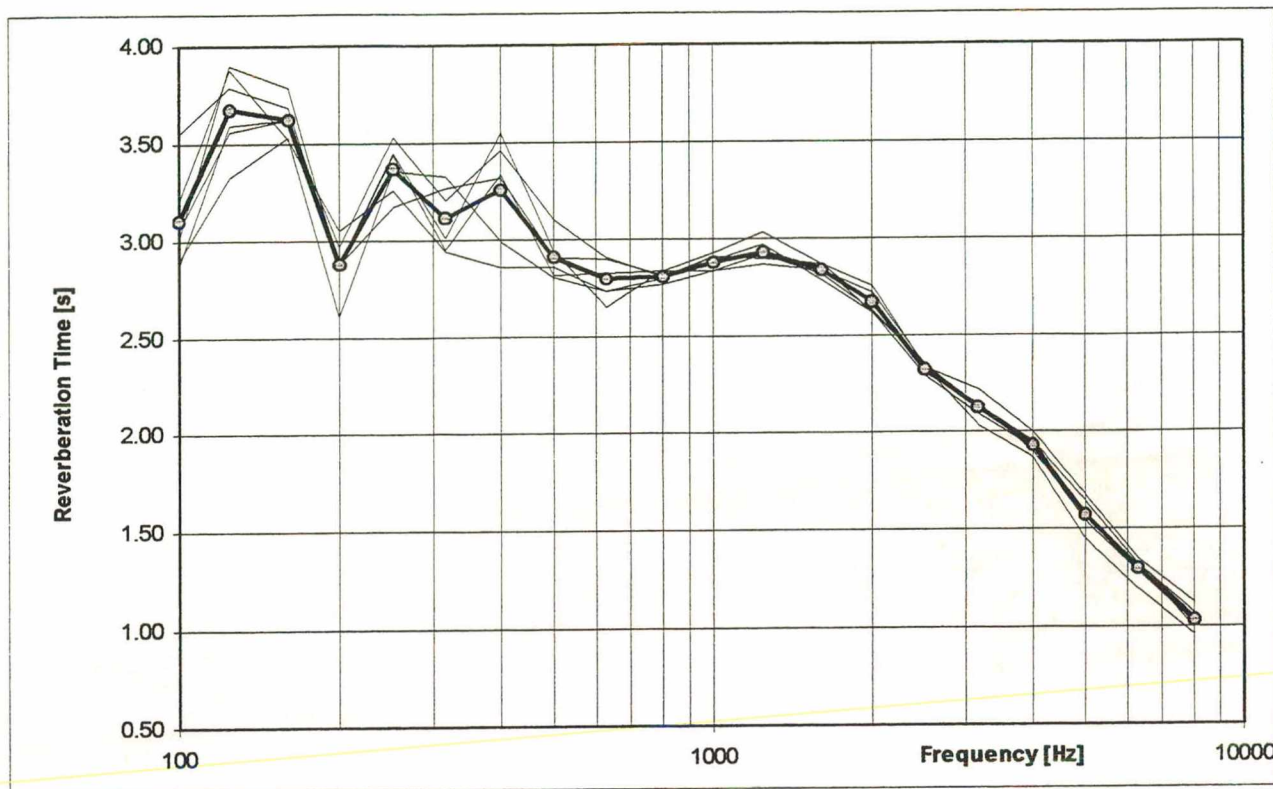


FIGURE 3.4 - Averaged reverberation time (thick line) and the six individual curves (thin lines) of the receiving room used for the louvre transmission loss measurements.

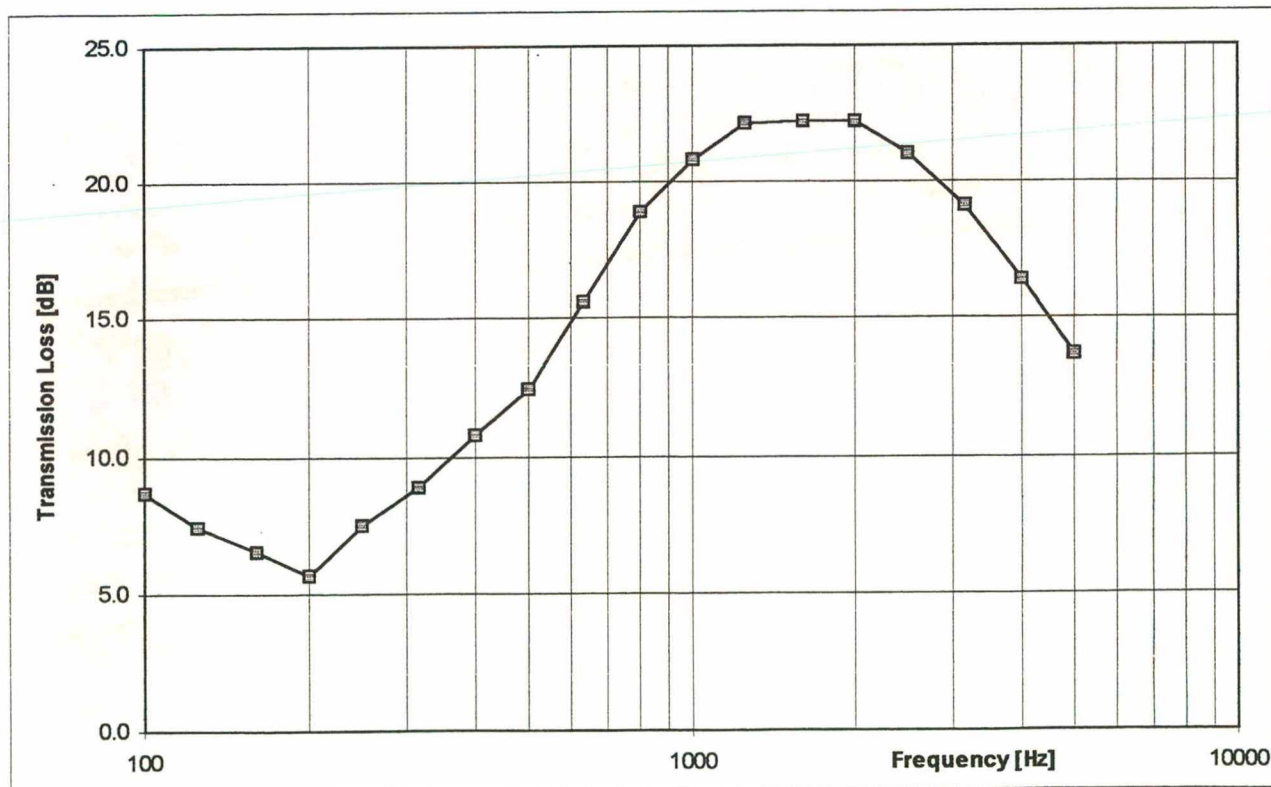


FIGURE 3.5 - Transmission loss of the louvre by ISO 140.

3. Louvre's Transmission Loss by Existing Methods

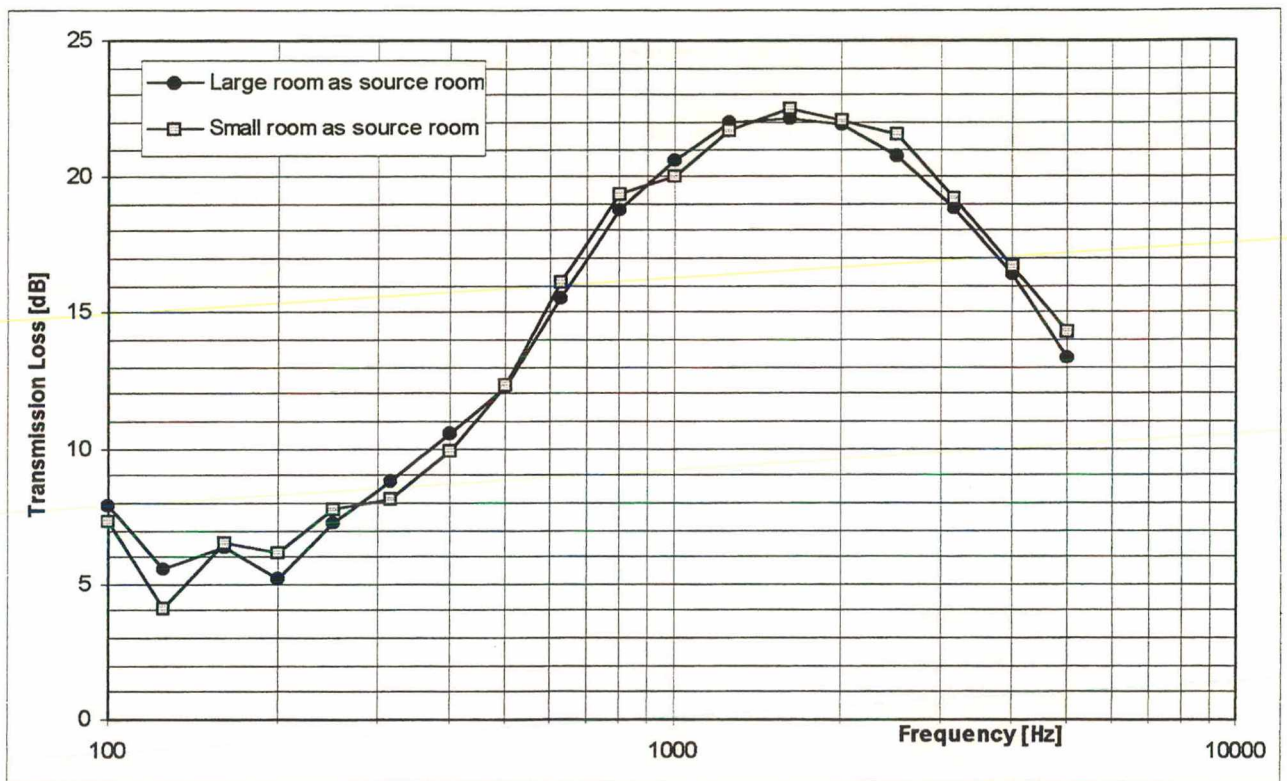


FIGURE 3.6 - Transmission loss for the louvre with respect to room orientation.

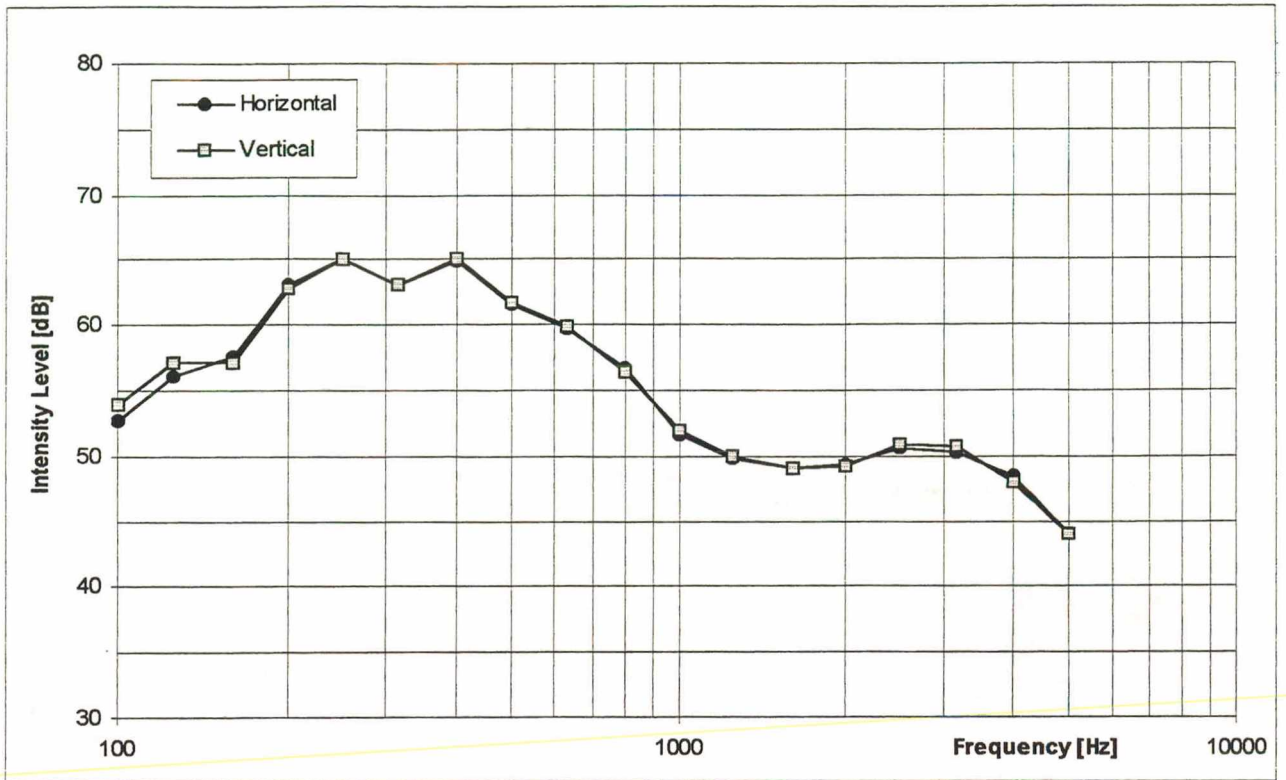


FIGURE 3.7 - Average transmitted intensity with respect to scanning direction.

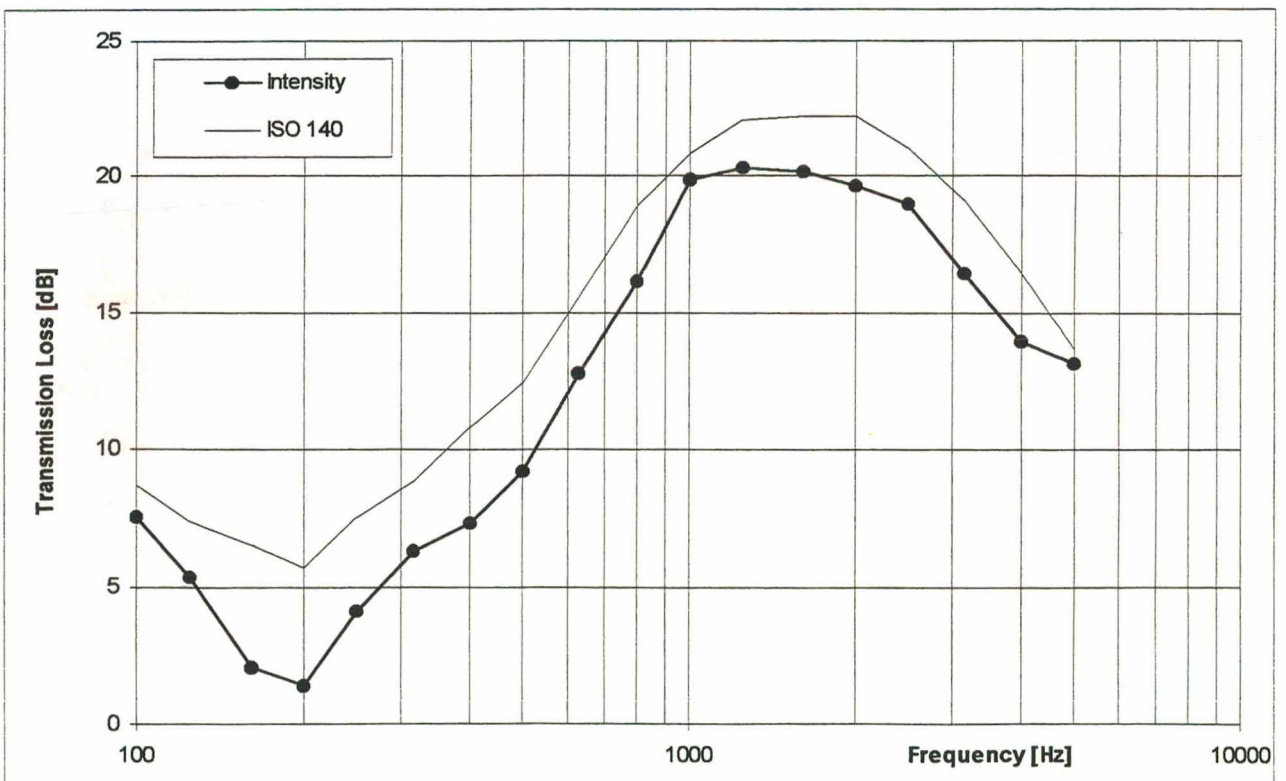


FIGURE 3.8 - Transmission loss of the louvre by intensity and ISO 140.

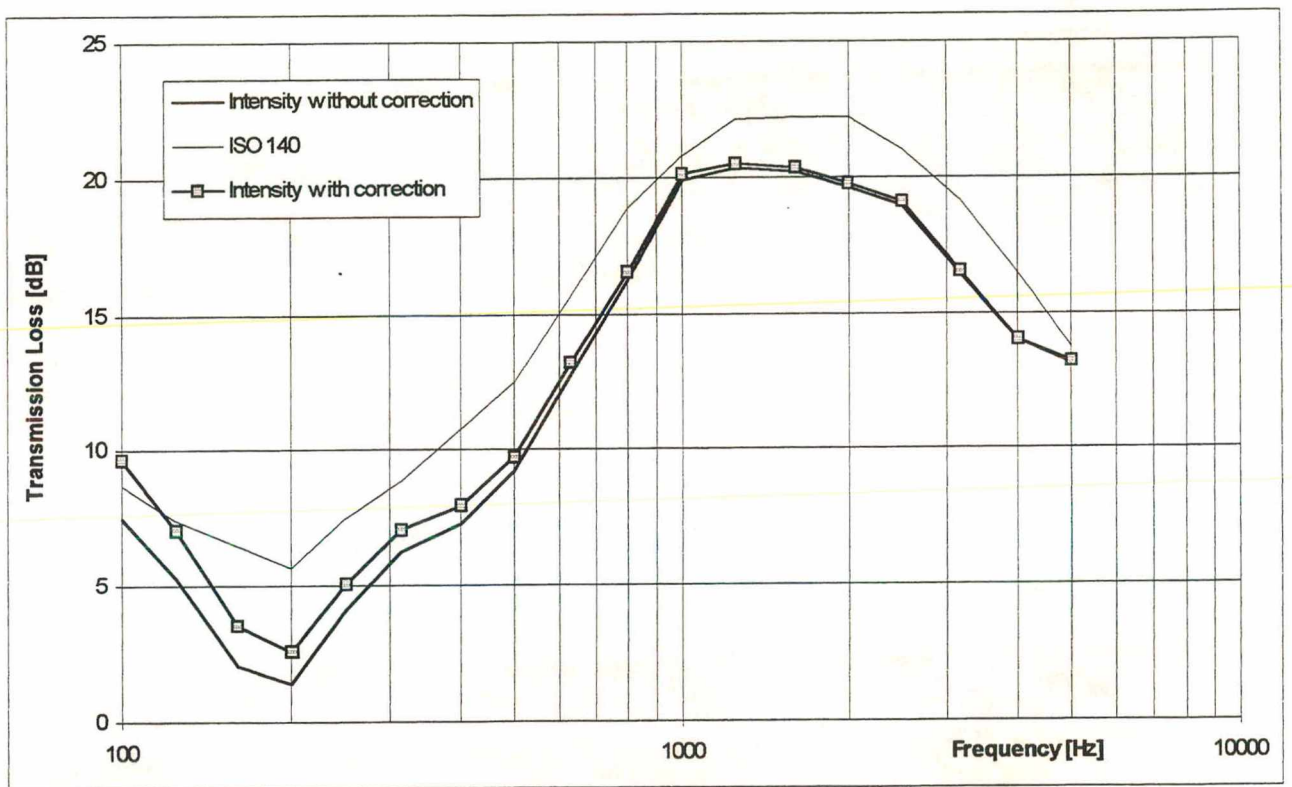


FIGURE 3.9 - Transmission loss for the louvre by intensity accounting for Waterhouse correction in the source room, without correction, and by ISO 140.

CHAPTER 4 IMPULSE RESPONSE ANALYSIS

- 4.1 Principle**
- 4.2 Maximum-Length Sequences (MLS)**
- 4.3 Measurement Method**
- 4.4 References**

4.1 PRINCIPLE

Impulse response analysis is applicable to linear time invariant systems (LTI). Linearity is an important prerequisite for applicability of Fourier's theorem, i.e. the correspondence of (transient) impulse responses and (stationary) frequency responses [1]. Measurements with a single pulse have the well-known disadvantage of low signal-to-noise ratio, caused by the limited maximum amplitude of transducers. Unlike impulsive excitation, maximum-length sequences have a very low crest factor, with the energy distributed uniformly over the measurement period.

To introduce the impulse response theory the delta function $\delta(t)$ is presented. Often termed the Dirac delta function, it has the following important properties:

$$(i) \delta(t) = 0, \text{ for } t \neq 0 \quad (ii) \int_{-\infty}^{\infty} \delta(t) dt = 1 \quad (4.1)$$

where t represents time. In the frequency domain it is represented as a constant level spectrum of unit amplitude.

For a system having an unit impulse input $x(t)$ and producing a well-defined output $y(t)$, the unit impulse response function $h(t)$, which is a complete description of that system's transfer function characteristics, can be measured directly:

$$h(t) = y(t) \quad \text{when} \quad x(t) = \delta(t) \quad (4.2)$$

where t is the time measured from the instant the delta function is applied.

On the other hand, if the system is excited by a stationary signal $n(t)$, the cross correlation of the input and the output is related to the autocorrelation of the input by a convolution with the impulse response:

$$\phi_{ny}(k) = \phi_{nn}(k) * h(k) \quad (4.3)$$

From equation (4.3) it is concluded that the input does not need to be a Dirac delta function, but only its autocorrelation. Thus the impulse response of the system $h(t)$ can be recovered by cross-correlating the special noise input $n(t)$ with the output $y(t)$.

MLS, or m-sequences, are periodic binary pseudostochastic signals and their most important property is that, except for a small DC error, their autocorrelation is a perfect impulse, as seen in Figure 4.1 [2]. The result of convolving $\phi_{nn}(k)$ with any function is the function itself, in this case, the impulse response.

4.2 MAXIMUM-LENGTH SEQUENCES (MLS)

MLS are generated by use of a register with feedback loops. Several of the references explain how to generate maximum-length sequences and provide a mathematical framework [3,4,5,6].

The generation of maximum-length sequences is most easily described by considering a specific case, such as the three-stage shift register shown in Figure 4.2. The grey boxes represent a unit-sample delay produced by memory elements or flip-flops. The operation designated by \oplus is a modulo 2 sum, or exclusive-or, defined by:

$$\begin{aligned}
 0 \oplus 0 &= 0 \\
 0 \oplus 1 &= 1 \\
 1 \oplus 0 &= 1 \\
 1 \oplus 1 &= 0
 \end{aligned}
 \tag{4.4}$$

A signal is fed back to the beginning of the shift register which is a modulo 2 sum of selected outputs. The sequences produced at each node of the three-stage shift register that are shown in Figure 4.2 were produced by initialising the shift register to all 1's. Choosing different initial conditions will change the sequences that are produced in a way that corresponds to delaying the sequences by some amount. With m stages in the binary shift register it is theoretically possible to describe 2^m states, but if the content of the shift register is all 0's, it will be impossible for a 1 to occur, and the shift register will remain frozen in this state. In order to avoid this degenerate case, the longest sequence that can be generated using linear feedback has length $2^m - 1$. A binary sequence whose length is $2^m - 1$ is called a maximum-length sequence [2]. Figure 4.3 a) shows a

maximum-length sequence of order 15, whose length is 32,767 and Figure 4.3 b) the two periods of the autocorrelation function.

4.2.1 Fast Hadamard Transform

When measuring with maximum-length signals, the MLS $s_{MLS}(t)$ is applied to the system under test and usually one period of the stationary pseudonoise response is sampled. The generating shift register and the receiving sampling device usually have to be clocked with the same rate ($1/T$). Due to the autocorrelation function of the MLS the impulse response of the device under test $h(nT)$ is obtained by convoluting the sampled data with the time reversed MLS $s_{MLS}(-nT)$ [7], according to:

$$\begin{array}{c}
 \text{cross-correlation} \leftrightarrow \text{FHT} \\
 \underbrace{S_{MLS}(nT) * h(nT) * S_{MLS}(-nT)}_{\text{measured}} = \underbrace{S_{MLS}(nT) * S_{MLS}(-nT)}_{\substack{\text{autocorrelation} \\ \text{function} = N \cdot \delta(t)}} * h(nT) \\
 \cong L \cdot h(-nT) \qquad \qquad \qquad (4.5)
 \end{array}$$

Due to the periodicity of the MLS the index (nT) is evaluated modulo L . Additionally, the factor L in equation (4.5) reflects the increase in dynamic range compared to single impulse measurements, assuming the same amplitude for the MLS and the single impulse.

Because the sequences are binary, the cross-correlation operation on the right hand side of equation (4.5) is particularly simple. By assigning the values ± 1 to the two binary levels, it is clear that the cross correlation requires no multiplication, only additions and subtractions. Multiplication usually requires much more time than addition, so eliminating the need for multiplication greatly speeds the processing. But even more significantly, an efficient algorithm based upon the Fast Hadamard Transform exists for performing the additions [2]. More information on the Hadamard transform can be found in the literature [2,5,6,8,9].

4.2.2 Signal to Noise Ratio

MLS has many advantages compared with other input signal generation. Firstly, when compared with single pulse technique, the amplitude gain of the MLS technique is theoretically given by [1]:

$$\Delta_{pulse} = 10 \log(L + 1) \approx m \cdot 3dB \quad (4.6)$$

where m is the sequence order.

Secondly, due to the deterministic nature of MLS, the signal should give exactly reproducible results. This allows the use of synchronous averaging, a procedure that reduces the effective background noise level by 3 dB per doubling of the number of averages. The reason is that the exactly repeated periods of the test signal add up “in phase” whereas background noise is not correlated between the different periods and only its energy is summed. This averaging process is an advantage of deterministic signals in general. The gain in signal to noise ratio, in dB, is [10]:

$$\Delta_{aver} = 10 \log N \quad (4.7)$$

where N is the number of averages.

Thirdly, signal-to-noise ratio does not completely characterise the noise immunity of MLS sequences. MLS are highly immune to noise transients of all kinds, such as clicks, door bang, and footsteps. All nonstationary interfering noise, whatever the source, is automatically converted to stationary noise and distributed evenly over the entire impulse response.

Lastly, after Hadamard transformation, the signal-to-noise ratio is already markedly improved, since the total signal energy is concentrated in the peaks of the impulse response. It is shown [10] that the gain in the effective S/N ratio, i.e. the difference between the stationary S/N ratio and the peak to noise ratio is:

$$\Delta_{FHT} = 10 \log\left(\frac{13.8t_{MLS}}{T}\right) \quad (4.8)$$

with t_{MLS} denoting the time elapsed during one MLS period and T the reverberation time of the (exponential) impulse response. In the worst case, when the sequence period equals reverberation time (should not be smaller, as it is shown in section 4.2.3), the “peak-to-noise” ratio is 11 dB larger than the S/N ratio [10].

It should be emphasised that in a practical application there will still be uncertainty due to noise in the system under test, but, unlike measurements based upon truly random noise, the excitation does not contribute to this randomness [2].

Zuomin and Chu [12] presented the following empirical formula for estimating the number of averages to be used for any given S/N ratio and accuracy:

$$N = \left(\frac{3.12e^{-0.18(S/N)}}{\Delta p} \right)^{1.23} \quad (4.9)$$

where Δp is the desired accuracy in dB.

The MLS measurement technique can still be improved by using digitally pre-emphasised signals. When measuring with spectrally white maximum-length signals, the result is always influenced by linear distortion of components that are within the measuring path but are not the subject of investigation. Equalising the signal to include exactly the inverse transfer characteristics of the transmission path without the device under test may be necessary in high precision measurements, as for loudspeaker responses for instance [7]. Coloured MLS can also be used to mimic the background noise spectrum and, therefore, improve S/N ratio [13].

The background noise in the laboratory where the transmission loss measurements would be carried out was investigated so as to decide the number of averages to adopt. The system used throughout this work, MLSSA (see section 4.3.1), can perform the synchronous average before or after the FHT is performed, because the process is linear. Pre-averages are limited up to 16 samples but it can be increased by averaging the resulting impulse response.

For the same power output of the loudspeaker, (S/N) was calculated for 1 sample and 16 pre-

averages, presented in Figure 4.4. The lowest ratio for averaged result is around 40 dB and for all measurements throughout this work 16 pre-averages was adopted.

4.2.3 Order of the Sequence

Although the room response is not of interest for the transmission loss measurements performed in this work, nevertheless the impulse response of the room must be taken into account when performing measurements. If the room response has not decayed sufficiently over one sequence period, the “tail” of its impulse response will overlap in the subsequent periods, causing what is called “time aliasing” [1]. Some guidelines relating the sequence length t_{MLS} and reverberation time T are found in the literature, such as $t_{MLS} = (1/3) T$ [14] and $t_{MLS} \geq (1/2) T$ [15].

Reverberation time measurements, shown in Chapter 3, gave a maximum less than 4 seconds in the receiving room. A MLS of 16th order was chosen. According to section 4.2, the sequence length was $L = 2^m - 1 = 65,535$, which at a sampling rate of 14.98 kHz (see section 4.3.3), gives 4.374 seconds. The order, and therefore the length, was used throughout this work.

4.3 MEASUREMENT METHOD

The impulse response technique is not new to the field of acoustics [16] and the various applications of impulse methods are briefly reviewed in section 4.3.4.

Raes introduced the terms “space insulation” and “time insulation” [16]. In the standard method [17] of measurement the space around the test element is insulated such that flanking transmission is negligible in terms of the energy transmitted directly through the test element. In time insulation the direct component of a short duration signal, which travels through the test element is isolated, in time, from those components that travel around the element. This is the principle of the impulse response technique.

Raes used two microphones, one on the source side and the other on the receiver side. An oscilloscope was used to obtain the amplitude of a short duration pure tone pulse from a loudspeaker and the transmission loss obtained from the expression:

$$TL = 20 \log\left(\frac{L_1}{L_2}\right) + k \quad (4.10)$$

where L_1 and L_2 are the amplitude readings at the source and receiver positions from an oscilloscope and k is a constant taking into account the calibration of the instruments and the reflection coefficient of the sample.

Raes had problems with inadequate signal to background noise ratios and limitations on the duration of the test signal due to the response time of the one third octave filters [18] but was able to investigate the relationship between steady state and transient transmission loss measurements [19]. A fundamental limitation to his approach, developed before the advent of Fourier analysis techniques, results from a conflict in the requirements of time versus frequency resolution. In order to give good frequency resolution, a sinusoidal wave train must be of great (theoretically infinite) duration. In order to locate in time and thence window a sinusoidal wave train, it must be of very small duration; however this will be at the expense of good frequency resolution. This limitation, which can be viewed as a form of Heisenberg uncertainty principle, is circumvented practically by Fourier analysis techniques.

Louden [20] used a single-pulse source and Fourier analysis techniques in measurements of freely suspended thin panels. A repeated pulse from a loudspeaker on one side of the test panel was captured by a microphone on the other side and a photograph obtained from an oscilloscope screen. The panel was then removed without altering the measurement set-up geometry and the measurement was repeated. Fourier analysis of both photographed traces yielded the transmission loss from the expression:

$$TL = 20 \log\left(\frac{H}{k}\right) + c \quad (4.11)$$

where H is the amplitude of the pulse component with no test panel, k is the amplitude of the pulse component with the panel present and c is the attenuate reading. The method showed agreement with mass law prediction although, as with the work of Raes, adequate signal to background noise ratios were difficult to maintain. The results were also for normal incidence only.

Both De Tricaud [21] and Roland [22] used pistol shots as the impulse sound source. De Tricaud performed field measurements of airborne sound insulation where the sound pressure level in both the source and receiver rooms due to pistol shot is recorded via sound level meters situated at the room centres. The signals were then replayed through one octave filters and the intensities in each room evaluated from

$$I_{1,2} = \int_0^T p^2(t) dt \quad (4.12)$$

where p is the pressure and T is the integration time for the pressure signal, typically one second, and depends on the source and receiver room characteristics. The sound insulation was then found in dB(A) for each octave in the range 125-4000 Hz by

$$R = 10 \log \left(\frac{I_1}{I_2} \right) \quad (4.13)$$

An analogue integrator attached to each sound level meter was used to quickly determine equation (4.13). Results gave good agreement with those obtained by standard methods.

In 1983 Guilhout and Gely [26] used a digital acquisition system and mini-computer to capture and analyse transmitted signals. A pistol was again used as the signal source but was unable to produce repeated identical signals for time averaging purposes. Instead the transmission losses calculated from each shot had to be averaged, resulting in what was then a time consuming procedure. In addition, tape recording of the signal for later analysis was necessary requiring more time and imposing limitations due to dynamic range of the recorder.

It is important to note that in general the use of pistol shots gives long time signals, and measurements of the test panels by such methods include room characteristics and internal reflections within the panel. The impulse technique proper is able to exclude these effects by windowing them out. Thus the pistol source is impulsive but it is not an impulse technique.

The impulse method proper was used by Davies and Mulholland [23] to measure normal impedance of porous materials. Their system employed an event recorder with input filter, A/D

converter, digital storage, and output via a D/A converter. The data in the event recorder was analysed into its Fourier components by interfacing directly with a digital computer and using a Fourier transform program. Davies and Gibbs [24] applied the impulse technique to oblique incidence measurements of transmission loss, employing a digital event recorder. The work, was similar to that of Loudon, but used a more sophisticated acquisition system, giving greater frequency resolution and enhanced signal to noise by averaging the repeated captured transient signal. The repeated signal was thus reinforced whilst the random background noise averaged to zero. The measurements were carried out on free standing perspex panels at normal and oblique incidence. Results were repeatable and agreement with theory was good, clearly indicating the coincidence dips at oblique angles.

With the increase in microprocessor technology such dedicated instrumentation as Fast Fourier analysers became common and Balilah and Gibbs [25,27] continued the work and applied the method to sound transmission and directivity of holes [28]. Again, good agreement with theory was obtained and the method was investigated in diagnosing acoustic failure in walls due to cracks. Problems arose in measurement of double panel constructions due to poor signal to noise [29]. Two unbridged panels gave over 80 dB above 2 kHz and were not measurable. However, measurements and simple theory for the same panels having a single tie beam showed reasonable agreement due to a much reduced and hence more easily obtained transmission loss.

Lyons [30] investigated solid and open building elements using a pulse signal generator and FFT analyser. From the measurement of a solid thin screen he concluded that the inclusion of the edge reflection component yielded a dip in insertion loss which was coincident-like but angle and frequency invariant. Exclusion of edge reflections allowed the contribution of the thin panel material to be identified. In the case of stiffened panels, due to additional internal reflections, it proved difficult but not impossible to obtain the unstiffened panel response. Open and freestanding screens were measured including the diffracted component of the time history. Measurement of thin panels gave good agreement with theoretical diffraction theory. Also, impulse response measurements for double picket screens gave values in close agreement with standard methods for normal incidence.

Zuomin and Chu [12] performed noise reduction measurements in laboratory with injected

background noise to simulate in-situ conditions. MLS excitation was first equalised so as to match the generated background noise spectrum, and measurements were performed for a flat (S/N) of -9.9 dB(A). With tolerance of 0.2 dB for sound pressure levels an estimate of the number of averages required to reduce the influence of noise was calculated according to equation (4.9). The results showed good agreement with conventional method. A procedure for field measurement was suggested. Continuing the investigation on sound transmission by impulse response in noisy environment Chu [31] found that the increase in (S/N) was not in agreement with expression shown here (equation (4.7)). It is suggested that MLS method provides a S/N enhancement of $10 \log (L/4)$ instead.

The work reported in this thesis involves applying the impulse method to assess sound insulation of an open screen. The method was also applied to obtain reflection factor. With the latter, field performance can be predicted without any measurement involving special facilities or acoustical conditions. The practicalities of impulse methods were explored.

Evaluation of sound insulation involves the digital acquisition of the room impulse response (and instrumentation) and the isolation of the direct component from other reflected and scattered components using time-of-flight methods and windowing. The captured time signal is Fourier transformed to the frequency domain giving the power spectrum. The power spectra with and without the element in position are used to obtain the transmission loss of the element. The main difficulties lie in determining the appropriate part of the time signal to window upon. On the other hand, many difficulties are naturally overcome by the fact that any systematic error in the measurement is cancelled when the differences between transmitted and direct sound are considered.

It should be emphasised that although the technique consists of measurements performed with and without the partition under test, it is not the insertion loss that is obtained, as defined in Chapter 2. So long as the direct component is isolated from the rest of the response time history, then the partition insulation characteristics only are obtained, independently of any environment conditions. Unlike any other measurement, such as the standard method [17] for instance, the impulse response analysis is independent of the measurement site and the transmission loss coefficient is obtained directly without any correction for room conditions.

4.3.1 Instrumentation

MLS methods offer advantages when compared with other techniques. For example, in FFT methods, the transfer function is often measured with random white-noise excitation and statistical computational methods [9]. Because of the random nature of the excitation, long measurement times are required to reduce random effects. Such statistical methods require that both the system input and output are measured simultaneously, whereas with MLS, because the stimulus is deterministic and repeatable, only a single acquisition channel is required. The commercial software Maximum-Length Sequence System Analyzer (MLSSA) was used throughout this work for data generation, acquisition and analysis, installed in a 486 PC with single channel input and output. Figure 4.15 presents the instrumentation used throughout this work for the impulse measurements.

A 16th order MLS, with 65,535 samples length and 4.374 s duration, was generated with an output amplitude of ± 0.4922 volts (variable). The clock frequency of the MLS generator is synchronised with the clock frequency of the A/D converter on the receiving side. The sequence was fed through a Quad 50E power amplifier and into a loudspeaker.

The power spectrum of the reference signal should, preferably, be as flat as possible. The flatter the spectrum the sharper the impulse shape, which in turn, increases the interval between components in the time history, easing the windowing process. As transmission loss coefficient and reflection factor are obtained from relative measurements the effect of an imperfect loudspeaker response is cancelled. A 50mm diameter Jordan Watt moving-coil loudspeaker unit was fitted facing out a wooden cubic box of 150mm side so that sound energy being radiated backwards would not cause destructive interference.

The acoustical signal was measured with an 1/2" Brüel & Kjær 4155 condenser microphone and a Brüel & Kjær 2231 sound level meter. Data was acquired, after one sequence lapsed time, at a sampling rate of 14.98 kHz (66.75 μ sec) at 12-bit resolution and passed through a Chebyshev antialiasing filter. The response was displayed in the time domain and by visual inspection a window was applied upon the desired component. A FFT routine generated the corresponding spectrum with a resolution of 14.63 Hz.

4.3.2 Temporal Window

The impulse under analysis, direct or transmitted, is extracted from the time history by a rectangular window, which is the best option for transient signals that can be contained within the time window [32]. The window function in the time domain has a zero value everywhere except over the interval $-T/2$ to $T/2$ where it has unit amplitude. The rectangular window was used throughout this research except for the reflection factor measurements, presented in Chapter 8, where it is shown that when the impulses are not easily separable, a different window is recommended.

If the desired component of the response signal time history has decayed to noise before the first room reflection arrives at the microphone, then the impulse is conveniently separated from that of the room by setting to zero all values beyond the sampling point set just before the first reflection. A premature termination of the window results in loss of low frequency information as it is in the “tail” of the impulse that resides most of the information about low frequency [33]. In general, where an impulse had no clear termination the end window was set at a point of zero value and zero slope.

4.3.3 Sources of Errors in MLS Analysis

Effects of nonlinearities are hardly noticeable in building acoustics measurements. According to Vorländer [10], weak nonlinearities can be tolerated and they appear as an apparent noise floor, typically at -40 dB, in the impulse response. Nonlinearity can be detected by checking whether the gain in S/N ratio by averaging is limited to a constant value. Reducing the signal level and accordingly increasing the number of averages or choice of a higher MLS order solves the problem. The order of the m-sequence is described in section 4.2.3.

Time variances can occur if extremely long MLS periods are used. If the time invariance assumption stated in section 4.1 is violated it can introduce change in amplitude, frequency, and phase. Whilst amplitude and frequency shifts are hardly likely to occur in building acoustics measurements, phase shift may take place caused by changes such as slow heating of a loudspeaker voice coil, air currents in a room, noise in the trigger or sampling circuits, or by

moving objects, which all normally cause a uniformly spread noiselike random fluctuation in the periodic impulse response [34]. Relative small changes in the sound speed and/or a change in temperature interfere with the averaging process.

A rule of thumb for the maximum permissible temperature drift $\Delta\vartheta$ (in K, equal distribution) in reverberation time measurements [10] is given by:

$$\Delta\vartheta \leq \frac{300}{fT} \quad (4.14)$$

where f is the midband frequency in Hz and T the reverberation time in s.

In outdoor measurements, the error in free-field sound pressure level ΔL in dB, caused either by a change in temperature or in wind speed is given by [10]:

$$\Delta L = k \cdot 10^{-9} (\sigma f d)^2 \quad (4.15)$$

where σ is either the temperature standard deviation in K (normal distribution) and k equals -1.1, or the wind speed standard deviation in m/s, when k takes the value of -3.2; d is measurement distance in meters and f the midband frequency.

Chu [35] investigated time variance over SPL and reverberation time measurements. The effect of air movement, rotating vane, temperature and tape recording were investigated. Temperature fluctuation was found to be the most influential parameter, as significant changes in average impulse response were produced by a change of 0.2° C.

In all measurements in this work the temperature variation in the room was monitored and observed not to exceed 0.1° C. For an impulse averaged over 16 samples, with the first sample skipped, the measurements took approximately 1.15 minutes; therefore not long enough for any significant change in temperature to take place.

4.3.4 Other Applications

The basic measurement results from MLS systems are impulse responses. All other quantities or functions must be derived from the impulse responses by subsequent transformations.

The pioneer in the use of impulse response in acoustical measurements was Schroeder [36] who later used MLS [37]. He showed that the ensemble average of the squared sound pressure decay $\langle p^2(t) \rangle$, at any point in a room is equal to the integral over the squared impulse response $h^2(\tau)$ of that point in the room as given by the following equation:

$$\langle p^2(t) \rangle = G \int_0^{\infty} h^2(\tau) d\tau \quad (4.16)$$

where G is proportional to the power of the source. When interrupted white noise excitation is used, the ensemble average requires a large number of measurements. By contrast, the right-hand side of equation (4.16) requires only a single measurement of the impulse response. A comparison of decay measurements using equation (4.16) and the decay-curve averaging method has been given by Chu [15]. More research on room acoustics can be found in [38,39,40,41].

A completely new edition of an old ISO standard of 1975 [42] has been developed in which, in addition to the reverberation time as the predominant indicator of the acoustical properties of a room, several other parameters and types of measurements are standardised. They are Sound Strength, Early Decay Time, Definition, Clarity, Centre Time, and early lateral energy ratios.

An investigation [43] into the influence of several sources of error on the above quoted room acoustical parameters showed that if measurements are performed according to the standard the overall uncertainty is of the same magnitude, or a little higher, than subjectively perceivable changes in these parameters. The impulse response measurements were highly reproducible, regardless of being measured by different teams and equipment.

Impulse response analysis have been used in assessing speech intelligibility [44], barrier attenuation [45], muffler characteristics [46], headphones [47,48], loudspeaker response [49, 33], and even to measure the maturity of fruits [50]. Relevant references on measurement of absorption and

impedance can be found in Chapter 8.

4.4 REFERENCES

- [1] Vorländer M., *Applications of Maximum Length Sequences in Acoustics*, Proc. I Simpósio Brasileiro em Metrologia Acústica e Vibrações, 35-43, (1996).
- [2] Borish J. and Angell J.B., *An Efficient Algorithm for Measuring the Impulse Response Using Pseudorandom Noise*, J. Audio Eng. Soc., **31**(7), 478-488, (1983).
- [3] Schroeder M.R., *Number Theory in Science and Communication*. Part IX, 2nd. ed., Springer, New York, (1990).
- [4] MacWilliams F.J. and Sloane N.J.A., *Pseudo-Random Sequences and Arrays*, Proc. IEEE, **64**, 1715-1729, (1976).
- [5] Nelson E.D. and Fredman M.L., *Hadamard Spectroscopy*, J. Opt. Soc. Am., **60**, 1664-1669, (1970).
- [6] Harwit M. and Sloane J.A., *Hadamard Transform Optics*, Academic Press, New York, (1979).
- [7] Mommertz E. and Müller S., *Measuring Impulse Responses with Digitally Pre-Emphasized Pseudorandom Noise Derived from Maximum-Length Sequences*, Appl. Acoustics, **44**, 195-214, (1995).
- [8] Kuttruff H., *Room Acoustics*, 3rd edition, chapter VIII, Elsevier Applied Science, London, (1991).
- [9] Rife D.D. and Vanderkooy J., *Transfer-Function Measurement with Maximum-Length Sequences*, J. Audio Eng. Soc., **37**(6), 419-444, (1989).
- [10] Vorländer M. and Kob M., *Practical Aspects of MLS Measurements in Building Acoustics*, Appl. Acoustics, **52**(3/4), 239-258, (1997).
- [12] Zuomin W. and Chu W.T., *Ensemble Average Requirement for Acoustical Measurements in Noisy Environment Using the M-Sequence Correlation Technique*, J. Acoust. Soc. Am., **94**(3), Pt.1, (1993).
- [13] Borish J., *An Efficient Algorithm for Generating Colored Noise Using a Pseudorandom Sequence*, J. Audio Eng. Soc., **33**(3), 141-144, (1985).
- [14] Maximum-Length Sequence System Analyzer (MLSSA) Manual, Version 9.0, DRA Laboratories.

- [15] Chu W.T., *Comparison of Reverberation Measurements Using Schroeder's Impulse Method and Decay-Curve Averaging Method*, J. Acoust. Soc. Am., **63**, 1444-1450, (1978).
- [16] Raes A.C., *A Tentative Method for the Measurement of Sound Transmission Losses in Unfinished Buildings*, J. Acoust. Soc. Am., **27**(1), 98-102, (1955).
- [17] ISO 140. *Methods of Measurement of Sound Insulation in Buildings and of Building Elements*. Part 1 to 12 (Revision 1994/1995).
- [18] Burd A.N., *The Measurement of Sound Insulation in the Presence of Flanking Paths*, J. Sound Vib., **7**(1), 13-26, (1968).
- [19] Raes A.C., *Static and Dynamic Transmission Losses of Partitions*, J. Acoust. Soc. Am., **35**(8), 1178-1182, (1963).
- [20] Louden M.M., *The Single-Pulse Method for Measuring the Transmission Characteristics of Acoustic Systems*, Acustica, **25**, 167-172, (1971).
- [21] Tricaud P.De, *Impulse Techniques for the Simplification of Insulation Measurement Between Dwellings*, Appl. Acoustics, **8**, 245-256, (1975).
- [22] Roland J., *Airborne Isolation Measurements by Impulse Technique*, Noise Control Eng., **16**(1), 6-14, (1981).
- [23] Davies J.C. and Mullholland K.A., *An Impulse Method of Measuring Normal Impedance at Oblique Impedance*, J. Sound Vib., **67**(1), 135-149, (1979).
- [24] Davies J.C and Gibbs B.M., *The Oblique Incidence Measurement of Transmission Loss by an Impulse Method*, J. Sound Vib., **74**(3), 381-393, (1981).
- [25] Balilah Y.A. and Gibbs B.M., *The Measurement of Transmission Loss of Single Leaf Walls and Panels by an Impulse Method*, J. Sound Vib., **123**(2), 229-245, (1988).
- [26] Guilhout J.P. and Gely D., *Transmission Loss Measurements of Transmission Loss by an Impulse Method*, J. Sound Vib., **74**(3), 381-393, (1981).
- [27] Balilah Y.A., *The Use of Impulse Techniques in the Measurement of Sound Insulation in Buildings*, Ph.D. Thesis, University of Liverpool, (1987).
- [28] Gibbs B.M. and Balilah Y.A., *The Measurement of Sound Transmission and Directivity of Holes by an Impulse Method*, J. Sound Vib., **133**(1), 151-162, (1989).
- [29] Gibbs B.M. and Balilah Y.A., *Measurement of Transmission Loss and Diagnosis of Acoustic Failure in Walls by an Impulse Method*, Proc. InterNoise 89, 617-620, (1989).
- [30] Lyons R., *Building Elements of Low Sound Insertion Loss*, Ph.D. Thesis, University of Liverpool, (1993).

- [31] Chu W.T., *Application of the M-Sequence Correlation Technique for Sound Transmission Measurements*, Proc. InterNoise 94, 1479-1484, (1994).
- [32] Randall R.B., *Frequency Analysis*, Brüel & Kjær, Chapter 5, (1987).
- [33] Fincham L.R., *Refinements in the Impulse Testing of Loudspeakers*, J. Audio Eng. Soc., **33**(3), 133-140, (1985).
- [34] Vanderkooy J., *Aspects of MLS Measuring Systems*, J. Audio Eng. Soc., **42**(4), 219-231, (1994).
- [35] Chu W.T., *Time-Variance Effect on the Application of the M-Sequence Correlation Method for Room Acoustical Measurements*, Proc. 15th ICA, 25-38, (1995).
- [36] Schroeder M.R., *New Method of Measuring Reverberation Time*, J. Acoust. Soc. Am., **37**, 409-412, (1965).
- [37] Schroeder M.R., *Integrated-Impulse Method Measuring Sound Decay without Using Impulses*, J. Acoust. Soc. Am., **66**(2), 497-500, (1979).
- [38] Vorländer M. and Bietz H., *Comparison of Methods for Measuring Reverberation Time*, Acustica, **80**, 205-215, (1994).
- [39] Barron M., *Impulse Response Testing Techniques for Auditoria*, Appl. Acoustics, **27**, 165-181, (1984).
- [40] Bodlund K., *On the Use of the Integrated Impulse Response Method for Laboratory Reverberation Measurements*, J. Sound Vib., **56**(3), 341-362, (1978).
- [41] Chu W.T., *Impulse-Response and Reverberation-Decay Measurements Made by Using PseudoRandom Sequence*, Appl. Acoustics, **29**, 193-205, (1990).
- [42] ISO 3382:1997, *Measurement of the Reverberation Time of Rooms with Reference to Other Room Acoustical Parameters*.
- [43] Lundeby A. et al, *Uncertainties of Measurements in Room Acoustics*, Acustica, **81**, 344-355, (1995).
- [44] Rife D.D., *Modulation Transfer Function Measurement with Maximum-Length Sequences*, J. Audio Eng. Soc., **40**(10), 779-790, (1992).
- [45] Papadopoulos A.I. and Don C.G., *A Study of Barrier Attenuation by Using Acoustic Impulses*, J. Acoust. Soc. Am., **90**(2), Pt.1, 1011-1018, (1991)
- [46] Singh R. and Katra T., *Development of an Impulse Technique for Measurement of Muffler Characteristics*, J. Sound Vib., **56**(2), 279-298, (1978).
- [47] Vorländer M., *Impulse Measurements of Headphones on Ear Simulators and on Head and*

- Torso Simulators*, *Acustica*, **76**, 66-72, (1992).
- [48] Vorländer M., *Impulse Measurement Technique for Headphones*, Proc. 9th FASE Symposium and 10th Hungarian Conference on Acoustics, (1991).
- [49] Berman J.M. and Fincham L.R., *The Application of Digital Techniques to the Measurement of Loudspeakers*, *J. Audio Eng. Soc.*, **25**(6), 370-384, (1977).
- [50] Duprat F. et al, *The Acoustic Impulse Response Method for Measuring the Overall Firmness of Fruit*, *J. Agric. Eng. Res.*, **66**(4), 251-259, (1997).

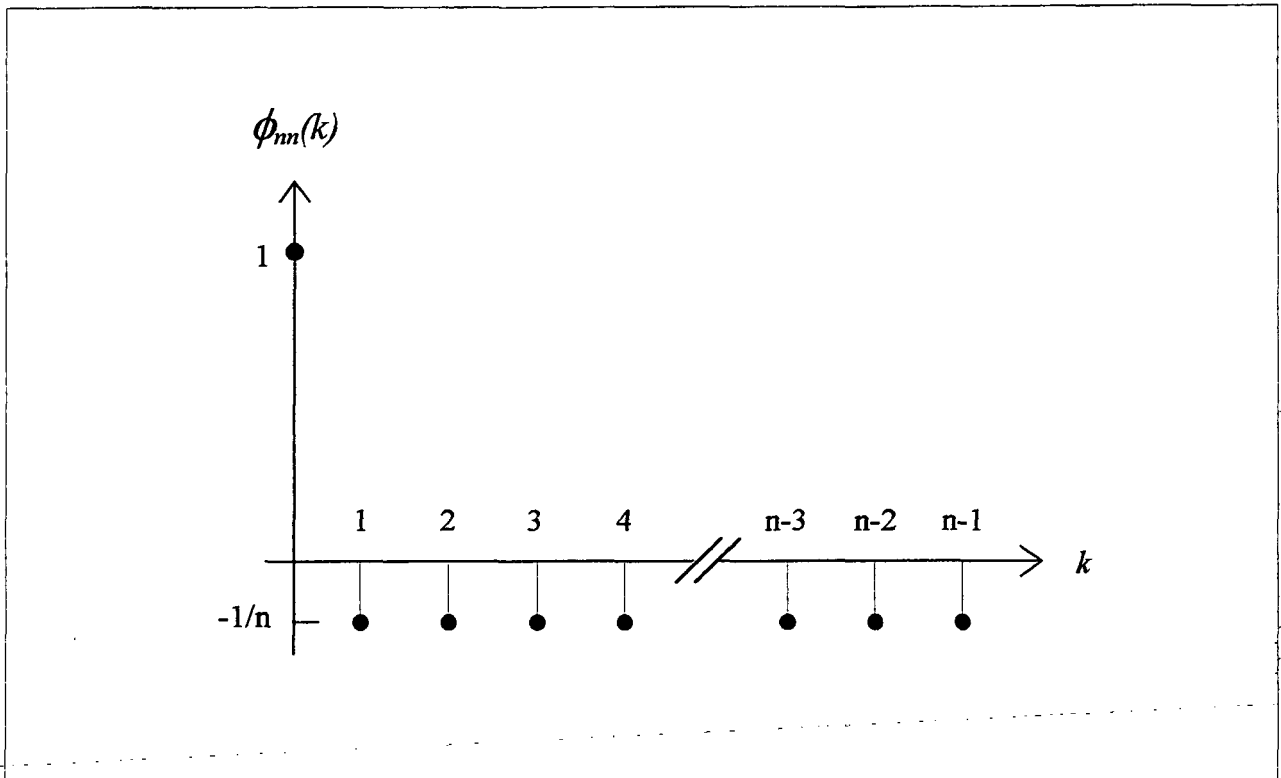


FIGURE 4.1 - Autocorrelation function of a maximum-length sequence with length n [2].

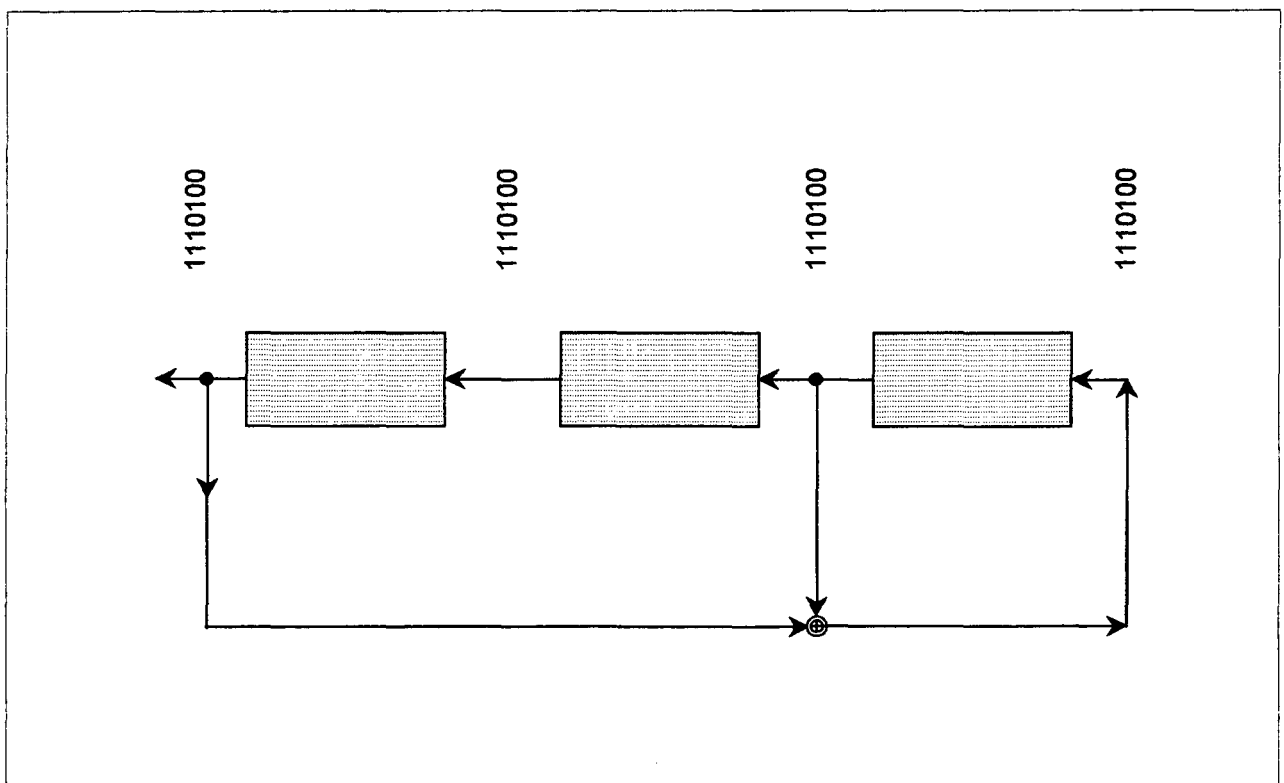


FIGURE 4.2 - Binary feedback shift register of length $m = 3$ for generating a maximum-length sequences of length $n = 7$.

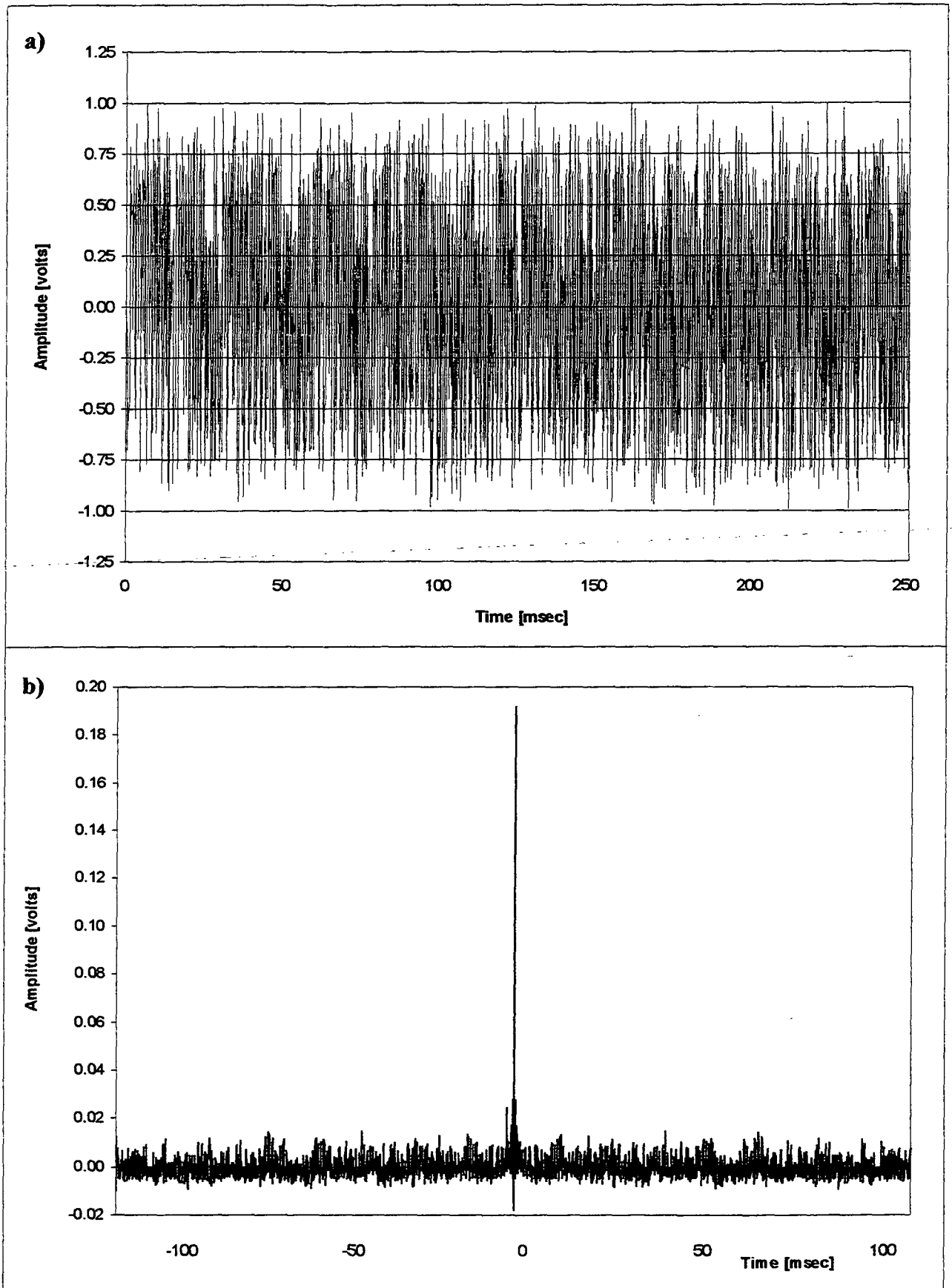


FIGURE 4.3 - a) One period of a maximum-length sequence of order 15 and b) two periods of the autocorrelation function.

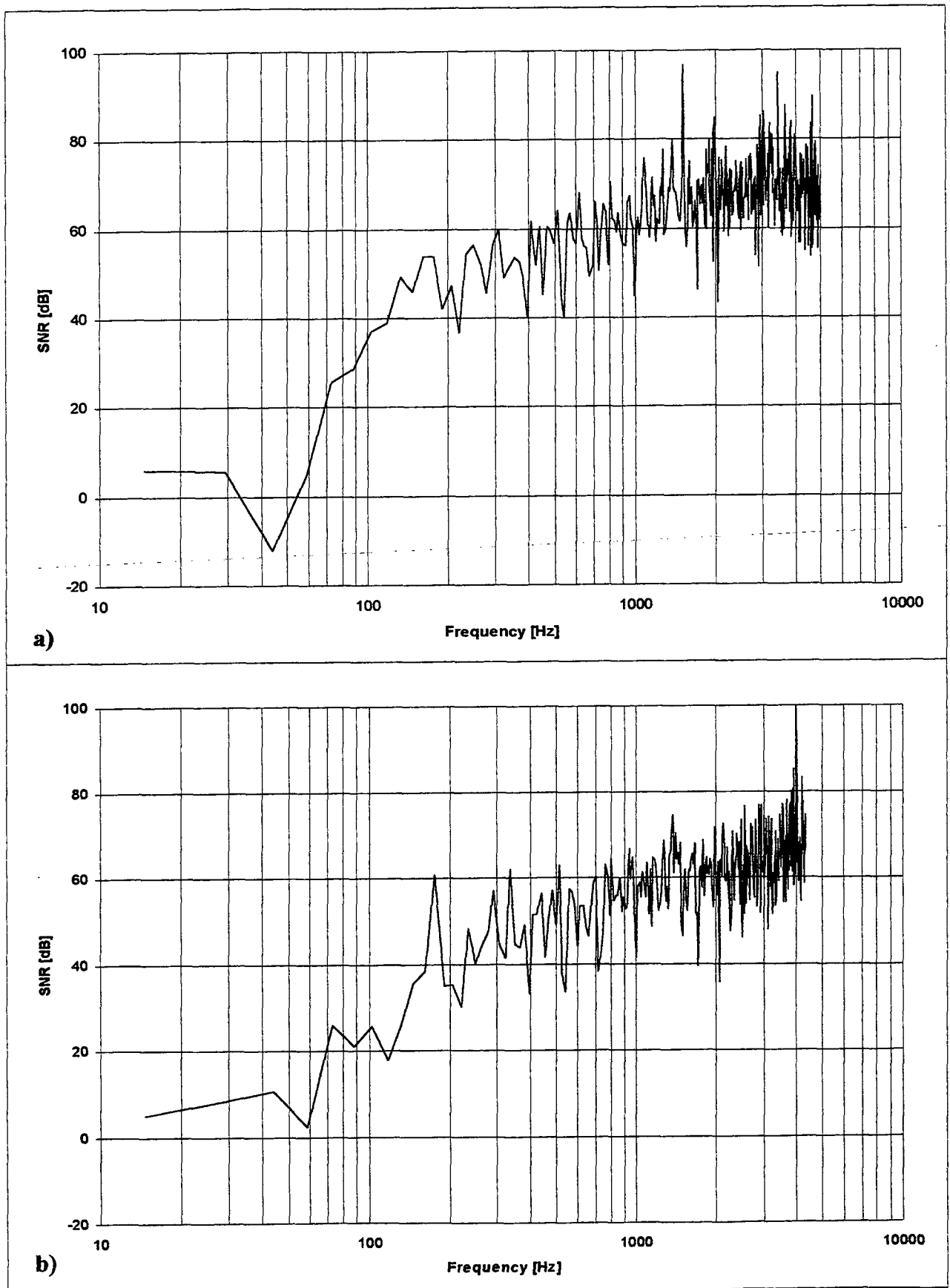


FIGURE 4.4 - S/N power ratio in the laboratory room for a) 1 sample and b) average over 16 samples.

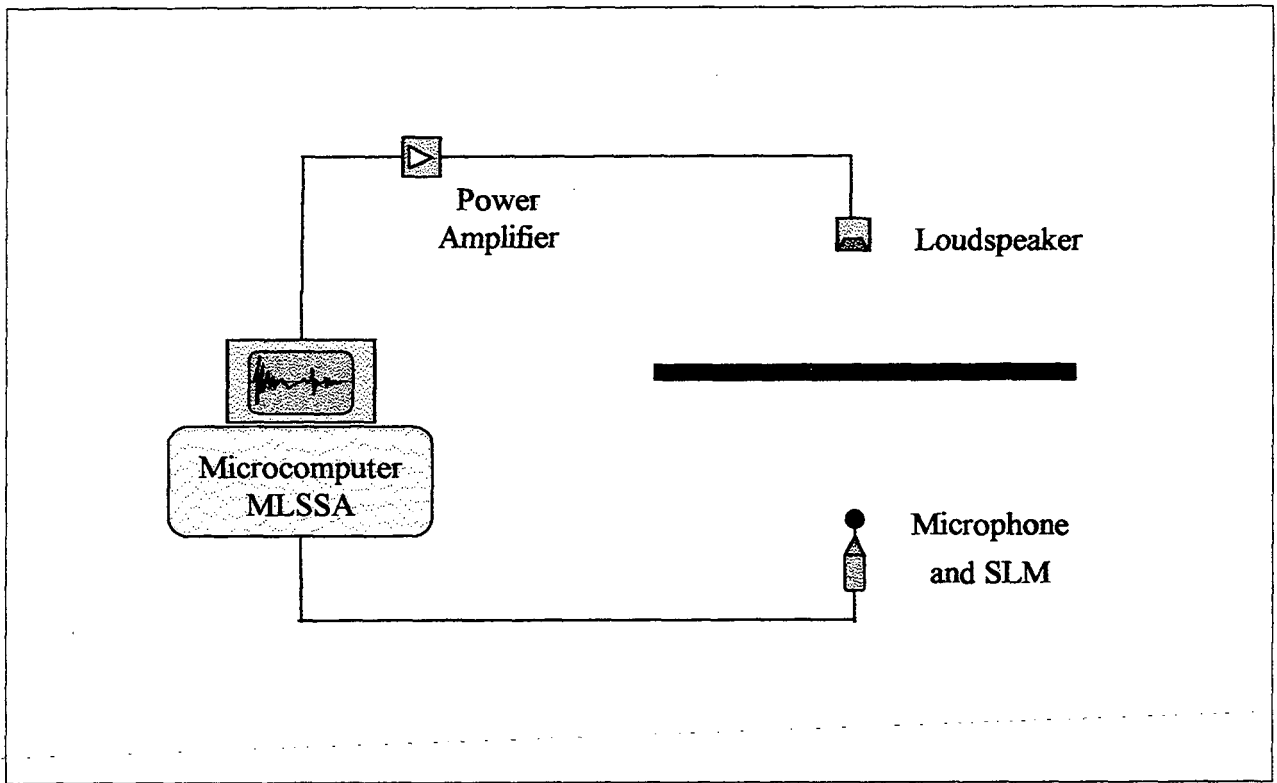


FIGURE 4.5 - Impulse response method instrumentation.

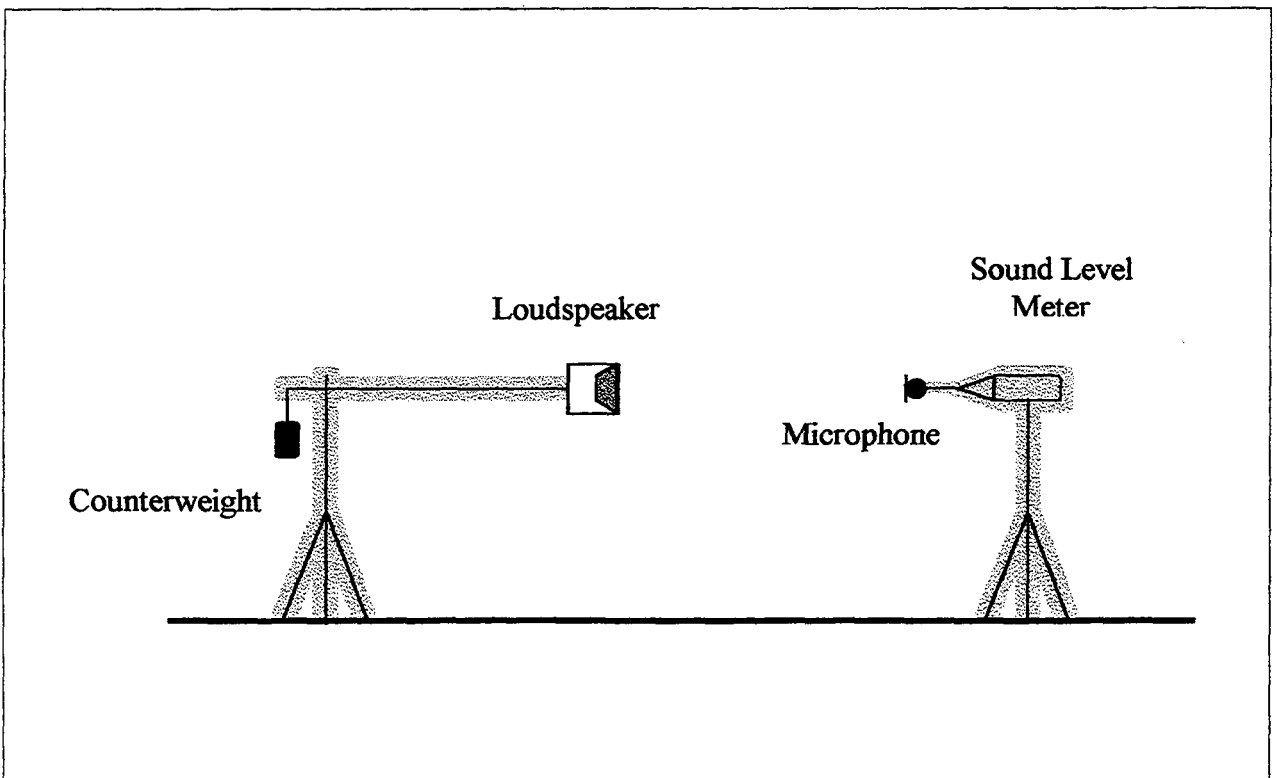


FIGURE 4.6 - Schematically set-up showing absorption material (foam) around equipment.

CHAPTER 5 TRANSMISSION LOSS BY IMPULSE RESPONSE

- 5.1 **Introduction**
- 5.2 **Preliminary Investigation of a Solid Screen**
- 5.3 **Transmission Loss at Different Frequency Regions**
- 5.4 **Comparison to Other Methods**
- 5.5 **References**

5.1 INTRODUCTION

The previous chapter has presented the theory and practical aspects of impulse response analysis, including the measurement method and chosen parameters for measuring transmission loss. In this chapter, preliminary investigations on solid screens and the measurements of the louvre for various incident angles are presented.

Impulse response analysis has been explained in Chapter 4, but is simply re-stated. The method requires the isolation in the time domain of the direct component from others reflected, scattered and/or diffracted so as to get the infinite response of the partition. By means of a rectangular time window and subsequent Fourier transformation, the attenuation offered by the partition is obtained from the comparison with a reference signal, which is the signal in free-field conditions. The instrumentation used was that presented in Figures 4.5 and 4.6.

As presented in section 4.3.2, one of the main aspects of impulse response analysis is the correct setting of the time window. The longer the window the wider (downwards) the frequency range of analysis, as the lowest frequency at which results are reliable is given by $(1/T_w)$, where T_w is the window length. Also, if a window is terminated after the impulse but late enough to include other components, for instance surface reflections, there will be a distortion on the spectrum, as shown in Figure 5.1. On the other hand, an earlier termination by the window results in the spectrum of Figure 5.2, where there is loss of low frequency information.

Infinite panels response, which includes in the time window the direct component only, or finite response, which includes the effect of discontinuities such as the free edges or fixings, are assessed independently of the surrounding acoustic conditions. The former is important since it identifies the contributions of the material, the latter is important since it corresponds to the partition performance in-situ. This is particularly important to the case of barriers for instance.

5.2 PRELIMINARY INVESTIGATION OF A SOLID SCREEN

The use of impulse response analysis in the evaluation of sound insulation of isotropic homogeneous panels has already been proved successful. Louden [1] showed agreement of

normal incidence measurements with mass law and the associated 6 dB per octave slope on freely suspended and lightly supported panels. Davies and Gibbs [2] found good agreement with mass law for perspex panels at normal incidence. At oblique incidence the coincidence dips at the expected frequencies were clearly indicated, though their depth was less than expected. Later work [3,4] was directed towards a better understanding of the impulse method and again showed good agreement with theory for normal and oblique incidence. Spatial averaging was employed to improve results for less homogeneous and thicker structures such as brick walls.

Lyons [5] investigated thin solid panels with different stiffness provided by external bracing. The finite and infinite panel response for the various elements was obtained, though for a large number of stiffeners it was found difficult to window correctly. In this situation, spatial averaging were applied and showed that unwanted components generated by reflections from the elements can be “averaged out”, giving an insertion loss which was close to that of the unstiffened panel.

The preliminary experiment involved the measurement of the transmission loss for normal incidence of an aluminium panel of 2.23 m x 1.78 m and 0.003 m thickness, freely standing on a hard floor. The panel had a surface density of 8.1 kg/m², and loudspeaker and microphone were positioned 0.7 m and 0.3 m away from the partition, respectively.

5.2.1 Normal Incidence

A typical time history of the reference signal is presented in Figure 5.3, which shows the direct impulse and the first room reflection. When the partition is in the transmission path the resulting time history is shown in Figure 5.4. The transmission loss of a partition of infinite dimension is obtained by windowing the direct component, which begins at the same time but will be slightly lengthened and strongly reduced in amplitude.

The experimental data were compared to the theoretical mass law prediction, valid below the critical frequency, given by [6]:

$$TL \approx 10 \log \left[1 + \left(\frac{\omega \rho_s \cos \theta}{2 \rho_0 c} \right)^2 \right] \quad (5.1)$$

where ρ_0 and ρ_s are density of air and panel surface density, respectively, ω is frequency and θ the incident angle.

For normal incidence $\cos \theta = 1$ and equation (5.1) becomes the usual normal incidence mass law,

$$TL = 10 \log \left[1 + \left(\frac{\omega \rho_s}{2 \rho_0 c} \right)^2 \right] \quad (5.2)$$

The result obtained, seen in Figure 5.5, has a good agreement with theoretical prediction given by equation (5.2) down to 300 Hz. The low frequency discrepancy is believed to be due to the window length used. To avoid the early arrival of diffracted components and, therefore, have a longer time window the panel area should be slightly bigger. Nevertheless, due to the agreement achieved over the whole frequency range the method was considered validated.

The finite response of the panel is obtained by lengthening the time window so as to include the direct and the edge reflected component. This component was first noted by Davies and Gibbs [2] who observed that it appears in the time history between the direct and diffracted components and causes a dip in the frequency domain. It was concluded that the edge reflected component is generated by the spherical pressure waves that strike the panel at concentric points with increased time delay forcing bending waves in the panel at the same speed. The free bending waves generated at the edges then suffer multiple reflections with bending waves repeatedly travelling back across the centre and registered as a fluctuation in the sound pressure time history [2], as observed in Figure 5.4. Investigations on the edge reflected component can be found in [2,3,7]. The resulting transmission loss is shown in Figure 5.6 and gives the normal incidence finite panel response. It is presented along with the mass law prediction given by equation (5.2). The frequency response shows the typical effect when edge reflected component, referred to in the literature is included. The frequency dip was not observed since it is predicted to occur beyond the upper frequency of analysis.

5.2.2 Oblique Incidence

When a plane wave strikes a panel at an angle θ , it causes a trace wavelength, λ_t , on the panel

equal to $\lambda/\sin\theta$. If a free bending wave exists in the panel of wavelength λ_b , and equals the trace wavelength then at that frequency coincidence occurs [6]. For every angle of incidence θ there is a unique coincidence frequency and vice versa. The lower limiting frequency for coincidence, the critical frequency, f_c , occurs at grazing incidence, 90° , so that $\sin\theta = 1$ and $\lambda_b = \lambda_t = \lambda$. The wave speed of the plate bending wave, c_b , and the acoustic wave in the fluid, c , are then equal, giving:

$$f_c = \frac{c^2}{1.8h} \sqrt{\frac{\rho_p(1-\sigma^2)}{E}} \quad (5.3)$$

where ρ_p is the panel density, E is the Young modulus, h is the thickness, and Poisson's ratio, σ , is assumed to be 0.3 for most materials [8]. The equation is valid for bending wavelengths greater than six times the panel thickness, ($\lambda_b > 6h$). For coincidence above the critical frequency $\lambda_{bco} = \lambda_{cco} = \lambda_{co}/\sin\theta_{co}$, therefore:

$$f_c = \frac{f}{\sin^2 \theta_{co}} \quad (5.4)$$

Above the critical frequency the acoustic wave in the panel is termed supercritical, travelling faster than that in air.

In Figure 5.7 is the resultant transmission loss of the panel for 45° of incidence. With a Young's modulus of $71.6 \times 10^9 \text{ N/m}^2$, the predicted coincidence frequency from equation (5.4) is 7934 Hz. The observed dip occurs earlier, at approximately 4.5 kHz and may correspond with the effect of edge reflections rather than coincidence.

5.3 TRANSMISSION LOSS AT DIFFERENT FREQUENCY REGIONS

Research on open screens has been limited and has been reported on Chapter 3. The understanding of the mechanisms of sound transmission through devices such as louvres has a theoretical basis on the transmission through slits and apertures, which has been advanced by many authors [9,10,11,12]. Some thirty years ago approximate theories were offered by Gomperts [10], Wilson and Soroka [11] and Sauter and Soroka [12]. More practical approaches, by means of

Statistical Energy Analysis, were offered by Trochidis [13]. A detailed review of work up to 1967 can be found in the work of Mulholland and Parbrook [14] who compared several theories for the sound transmission through thin circular apertures.

Balilah [7] has also reviewed much of the work on the transmission loss of apertures up to 1985. In 1979 Tinti [15] investigated diffraction through a slit in a thick screen using numerical methods based on Green's function theory, and in 1985 Rosenhouse [16] gave a theoretical description of sound transmission through an aperture of arbitrary shape using a numerical methodology which combined Kirchhoff's integral and a so-called "Z-lines method". Oldham and Shen [17,18] have considered very large apertures in which they mathematically model the radiation pattern from rectangular openings. The results of measurements on a 1:20 scale model of a large aperture were compared with a simple theoretical model.

The first application of the impulse response method to the transmission loss of apertures appears to be that of Balilah [7], who compared measurements with the approximate solution for the diffraction of sound by a circular aperture according to Wilson and Soroka [11]. There was good agreement where measurements were taken with the microphone close to the aperture.

Slow-waveguide filters were incorporated into conventional barriers in the work of Nicolas and Daigle [19] and Amram et al [20]. The waveguide consisted of an open network of rigid plates with expansion chambers that retard the low frequency sound propagated by increasing the apparent density of the air surrounding the plates. The field at the receiver is the result of interference between the field diffracted over the top of the barrier and the propagated through the waveguide. For a certain frequency the system could be tuned by adjusting the geometry of the waveguide to produce an 180° phase lag between the diffracted and retarded sound waves at the receiver and hence maximum attenuation [20]. However, this is at the expense of a reduction in attenuation at other frequencies due to constructive interference. In general, these screens are most useful in attenuating noise with dominant low frequency tones.

Tanoiku and Konishi [21] calculated the noise reduction of a slit type barrier using the line integral method. They showed that, for a 3% slit opening, there was negligible difference in performance in the far field when compared with normal barriers. However, as a louvre, 3% open area

provides insufficient ventilation and would result in high pressure drops across the louvre.

Wassilieff [22] also considered the attenuation by a regular slit screen or picket barrier. Comparisons of measurements with optical diffraction and mass-layer models showed that careful selection of gap width could provide significant improvement at low frequencies when compared with solid barriers. Again, destructive interference and improved insertion loss is accompanied by constructive interference at other frequencies with reduce performance.

5.3.1 Mechanisms of Attenuation

Low insertion loss elements are not only found as part of building façades but very often are present as part of an acoustic device for the noise control from building services and industrial equipment.

Maybe due to the lack of research, commercially available louvres follow a standard design: an infill of sound absorption material enclosed by an upper layer of solid metallic sheet and a perforated sheet underside, seen in detail in Plate 2. The blades, which are enlarged schematically in Figure 5.8, are equally spaced along the axis of the louvre and typically at an angle by 45° . Sound passing through the “channel” formed by each pair of blades is absorbed in a manner analogous to a parallel baffle. Thus the assumption was that the mechanism involved in louvre attenuation process could be simply stated as:

- i) Acoustical energy is reflected back to the source room due to an impedance change in the medium, mainly offered by the mass of the blades.
- ii) Destructive interference generated by the periodic pattern of blades and gaps, which can be interpreted as secondary sound sources.
- iii) Losses that occur when the sound waves travel with high absorption coefficient material at the boundary of the transmission path, through the louvre gaps.

All the above effects are frequency dependent. With the impulse response measurements presented next, their role in the insulation performance of the louvre was investigated and is discussed in Chapter 6. The louvre was measured for nine incident angles as indicated in Figure 5.9.

5.3.2 Frequency Dependency

Figure 5.11 presents the resulting transmission loss for the measured incident angles. At low frequency (below 1 kHz), louvre performance is nearly independent of the incident angle and a mass effect can be identified, as described in section 5.3.1.

Above 1 kHz, the performance is characterised by fluctuations about plateaux due to destructive and constructive interference from the different transmission paths through the separate slits.

5.3.3 Angular Dependency

At mid and high frequencies the interference is a function of louvre periodicity, incident angle and wavelength and is shown in Figure 5.11. The directional characteristics of the louvre are shown in Figure 5.12, where transmission loss is plotted against incident angle in third octave bands. It is observed that at low frequencies transmission loss is nearly angle independent and increases with increased frequency. Above 1.6 kHz, transmission loss is a function of incident angle, decreasing with increased angle.

Although dependent on the incident angle, Figure 5.13 shows that the path parallel to the blade pitch (in this case at 45°) strongly influences the overall performance.

5.4 COMPARISON TO OTHER METHODS

Figure 5.14 shows the angle average impulse response, along with intensity and pressure measurements presented in Chapter 3. As anticipated, intensity and impulse methods have a better agreement apart from the very low frequency, where impulse measurements also have some limitations. The results confirm that the standard method overestimates the screen performance.

On the other hand, the impulse measurements display fluctuations at high frequencies. It is suggested that these fluctuations would be eliminated or reduced if measurements were repeated and averaged for different source to receiver distances, thereby, yielding results independent of set-up geometry. In Figure 5.15 is seen the difference between the two set of measurements.

5.5 REFERENCES

- [1] Louden M.M., *The Single-Pulse Method for Measuring the Transmission Loss of Acoustic Systems*, *Acustica*, **25**, 167-172, (1971).
- [2] Davies J.C. and Gibbs B.M., *The Oblique Incidence Measurement of Transmission Loss by an Impulse Method*, *J. Sound Vib.*, **74**(3), 381-393, (1981).
- [3] Balilah Y.A. and Gibbs B.M., *The Measurement of Transmission Loss of Single Leaf Walls and Panels by an Impulse Method*, *J. Sound Vib.*, **123**(2), 229-245, (1988).
- [4] Gibbs B.M. and Balilah Y.A., *Measurement of Transmission Loss and Diagnosis of Acoustic Failure in Walls by an Impulse Method*, *Proc. InterNoise 1989*, 617-620.
- [5] Lyons R., *Building Elements of Low Sound Insertion Loss*, Ph.D. Thesis, University of Liverpool, (1993).
- [6] Cremer L., Heckl M. and Ungar E.E., *Structure-Borne Sound: Structural Vibrations and Sound Radiation at Audio Frequencies*, Springer-Verlag, 2nd. Edition, (1973).
- [7] Balilah Y.A., *The Use of Impulse Techniques in the Measurement of Sound Insulation in Buildings*, Ph.D. Thesis, University of Liverpool, (1987).
- [8] Kinsler L.E., Frey A.R., Coppens A.B. and Saunders J.V., *Fundamentals of Acoustics*, 3rd. edition, (1982).
- [9] Bouwkamp C.J., *On the Transmission of a Circular Aperture*, *Physic. Rev.*, **75**, p 608, (1949).
- [10] Gomperts M.C., *The Sound Insulation of Circular and Slit Shaped Apertures*, *Acustica*, **14**(1), 1-16, (1964).
- [11] Wilson G.P. and Soroka W.W., *Approximation to the Diffraction of Sound by a Circular Aperture in a Rigid Wall of Finite Thickness*, *J. Acoust. Soc. Am.*, **37**(2), 286-297, (1965).
- [12] Sauter A.Jr. and Soroka W.W., *Sound Transmission Through Rectangular Slots of Finite Depth Between Reverberant Rooms*, *J. Acoust. Soc. Am.*, **47**(1), 5-11, (1970).
- [13] Trochidis and Papanikolaou, *Sound Transmission Through Slits and Circular Apertures*, *Archives of Acoustics*, **9**(3), 317-326.
- [14] Mulholland K.A. and Parbrook H.D., *Transmission of Sound Through Apertures of Negligible Thickness*, *J. Sound Vib.*, **5**(3), 499-508, (1967).
- [15] Tinti S., *Diffraction by a Thick Slitted Screen*, *J. Acoust. Soc. Am.*, **65**(4), 888-895, (1979).
- [16] Rosenhouse G., *A Hole Spoils a Wall - Acoustics Analysis of Sound Transmission Through*

- Slits by the Theory of Diffraction*, *Acustica*, **58**(4), 181-195, (1985).
- [17] Oldham D.J., *The Directivity of Sound Radiated from a Large Aperture*, *Acoustics Letters*, **2**, 1-5, (1978).
- [18] Oldham D.J. and Shen Y., *A Scale Model Investigation of Sound Radiation from a Large Aperture in a Building*, *Appl. Acoustics*, **15**, 397-409, (1982).
- [19] Nicolas J. and Daigle G.A., *Experimental Study of a Slow-Waveguide Barrier on Finite Impedance Ground*, *J. Acoust. Soc. Am.*, **80**(3), 869-876, (1986).
- [20] Amram M. and Tartas R., *Improved Transformer Noise Control with a Tuned Interference Device*, *Proc. InterNoise 1988*, 1495-1498.
- [21] Tanioku Y., Konishi K. and Maekawa Z., *Noise Reduction of a Slit-Type Barrier by Using Line Integral Method and Full Scale Model Measurement*, *Proc. InterNoise 1987*, 395-398.
- [22] Wassilief C., *Improving the Noise Reduction of Picket Barriers*, *J. Acoust. Soc. Am.*, **84**(2), 645-650, (1988).

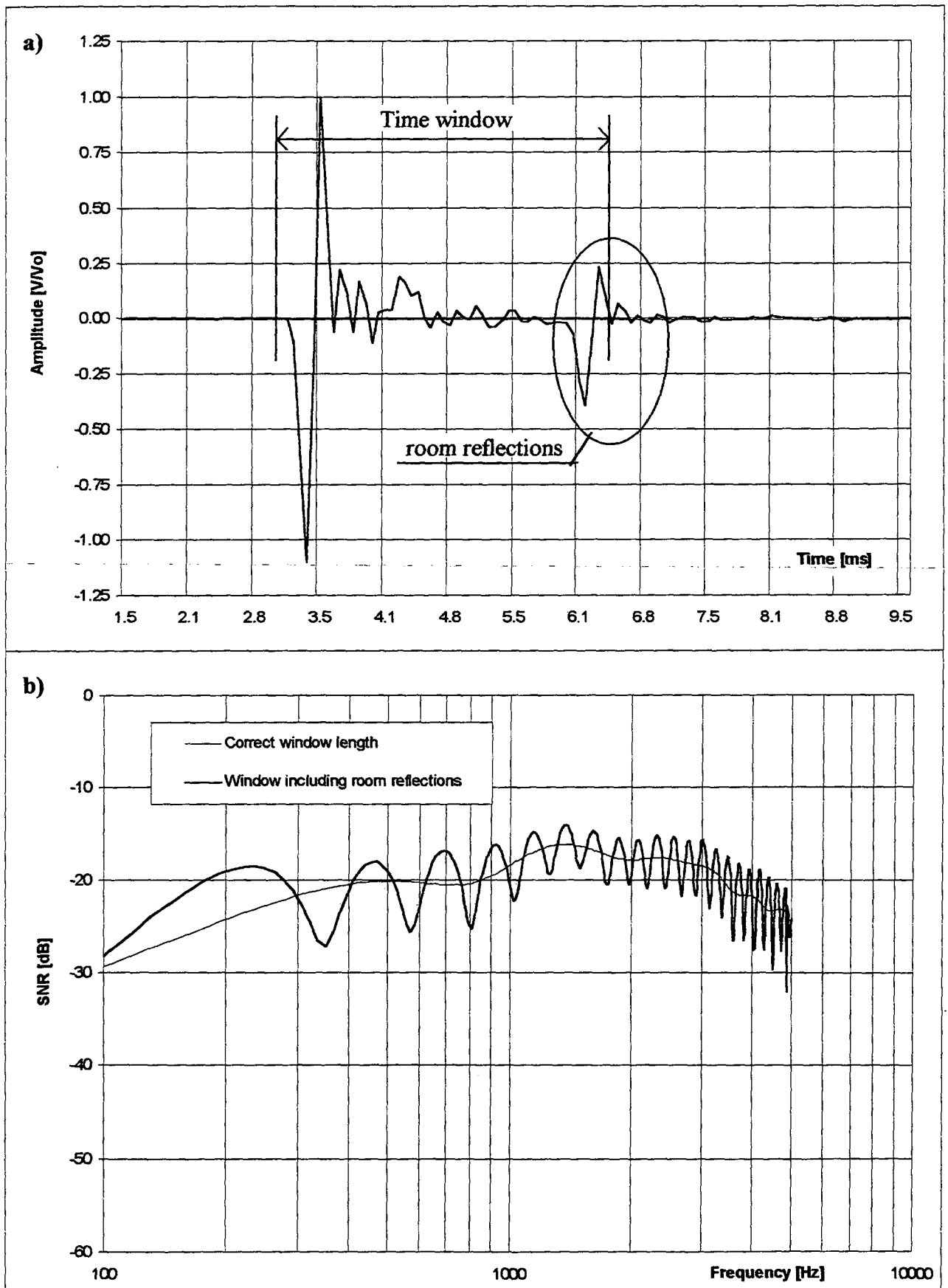


FIGURE 5.1 - a) Time history showing a time window where room reflections were included; b) Spectra for window as set in a), and the correct spectra.

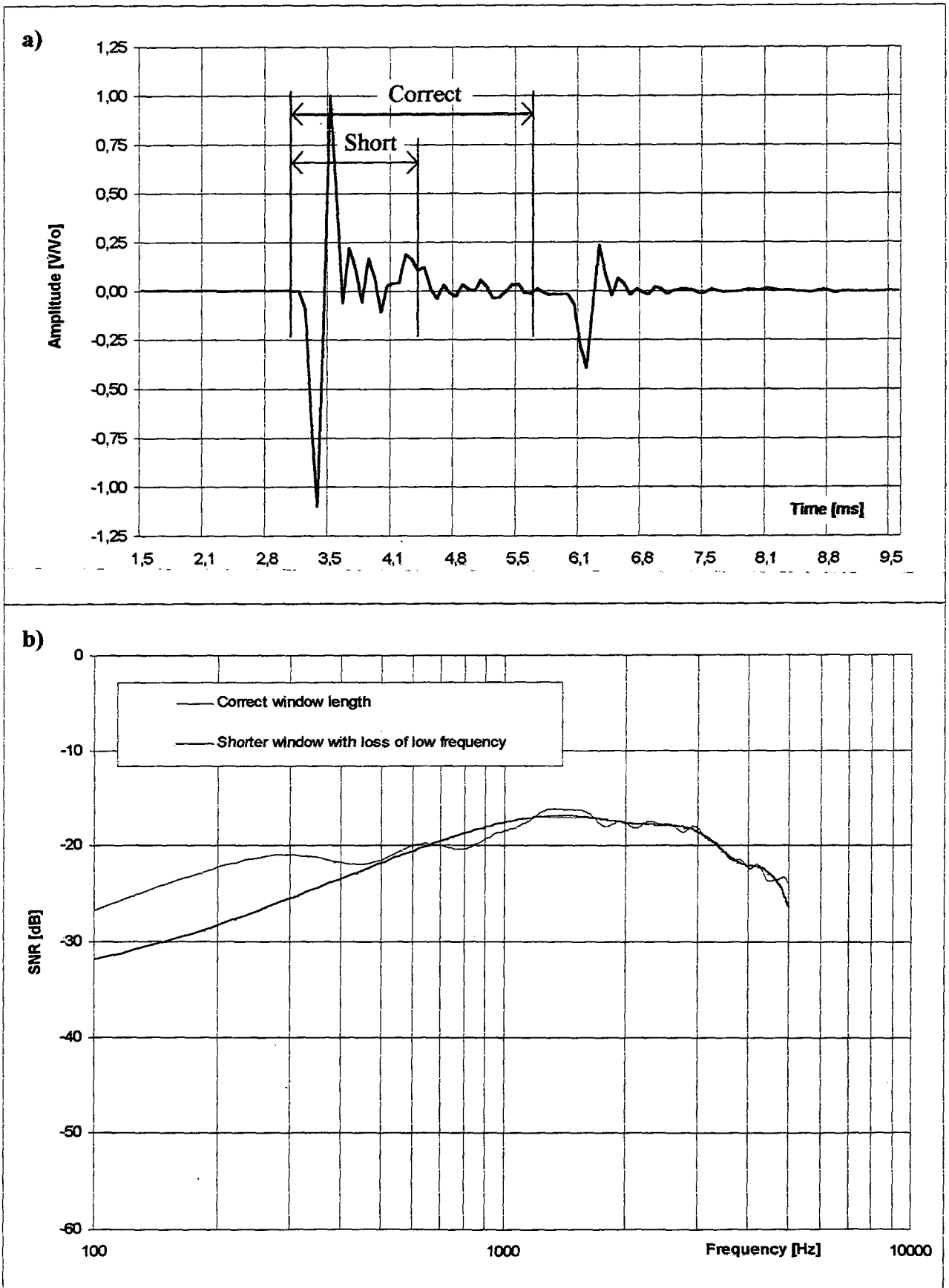


FIGURE 5.2 - a) Time history showing different length of time windows; b) spectra for window as set in a) indicating a loss of low frequency information and the correct spectra.

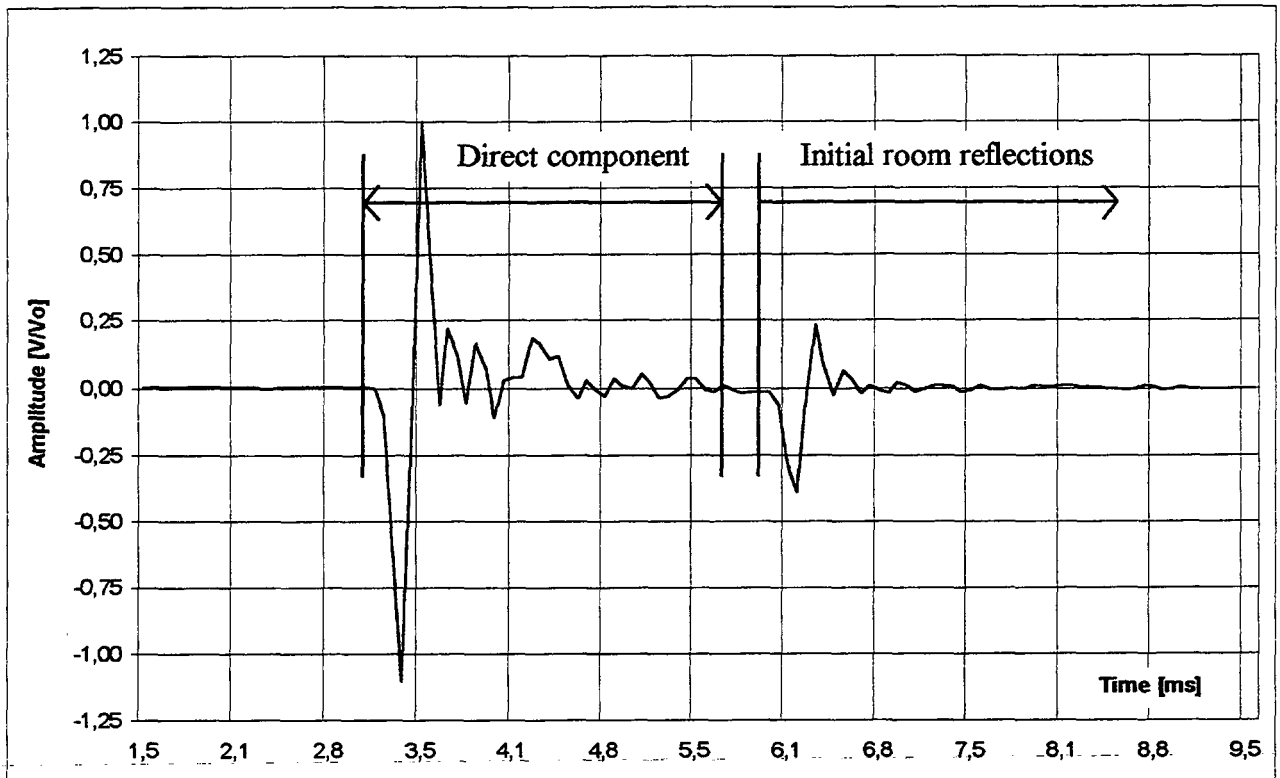


FIGURE 5.3 - Typical time history for impulse response of reference signal.

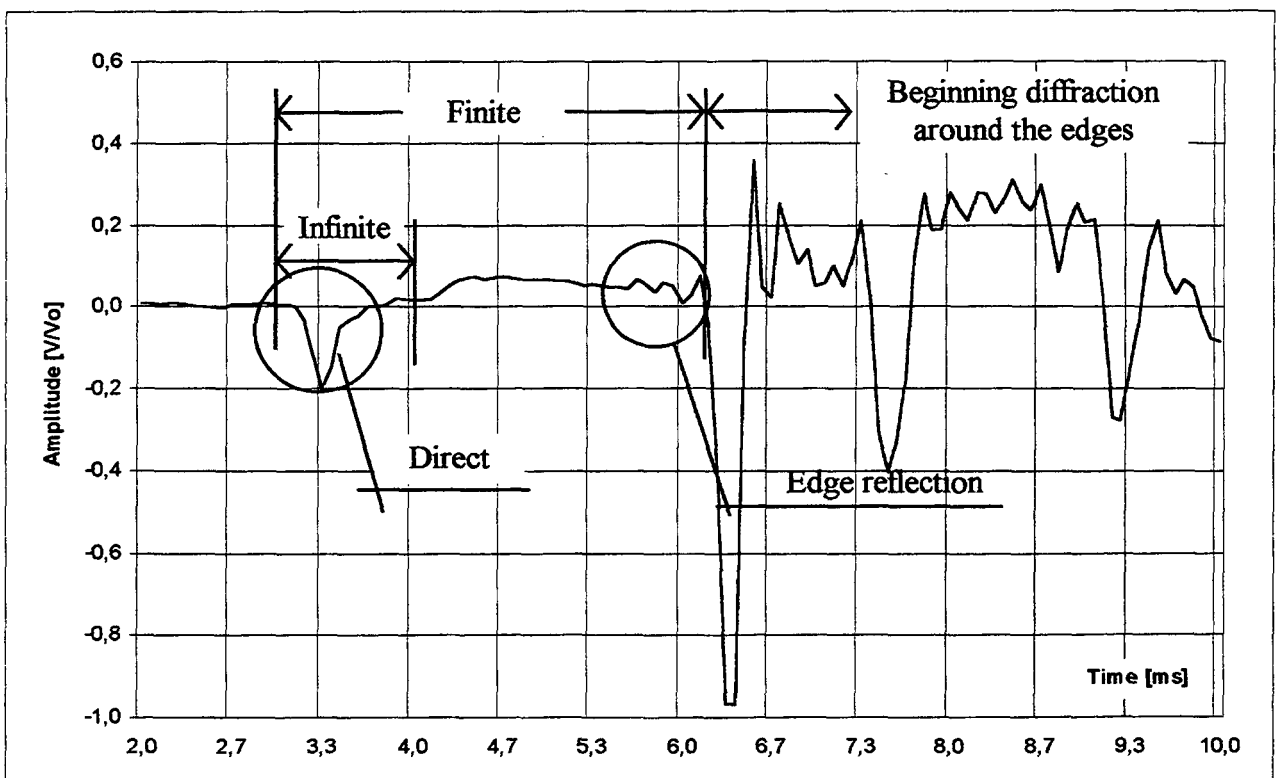


FIGURE 5.4 - Time history for impulse response of transmitted signal for normal incidence.

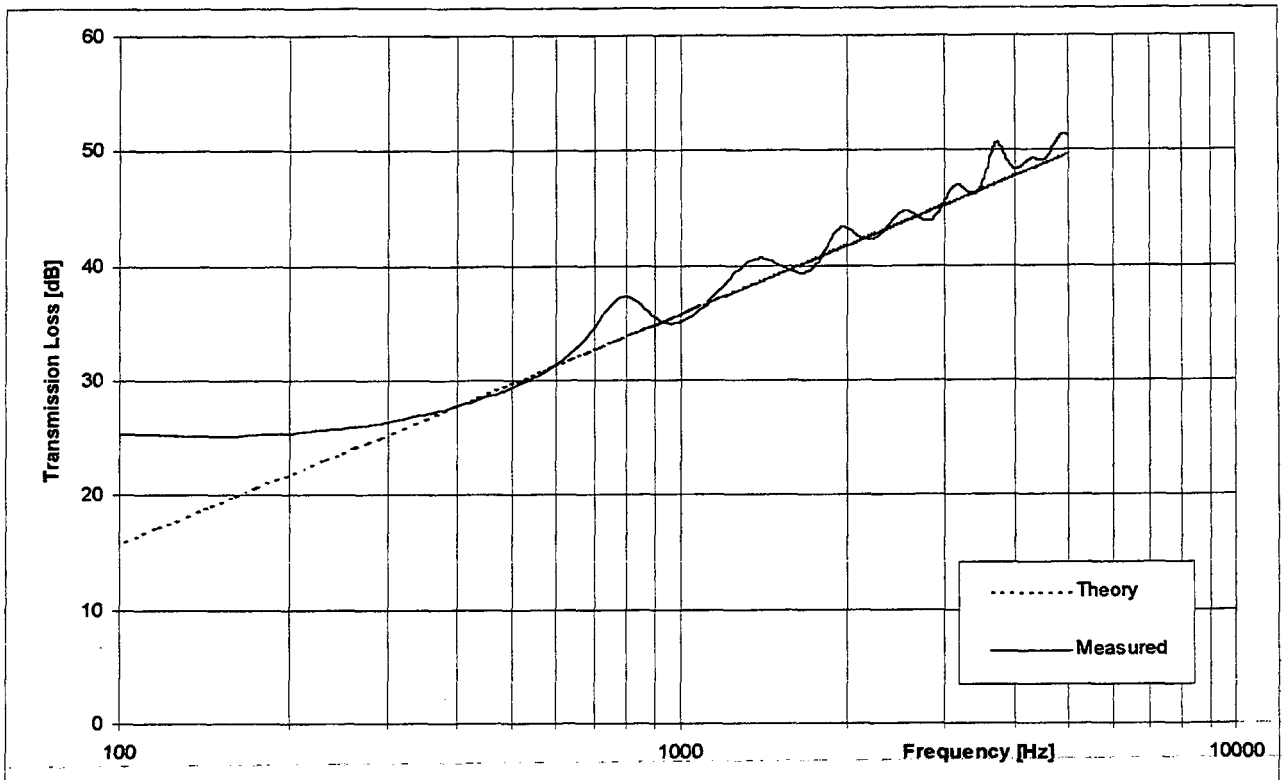


FIGURE 5.5 - Infinite response of an aluminium panel measured at normal incidence.

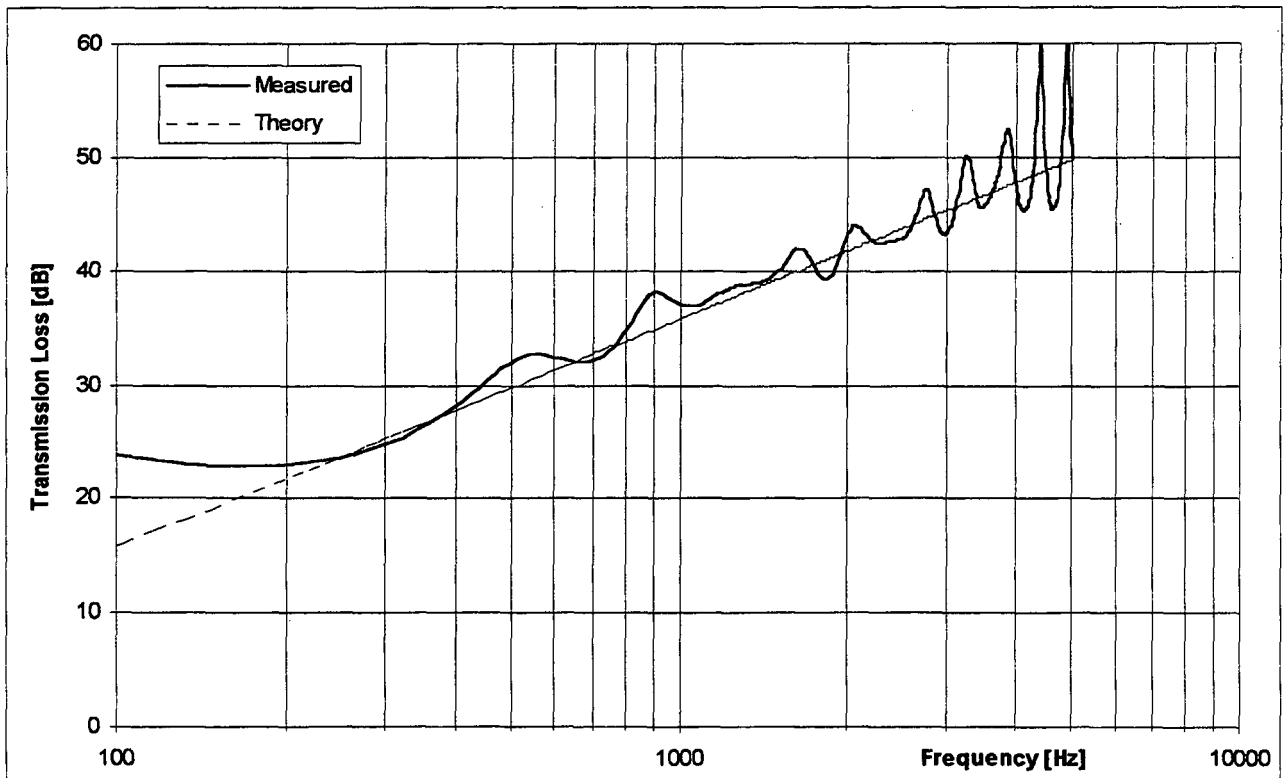


FIGURE 5.6 - Finite response of an aluminium panel measured at normal incidence.

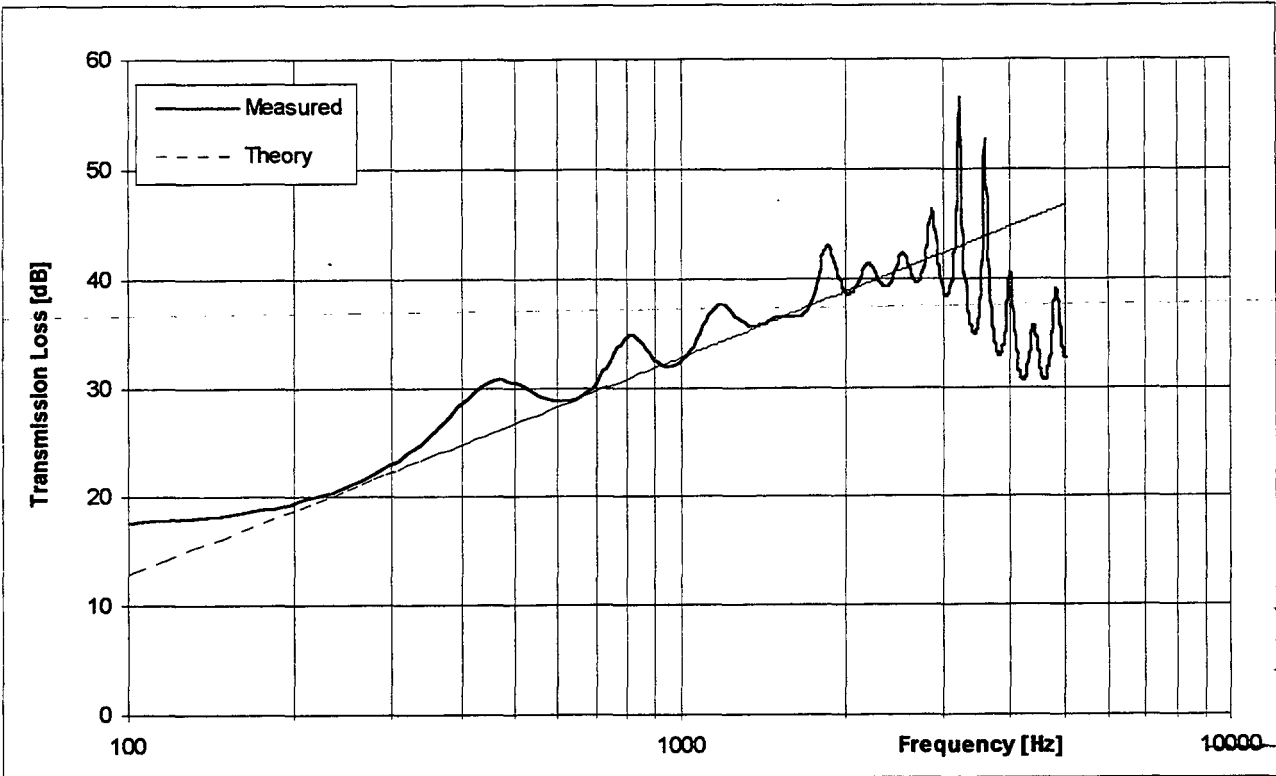


FIGURE 5.7 - Transmission loss of the aluminium panel for 45° of incidence.

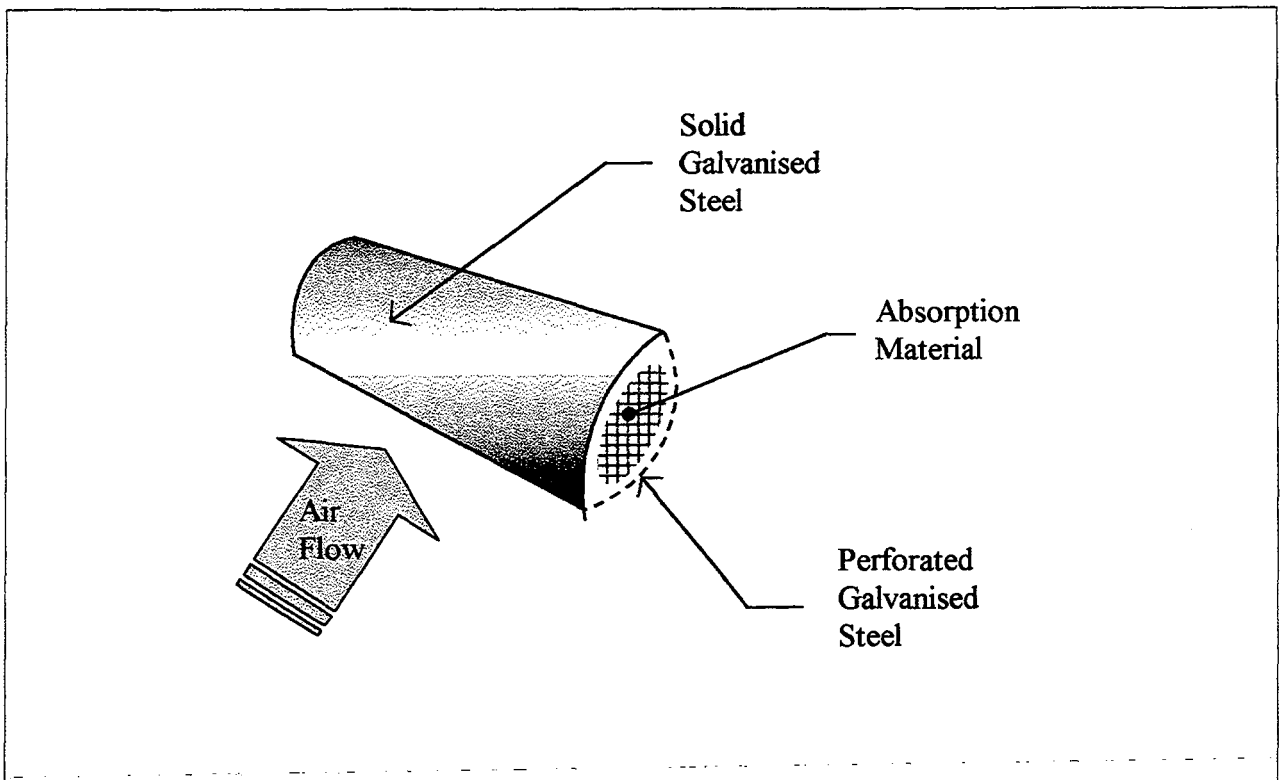


FIGURE 5.8 - Detail of the blade of the louvre.

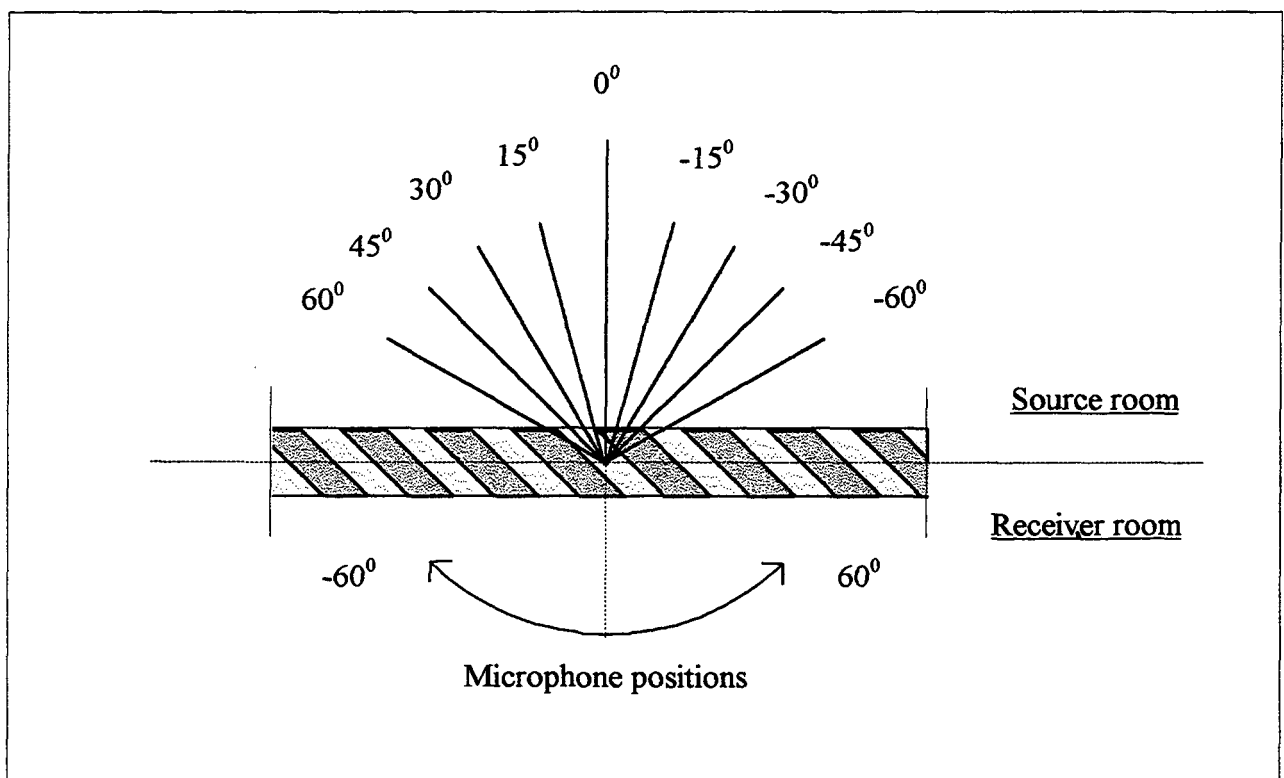


FIGURE 5.9 - Measured incident angles for the louvre performance analysis.

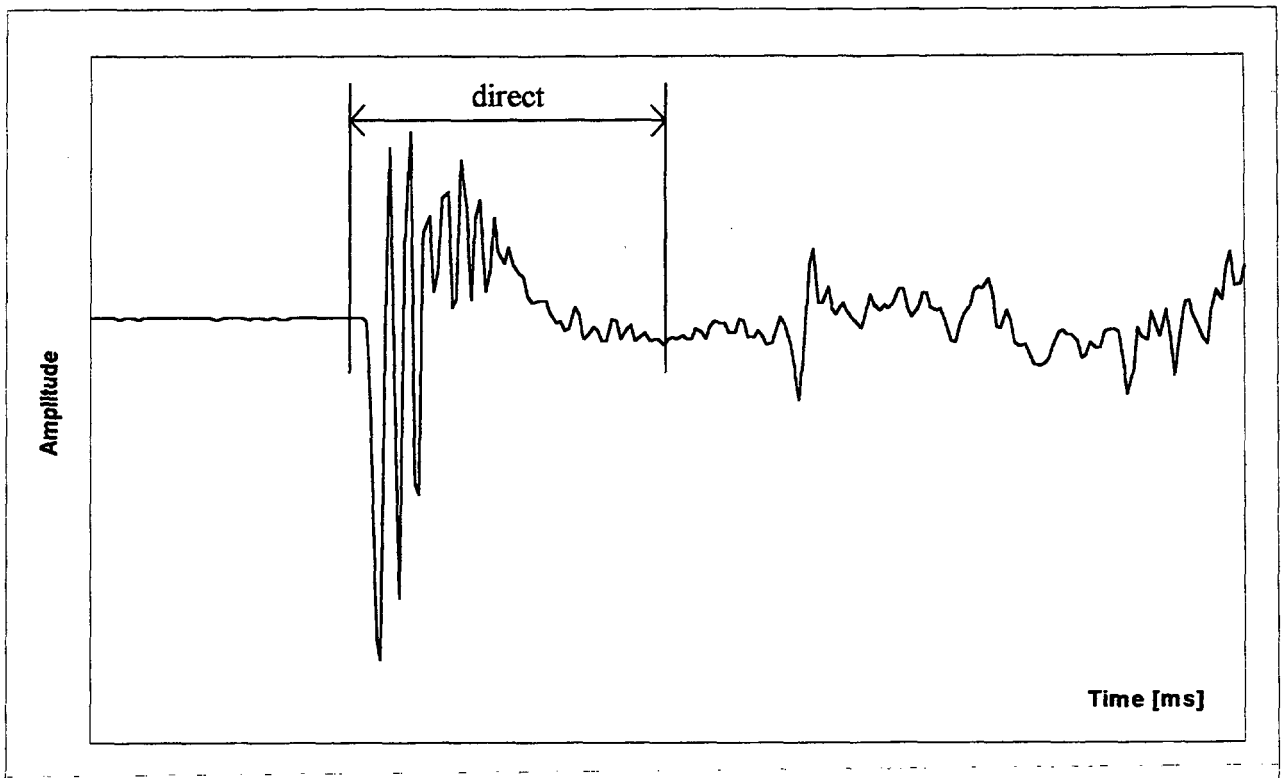


FIGURE 5.10 - Typical time history of the transmitted signal through the louvre.

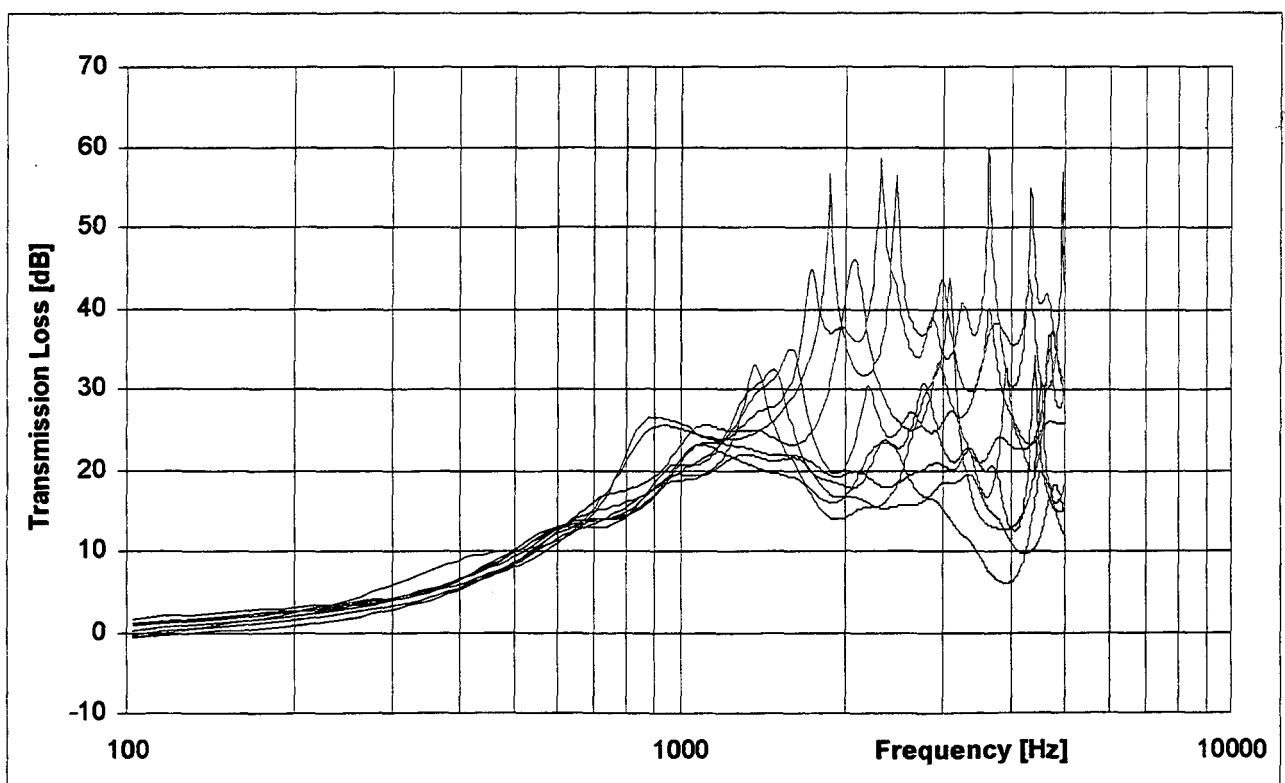


FIGURE 5.11 - Transmission loss of the louvre by impulse response for 9 incident angles.

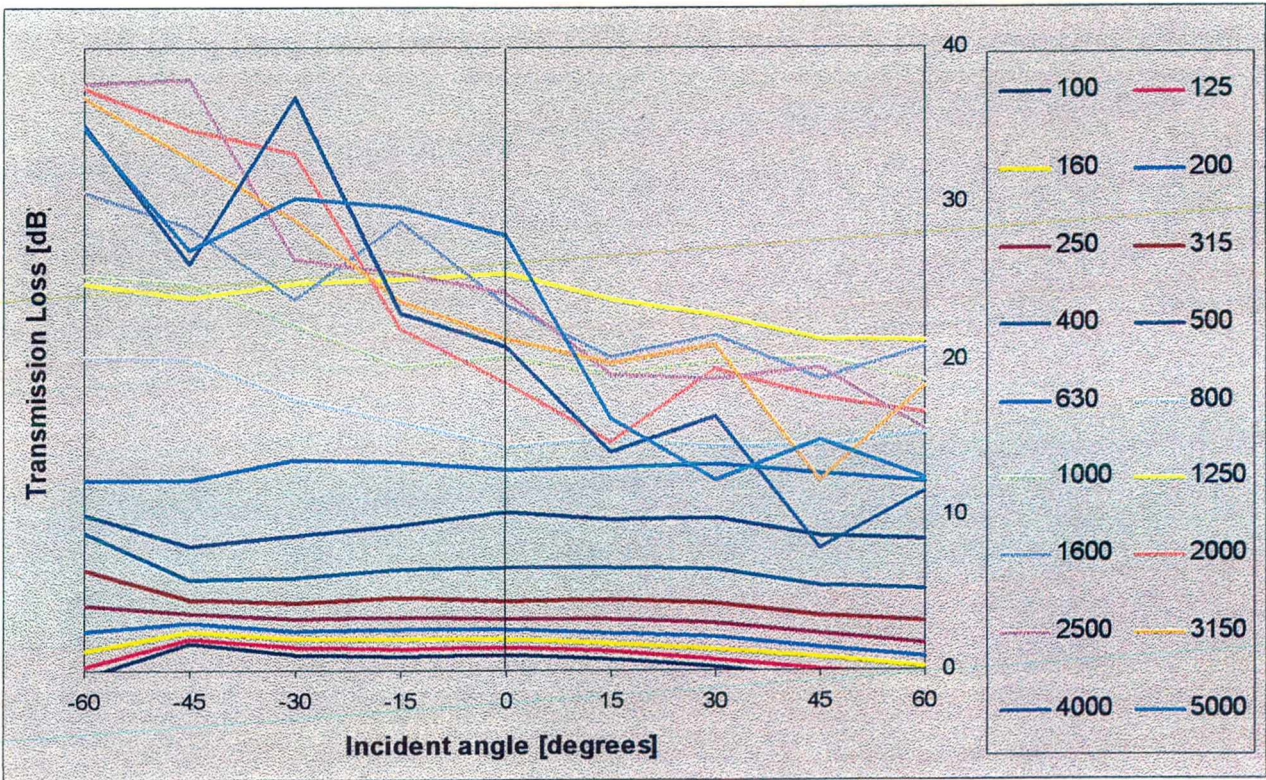


FIGURE 5.12 - Transmission loss of the louvre by impulse response for 1/3 octave bands.

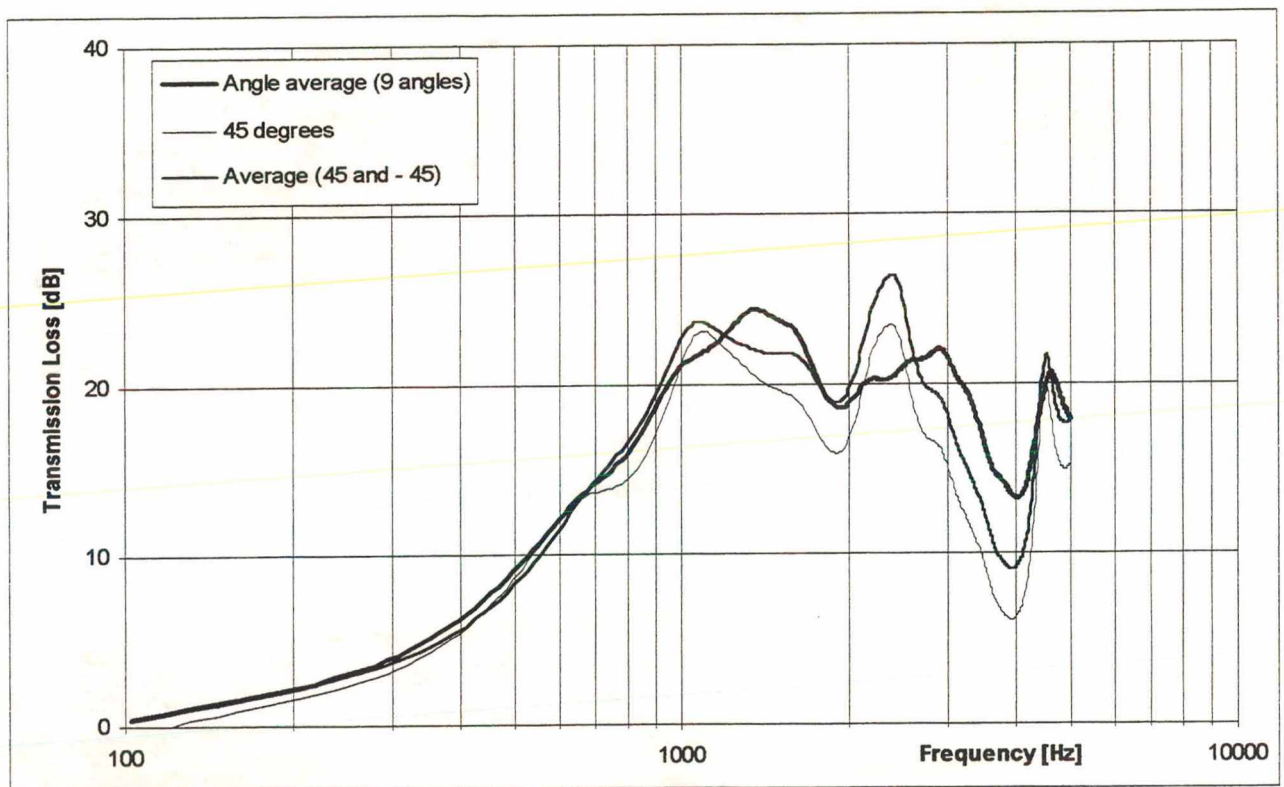


FIGURE 5.13 - Transmission loss for 45° of incidence and angle averages over 45° and -45° and all angles.

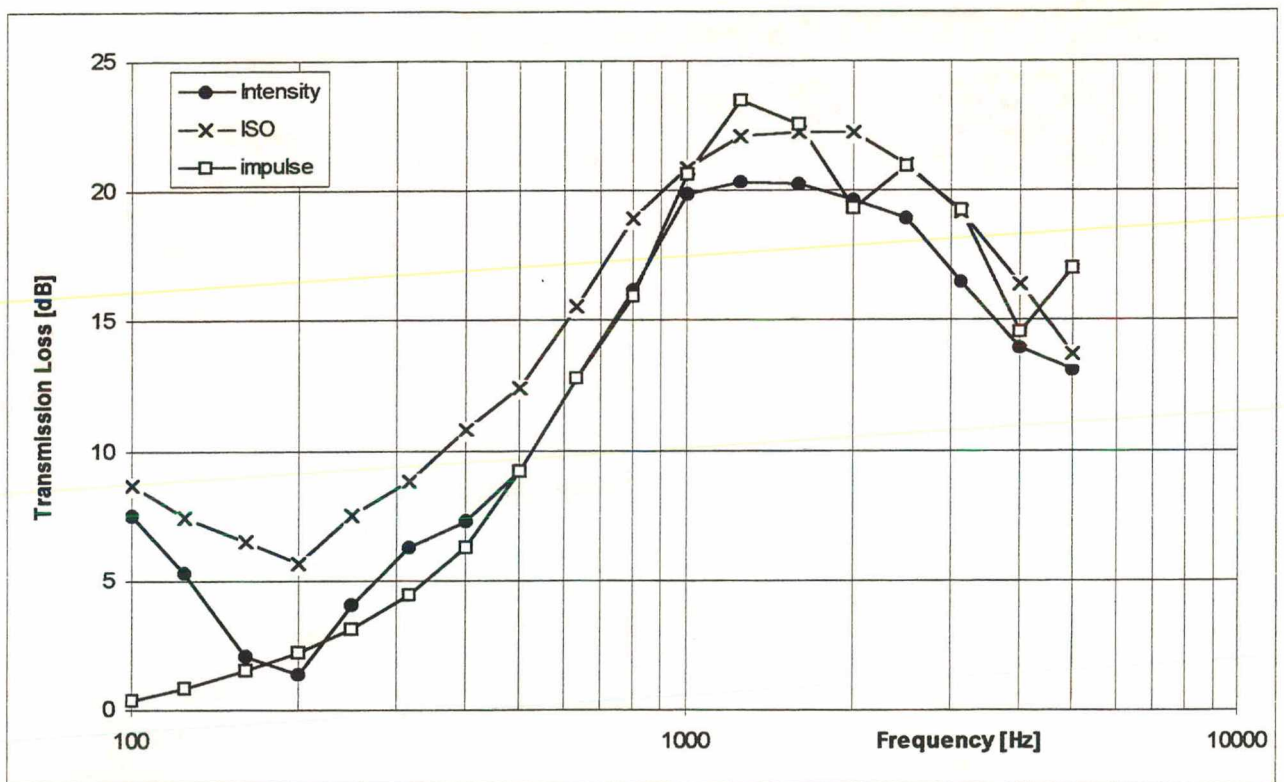


FIGURE 5.14 - Transmission loss of the louvre measured by ISO 140, intensity and impulse response.

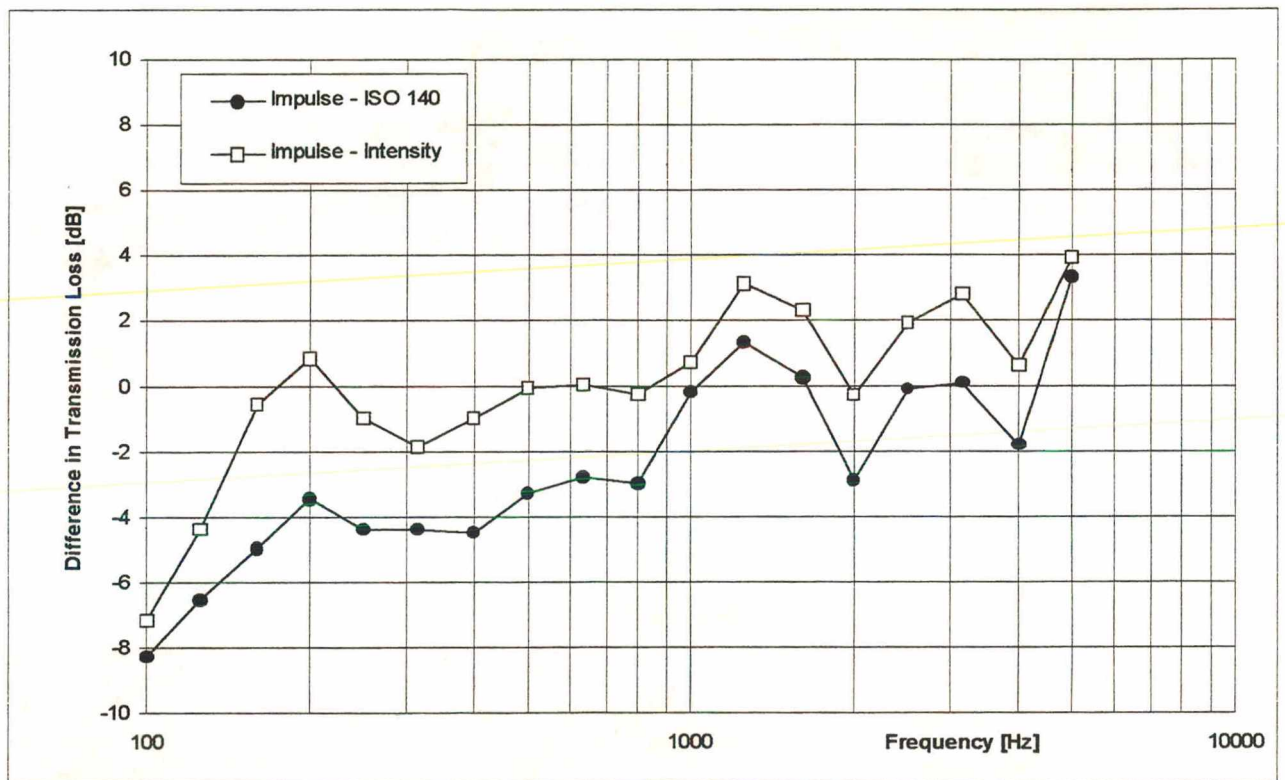


FIGURE 5.15 – Difference between impulse, intensity and ISO 140 measurements.

**CHAPTER 6 SIMULATION OF TRANSMISSION THROUGH
ACOUSTIC LOUVRE**

- 6.1 Introduction
- 6.2 Wave Diffraction Model
- 6.3 Preliminary Simulation
- 6.4 Prediction Model for the Louvre
- 6.5 Results
- 6.6 References

6.1 INTRODUCTION

As shown in the previous chapter, the sound transmission through louvres is strongly frequency dependent. At low frequencies, the transmission loss increases monotonically with frequency. At mid- to high- frequencies, the performance varies with frequency, showing dips and peaks.

In order to validate the measurement results, an investigation into the mechanisms of sound transmission through openings and perforated screens was carried out, and formed the basis for a numerical simulation. The approach, in developing the computer model was to identify the characteristics of the sound transmission through the louvre in different frequency regions and then assign the appropriate theoretical model for each region. Kirchhoff's mathematical formulation for diffraction theory was used for mid- and high- frequencies and a mass layer model was used to predict the results for low frequencies. The wave diffraction model was also used for the preliminary investigations and will be described in detail next.

6.2 WAVE DIFFRACTION MODEL

The concept of sound rays leads to simple propagation involving only specular reflections [1]. When other phenomena take part, such as diffraction or interference, the model is less simple and involves the wave characteristic of sound [2]. As the louvre is composed of solid and open parts, a complex field pattern is generated behind the screen. In this case, the sound behaviour cannot be described by geometric acoustics alone. The wave nature of sound propagation must be taken into account [3].

The propagation of a wave can be conveniently described by means of wavefronts. Huygens' principle describes the propagation as points on a wavefront, at any instant, being considered as new sources of secondary wavelets [4]. The wavefront at a later instant can be found by constructing the 'envelope' of the secondary wavelets, due to point sources distributed over the previous wavefront. The principle is illustrated in Figure 6.1.

Where a wavefront is unobstructed each element of the wavefront travels along a straight line, as a ray. If a finite barrier is placed along the transmission path, propagation ceases to be rectilinear

and diffraction occurs around the edges [5]. Likewise, when a wave strikes a perforated screen, the wave beyond the screen no longer propagates only in the direction of the incident wave. Instead, it spreads over a range of new directions. Figure 6.2 illustrates wavefronts of a plane propagating wave when an infinite barrier with a single slit is in the transmission path. The diffracted path propagation beyond the screen is constructed according to Huygens' principle [6].

Fresnel developed Huygens' envelope construction to include Young's principle of interference. These ideas were put on a mathematical foundation by Kirchhoff making use of the theory of Green's function to give the Rayleigh-Sommerfield diffraction theory [7]. Sommerfield's exact solution has the advantage that it can be applied to more complex barriers such as wedge shaped screens, though Kirchhoff's approximation is less complicated and can give accurate results, as highlighted by Lyons [8]. Measurements, obtained by Lyons for single leaf picket screens, confirm this approach. This mathematical formulation for diffraction was used as the basis of the model of sound transmission through the louvre and is summarised here.

6.2.1 Mathematical Foundation

Consider an infinite opaque screen with an aperture, as shown in Figure 6.3. The disturbance at point p_1 , generated by a sound source emitting a single spherical wave positioned at point p_2 , is given by:

$$\tilde{P}(p_1) = \frac{Ae^{jk r_{21}}}{r_{21}} \quad (6.1)$$

where A is proportional to the source power, k is the wavenumber ($k = 2\pi / \lambda$), and r_{21} is the distance between source and receiver. The Fresnel-Kirchhoff diffraction formula expresses the disturbance at point p_0 by [9]:

$$\tilde{P}(p_0) = \frac{-A}{4\pi} \iint_{\text{aperture}} \frac{e^{jk(r_{21} + r_{01})}}{r_{21}r_{01}} \left[\left(jk - \frac{1}{r_{21}} \right) \cos \theta_{21} + \left(jk - \frac{1}{r_{01}} \right) \cos \theta_{01} \right] ds \quad (6.2)$$

where r_{2l} and r_{0l} are the distances from the source and receiver to the elemental area ds on the aperture, at angles θ_{2l} and θ_{0l} , respectively, to the normal of the surface, according to Figure 6.3. Equation (6.2) formed the basis for the simulation approaches.

An interpretation of the diffraction formula (6.2) can be presented. Let equation (6.2) be rewritten as follows:

$$\tilde{P}(p_0) = \iint_{\text{aperture}} \tilde{P}'(p_1) \frac{e^{jk r_{0l}}}{r_{0l}} ds \quad (6.3)$$

where $\tilde{P}'(p_1)$ is given by:

$$\tilde{P}'(p_1) = \frac{1}{4\pi} \left[\frac{-Ae^{jk r_{2l}}}{r_{2l}} \right] \left[\left(jk - \frac{1}{r_{0l}} \right) \cos \theta_{0l} + \left(jk - \frac{1}{r_{2l}} \right) \cos \theta_{2l} \right] ds \quad (6.4)$$

Equation (6.3) may be interpreted as follows; the field at point p_0 arises from an infinity of secondary point sources located within the aperture. The amplitude $\tilde{P}'(p_1)$ of the secondary source located at p_1 is proportional to the amplitude $(Ae^{jk r_{2l}}) / r_{2l}$ of the wave emitted at p_2 .

Kirchhoff's theory, as expressed in equation (6.2), contains two assumptions:

- i. Across the aperture surface, the field distribution and its derivative is exactly the same as it would be in the absence of the screen.
- ii. Over the portion of the screen that lies in the geometrical shadow, the field distribution and its derivative are identically zero.

These conditions are commonly known as Kirchhoff boundary conditions. Actually, neither can be exactly true. The presence of the screen will invariably perturb the field to some extent and fringing effects will take place in the shadow zone behind the screen. Yet, if the aperture dimensions are large compared with the wavelength, these effects can be neglected [7]. The

formula can fail to reproduce the assumed boundary conditions if the diffracted fields are observed too close to the aperture [8].

6.3 PRELIMINARY SIMULATION

Prior to the analysis of the transmission measurements of the louvre, a simpler simulation was carried out, for a solid aluminium screen. Measured results are shown in Chapter 5. Fresnel-Kirchhoff's theory was also used to describe the diffraction around the edges of the barrier.

Equation (6.2) applies for an aperture in an absorbing screen. However, if Babinet's principle [10] is invoked, an exact complement is obtained: an absorbing screen in free space, of same shape and size as the aperture. Thus, the field that is diffracted around the screen is given by:

$$\tilde{P}(p_0) = \frac{Ae^{jk r_{21}}}{r_{21}} + \frac{A}{4\pi} \iint_{\text{screen}} \frac{e^{jk(r_{21} + r_{01})}}{r_{21}r_{01}} \left[\left(jk - \frac{1}{r_{21}} \right) \cos \theta_{21} + \left(jk - \frac{1}{r_{01}} \right) \cos \theta_{01} \right] ds \quad (6.5)$$

which is the net result obtained when the field incident upon the screen is subtracted from the field that would reach the observation point in free space, equation (6.1) minus equation (6.2).

Provided the screen has sufficient mass, the direct transmission can be disregarded and equation (6.5) yields the attenuation due to the presence of the panel. However, at low frequencies and for the panel tested the transmitted component is not negligible and must be considered. The transmission coefficient, τ_θ , is given by:

$$\tau_\theta = \frac{1}{1 + \left(\frac{\omega m \cos \theta}{2\rho c} \right)^2} \quad (6.6)$$

where θ is the angle of incidence, m is the surface mass density and c is the sound speed in the air. The phase shift, ϕ , between the incident and transmitted waves is of the form:

$$\phi = \tan^{-1}\left(\frac{\omega m \cos \theta}{2\rho c}\right) \quad (6.7)$$

The effect at the receiver due to the field transmitted through the screen only is obtained by integrating the sound field over the screen area, now reducing the incident pressure by including the transmitted component and considering the phase shift. Hence, the transmitted field through the screen is given by:

$$\frac{-A}{4\pi} \iint_{\text{screen}} \sqrt{\tau} e^{j\theta} \left(\frac{e^{jk(r_{21} + r_{01})}}{r_{21}r_{01}} \left[\left(jk - \frac{1}{r_{21}} \right) \cos \theta_{21} + \left(jk - \frac{1}{r_{01}} \right) \cos \theta_{01} \right] \right) ds \quad (6.8)$$

The total disturbance is now the addition of the fields that are diffracted around and transmitted through the screen, equation (6.5) plus equation (6.8):

$$\begin{aligned} \tilde{P}(P_0) = & \frac{Ae^{jk r_0}}{r_{21}} + \frac{A}{4\pi} \iint_{\text{screen}} \frac{e^{jk(r_{21} + r_{01})}}{r_{21}r_{01}} \left[\left(jk - \frac{1}{r_{21}} \right) \cos \theta_{21} + \left(jk - \frac{1}{r_{01}} \right) \cos \theta_{01} \right] ds \\ & \frac{-A}{4\pi} \iint_{\text{screen}} \sqrt{\tau} e^{j\theta} \left(\frac{e^{jk(r_{21} + r_{01})}}{r_{21}r_{01}} \left[\left(jk - \frac{1}{r_{21}} \right) \cos \theta_{21} + \left(jk - \frac{1}{r_{01}} \right) \cos \theta_{01} \right] \right) ds \end{aligned} \quad (6.9)$$

The computer program used equation (6.9) to predict the sound field in the receiver point when a screen is placed in the transmission path. The program listing is shown in Appendix 1. The solid barrier was discretised into elements no greater than $\lambda/5 \times \lambda/5$ [9] that should be divisible by blade and gap width (both 100 mm). This gave an element of 6.25 mm x 6.25 mm, corresponding to an upper wavelength and frequency of 0.0137 m and 5004 Hz, respectively. In the measurement set-up, the source, receiver, and screen were placed on a perfectly reflecting surface, at source to louvre and receiver to louvre distances of 1.0 m to the axis of the louvre. The simple mirror image method simulates a screen twice the height of the measured screen. The microphone and source were as used in earlier measurements as described in section 4.3.1.

Figure 6.4 shows the measured results for the aluminium panel at normal incidence, presented in Chapter 5, along with predicted values. The upper chart represents the infinite panel response. As

described in section 5.2, the measurement of the infinite response was obtained by setting the time window in such a way to include only the direct component. Likewise, the prediction is for the attenuation across the screen only, obtained from equation (6.8). On the other hand, the measured finite response (lower chart) is obtained by including the diffraction over the top, together with the direct component transmitted through the screen, in the time window. The prediction given by equation (6.9) considers the incident field as being diffracted around the four edges of the panel.

The agreement for the infinite result is promising (within 4 dB) in the frequency range 500-5kHz. Discrepancy between measurement and prediction increases with decreased frequency below 500 Hz and is a maximum of 15 dB at 100 Hz. The discrepancy is due to three causes. Firstly, as presented in 4.2.3, there is a low frequency limit to the impulse method, depending upon time window duration. A second reason arises from the assumption that the observing point is in the far field. In fact, at such low frequencies, Kirchhoff boundary conditions do not apply when the diffracted field is observed close to the screen [7]. The third reason is that the loudspeaker efficiency decreased with decreased frequency, plus high background noise at low frequencies, increased signal-to-noise errors (see Figure 4.4 on S/N ratio in Chapter 4).

The finite response simulation predicts, in general, a lower transmission loss than measured at all frequencies, with some peaks in performance not present in the measured data. This is expected, since the measured data took into account the diffraction over the top of the screen only. The frequencies where the prediction showed higher values of transmission loss can be related to destructive interference of other diffracted components. In general, the agreement is reasonable and results remained promising. The method was now applied to louvres.

6.4 PREDICTION MODEL FOR THE LOUVRE

The computer simulation was used to predict the transmission loss at an incident angle of 45 degrees. The choice for this angle was made from results obtained for the far-field measurements. It has been shown in section 5.3.3 that this angle is the dominant contribution to the overall performance, i.e. when measured transmission loss was angle averaged.

The computer model incorporated three aspects. Firstly, for low frequency, the mass layer theory

was used. Secondly, for the mid- and high- frequencies, the diffraction theory was applied. Thirdly, transmission across the louvre was also considered by means of measured transfer functions.

6.4.1 Low Frequency Range

For this region, where the wavelength is much greater than gap dimension, the louvre was assumed to be a partially transmitting, solid screen, with an effective surface mass density.

Below the frequency at which the openings become comparable to the wavelength, there will be a nearfield interaction between adjacent sources. Thus, unlike the wave behaviour at mid- and high-frequencies, the gaps behave as an inert mass per unit area. This is the so-called mass layer effect [11] and the effective mass per unit area, m_o , is given by:

$$m_o = \frac{\rho}{\sigma} (l_o + 2\Delta l) \quad (6.10)$$

where ρ is the density of the air, σ is the open area ratio, given by b/B , where b is the gap width and B is the total width of gap and blade, l_o is the gap depth and $2\Delta l$ is the gap end correction, which in turn depends on the inverse of the open area ratio and the distance between screen and back wall.

Equation (6.10) shows that the small amount of air confined in the apertures of the louvre can contribute to an increased surface mass density and should not be disregarded. Therefore, this equivalent mass was used in equation (6.6), as well as in equation (6.7), and the low frequency range was predicted by modifying equation (6.8) as follows:

$$\frac{-A}{4\pi} \iint_{\text{screen}} \sqrt{1 + \left(\frac{\alpha m_o \cos \theta}{2\rho c} \right)^2}^{-1} e^{j\theta} \left(\frac{e^{jk(r_{2l} + r_{0l})}}{r_{2l}r_{0l}} \left[\left(jk - \frac{1}{r_{2l}} \right) \cos \theta_{2l} + \left(jk - \frac{1}{r_{0l}} \right) \cos \theta_{0l} \right] \right) ds \quad (6.11)$$

The computer program listing is given in Appendix 2.

6.4.2 Mid- and High- Frequency Range

The periodical slit opening pattern of the louvre was modelled as follows; the transmitted sound field was composed by two components, representing blades and gaps. It was assumed that the sound transmission over the blades was negligible compared to the transmission through the gaps. The sound waves incident on the openings had their behaviour modelled by the diffraction theory.

The field generated at the receiving point by the transmission through the apertures involved two further considerations. Initially, the sound transmission through the louvre gaps can be approached as a multiple slit problem, which combines the mechanisms of diffraction and interference. Both are, in essence, superposition effects. Fresnel-Kirchhoff theory, presented earlier, yields the phase of the components of the sound field generated at the multiple openings. It predicts the effect of constructive and destructive interference at the receiver position. In addition, the computer model also considered the transmission through the louvre as a frequency dependent complex transfer function, $TF(f)$. Consequently, the expression governing the diffracted field produced by the gaps, equation (6.2), was replaced by:

$$\frac{-A}{4\pi} \iint_{\text{screen}} \frac{e^{jk(r_{21}+r_{01})}}{r_2 r_{01}} \left[\left(jk - \frac{1}{r_{21}} \right) \cos \theta_{21} + \left(jk - \frac{1}{r_{01}} \right) \cos \theta_{01} \right] TF(f) ds \quad (6.12)$$

The program listing, predicting the transmitted field for mid- and high- frequency range is presented in Appendix 3.

6.4.3 Transfer-Function Measurements

The first approach was to measure the transfer function placing the microphone on two different positions, before and after the screen, named “entrance” (microphone 1) and “exit” (microphone 2) of the gap, according to Figure 6.5. The measurement would thus allow the amplitude and phase changes imposed by the louvre to be detected. The microphone was placed at a height of 1.07 m above the hard floor. The two microphone positions were at a set distance of 420 mm.

The set-up was chosen to ensure that the loudspeaker was sufficiently distant from the louvre so

that the incident sound approximated a plane wave field. Consequently, all gaps should give the same transfer function, as the sound waves enter the opening at approximately the same angle. In addition, measurements were previously performed to investigate the contribution of different paths to the response obtained at microphone 2, at the exit of the opening. All gaps were sealed with a wooden panel, leaving solely the transmission path along the measured gap. Figure 6.6 shows the difference in amplitude (upper chart) and phase (lower chart) between the transfer functions measured with and without the gaps sealed, indicating that the contribution from other paths could be disregarded.

The acquisition of transfer function involved two measurements. The transfer function at the louvre's position, TF_{lou} , was obtained by the ratio given by microphones 1 and 2, according to:

$$TF_{lou} = \frac{mic_{lou,2}}{mic_{lou,1}} \quad (6.13)$$

where $mic_{lou,2}$ and $mic_{lou,1}$ are the impulse responses of the microphones positioned by the louvre, at the exit and entrance of the opening, respectively.

As for other impulse response measurements, a reference measurement was also necessary, so as to cancel the effect of distance and system response. The loudspeaker, microphones 1 and 2 were put at the same geometry as for the measurement by the louvre, and the reference transfer function was obtained according to:

$$TF_{ref} = \frac{mic_{ref,2}}{mic_{ref,1}} \quad (6.14)$$

The ratio between the result obtained by the louvre, equation (6.13), and that measured in reference conditions, equation (6.14), gives the transfer function of the louvre between the entrance and exit planes, in agreement with:

$$TF_{LOUVRE} = \frac{TF_{lou}}{TF_{ref}} \quad (6.15)$$

Two preliminary tests were performed in order to investigate the accuracy of the measurements, one regarding errors inherent in the method and the other concerning the phase delay detection.

Firstly, the repeatability of the transfer function measurement was evaluated. Six measurements were performed with microphone and loudspeaker distance kept constant. The transfer functions between three pairs of impulse responses were processed and the results expected to be unity. If two different microphone positions were measured, the difference from the unit in the result of the transfer function would be dictated by sphericity effect and air attenuation.

Each impulse response was inspected separately and the window set for that time history. The three results, showing the amplitudes responses, are presented in Figure 6.7. The difference from the expected result, a unit transfer function, was never greater than 0.006. The phase difference for the three sets of measurements was zero over the frequency range, showed in Figure 6.8. This is particularly significant since measurement is likely to be very sensitive to erroneous phase differences introduced as a result of variation in windowing and other test conditions. Therefore, a second test was set to detect the phase delay between two different microphone positions. A preliminary measurement was performed with two microphones placed 0.67 m apart. An 180° phase delay was expected to occur at around every 257 Hz, corresponding to a half wavelength. Figure 6.9 shows that the phase delay was correctly measured. When measuring the transfer function through the louvre, it was likely that microphone 2 would present a phase difference compared to its reference signal. This is due to the sound waves travelling at grazing incidence to the absorption material in the blades. Hence, the time windows were set at the same point in both reference and the measurement itself so as to detect the changed phase difference.

As far as the louvre's transfer function is concerned, it was realised later that the louvre's presence would disturb the sound field detected by microphone 1, as reflections would occur at the screen. Consequently, a simplified way of measuring the transfer function was proposed, using one microphone only. The transfer function, TF_{LOUVRE} , obtained from the relation between transfer functions measured at the louvre and reference set-up, is obtained from:

$$TF_{LOUVRE} = \frac{TF_{lou}}{TF_{ref}} = \frac{mic_{lou,2}}{mic_{lou,1}} \cdot \frac{mic_{ref,1}}{mic_{ref,2}} = \frac{mic_{lou,2}}{mic_{ref,2}} \cdot \frac{mic_{ref,1}}{mic_{lou,1}} \quad (6.16)$$

If ideal measurements conditions could be achieved, the sound waves incident at the entrance plane of the perforated screen would only have suffered attenuation due to the distance travelled, the same as the reference measurement. Assuming that free-field microphone response at position 1 is the same as that in the presence of the screen, then:

$$\frac{mic_{ref,1}}{mic_{lou,1}} \cong 1 \quad (6.17)$$

and expression (6.16) reduces to:

$$TF_{LOUVRE} = \frac{mic_{lou,2}}{mic_{ref,2}} \quad (6.18)$$

The transfer function is then obtained according to equation (6.18), using only one microphone for both louvre and reference measurements.

6.5 RESULTS

The simulation was performed in three steps, with increased complexity. Firstly, the louvre was treated as a thin picket screen, with infinitesimal thickness, hence source and receiver related to the normal by the same angle. Figure 6.10 shows the model layout, where the parameters signed are those in equation (6.11) and (6.12), although the latter disregarded the transfer function ($TF(f) = 1.00$). The equation produced the results shown in Figure 6.11, where transmission loss is nearly frequency independent. The measured transmission loss, presented in Chapter 5, is also shown.

For the same set-up, but a different pattern of gaps and blades, the result can be quite different, as shown in Figure 6.12. The simulated transmission loss for a louvre with 0.20 m wide blades, spaced by 0.025 m (gap width) demonstrates diffraction as sheer result of geometry.

Secondly, the louvre was treated as a slitted secondary source and its thickness taken into account. Figure 6.13 shows schematically the model. The transfer function of the louvre was not yet considered, but the function $e^{jk_1 l}$ described the phase change. The amplitude of the sound waves

was assumed unchanged due to a “channelling” along the transmission path. Equation (6.11) was substituted by

$$\frac{-A}{4\pi} \iint_{\text{screen}} \frac{e^{jk(r_{2l}+r_{0l})}}{r_{2l}r_{0l}} \left[\left(jk - \frac{1}{r_{2l}} \right) \cos\theta_{2l} + \left(jk - \frac{1}{r_{0l}} \right) \cos\theta_{0l} \right] e^{jk\ell} ds \quad (6.19)$$

Figure 6.14 shows the transmission loss simulated using the above equation. It is noticeable the interference effect caused by the new geometry, but not yet describes the measured curve.

Figure 6.15 presents the data obtained in the last step of the simulation, where the function $e^{jk\ell}$ is substituted by the measured transfer function. It can be seen that the mass layer model predicts the measured louvre’s transmission loss up to about 400 Hz. The mass effect was expected to decrease with increasing frequency, because the distance between the gaps starts to be of the same magnitude of, or greater than the wavelength, where the wave approach takes over. As indicated in Chapter 5, two sound sources do not interact whenever their separation is greater than about a sixth of the wavelength.

The geometry of the louvre for the computer simulations approximated the curved blades by a rectangular section with 0.10m width (see Figure 6.5). This may contribute to the difference between predicted and measured results up to 580 Hz, which is the frequency that has its sixth of the wavelength corresponding the distance modelled. The maximum difference in that frequency region is 3.3 dB.

Above this frequency region, the louvre’s performance is dictated by the wave diffraction model. For the mid- and high- frequencies, the simulation is even more sensitive to the geometry, which is responsible for the constructive and destructive interference patterns. It can be seen as a shift in frequencies for the peaks of high transmission loss. The first predicted peak is 88 Hz apart from the measured value, with 2 dB difference, and the second, where the prediction shows a difference of 424 Hz the performance is 5.5 dB higher. For the last peak, above 4 kHz, the difference is about 12 dB. Taking the simplicity of the geometrical modelling into account, the achieved agreement was considered good.

6.6 REFERENCES

- [1] Sabine W.C., *Collected Papers on Acoustics. Theatre Acoustics*. Peninsula Publishing, (1982).
- [2] Rayleigh J.W.S., *The Theory of Sound*, vol. 1, Dover Publications, (1945).
- [3] Cremer L. and Müller H. (Translated by Schultz T.J.), *Principles and Applications of Room Acoustics*, Applied Science Publishers, vol. 1, chapter I.1, (1982).
- [4] Ohanian H.C., *Principles of Physics*, W.W. Norton & Company, chapter 11, (1994).
- [5] Woods A., *Acoustics*, Blackie & Son Limited, chapter IX, (1950).
- [6] Eisberg R. and Lerner L., *Physics. Foundations and Applications*, McGraw-Hill, combined volume, chapter 28, (1982).
- [7] Godman J.W., *Introduction to Fourier Optics*, McGraw Hill, chapter 3, (1968).
- [8] Lyons R., *Building Elements of Low Insertion Loss*, Ph.D. Thesis, Liverpool University, (1993).
- [9] Wassilieff C., *Improving the Noise Reduction of Picket Barriers*, J. Acoust. Soc. Am., **84** (2), pp 645 - 50, (1988).
- [10] Longhurst R.S., *Geometrical and Physical Optics*, Logman, 3rd. Edition, chapter 10, (1981).
- [11] Cremer L. and Müller H. (Translated by Schultz T.J.), *Principles and Applications of Room Acoustics*, Applied Science Publishers, vol. 2, pp 181-190, (1982).

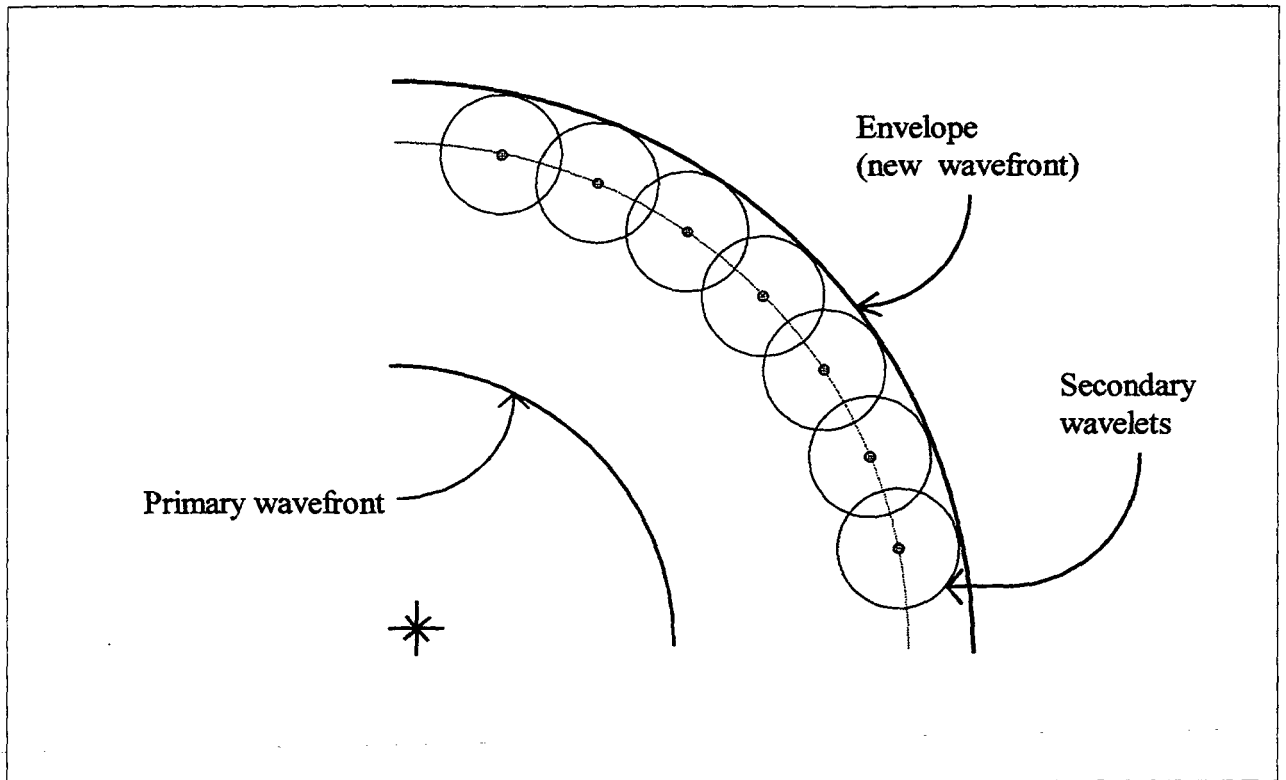


FIGURE 6.1 - Huygen's construction for the propagation of a spherical wavefront.

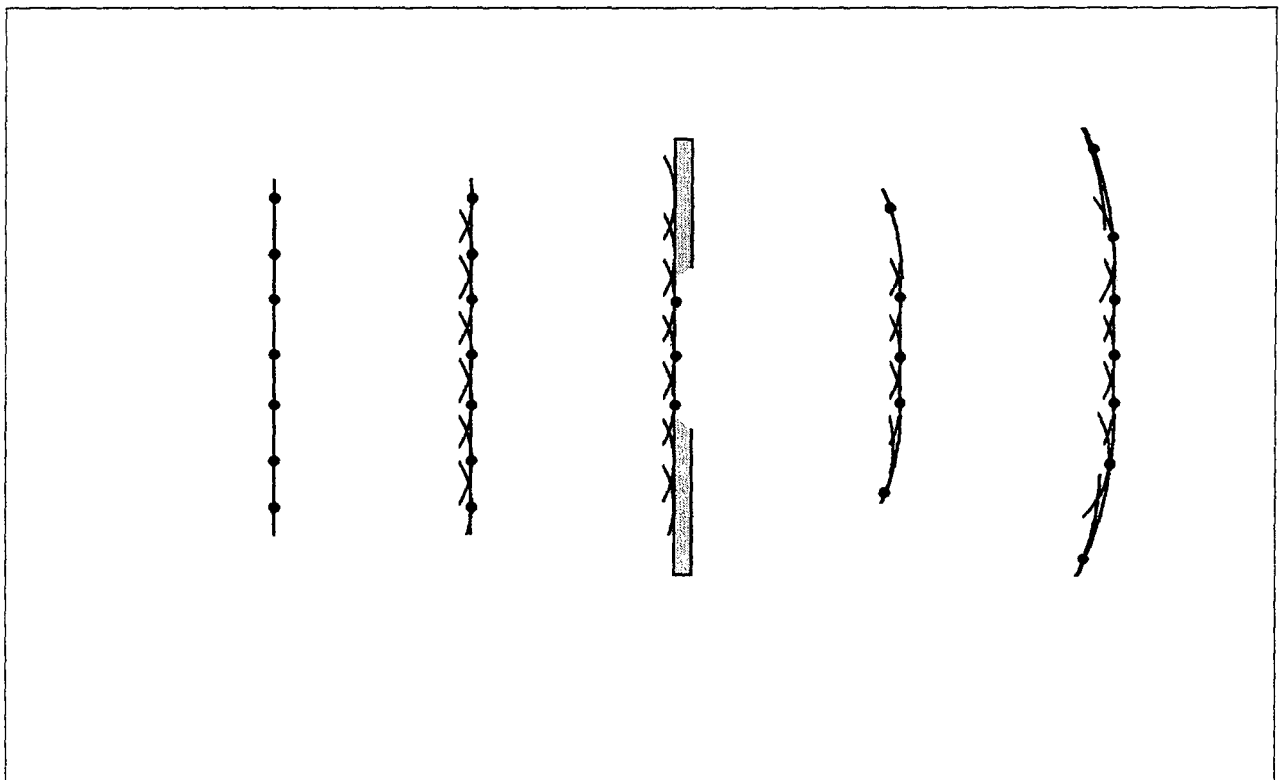


FIGURE 6.2 - Huygen's construction for single-slit diffraction from a slit whose width is three times the wavelength of the incident wave.

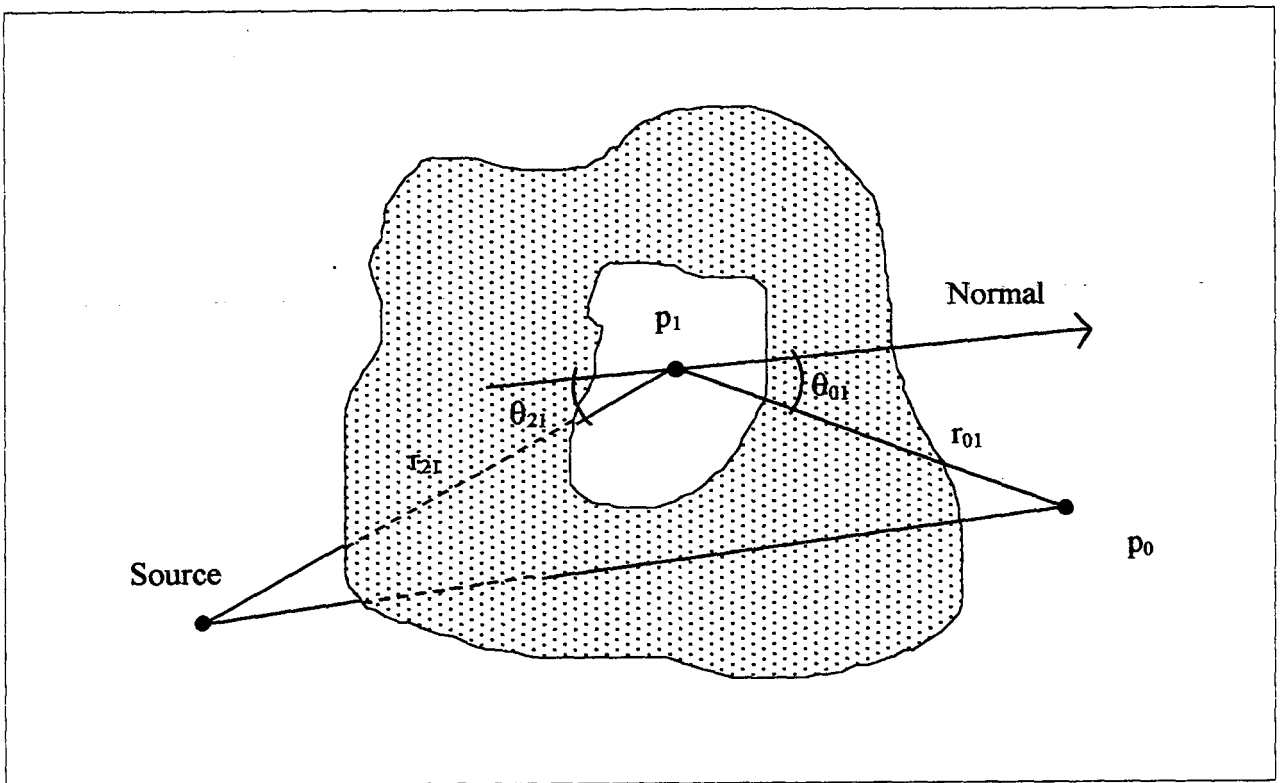


FIGURE 6.3 - Diffraction geometry.

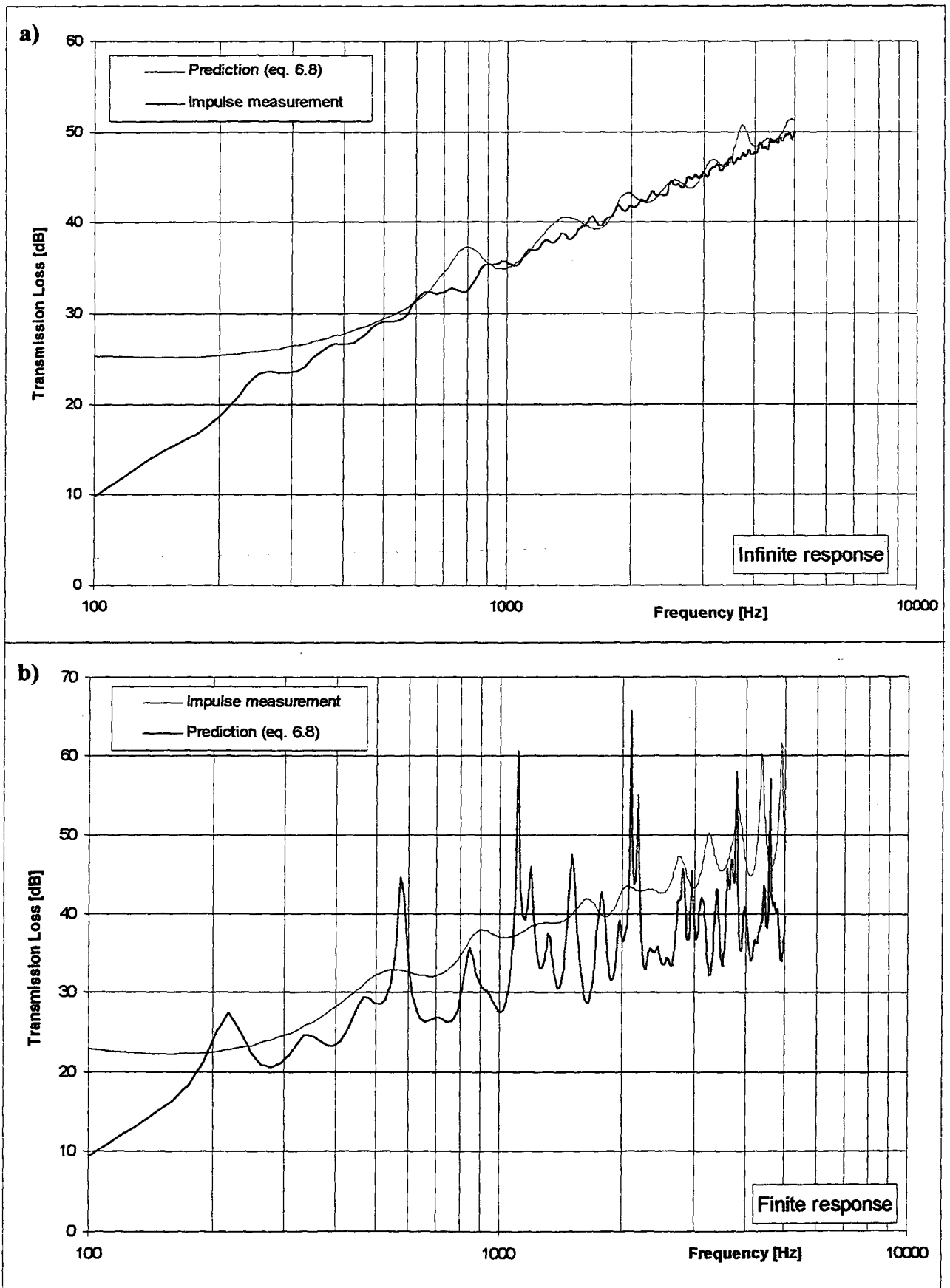


FIGURE 6.4 - a) Transmission loss of an infinite, and b) finite aluminium panels at normal incidence.

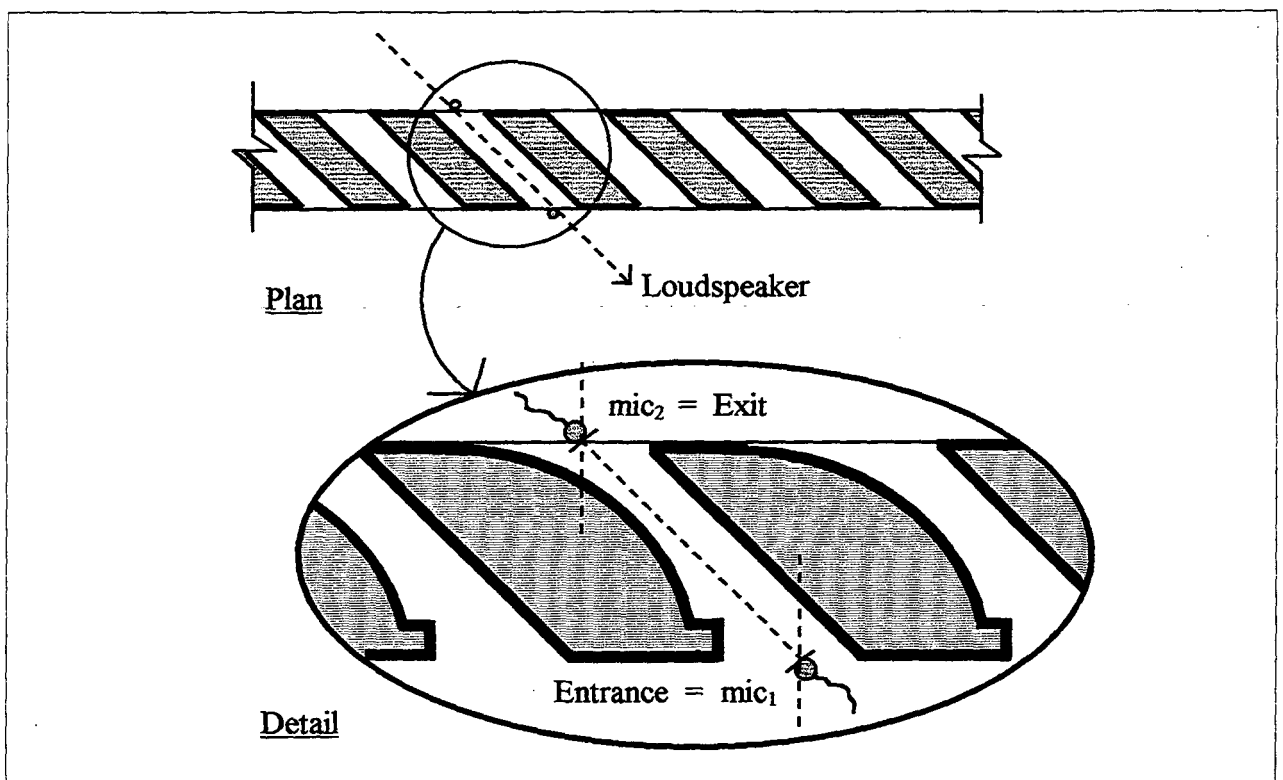


FIGURE 6.5 - First measurement setup of the louvre's transfer function using two microphone positions.

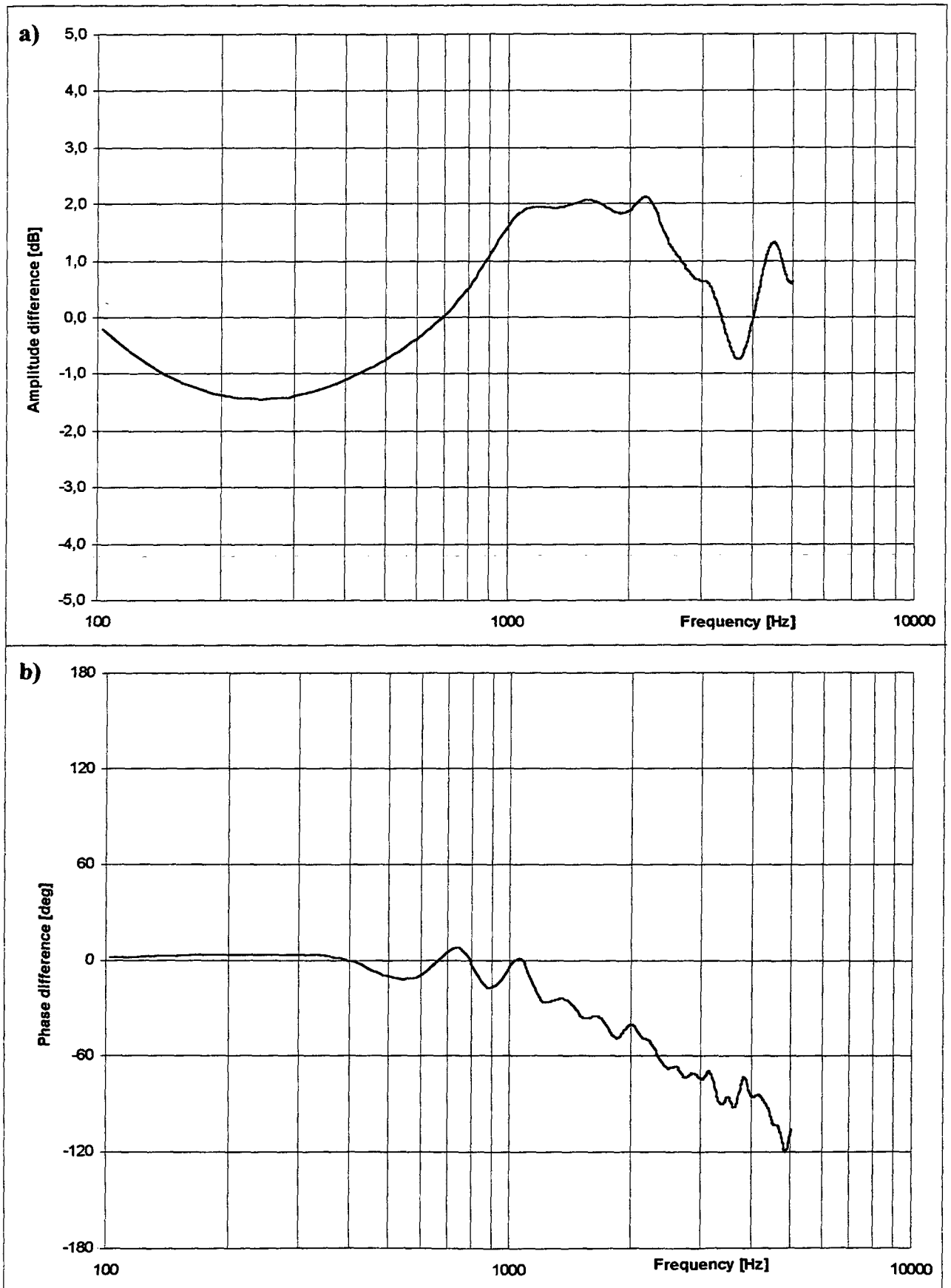


FIGURE 6.6 - Transfer function differences between measurements with gaps open and closed: a) amplitude, and b) phase differences.

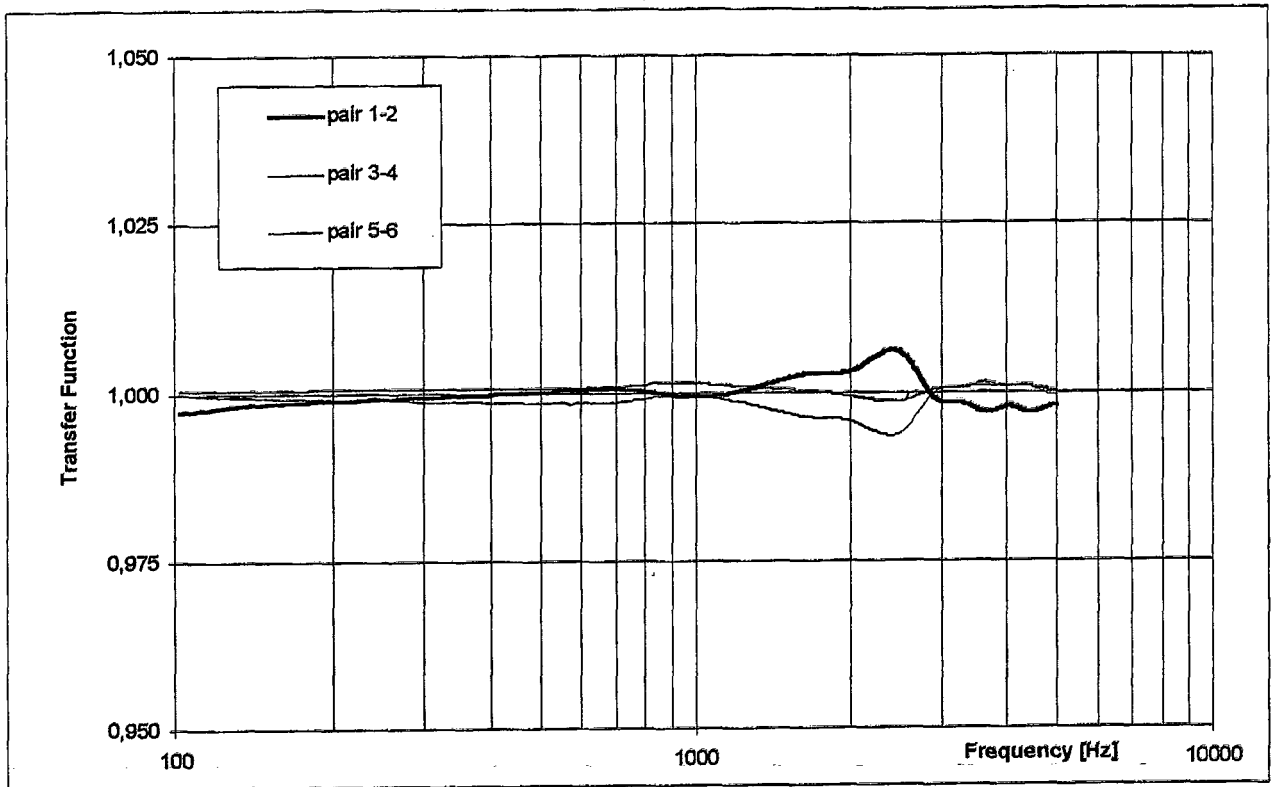


FIGURE 6.7 - Amplitude response of three transfer function measurements.

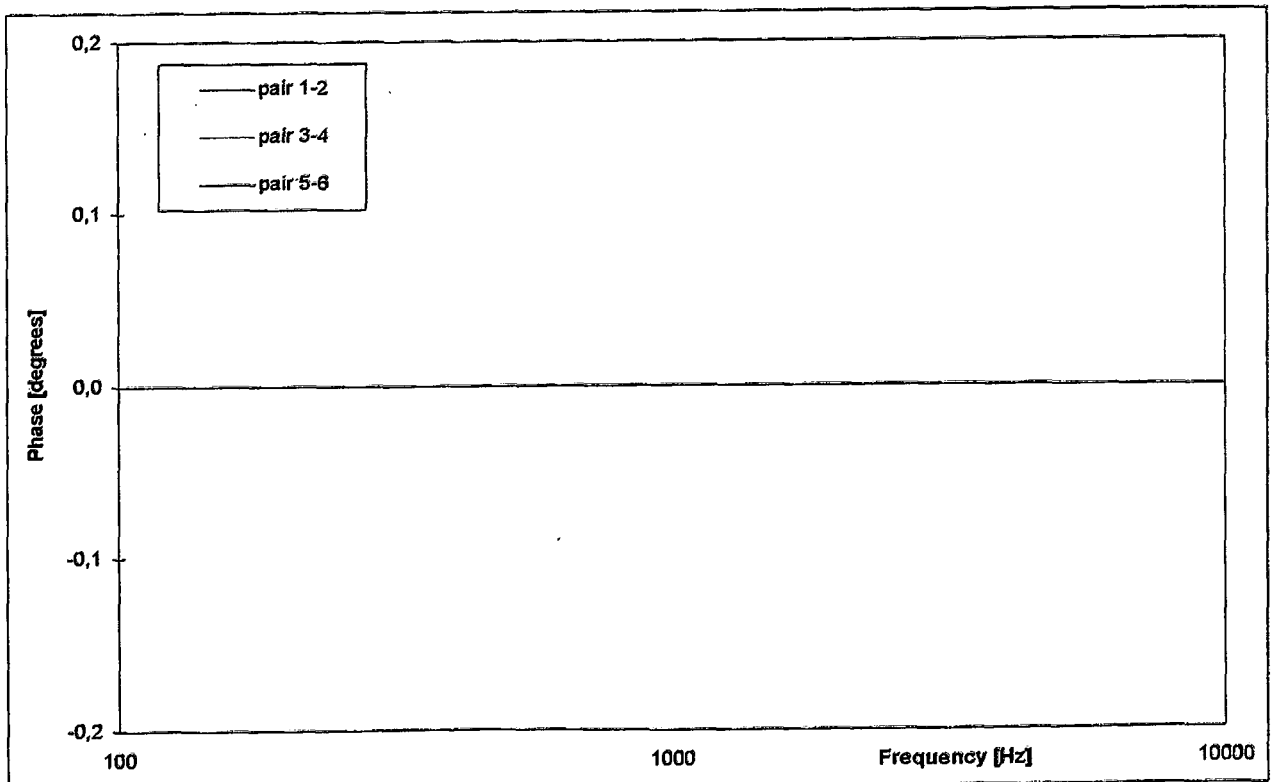


FIGURE 6.8 - Phase of three transfer function measurements.

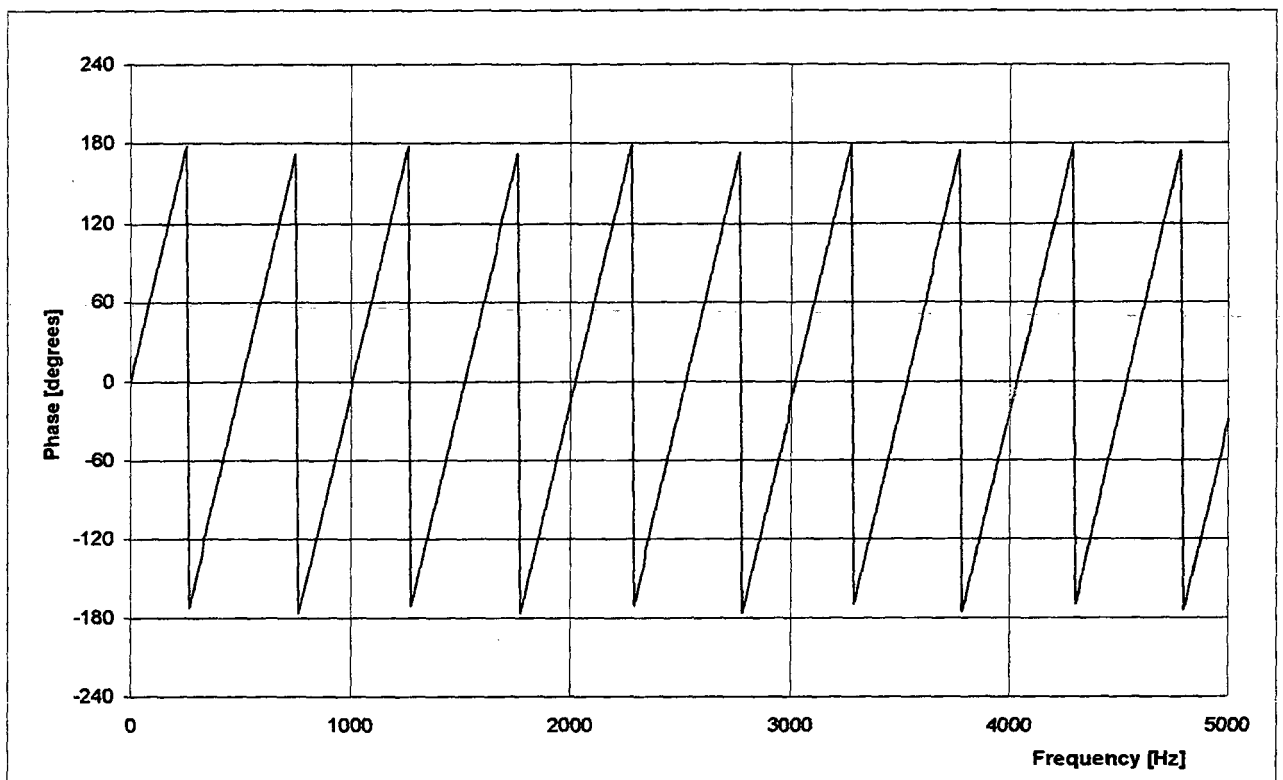


FIGURE 6.9 - Phase delay between a pair of microphones 0.67 m apart.

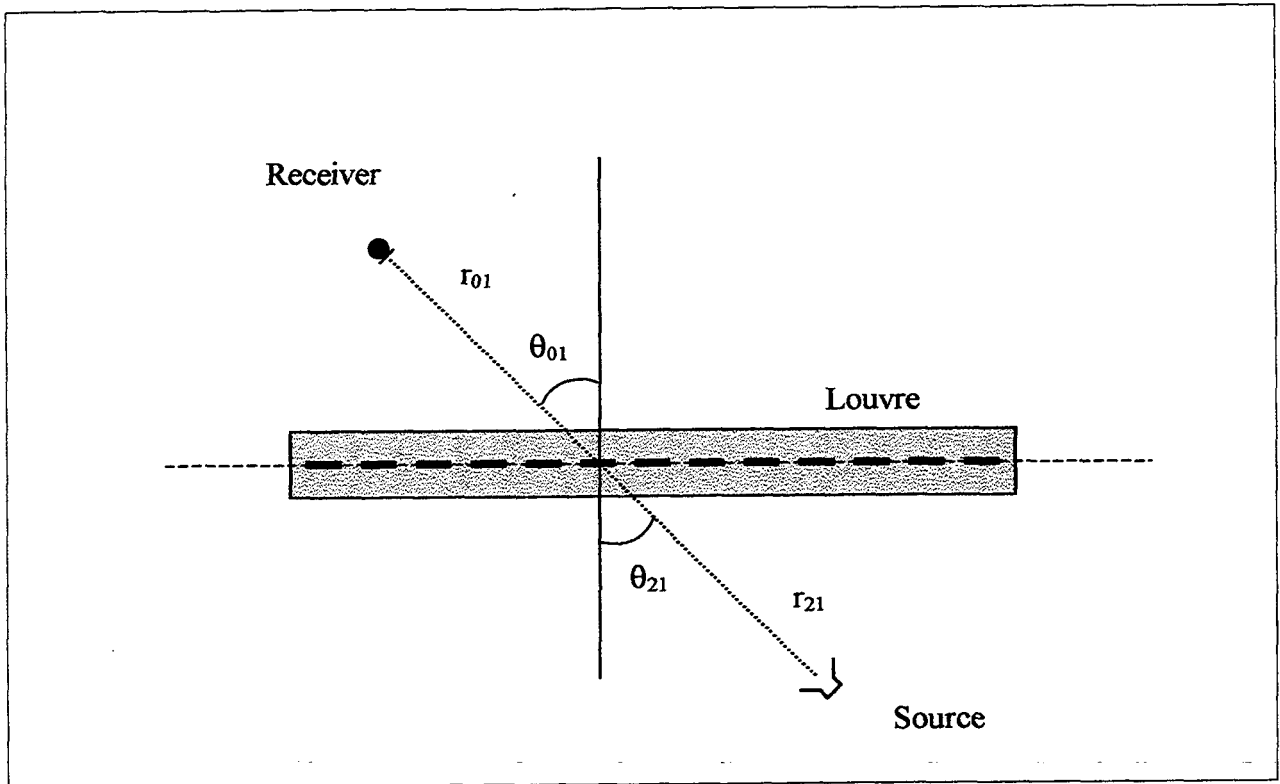


FIGURE 6.10 – First simulation approach; louvre with infinitesimal thickness.

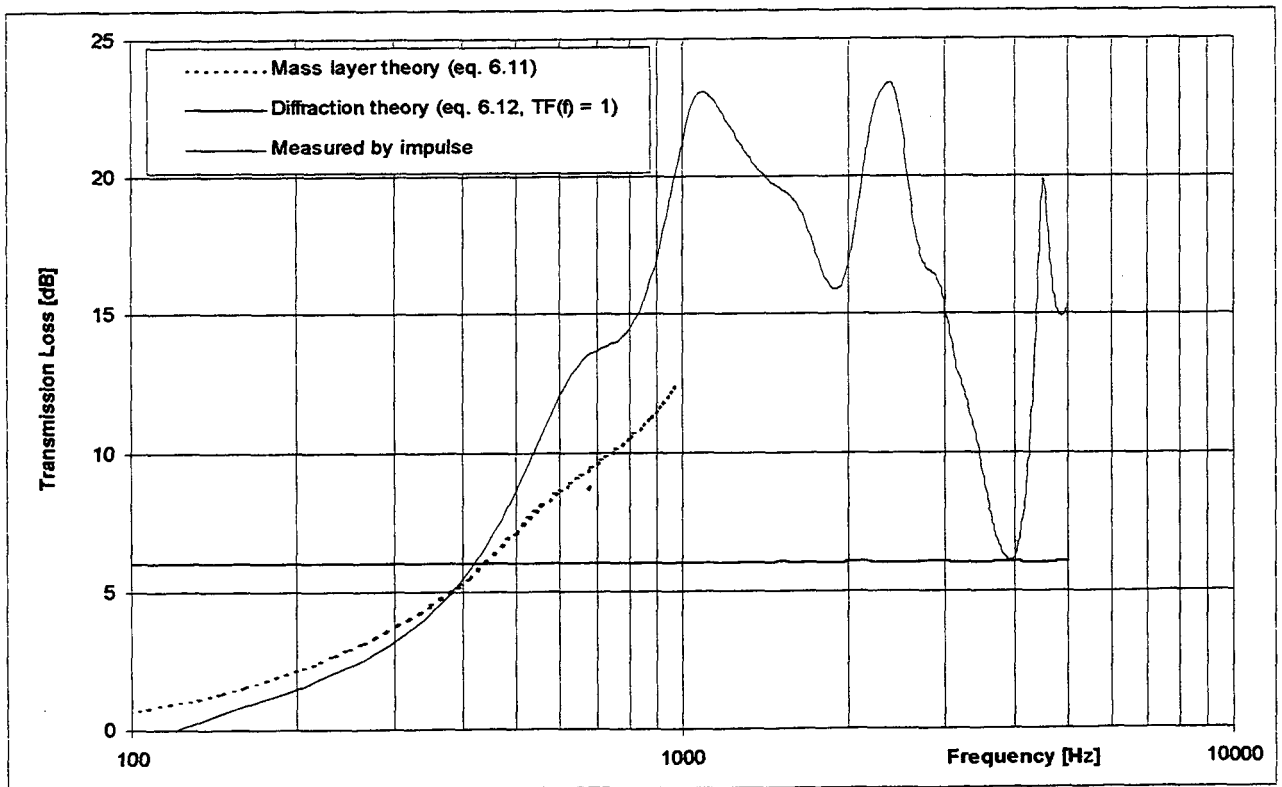


FIGURE 6.11 - Measured and predicted transmission loss of the louvre for 45° of incidence, as model shown in Figure 6.10.

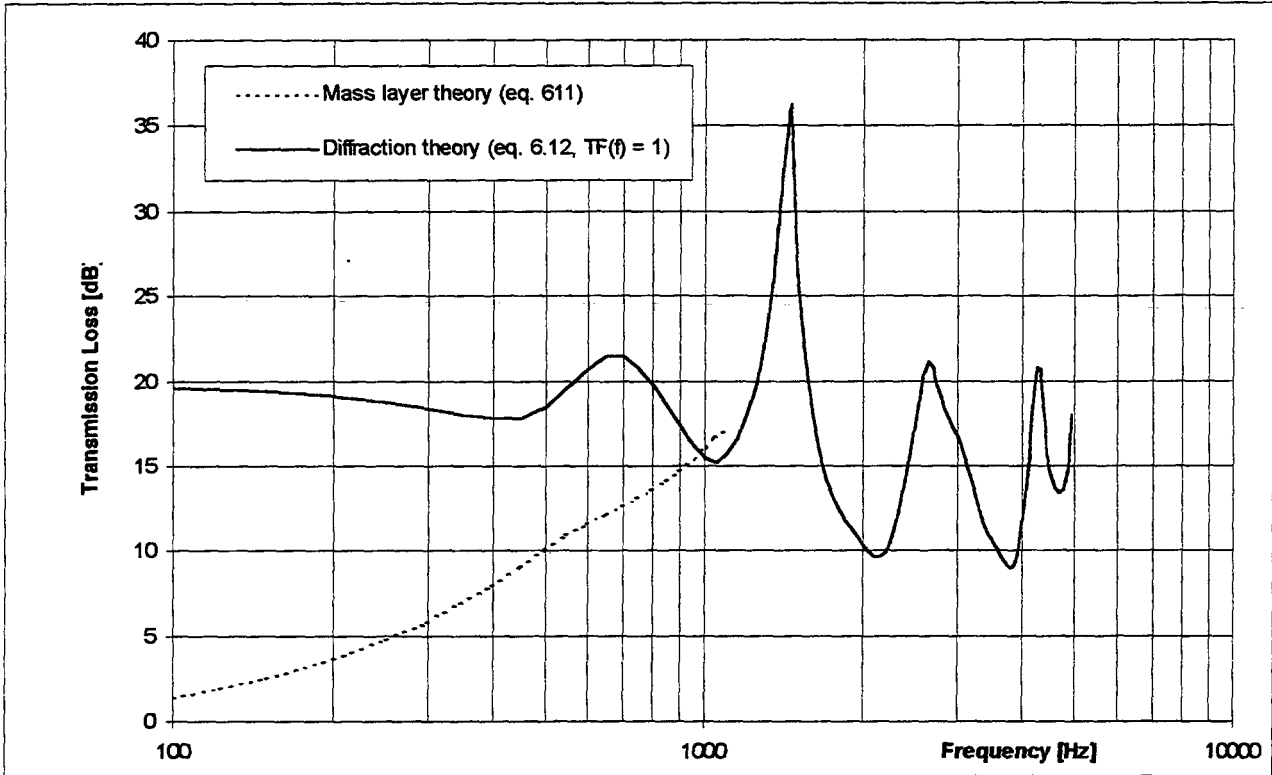


FIGURE 6.12 - Predicted transmission loss for 45° of incidence of a louvre with 0.20 m wide blade spaced by 0.025 m (gap width).

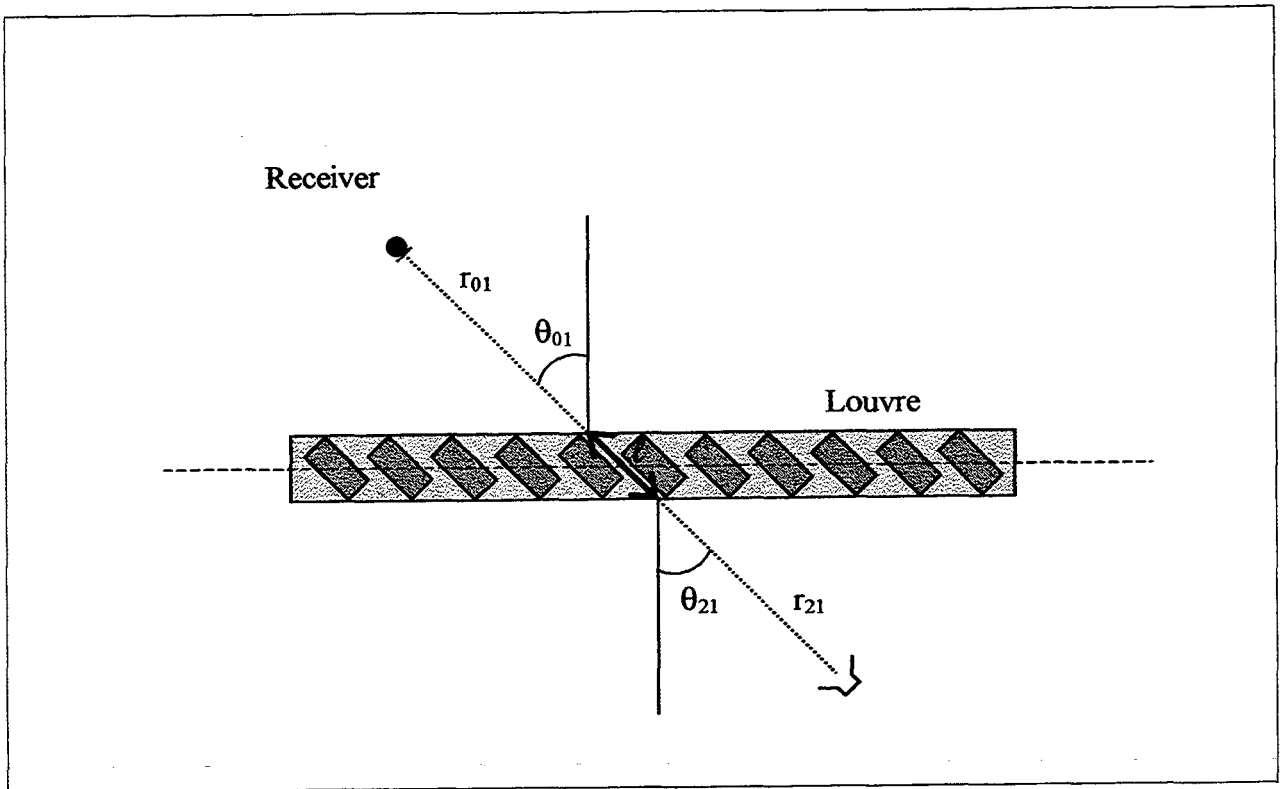


FIGURE 6.13 - Simulation model; louvre with real thickness and function to account for ℓ -distance travelled along the “channel” of the louvre.

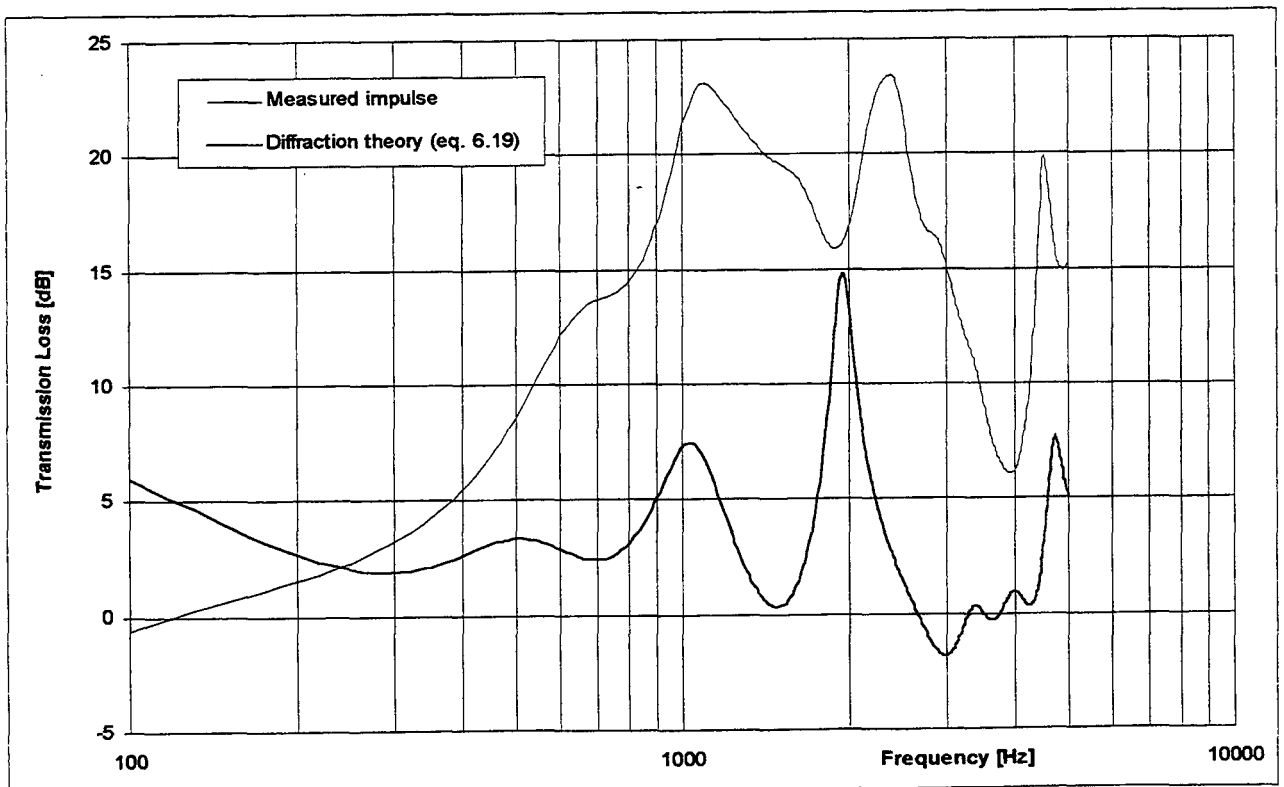


FIGURE 6.14 – Transmission loss of the louvre for 45° of incidence, as model shown in Figure 6.13, using the function $e^{jk\ell}$ to describe the propagation along the “channel”.

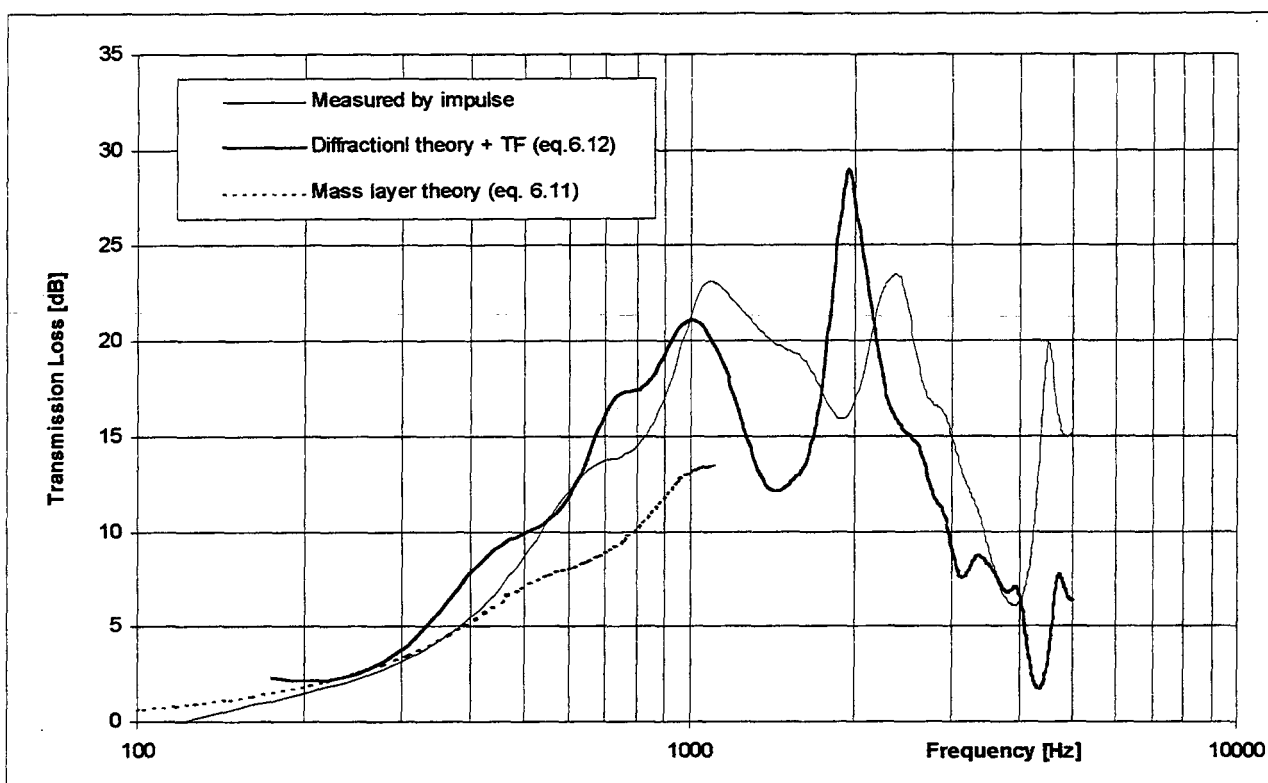


FIGURE 6.15 – Measured and predicted transmission loss of the louvre for 45° of incidence.

CHAPTER 7 ACOUSTIC MODELLING

7.1 Types of Modelling

7.2 Insertion Loss Simulation by Image Methods

7.3 References

7.1 TYPES OF MODELLING

Physical scale modelling is a powerful tool in evaluating acoustic properties of materials and enclosures prior to construction and has the advantage of being economical and timesaving. It has been used, with success, to predict the performance of auditoria and has been employed in noise control research, such as in the study of traffic noise propagation in urban areas.

The first applications to room acoustics date back to some eighty years, with the experiments involving the use of simple optical devices [1] and ripple tank methods [2], and were primarily employed in a study of diffraction, reflection and transmission phenomena.

More recently, the development of reliable and accurate electro-acoustic transducers and associated instrumentation has resulted in improvements in the technique [3]; particularly in the assessment of the effect on the steady state and transient sound fields within rooms of surface modelling and absorption, audience absorption, room geometry and source/receiver position. The constant and fast improvement in digital signal processing equipment has allowed advanced measurements to be performed [4]. The method is now an acceptable tool for assessment of room acoustics at design stage and some references are suggested [5,6,7,8].

With the advent of computers and powerful numerical techniques, physical scale modelling has been replaced by virtual modelling. The main categories, as suggested by McCulloch, are [9]:

- i. Empirical models, based upon observed acoustics relations.
- ii. Modal simulations, which base their concept on mathematical expressions derived from the wave nature of sound.
- iii. Geometrical or energy methods, which rely on some geometrical description of the sound field(s), together with formulae that describe the physics of that propagation.

The computational time required to perform such tasks has been much reduced and all approaches are now routinely applied.

This chapter reviews acoustic modelling by computer as a prelude to modelling the performance

of acoustic louvres when installed in a HEVAC test facility. It has been shown, in Chapter 2, that the HEVAC proposal represents a good approximation to open screen performance in-situ. Therefore, if the HEVAC condition can be correctly modelled, the field performance conditions will be likewise correctly modelled. The categories of acoustic modelling are presented and the method adopted described in detail.

7.1.1 Empirical Models

One of the classical empirical relations in Acoustics governs the statistical behaviour of sound decay in rooms. Sabine [10], after laborious experiments introducing cushions in a room and observing the change in what he called “the duration of audibility of the residual sound”, derived the expression relating the room dimensions and average sound absorption, as:

$$T = \frac{0.16V}{A} \quad (7.1)$$

where T is the so-called Reverberation Time in seconds, V is the room volume in m^3 and A its average sound absorption in m^2 Sabins.

Later, Eyring [11], and after him, Millington [12], introduced some alterations to this classical expression that would govern more precisely the relationship for some special cases.

The great advantage of these statistical approaches lies on their simplicity, permitting a first and quick means of evaluation. Having reverberation time as a parameter recommended ranges were proposed for different room uses, such as speech and music performance. Other criteria that complement the analysis of room acoustics were presented in section 3.2.1.2 and are found in the literature and international standards [13].

Other examples of empirical approach include prediction of outside road traffic noise propagation now contained in the procedure for calculation of road traffic noise [14] and the relation between sound attenuation given by barriers and its geometry, source, and receiver positions [15].

This approach was rejected because there was insufficient existing field data to allow empirical relationships to be developed. This may not always be true since if the HEVAC proposal were to be adopted as an international standard, then a database of sufficient depth and detail would evolve to allow a comparison of insertion loss measurement in situ and HEVAC to allow the establishment of consistent relationship.

7.1.2 Modal Simulation

Analytical methods are available, describing sound in rooms [16] but are confined to simple systems with idealised boundary conditions, and thus were rejected for this study. Numerical simulation also involves applying equations governing the wave phenomena of sound but is not restricted to rectangular room shapes or simply defined absorbing surfaces. Two methods are used in acoustics, when wave phenomena dominate, Finite Element Methods (FEM) and Boundary Element Methods (BEM). The theory and some applications of FEM and BEM can be found in [17,18,19,20] and will be summarised here.

Consider the wave equation, where all acoustical quantities depend only on the distance from the origin, but not on direction:

$$\frac{\partial^2 p}{\partial t^2} = c^2 \nabla^2 p \quad (7.2)$$

where $\partial^2/\partial t^2$ is the second derivative with respect to time, p is the pressure disturbance with respect to ambient field, c is the sound speed and ∇^2 is the Laplacian operator.

Assuming that the variation in time of the pressure at any given point is harmonic, described by:

$$p(\mathbf{r}, t) = \tilde{p}(\mathbf{r}) \cdot e^{i\omega t} \quad (7.3)$$

where (\mathbf{r}, t) indicates that the pressure field is a function of both space and time, an expression for the complex pressure $\tilde{p}(\mathbf{r})$, is obtained by substituting equation (7.3) into the wave equation (7.2):

$$\nabla^2 \tilde{p} + k^2 \tilde{p} = 0 \quad (7.4)$$

Noise sources interior to an enclosed cavity can be included as forcing terms in equation (7.4). The boundary conditions for \tilde{p} determine the reflection, absorption, and transmission of the sound waves at the enclosure's surfaces and are derived from fluid mechanical considerations.

By definition, finite element methods involve dividing the acoustic medium into volume elements to produce a linear set of equations, which can be solved numerically, rather than analytically. An advanced feature, called Wave Envelope Elements or Infinite FEM, allows the modelling of external radiation to an infinite (or semi-infinite) field as well [17].

On the other hand, boundary element methods can be applied both to closed and opened regions. The indirect variational method is also able to solve simultaneously an internal and external acoustic radiation and scattering problem. BEM has a two step approach; it divides the boundary surfaces into elements and use further mathematics to transform it into a surface integral problem.

For both approaches, the number of nodes of the element mesh, which divides the volume or surface into elements, will set the highest frequency under analysis. Usually, a minimum of six linear elements per wavelength is necessary to avoid "spatial aliasing". At high frequencies, wavelengths become small and the number of elements increases. Computational speed and storage capacity is limited and this sets a limit to the frequency range of study. Another upper limit is imposed by the assumption upon which both methods are based, namely the coherence and interaction between waves. As the frequency increases so increases the modal density and the presumption loses its applicability. At this limit, other models should be applied instead, like geometrical acoustics.

This approach was rejected for this study since it was unnecessarily complex and time consuming, requiring the calculation of all modes within the frequency range of interest, plus corrections for those outside this range. In addition, it will be shown in section 7.2.5 that the difference between impulse response measurements and HEVAC measurement of insertion loss would likely be greatest when louvre absorption became influential, i.e. at mid- and high- frequencies. In this frequency range, FEM and BEM become computationally intractable but conversely, the ray

nature of sound becomes applicable allowing simpler numerical modelling.

7.1.3 Geometrical and Energy Approaches

In geometrical room acoustics, the concept of a sound wave is replaced by the concept of a ray or beam. Rays have infinitesimal cross-section and reach a finite receiver volume, whilst the latter are generated by circle or triangle sections and intersect a point receiver.

The acoustic model is described by geometrical laws, together with expressions that rule the physics of propagation. Typically, there is a distinction between purely acoustic methods, like ray-tracing, and vibro-acoustic methods, such as statistical energy analysis (SEA)[21,22], where the latter can include acoustic calculations, but is usually concerned with structural vibration [9].

Ray-tracing techniques follow numerous sound rays emitted by a source, through the medium, which suffer attenuation by air absorption and divergence. It has been extensively applied to room acoustics [23,24,25,26,27].

When the ray strikes a room boundary (or any other element), its energy content is reduced by an amount dictated by the absorption of the surface. If only specular reflections are assumed, the portion reflected respects the reflection laws from optics [28]. Therefore, the transmission path is along the same plane formed by the incident ray and the normal to the surface, as well as the angles formed by the normal to the surface, incident and reflected rays are the same.

As soon as the energy of the ray has fallen below an assigned value another ray will be followed up and the whole process takes place again, until all rays are “traced”. At the receiver position the result is obtained by adding up energy contents at arrival time intervals. The principle is illustrated in Figure 7.1.

Some refinements can be introduced to the simulation and, for instance, wave characteristics taken into account. Recent developments include diffuse coefficients applied to surfaces, transmission through surfaces, and coherency between sound sources (Phase Ray-Tracing).

An alternative to the ray-tracing technique is the so-called image method, which applies to rooms of simple geometry. Like the former, the method is based on geometrical propagation of sound rays emitted by an omnidirectional sound source, but takes into account specular reflections only. The ray paths within the room are constructed by means of mirror images. The method offers advantages with respect to ray tracing in being easy to implement and computationally economical. It is likely that HEVAC test facilities will consist of simple rectangular spaces and therefore the method was adopted to simulate the in-situ performance of the louvre. It is argued that the physical insights gained in developing the set of programmes, employing the image approach, is greater than when importing commercially available software. In addition, the programs could be carefully tailored to the particular needs of this study. The applicability of the concept of image sources for simulating the HEVAC test procedure is presented next.

7.2 INSERTION LOSS SIMULATION BY IMAGE METHODS

A description of the measurement of the transmission loss of louvres by impulse response analysis has been described in Chapter 5. It was demonstrated that the method is simple, accurate and does not require special installations or any acoustic conditions for the measurement site. The question that remains is how the measured data can be applied to predict field performance.

Therefore, the aim was to correlate the impulse data to the HEVAC method of measuring insertion loss so as to obtain the louvre's field performance thereby preserving the ability of the method in acquiring all data necessary by means of portable equipment with no need for special acoustic facilities.

HEVAC's test procedure is to be performed in a room with regular shape and hard surfaces. The image method is a convenient simulation tool when the boundary walls of the room are rigid, as it is the case under consideration, the image solution of a rectangular enclosure rapidly approaches an exact solution of the wave equation [29]. The exact relationship between the normal-mode solutions and the image solution for a room with rigid walls is presented in Appendix 4.

A computer simulation was used to predict the sound pressure level at the receiver position with and without the louvre placed in the aperture, as indicated by the test method. The level

difference at the receiver gives the insertion loss, as it is going to be shown in details. The relation between sound pressure levels within an enclosure that basis the theory of the image method is presented next, together with previous research on the subject.

7.2.1 Introduction

One of the main relations in room acoustics is that between the sound absorption of the room surfaces and the distribution of sound energy density within the enclosure. Sabine [10] assumed a diffuse field, i.e. the energy density was equally distributed throughout the room, and at any point the energy flow was the same in all directions. With this consideration, he derived the expression governing the transient decay rate, shown in equation (7.1). The expression fails for high values of absorption and predicts a finite value of $0.16V/S$ for reverberation time when $\bar{\alpha} = 1$.

Later, Eyring [11] considered a wavefront travelling a fixed distance (the mean free path) between successive reflections at which it loses the same fraction of its incident energy. Eyring's expression for the reverberation time, more generally accepted, is given by:

$$T = \frac{0.16V}{-S \ln(1 - \bar{\alpha})} \quad (7.5)$$

with,

$$\bar{\alpha} = \frac{1}{S} \sum_i S_i \alpha_i \quad (7.6)$$

Millington's [12] formula differs from equation (7.6) in the way the different absorption coefficients are averaged only, which is replaced by an "absorption exponent",

$$\bar{\alpha} = -\frac{1}{S} \sum_i S_i \ln(1 - \alpha_i) \quad (7.6a)$$

which predicts a reverberation time of zero if a ray strikes a surface having a coefficient absorption $\alpha_i = 1$.

All expressions can be completed by taking into account the air attenuation constant m , which is

responsible for the attenuation of sound during its free propagation, and adding a term $4mV$ to the denominator [30].

The steady-state method of measuring room absorption was investigated by Knudsen [31]. Using a constant source power with output Q , he obtained values for the room absorption in agreement with those deduced from the reverberation time method, using the relation:

$$\bar{\alpha} = \frac{4}{cS} \frac{Q}{E_0} \quad (7.7)$$

where E_0 is the average energy density measured in the far field.

In both steady state and transient methods, the assumption is of a diffuse sound field, only achieved in very careful acoustical conditions, if so. Frequently, either the absorption is not evenly distributed along the room surfaces, contributing to the non-random energy patterns or one of the room dimensions is greatly different from the other two, like in open plan offices. The uneven distribution of absorption is present in HEVAC's test method, as the room has all surfaces highly reflective but one, which contains either the aperture or the louvre. Both situations have a distinguished high absorption coefficient compared to the other surfaces. Therefore, this classical approach should not be used to predict the sound pressure levels in the room and, consequently, relate them later to the sound field at the receiver position, outside HEVAC's test room. It is desirable to relate the energy distribution to the absorption pattern on the boundary surfaces, rather than the average values of energy to average absorption in the room.

7.2.2 Theory

The image method bases its concept on the optical analogy stating that when a sound source of power Q is placed near a boundary plane an image source will result with a power $(1-\alpha)Q$, where α is the absorption coefficient of the boundary averaged over all angles of incidence. The principle of the method is shown in Figure 7.2. Provided that the surface is plane, the reflection of sound rays originating from a certain point can be illustrated by the construction of an image source. The propagation path of the reflected ray takes place along the lines that connect the

image source to the receiving point and from the source position to the point of intersection of the line image-source/receiver with the plane. Once the associated image source is constructed, the wall can be disregarded altogether, the effect of which is now replaced by that of the image source [32].

A second order image source is generated by the mirror image of one of first order, corresponding to a ray that has suffered two successive reflections, as shown in Figure 7.3. The succession of reflections continues until the rays either arrives at a perfectly absorbent surface or its energy content becomes vanishingly small. All this higher order reflections are constructed by the same principle applied to generate the first image source. Continuing in this way, more and more image sources are generated, while the propagation path increases and the correspondingly energy contribution decreases. Figure 7.4 illustrates the construction of image sources of some higher orders in an infinite flat room.

In the past, some applications of the image method have been made, as for instance, in theoretical studies of sound behaviour in rooms [33,34].

Power [35] used the assumption of an image source with an effective power determined by the absorption of the surface mirror to predict the acoustic response of large offices, where the ceiling height is much smaller compared to the plan dimensions. If the source has a power Q then an image source was assumed to have a power given by:

$$Q_n = (1 - \alpha)^n Q \quad (7.8)$$

where n is the order of the image. Having assumed the ceiling as totally absorbent, the images of the sources were consequently confined to two planes, one through the real source and the second resulting from the first reflection from the source. The energy density at the receiver was given as the summation of the energy densities due to each point and a time dependent expression was derived to obtain the reverberation time.

Gibbs [36] applied the method to predict variations in sound pressure level throughout a rectangular room possessing various absorption configurations. It was found out that varying the

absorption coefficient with angle of incidence gives little or no improved correlation with measured values than the simpler model that assumes a constant value of absorption coefficient. The predicted values correlated better with experimental data than the classical prediction, which assumes a diffuse sound field. Dance developed a model based on the earlier one by Gibbs, and later improved by considering the sources as coherent and the phase information due to different path lengths taken into account simulating interference effects [37,38].

Lindqvist [39] used the method to account for the presence of furnishings under the assumption that they are isotropically distributed in random fashion throughout the room. In this case, the furnishings, as well as the sources, are mirrored in the room surfaces. The steady state and decaying sound fields are formed as before. However, the contribution of each image source is modified due to scattering and absorption by the furnishings; absorption at surfaces is also increased due to scattering.

Arbitrarily shaped rooms, bounded by planes, have also been modelled by image methods [40]. Further applications of the method in architectural acoustics and studies of properties of rooms can also be found elsewhere [29,41].

7.2.3 General Model

The image method proposed is based on that presented by Gibbs [36] for a room with one surface covered by highly absorbent material. In the present case, the surface under consideration will contain either the louvre or the aperture.

Consider a simple rectangular room of dimensions α , β , γ metres in the x , y and z directions of a co-ordinate system with the origin at the room centre. If the six surfaces are plane and have a low absorption coefficient then, by optical analogy, a three-dimensional array of image cells, each one containing an image-source with same power output as the real source, is generated. Figure 7.5 illustrates the concept where it is seen the image-sources spatially distributed over the xy -plane. The darker cell represents the original room with the real sound source. The source and receiver co-ordinates are given by $[x_s, y_s, z_s]$ and $[x_r, y_r, z_r]$, respectively, and are both placed away from the room boundaries.

To describe each room (or cell) the integers l , m and n are used. Thus, the real room is described by the $(0,0,0)$ cell, whilst its neighbour along the positive x -axis is the $(l,0,0)$ cell. Figure 7.6 presents a segment of the xz -plane, which shows how the column $(0,0,n)$ is numbered. As a cell is a mirror image of its neighbour, it will be orientated as the real cell only if l , m , and n are even.

The distance vector d , from the image-source in cell (l,m,n) to the real receiver has its components given by:

$$\begin{aligned}d_x &= (\alpha l \pm x_s) - x_r \\d_y &= (\beta m \pm y_s) - y_r \\d_z &= (\gamma n \pm z_s) - z_r\end{aligned}\tag{7.9}$$

The positive terms in the brackets are used when l , m and n are positive, similarly for negative integers the negative sign is used.

The distance is given by:

$$d_{l,m,n} = \sqrt{d_x^2 + d_y^2 + d_z^2}\tag{7.10}$$

The contribution to the energy intensity at the receiver position from each image will be modified by:

- i) a reduction in intensity obeying the inverse square law;
- ii) absorption at each real and imaginary boundary between the image and receiver;
- iii) attenuation due to air absorption.

For an image sound source of power Q [watts] at a distance d [metres] from the receiver the intensity at the receiver is given by:

$$I = \frac{Q}{4\pi d_{l,m,n}^2} \text{ [W/m}^2\text{]}\tag{7.11}$$

The number of boundary reflections suffered by a sound ray assumed to have come from the source in an image cell (l,m,n) can be seen to be equal to $N_b = |l| + |m| + |n|$. Therefore, modifying equation (7.11) to include boundary absorption gives,

$$I = \frac{Q}{4\pi d_{l,m,n}^2} (1 - \alpha')^{N_b} \quad (7.12)$$

where α' is the absorption coefficient of the surface averaged over all angles of incidence. To take into account air absorption, equation (7.12) is multiplied by an exponential term giving,

$$I = \frac{Q}{4\pi d_{l,m,n}^2} (1 - \alpha')^{N_b} e^{-m_a d_{l,m,n}} \quad (7.13)$$

where d is that given by equation (7.10). Expressed as sound pressure level, the contribution of an image source in a cell (l,m,n) to the sound pressure level at the receiver is given by,

$$SPL = 10 \log \frac{Q}{4\pi d_{ref}^2} + 10 \log [d^{-2} (1 - \alpha')^{N_b}] \quad (7.14)$$

Summation of all the contributions from real and imaginary source gives the total sound intensity at the receiver,

$$IL = 10 \log \left(\sum_{l=0}^{|B-A|} d_{l,m,n}^{-2} (1 - \alpha')^{N_b - l_2} (1 - \alpha'')^{l_2 - 1} \tau e^{m_a (l - d_{l,m,n})} \right) \quad (7.15)$$

The range of values of the integers l,m,n is determined with respect to the desired accuracy required of the prediction. This will be discussed in the section dealing with the preliminary simulations.

If equation (7.15) is rewritten in the form

$$I_t = KI_0 \quad (7.16)$$

then if

$$I_0 = \frac{Q}{4\pi} e^{-m_a} \quad (7.17)$$

is the intensity at a distance of 1 metre from the sound source in free field conditions and

$$K = \sum_{-l}^l \sum_{-m}^m \sum_{-n}^n d_{l,m,n}^{-2} (1 - \alpha')^{N_b} e^{m_a(1 - d_{l,m,n})} \quad (7.18)$$

the total sound pressure level at the receiver is given by

$$SPL_r = SPL_{lm} + 10 \log K \quad (7.19)$$

Now, let the wall described by the equation,

$$x = \frac{\alpha}{2} \quad (7.20)$$

contain either the louvre or the aperture having an absorption coefficient α'' greater than that of the remaining five surfaces. For an image cell (l, m, n) there will be a total of $N_b = |l| + |m| + |n|$ reflections of which l_2 will involve the wall with the higher absorption coefficient. l_2 is given by the expression,

$$\begin{aligned} l_2 &= |l|/2 && \text{for } l \text{ even} \\ l_2 &= (l+1)/2 && \text{for } l \text{ odd positive} \\ l_2 &= (|l|-1)/2 && \text{for } l \text{ odd negative} \end{aligned} \quad (7.21)$$

Therefore, the factor K in equation (7.18) now becomes,

$$K = \sum_{-l}^l \sum_{-m}^m \sum_{-n}^n d_{l,m,n}^{-2} (1 - \alpha')^{N_b - l_2} (1 - \alpha'')^{l_2} e^{m_a(1 - d_{l,m,n})} \quad (7.22)$$

7.2.4 Implementation of the Method

Prior to the simulation of the HEVAC test facility, some investigations were carried out. Firstly, a set of preliminary tests of the model considered the measurements as performed in the transmission suite. If this condition were correctly modelled, then the HEVAC simulation would be properly implemented. Some changes introduced to the general model, presented in section 7.2.3, are common features of both the HEVAC method and impulse measurements. New expressions that govern the number of total reflections suffered by the ray are presented.

Figure 7.7, which shows the set-up for 45 degrees of incidence as an example, presents the xy -plane of the image diagram common to both methods. Regardless of room dimensions, both situations are similar as far as the requirements of the simulation are concerned. The microphone is placed in an adjacent room to the source room, where the latter now plays the role of cell $(0,0,0)$ for the image method approach. For both cases, five out of six surfaces are reflective, with absorption coefficient α' , and the wall that contains either the louvre or the aperture, has an absorption coefficient α'' .

Thus, with the microphone outside the source room, the number of total reflections is now

$$N_b = |l| + |m| + |n| + 1 \quad (7.23)$$

Among all image cells, which can be of infinite number, some of them do not contribute to the total intensity at the receiver position. If an image-cell falls within a solid angle (three-dimensional) that is “out of sight” for the microphone, then there is no contribution from this source. For an image cell to be considered, the angles on the xy - and xz -plane formed by the image ray line and the normal to the surface of absorption coefficient α'' must fall within the angle given by θ_y and θ_x , as indicated in Figure 7.7 and 7.8, respectively. This angle is determined by the “line of sight” of the microphone, which means that the cells outside this “visible” area do not contribute to the overall level; these cells are shaded in both Figures 7.7 and 7.8. This restriction applies because any image outside these limits produces a ray with a last reflection not at the aperture or louvre but at the room boundaries. This is correct neither for the impulse response measurements, which deals with direct transmission only, nor for the HEVAC

measurements, as the microphone is placed outdoors and the environment was modelled as free-field.

As the negative cells do not exist, in consideration of the microphone's line-of-sight, l_2 for the positive cells is now given by:

$$\begin{aligned} l_2 &= l + 1 && \text{for } l = 0 \\ l_2 &= (l/2) + 1 && \text{for } l \text{ even} \\ l_2 &= (l+1)/2 && \text{for } l \text{ odd} \end{aligned} \quad (7.24)$$

Another common characteristic to both simulations is regarding the aperture and louvre dimensions. As insertion loss measurement is a relative parameter, the whole surface in between source and receiver rooms was considered containing either the aperture or the louvre. Therefore, the two configurations had the surface α' increased by the same area and any ray that strikes the connecting wall will be transmitted whilst attenuated by the transmission coefficient of the element (the transmission coefficient of the louvre or the unity for the aperture).

Modifying expression 7.22 to include attenuation suffered by the image ray when it crosses the room boundary gives,

$$K_{\text{louvre}} = \sum_0^l \sum_{-m}^m \sum_{-n}^n d_{l,m,n}^{-2} (1 - \alpha')^{N_b - l_2} (1 - \alpha'')^{l_2 - 1} \tau e^{m_a(1 - d_{l,m,n})} \quad (7.25)$$

where τ is the transmission coefficient of the louvre. When the model deals with the aperture, to calculate the original sound pressure levels without the partition in analysis, K takes the form of

$$K_{\text{aperture}} = \sum_0^l \sum_{-m}^m \sum_{-n}^n d_{l,m,n}^{-2} (1 - \alpha')^{N_b - l_2} e^{m_a(1 - d_{l,m,n})} \quad (7.25a)$$

Although for the aperture, α'' is equal to unity and hence $(1 - \alpha'')$ is equal to zero, the term $(1 - \alpha'')^{l_2 - 1}$ present in equation (7.25) must be removed from equation (7.25a). It is assumed that there is no reflection from the aperture and a ray crossing an image surface of α'' is

meaningless. Therefore, any cell that has I_2 greater than unity is disregarded by the model since a mathematical non-determination (0^0) would arise if the term were left in the expression.

By definition (as presented in section 2.1.3), the insertion loss of the louvre is the difference in sound pressure levels before and after the partition is placed in the aperture, given by:

$$IL = SPL_{before} - SPL_{after} \quad (7.26)$$

Substituting equation (7.19) into equation (7.26) and using equation (7.25) and (7.25a) gives the predicted insertion loss by the image model

$$IL = SPL_{1m} + 10 \log K_{aperture} - SPL_{1m} - 10 \log K_{louvre}$$

$$IL = 10 \log K_{aperture} - 10 \log K_{louvre} \quad (7.27)$$

The calculations from these simple equations were very fast and the problem of summing the contributions of many image sources to the sound field at a receiver point was easily handled. Equation (7.27) was the basis for the computer programs, written in Fortran, for all simulations by the image method (see listing in Appendix 6).

Although the number of images can be thought of being infinite, it is necessary to consider only the contributions of images within a sphere of influence the centre of which coincides with the real room. The radius of this sphere of influence is dictated by the room absorption, the required accuracy of the prediction of sound pressure level at a point, and, finally, the time of computation. The last point is important in that if the sphere radius is doubled the computation time is increased eight-fold.

An investigation was carried out to set the radius to all simulations, which would determine the number of cells to be considered in equation (7.25) and (7.25a). A computer program was produced, which calculated the sound pressure level at a receiver position for various radii of the sphere of influence for two configurations, that of the aperture and of the louvre. Table 7.1 shows the radii investigated and the number of cells considered in each case. Figures 7.9 and 7.10

show the resulting sound pressure levels at a fixed receiver position for the louvre and aperture configurations, respectively, for the various radii. Considering that for a radius of 100 metres the computational time was quite long (19 minutes) and that insertion loss is a relative calculation, a radius of 50 metres was considered sufficiently accurate and was adopted throughout all computations.

TABLE 7.1 - Number of cells considered for different radii of influence

Number of cells	Radius [metres]					
	6	20	50	100	200	468
<i>L</i>	3	9	21	41	83	193
<i>M</i>	3	7	19	35	71	163
<i>N</i>	3	11	25	47	95	221
Total	9	27	65	123	249	577

Another input parameter for the model is the absorption coefficient of the hard walls, α' . Gibbs [36] compared the results of an image model assuming a random incidence and assuming that the absorption coefficient varied with angle of incidence of the sound ray. The conclusion was that the difference between the two distributions of sound pressure levels within the room was too slight to justify the additional computational time. This will not be true for the louvre, which has transmission strongly dependent upon the incident angle, as seen in Chapter 5. However, for the initial simplified model, an angle independent absorption coefficient for the louvre was adopted and a diffuse coefficient of the hard walls used throughout the simulations. As far as the latter is concerned, Chapter 3 presented the transmission loss measurements of the same configuration that of the louvre covered by wooden panels. To obtain the *TL* for this partition a measurement of the reverberation time of the receiving room was necessary. Therefore, the diffuse absorption coefficient was derived from this measurement.

The attenuation of sound in air, another input parameter for the model, has been determined experimentally by several authors and the data in Kuttruff [42], shown in Table 7.2, were used.

TABLE 7.2 - Air attenuation constant m for different frequency bands.

Freq.	500	1k	2k	3k	4k	6k
m	0.00047	0.00074	0.00164	0.00312	0.00518	0.01098

7.2.5 Preliminary investigation

The new set of equation was first tested in some preliminary relations of transmission loss measurements by impulse. A basic image model, considering all parameters angle independent and with the louvre with no absorption (i.e. the energy is partially transmitted and/or reflected), was related to some results. Table 7.3 summarises the procedure adopted in the validation of this basic model. It describes the adopted reflection factor of the louvre, which components of equation (7.27) were taken into account, which result the simulation was compared with and the frequency resolution of the analysis. In the general model, the reflection factor R was given by $(1-\alpha)$, where α represented all energy that was not reflected back. The reflections from the louvre, R contains terms that depend on partially transmitted and partially absorbed components. Naturally, any change in variable represents some modification to the model, and they will be described along with the results. Except when stated differently, all tests have the model related to the set-up of 45° of incidence.

The first test, with results shown in Figure 7.11 assumed the reflection factor and transmission coefficient are constant with frequency and angle of incidence ($R = 0.9$ and $\tau = 0.1$). As the reverberant field inside the HEVAC enclosure is lower with the aperture, then, less image cells contribute to the overall level and equation (7.25a) has fewer terms in the summation than equation (7.25). The contribution from the remaining cells is frequency dependent, and so is the resulting insertion loss, as observed.

The second investigation does not require the reflection factor of the louvre because it predicts the direct field only. The angle average transmission loss coefficient, $\bar{\tau}_\theta$, which the direct component is attenuated by, is presented in Figure 7.12. The transmission loss measured by impulse response, where $\bar{\tau}_\theta$ was derived from, was presented in Chapter 5.

TABLE 7.3 - Image model parameters for different angle independent preliminary tests

Figure Number	Reflection Factor of Louvre, R	Components Considered	Results Compared to	Freq. Resolution
7.11	$R = \text{constant}$	All components	Theory	1/3 oct.
7.13	—	Direct only	Impulse aver.	MLSSA
7.14	$R = 1 - \bar{\tau}_\theta - \alpha''_{\Delta=0}$	All components	Impulse aver.	MLSSA
7.15	$R = 1 - \bar{\tau}_\theta - \alpha''_{\Delta=0}$	All components	Impulse aver.	1/3 oct.
7.16	$R = 1 - \bar{\tau}_\theta - \alpha''_{\Delta=0}$	All components	Impulse 45°	1/3 oct.
7.17	$R = 1 - \bar{\tau}_\theta - \alpha''_{\Delta=0}$	All components	Impulse -45°	1/3 oct.
7.18	$R = 1 - \tau_{-45^\circ} - \alpha''_{\Delta=0}$	All components	Impulse -45°	1/3 oct.
7.19	$R = 1 - \tau_{45^\circ} - \alpha''_{\Delta=0}$	All components	Impulse 45°	1/3 oct.

This investigation confirms the equivalence of transmission loss and insertion loss when the latter deals with a direct field only. To model this situation, the image model takes into account cell $(0,0,0)$ solely and disregards the contribution of the reverberant field. Figure 7.13 shows the agreement obtained between the image model and the curve for angle averaged impulse response.

Direct and reverberant fields were taken into account for the next step; the resulting curve is presented in Figure 7.14 along with the same measured impulse data presented as in Figure 7.13. The model disregards any absorption given by the louvre ($\alpha'' = 0$), and the reflection factor depends upon the angle average transmission coefficient $\bar{\tau}_\theta$ only, presented in Figure 7.12. In this case, where absorption coefficient is not taken into account, the predicted insertion loss is lower than the measured transmission loss. This will be discussed in the section dealing with HEVAC test simulation.

The next modification introduced to the model concerned the frequency resolution. In the process of constructing the image model the results have been compared to the impulse

measurements so far, whose frequency resolution is 14 Hz. As HEVAC test procedure is performed in 1/3 octave bands, the model was altered accordingly as shown in Figure 7.15.

These preliminary tests show that the computer model is correct but it is not a simulation of the HEVAC test facility, as the angle of incidence of the image rays has not been considered. Whenever an image ray strikes the room boundaries it is reflected back attenuated by an angle average reflection coefficient. Figure 7.16 illustrates this condition and shows the disagreement when, instead of an average transmission coefficient, the model includes values of τ for 45° degrees. The discrepancy between measured transmission loss and predicted insertion loss is greater if a different set-up is used, since 45° is the dominant incident angle to the overall performance, as seen in Chapter 5. With the set-up changed to -45° degrees, but the model still using average τ , Figure 7.17 shows the curve for the image model compared to the impulse response for this set-up.

Not only the average incident angle was investigated. Figures 7.18 and 7.19 show the results when the model had specific transmission coefficient for 45° and -45° of incidence as input and the respective impulse response curves. Although a nearly constant displacement from the experimental results can be observed, the model is not angle independent yet, as it is still independent of the incident angle.

In the process of improving the model, the next component taken under consideration was the absorption coefficient of the louvre. For this purpose, reverberation time measurement was carried out according to ISO 354 [43] with the same procedure and equipment already presented in Chapter 3. To obtain the absorption coefficient of the louvre, shown in Figure 7.20, the reverberation time of the room was measured twice, with and without the louvre covered by a heavy wooden panel. Figure 7.21 shows the model result for the set-up of 45° of incidence using $R = 1 - \tau_{45^\circ} - \alpha_{diffuse}$ as the reflection factor of the louvre and compared to the transmission loss measurement of this set-up. The same relation is shown in Figure 7.22 for -45° of incidence.

All set-ups have been tested and the agreement showed here was observed in all configurations. Figure 7.23 and 7.24 show the difference between TL measured by impulse and IL given by the image model for -45° and 45° set-ups, respectively, with and without the absorption of the louvre

is taken into account.

From these last comparisons, the importance of assessing the absorption of the device in characterising insertion loss is confirmed. When absorption coefficient of the louvre is taken into account the agreement between the model and measurement increases. To confirm the important role played by absorption the model has had different coefficients as input. Figure 7.25 shows the model results for angle average attenuation when no absorption, half of the real values for diffuse incidence and the measured absorption coefficient are used as input data. It can be seen that as long as the absorption approximates to its real values the model shows increased agreement with measurements.

7.2.6 Simulation

With the model validated changes were introduced so as to simulate the HEVAC test procedure. The angle dependency for the transmission coefficient of the louvre was included and the room geometry, receiver and source position modified in the image diagram so as to simulate the specifications presented in Chapter 2. Absorption coefficients of room and louvre were kept angle independent, the former based on previous research that showed the refinement is unnecessary and the latter would be made angle dependent later.

Figure 7.26 presents the lay-out for source room, which is cell $(0,0,0)$ and has the origin of coordinates in its centre, as before. The region where the microphone is positioned (outside) is assumed free field. Therefore, all specifications concerning minimum distances between louvre and building elements that could be an obstruction are contemplated. The model has considered one point source.

The introduction of angle dependency transmission coefficient for the louvre modifies equation (7.25) into:

$$K_{louvre} = \sum_0^l \sum_{-m}^m \sum_{-n}^n d_{l,m,n}^{-2} (1 - \alpha')^{N_b - l_2} (1 - (\tau_\theta + \alpha'') \sin \theta_z)^{l_2 - p - 1} (1 - (\tau_{-\theta} + \alpha'') \sin \theta_z)^p \tau \sin \theta_z e^{n\alpha(1 - d_{l,m,n})} \quad (7.28)$$

where τ_θ and $\tau_{-\theta}$ are the transmission coefficients of the louvre for an incident angle θ and for its complementary angle $-\theta$, respectively, p is the number of reflections occurred from this complementary angle and θ_z is the azimuth angle of the incident ray.

Every ray crosses a certain number of α'' surfaces by a different angle because, as explained in section 7.2.3, the louvre will be orientated as it is in the real cell only if l, m, m are all even. Consequently, an image ray line forms an angle of 35° with some of the image louvre and of -35° with other image louvres, for example. The term dependent upon θ_z reflects the behaviour of all surfaces due to grazing incidence, in that reflection and transmission are cancelled by the term $\sin\theta$. An angle dependent transmission coefficient means that a value for each possible incident angle is necessary.

The measurements by impulse response were performed for nine angles in 15° step, analysed in 18 frequency bands. Therefore, a function to describe the measured results was necessary.

To the nine measured data in each frequency band the known results at the extremes of the scale was added, which describe sound transmission as null for grazing incidence. A polynomial fit was chosen and although a 10th order polynomial would be necessary to get an exactly result along the points, a polynomial fit of 9th order was considered sufficiently good. Figures 7.27, 7.28, 7.29 and 7.30 show the measured points and the polynomial fit for the frequency bands from 100 to 315 Hz, 400 to 800Hz, 1k to 2k and 2.5k to 5k, respectively.

For the low frequency range, where τ varies smoothly with incident angle, the polynomial curve describes the measured data accurately. On the other hand, at higher frequencies, where interference results in a sharply varying transmission coefficient (although the absolute values are low), the polynomial fits may deviate from the measured results. If the function resulted in negative values, as seen in Figure 7.30 for -15° at 4 kHz, the program sets the value of τ to zero.

7.2.7 Results

Figure 7.31 presents the result for the HEVAC insertion loss simulation, considering an angle dependent transmission coefficient and diffuse absorption coefficient for the louvre.

For low frequencies, up to 1 kHz, insertion loss is dictated by the mass layer effect, with increased performance with increasing frequency. In this region, insertion loss is independent of incident angle, as it has been observed in the transmission loss measurements, the results of which are shown in Chapter 5.

For mid- frequencies, the two parameters show different characteristics. While *TL* measurements indicate a spread of values over a range of about 23 dB due to interference, *IL* varies about 5 dB only. In the high frequencies this behaviour is accentuated, with nearly 30 dB difference between highest and lowest values of *TL*, whereas *IL* changes by less than 10 dB. As the measurements by impulse were dealing solely with direct paths through the gaps the effect of interference is clearly observed, while the simulated HEVAC test is performed in diffuse to free-field conditions. Therefore, multiple rays arrive at the receiver and the total contribution is made up of peaks and anti-peaks cancelling each other as they are add up at the receiver point. For the same reason, the overall performance for each incident angle shows lower absolute values than that for *TL*.

This analysis is qualitatively only, because *IL* simulation and *TL* measurements have different set-ups. Impulse measurements were performed with the loudspeaker aligned with the receiver, whereas the simulated HEVAC procedure allows changes in microphone position only. Figure 7.32 illustrates the layout for *IL* simulation for the 30° set-up as an example, which corresponds to an incident angle of 9.4° in *TL* impulse measurement. Thus, in order to compare the two results, the transmission loss for all corresponding *IL* simulation was calculated from the measured results using the polynomial fits presented in Figures 7.27 to 7.30. For each incident angle a Fortran program calculated from the 18 polynomial functions, one for each frequency band, the predicted transmission loss for this set-up. The correspondence between angles of incidence for the two set-ups is shown in Table 7.4.

TABLE 7.4 - Correspondent incident angles between *TL* and *IL* set-ups.

Angle of Incidence									
<i>IL</i>	- 60	- 45	- 30	- 15	0	15	30	45	60
<i>TL</i>	1.35	5.08	9.40	14.12	19.08	24.20	29.38	34.56	39.66

Figure 7.33 presents the result for the eight *IL* simulations that have had the correspondent *TL* calculated from the prediction polynomial curve. It is worth emphasising that *TL* and *IL* deal with attenuation through different media. *TL*, obtained by the impulse method is calculated by comparison of direct components (free-field responses) and *IL* is obtained from simulation performed from diffuse to free field. Hence the *IL* simulation for each set-up will have infinite incident angles and the nine receiver positions quantify the louvre directionality. On the other hand, each *TL* set-up is the response for one incident angle only. The difference in source fields alters the mid- and high- frequency region, with *IL* simulation tending to vary less with frequency than *TL*.

The simulation for the set-up of 45° , the result of which is presented in Figure 7.34, is the only one that can be compared directly, as both *TL* and *IL* have source and receiver aligned and the same incident angle. The agreement is within 0.5 dB at the low frequency range and is within 1 dB at the mid- frequencies. The difference presented in the high frequency is between 2 and 4 dB.

HEVAC guide test procedure indicates that the Static Insertion Loss, *SIL*, should be calculated according to:

$$SIL = \bar{L}_{p2} - \bar{L}_{p1} \quad (7.29)$$

where \bar{L}_{p2} and \bar{L}_{p1} are the logarithmic mean octave band sound pressure level outside the building averaged over the nine specified angles without and with the louvre fitted in the aperture, respectively.

Figure 7.35 presents average *IL* calculated according to expression 7.27 and the predicted average *TL*. The slight difference at mid- and high frequencies is due to the characteristics of insertion loss itself. While *TL* is a property of the partition and its mounting conditions only, *IL* is a parameter that is result of the interaction of the partition under test and the test conditions.

Another parameter to evaluate is the Directivity Index *DI*. For each octave band, the *DI* in dB is obtained by the following formula:

$$DI = \bar{L}_p - L_p \theta, \quad (7.30)$$

where $L_p \theta$ is the value measured at angle θ for that octave band. Directivity of less than 2 dB may be ignored.

Figure 7.36 shows the directivity index calculated according to equation (7.30). It is observed that any significant directivity is within the range from 3k to 5k Hz.

This chapter has shown that by measuring the transmission loss coefficient by impulse response, which does not require any special facilities, a simple image method can simulate the field performance of the louvre. As the computer simulation has had the diffuse absorption coefficient as an input data, it so far does not comply with the thesis proposal, which was to have all data measured by impulse response. The next chapter presents the measurement of the reflection factor of the louvre. Then the data required for the field simulation is acquired by impulse response methods only.

7.3 REFERENCES

- [1] Davis A.H. and Fleming N., *Sound Pulse Photography as Applied to the Study of Architectural Acoustics*, J. Sci. Instrum., **3**, (1926).
- [2] Davis A.H., *The Analogy Between Ripples and Acoustic Wave Phenomena*, Proc. Phys. Soc., **38**, 234-239, (1925/1926).
- [3] Hodgson M. R. and Orłowski R. J., *Acoustic Scale Modeling of Factories. 1. Principles, Instrumentations and Techniques*, J. Sound Vib., **113**(1), 29-46, (1987).
- [4] Xiang N. and Blauert J., *Binaural Scale Modeling for Auralisation and Prediction of Acoustics in Auditoriums*, Appl. Acoustics, **38**(2/4), 267-290, (1993).
- [5] Harwood H.D. and Burd A. N., *Acoustic Scaling of Studios and Concert Halls*, Acustica, **28**, 330-340, (1973).
- [6] Hegrold L. W., *A 1:8 Scale Model Auditorium*, Appl. Acoustics, **4**, 237-256, (1971).
- [7] Day B. and White R. J., *A Study of the Acoustic Field in Landscape Offices with the Aid of a Tenth-Scale Model*, Appl. Acoustics, **2**, 161-183, (1969).
- [8] Barron M., *Auditorium Acoustic Modeling Now*, Appl. Acoustics, **16**(4), 279-290, (1983).

- [9] McCulloch C., *Acoustic Modelling - A personal view*, Acoustics Bulletin, **22**(4), 5-12, (1997).
- [10] Sabine W.C., *Collected Papers on Acoustics*, Peninsula Publishing, (1992).
- [11] Eyring C.F., *Reverberation Time in 'Dead' Rooms*, J. Acoust. Soc. Am., **1**, 217-241, (1930).
- [12] Millington G., *A Modified Formula for Reverberation*, J. Acoust. Soc. Am., **4**, 69-82, (1932).
- [13] ISO 3382 - *Measurements of the Reverberation Time of Rooms with Reference to Other Acoustical Parameters*, (1996).
- [14] Department of Transport, Welsh Office, HMSO, *Calculation of Road Traffic Noise*, Her Majesty's Stationery Office, (1988).
- [15] Maekawa Z., *Noise Reduction by Screens*, Applied Acoustics, **1**(3), 157-173, (1968).
- [16] Morse P.M. and Ingard K.U., *Theoretical Acoustics*, McGraw-Hill, New York, (1968).
- [17] Sysnoise, *Theoretical Manual*, Revision 5.1, Numerical Integration Technologies, (1993).
- [18] Zienkiewicz O.C., *The Finite Element Method*, McGraw-Hill, London, (1977).
- [19] Huebner K.H and Thornton E.A., *The Finite Element Method for Engineers*, Wiley, New York, (1982).
- [20] Ciskowski R.D. and Brebbia C.A., *Boundary Element Methods in Acoustics*, Elsevier Applied Science, London, (1991).
- [21] Lyons R.H., *Statistical Energy Analysis of Dynamical Systems. Theory and Applications*, Massachusetts: MTI Press, Cambridge, (1975).
- [22] Craik R.J.M., *Sound Transmission Through Buildings Using Statistical Energy Analysis*, Gower Publishing Limited, Hampshire (1996).
- [23] Ondet A.M. and Barbry J.L., *Modeling of Sound-Propagation in Fitted Workshops Using Ray Tracing*, J. Acoust. Soc. Am., **85**(2), 787-796, (1989).
- [24] Krokstad A., Strom S. and Sorsdal S., *Calculating the Acoustical Room Response by the Use of a Ray-Tracing Technique*, J. Sound Vib., **8**(1), 118-125 (1968).
- [25] Hodgson M. and Lewis D.N., *Case History: Application of Ray Tracing to the Modelling of Noise in a Food-Production Hall*, Noise Control Eng. J., **44**(5), 249-255, (1996).
- [26] Hodgson M.R., *Case History: Factory Noise Prediction Using Ray Tracing - Experimental Validation and the Effectiveness of Noise Control Measures*, Noise Control Eng. J., **33**(3), 97-104, (1989).

- [27] Giner J. and Militello C., *Ray-Tracing for Room Acoustics - Experiences and New Possibilities*, *Acustica*, **82**(S1), S 152, (1996).
- [28] Kuttruff H., *Room Acoustics*, 3rd. edition, Elsevier Applied Science, chapter IX, (1991).
- [29] Allen J.B. and Berkeley D.A., *Image Method for Efficiently Simulating Small-Room Acoustics*, *J. Acoust. Soc. Am.*, **65**(4), 943-950, (1979).
- [30] Kuttruff H., *Room Acoustics*, Elsevier Applied Science, Chapter V, 3rd edition (1991).
- [31] Knudsen V.O., *The Measurement of Sound Absorption in a Room*, *Phil. Mag.*, **5**, (1928).
- [32] Kuttruff H., *Room Acoustics*, Elsevier Applied Science, Chapter IV, 3rd. edition (1991).
- [33] Bolt R.H., Doak P.E. and Westervelt P.J., *Pulse Statistics Analysis of Room Acoustics*, *J. Acoust. Soc. Am.*, **22**(3), 328-340, (1950).
- [34] Mintzer D., *Transient Sounds in Rooms*, *J. Acoust. Soc. Am.*, **22**, 341-352, (1950).
- [35] Power J.R., *Measurement of Absorption in Rooms with Sound Absorbing Ceilings*, *J. Acoust. Soc. Am.*, **10**, 98-101, (1938).
- [36] Gibbs B.M., *The Inter-Relation Between the Distribution of Absorbent Material Amongst the Room Surfaces and the Distribution of Sound Energy and Reverberation Times within the Room*, Master Dissertation, University of Sheffield, (1970).
- [37] Dance S., Roberts J. and Shield B., *Computer Prediction of Sound Distribution in Enclosed Spaces Using an Interference Pressure Model*, *Appl. Acoustics*, **44**, 53-65, (1995).
- [38] Dance S.M. and Shield B.M., *Computer Prediction of Sound Propagation in Enclosed Spaces Using a Pressure Based Model*, *Proc. of 5th International Congress on Sound and Vibration*, 765-772, Australia, (1997).
- [39] Lindqvist E.A., *Noise Attenuation in Factories*, *Appl. Acoust.*, **16**, 183-214, (1983).
- [40] Borish J., *Extension of the Image Model to Arbitrary Polyhedra*, *J. Acoust. Soc. Am.*, **75**, 1827-1836, (1984).
- [41] Mayo C.G., *Standing Wave Patterns in Studio Acoustics*, *Acustica*, **2**, 49-64, (1951).
- [42] Kuttruff H., *Room acoustics*, Elsevier Applied Science, 3rd. edition (1991).
- [43] ISO 354:1985. *Measurement of Sound Absorption in a Reverberant Room*.

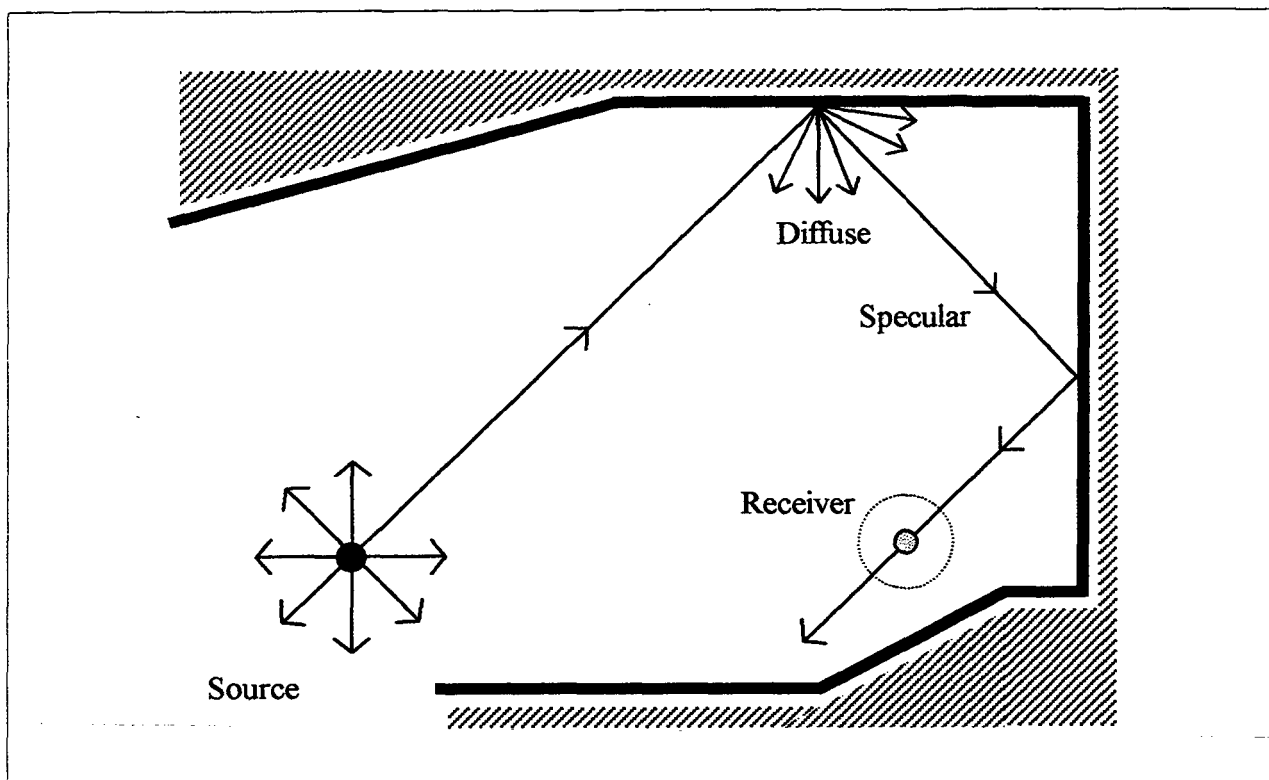


FIGURE 7.1 - Principle of ray-tracing: a ray is reflected, either specularly or diffusely, from a room boundary and it is followed until the receiver position.

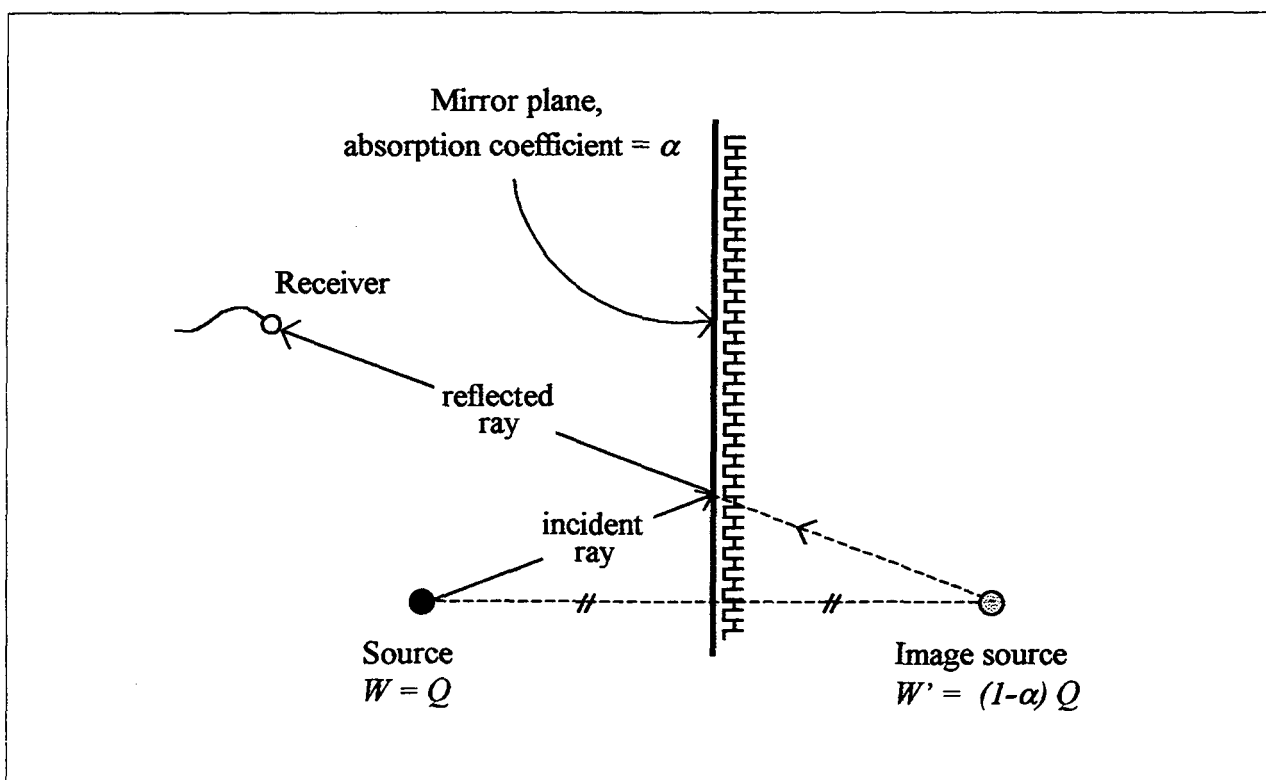


FIGURE 7.2 - Construction of the image source and its corresponding reflected ray.

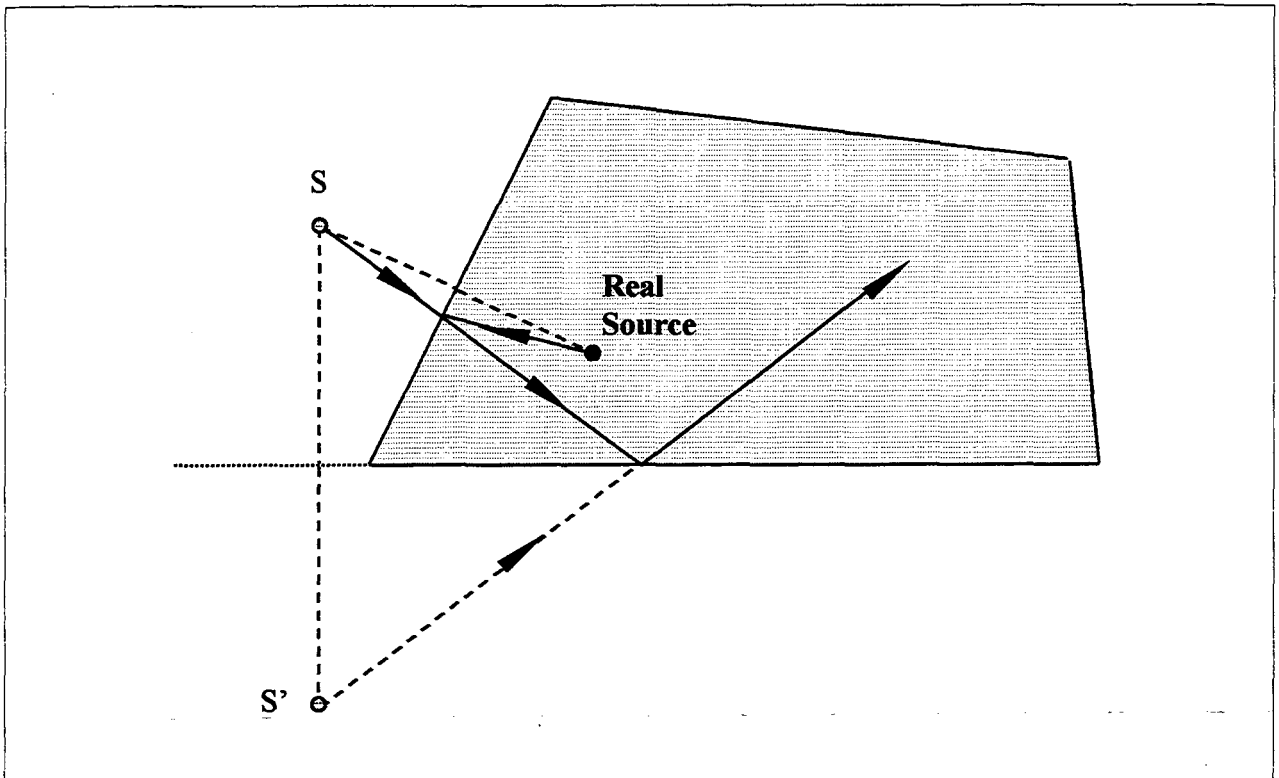


FIGURE 7.3 - Image sources of first and second orders [28].

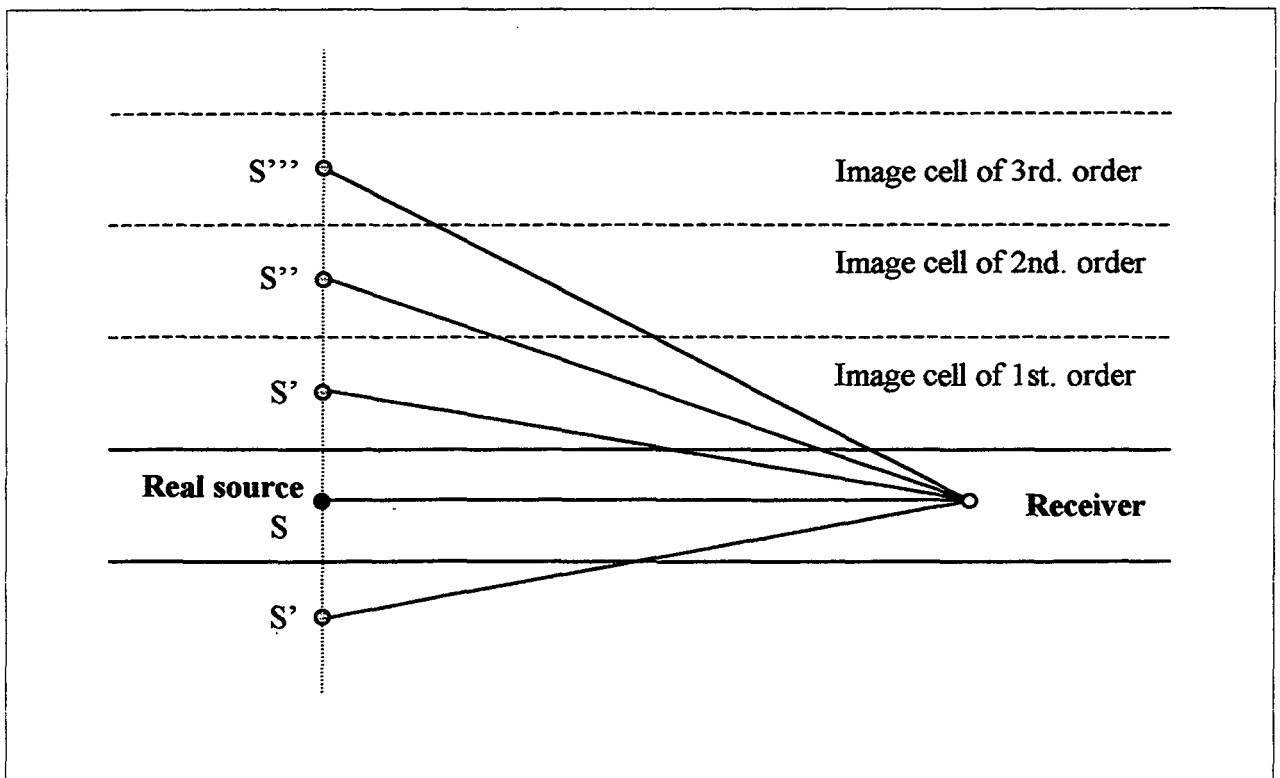


FIGURE 7.4 - System of image sources of an infinite flat room showing the first higher order image cells and their respective image sources and reflection contributions [28].

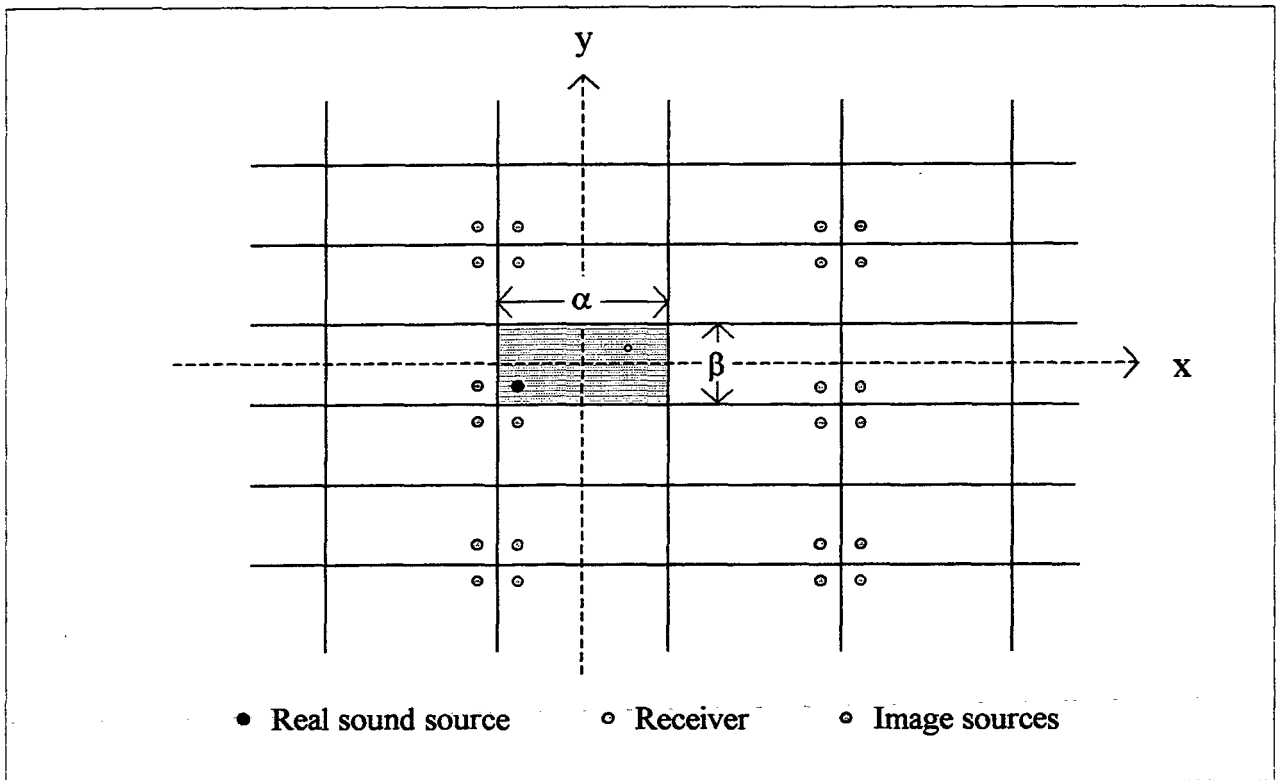


FIGURE 7.5 - Cross-section of the image system showing the xy -plane; the system repeats itself along the z -axis, from $-\infty$ to $+\infty$. The darker cell is the original room.

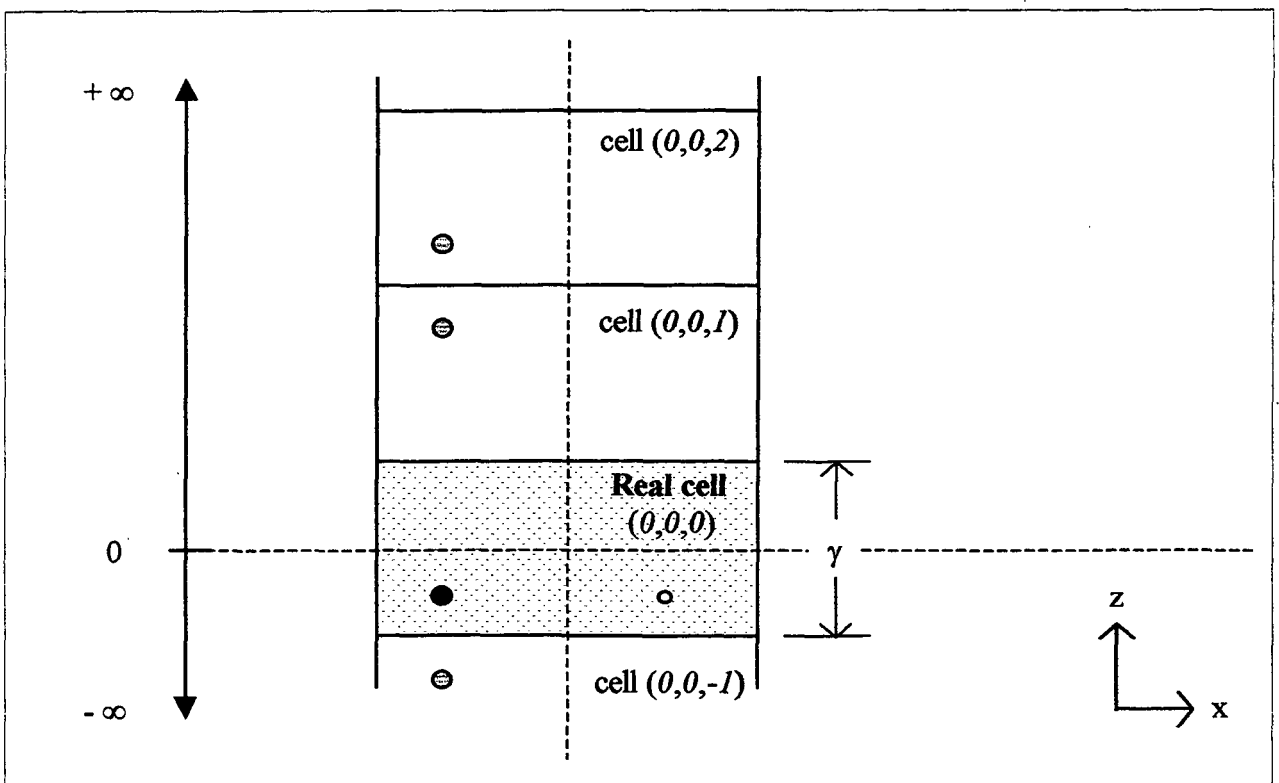


FIGURE 7.6 - Cross-section of the image system showing some elements along the $(0,0,n)$ on the xz -plane; cell $(0,0,0)$ is the real cell.

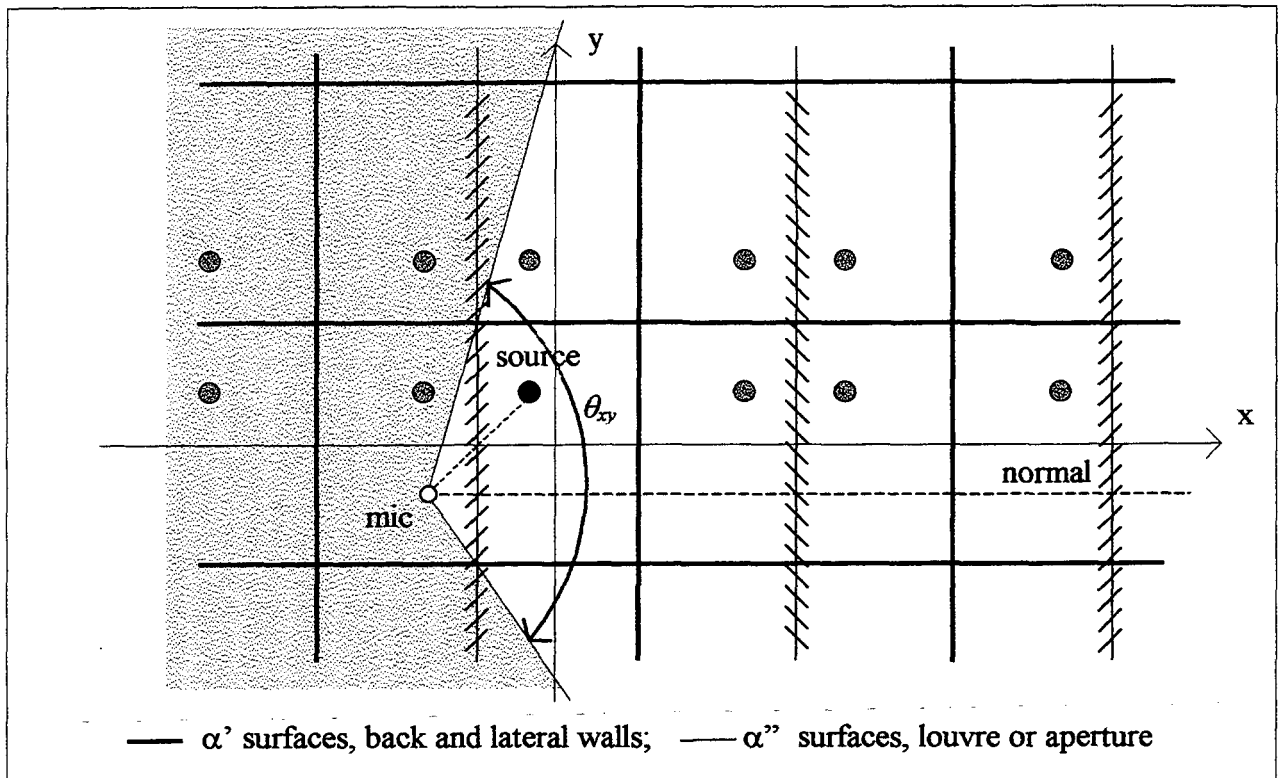


FIGURE 7.7 - xy -plane of image diagram for impulse measurements and HEVAC simulations; non-contributing image sources (shaded) are outside receiver's "line-of-sight".

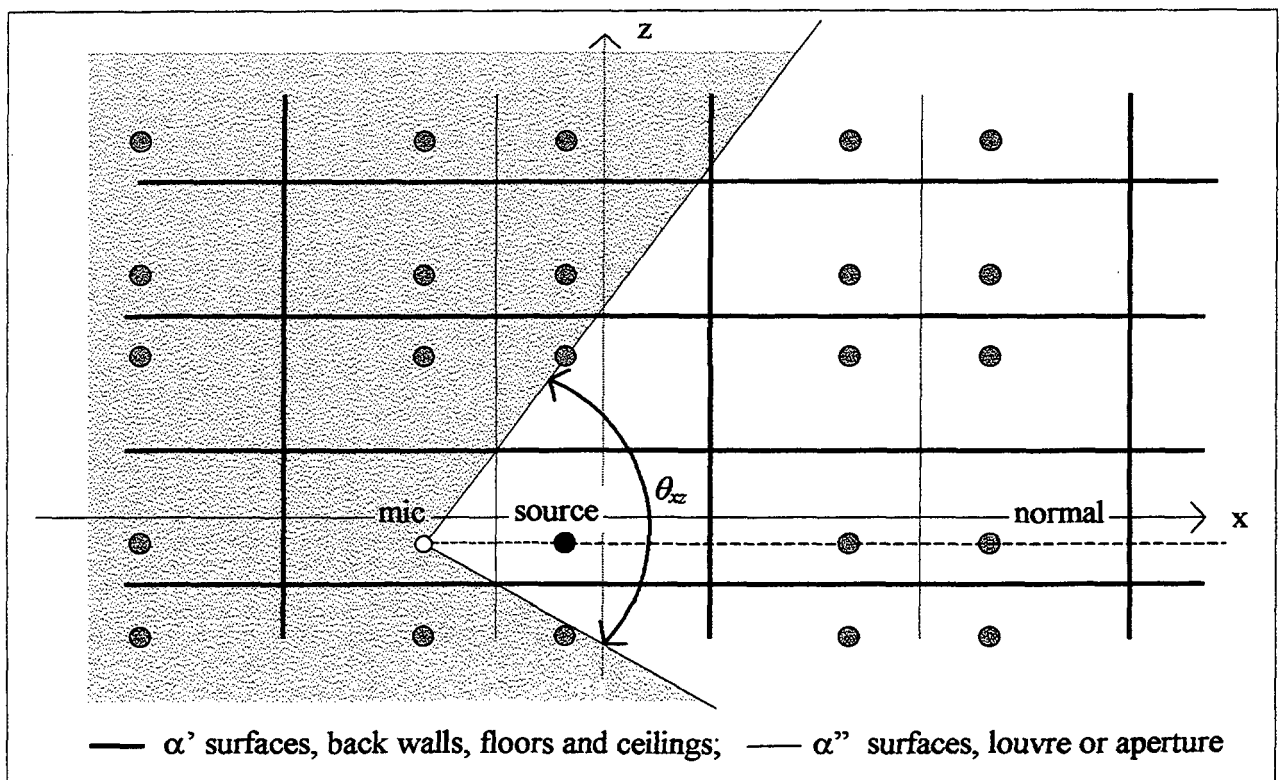


FIGURE 7.8 - xz -plane of image diagram for impulse measurements and HEVAC simulations; non-contributing image sources (shaded) are outside receiver's "line-of-sight".

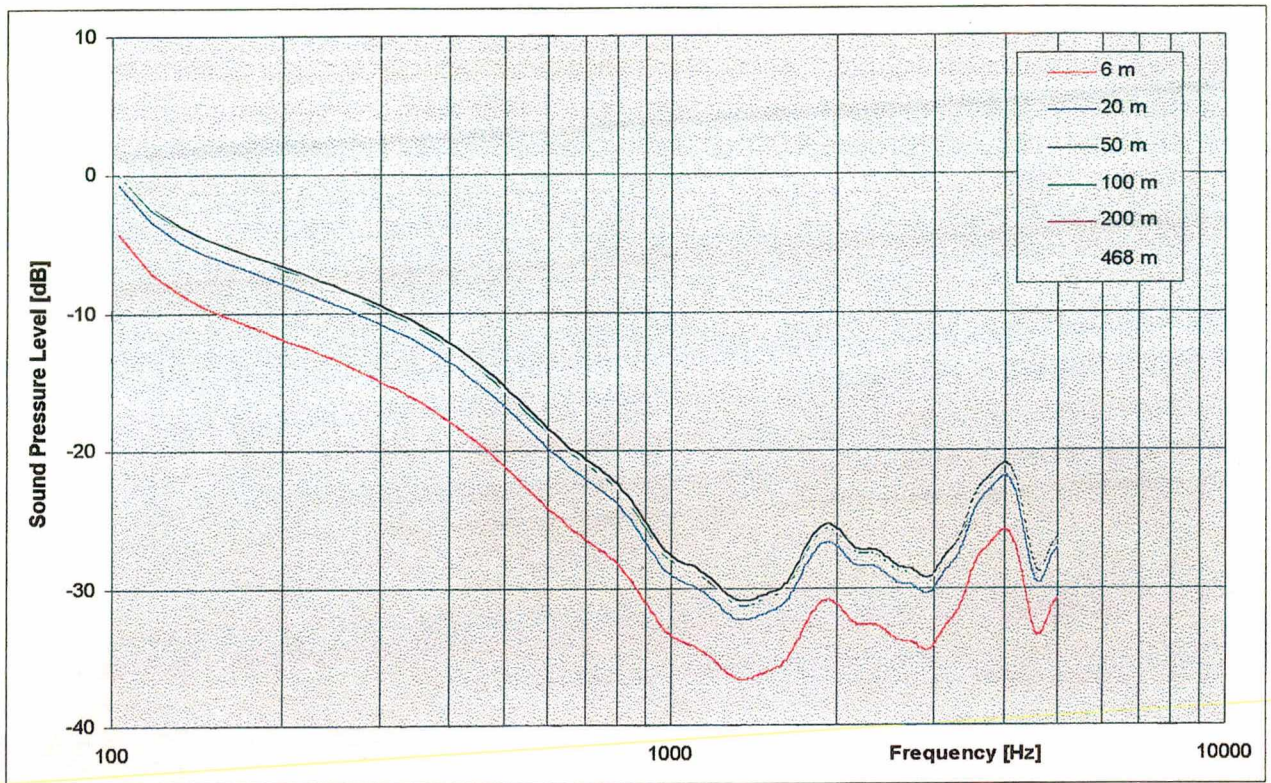


FIGURE 7.9 - Sound pressure levels for different radii of influence for the louvre.

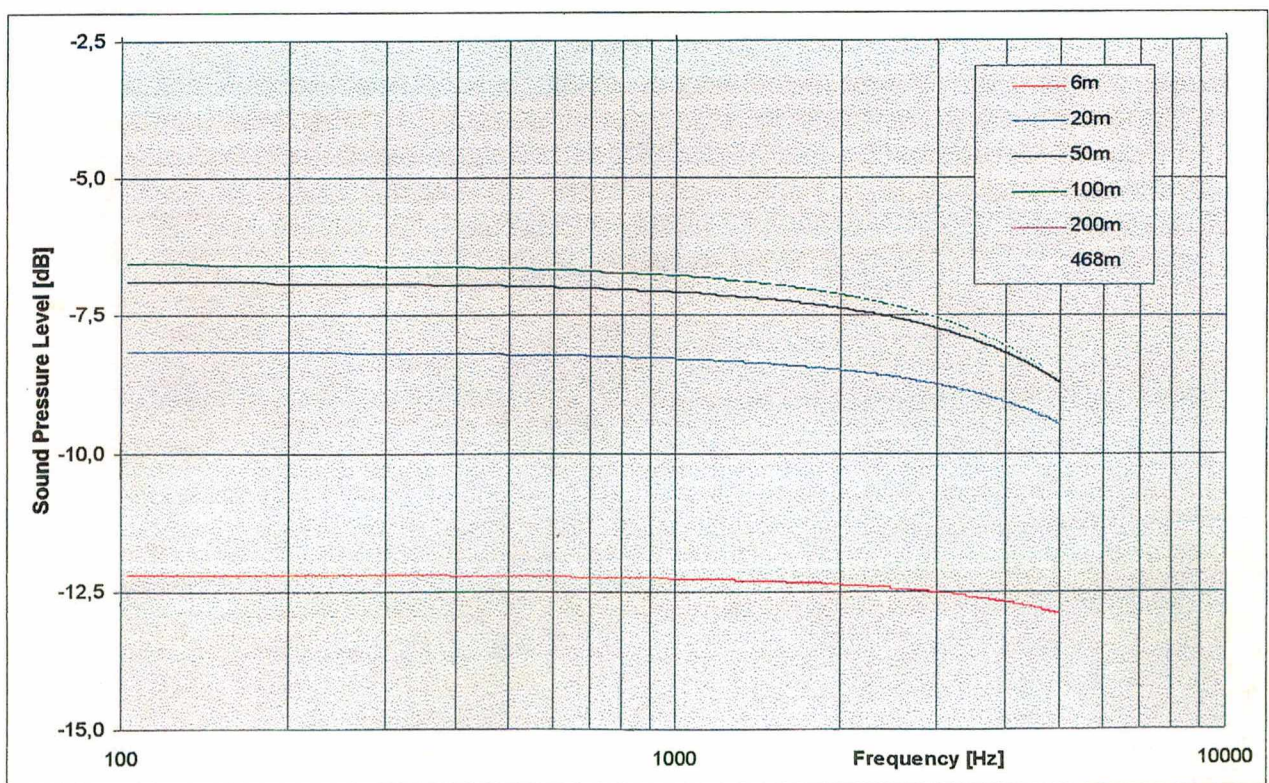


FIGURE 7.10 - Sound pressure levels for different radii of influence for the aperture.

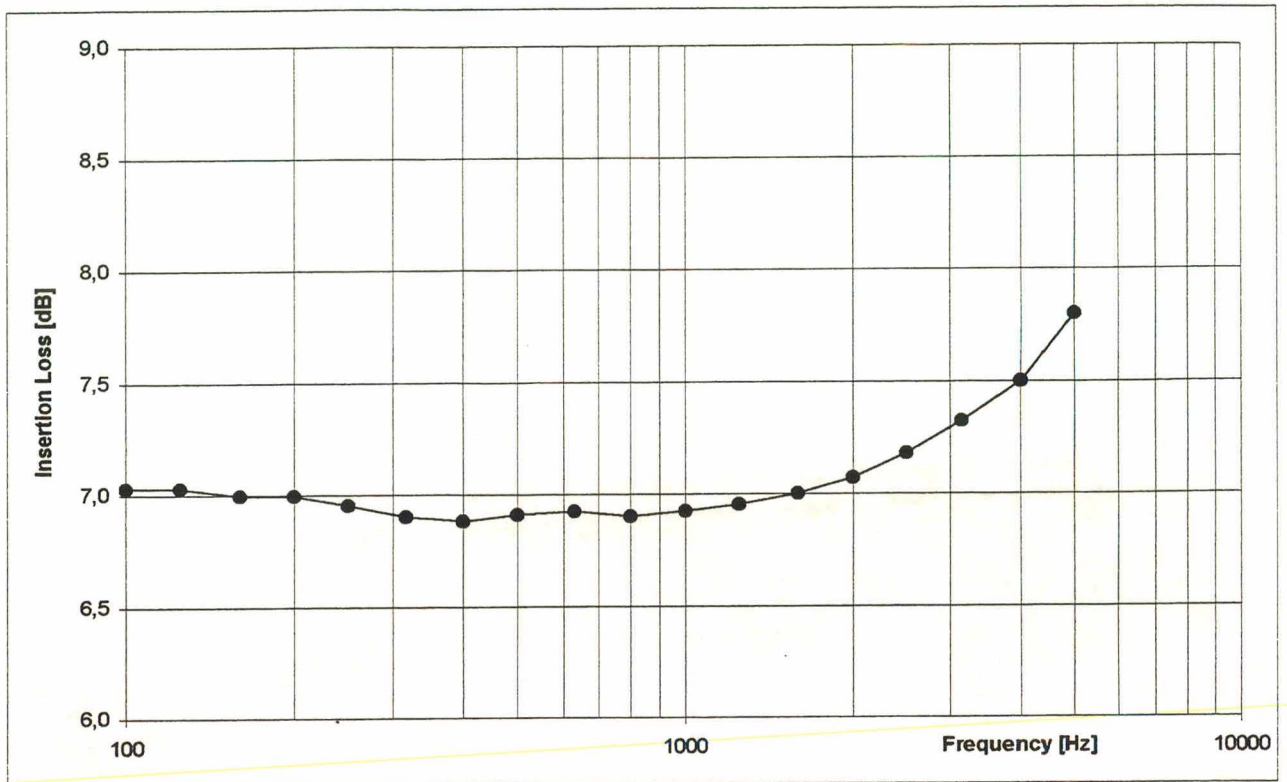


FIGURE 7.11 - Insertion loss simulation by image model for a constant reflection factor of the louvre.

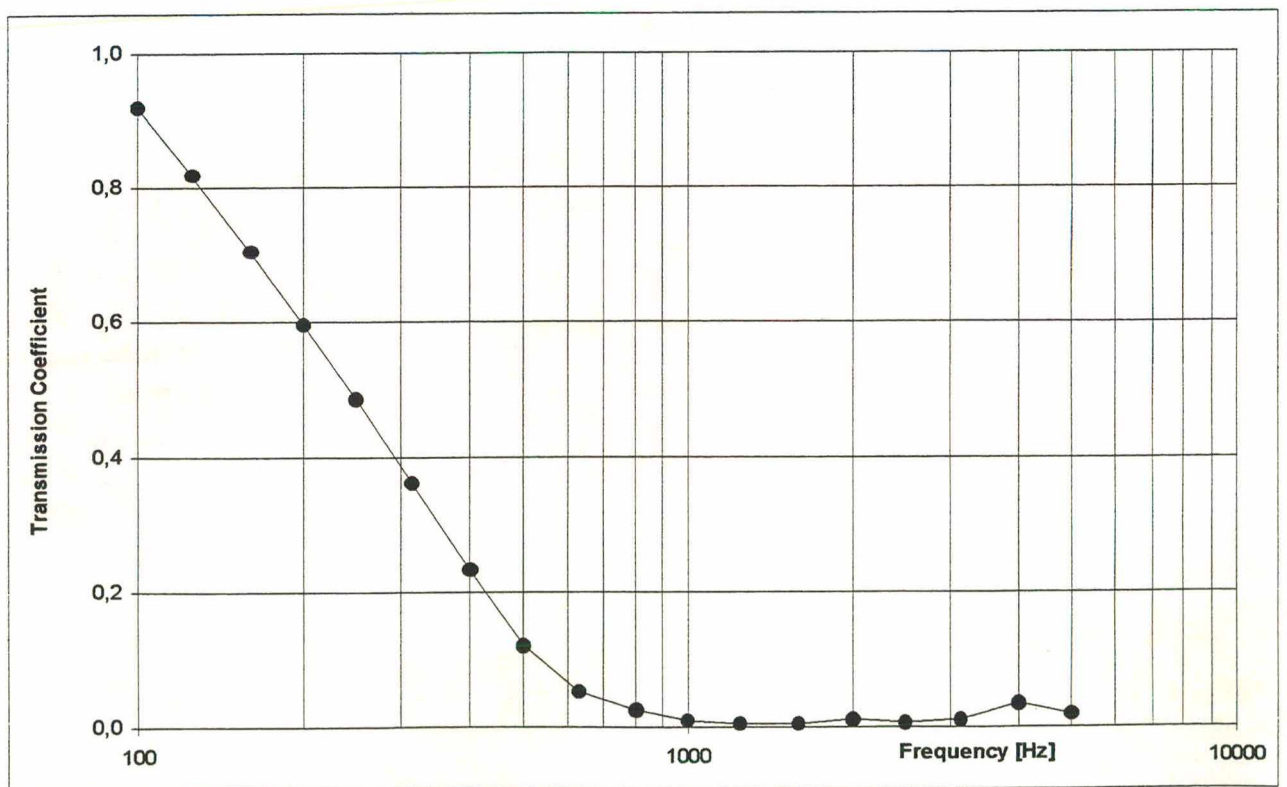


FIGURE 7.12 - Angle average transmission coefficient of the louvre measured by impulse and used as input data into the image method.

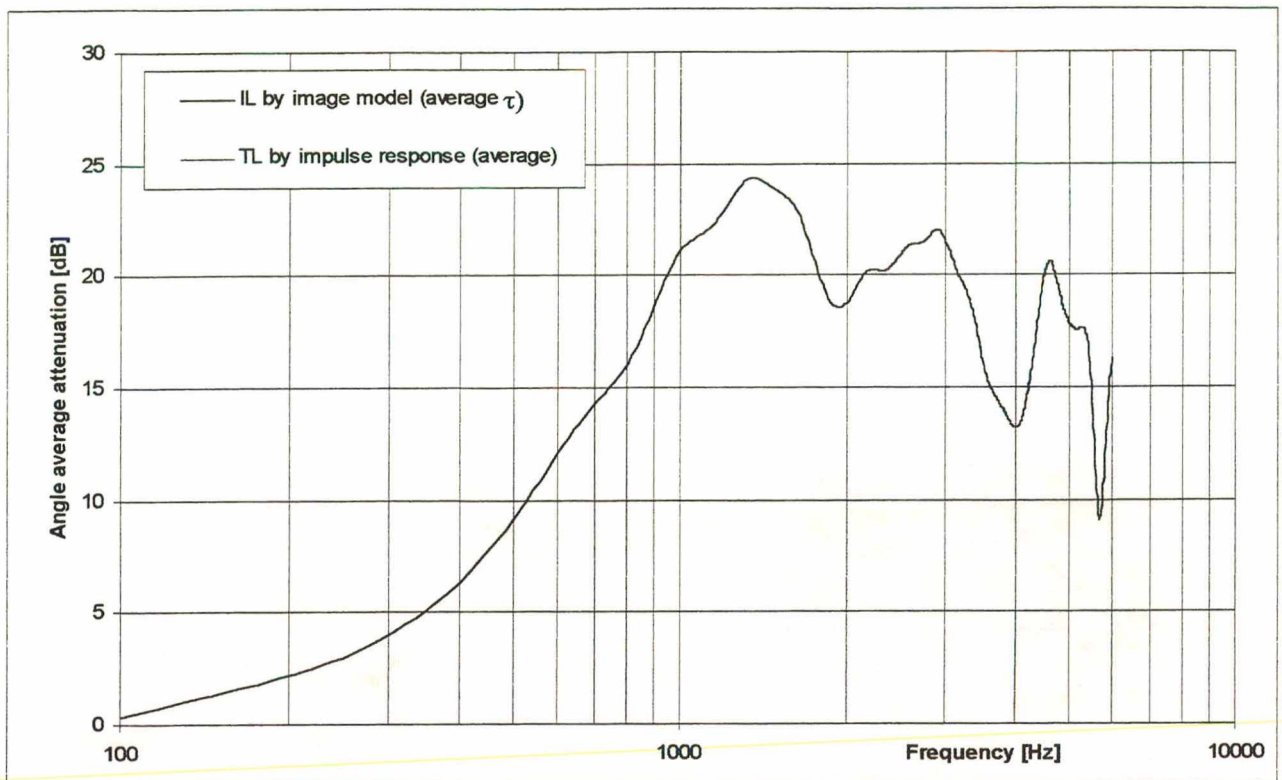


FIGURE 7.13 - Angle average insertion loss by image model (set-up = 45°) considering direct component only and angle average transmission loss measured by impulse.

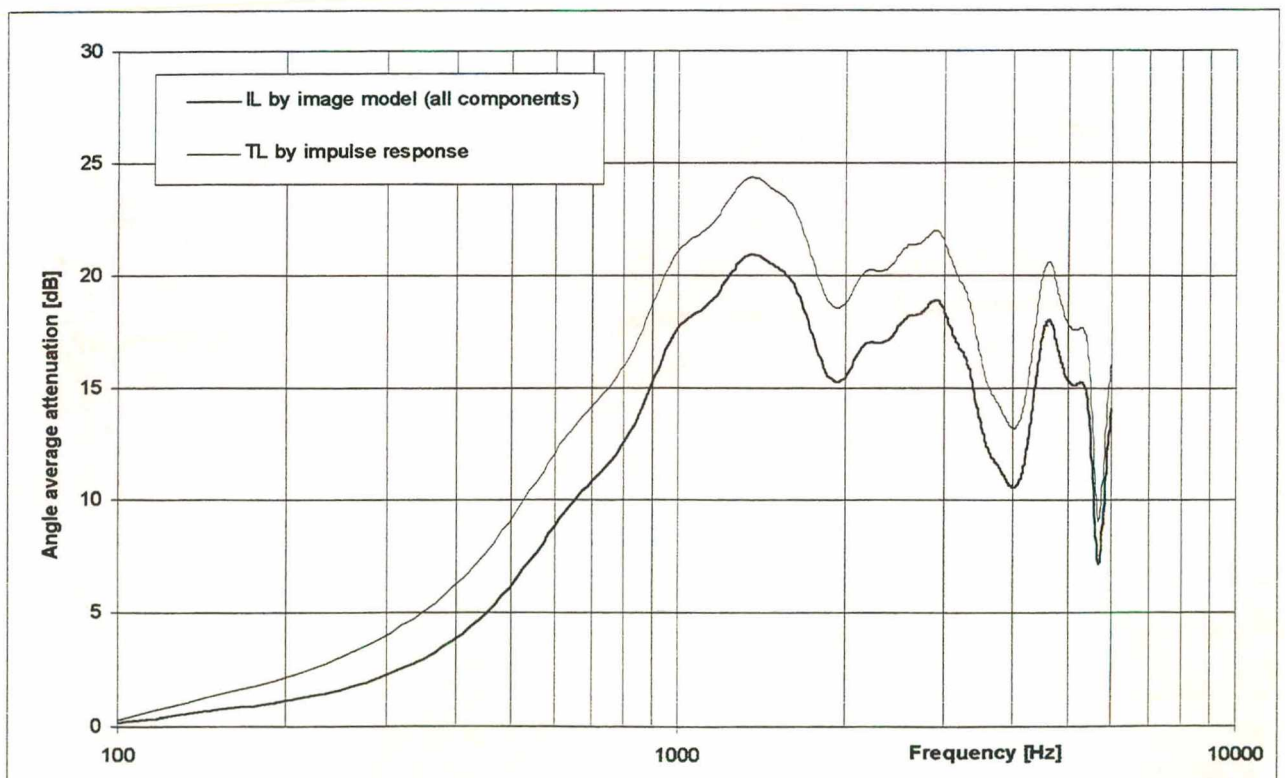


FIGURE 7.14 - Angle average insertion loss by image model (set-up = 45°) considering direct and reverberant fields and angle average transmission loss measured by impulse.

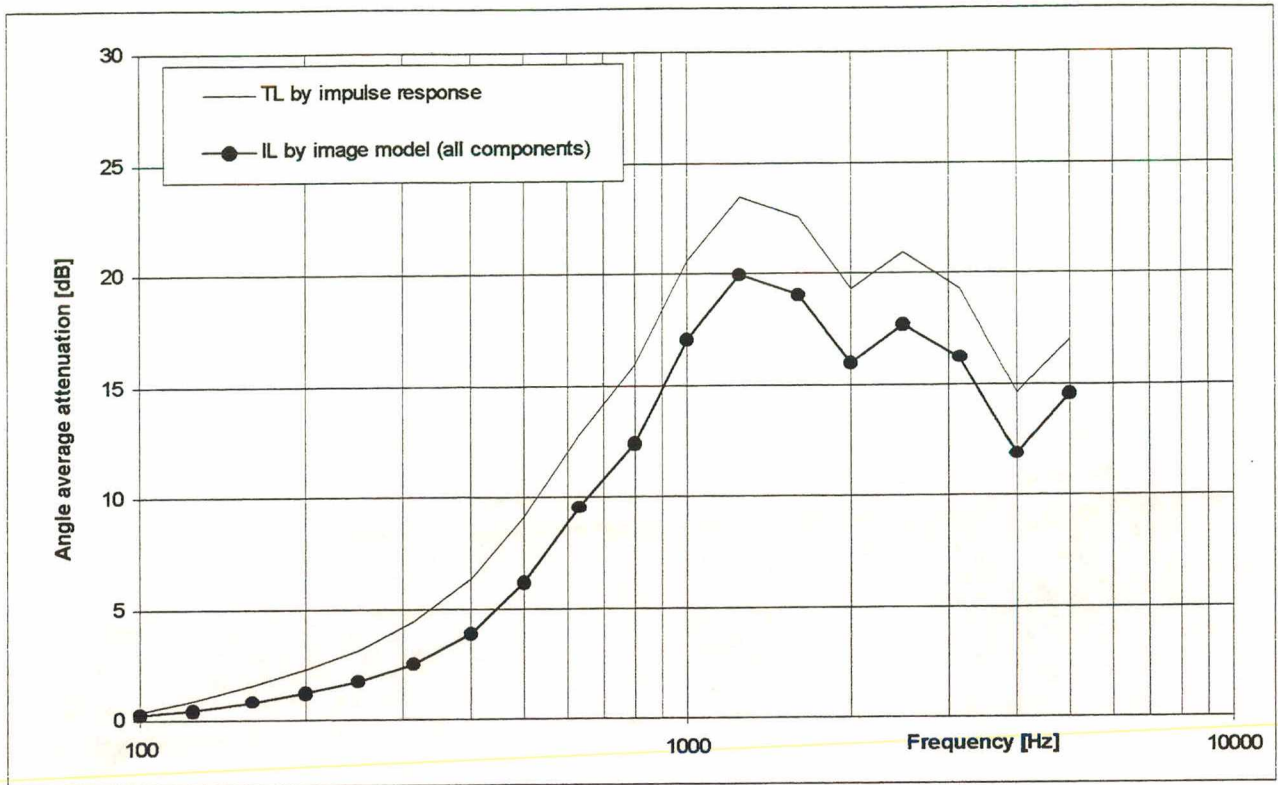


FIGURE 7.15 - Angle average insertion loss of the louvre by image model (set-up = 45°) and angle average transmission loss measured by impulse, in 1/3 octave bands.

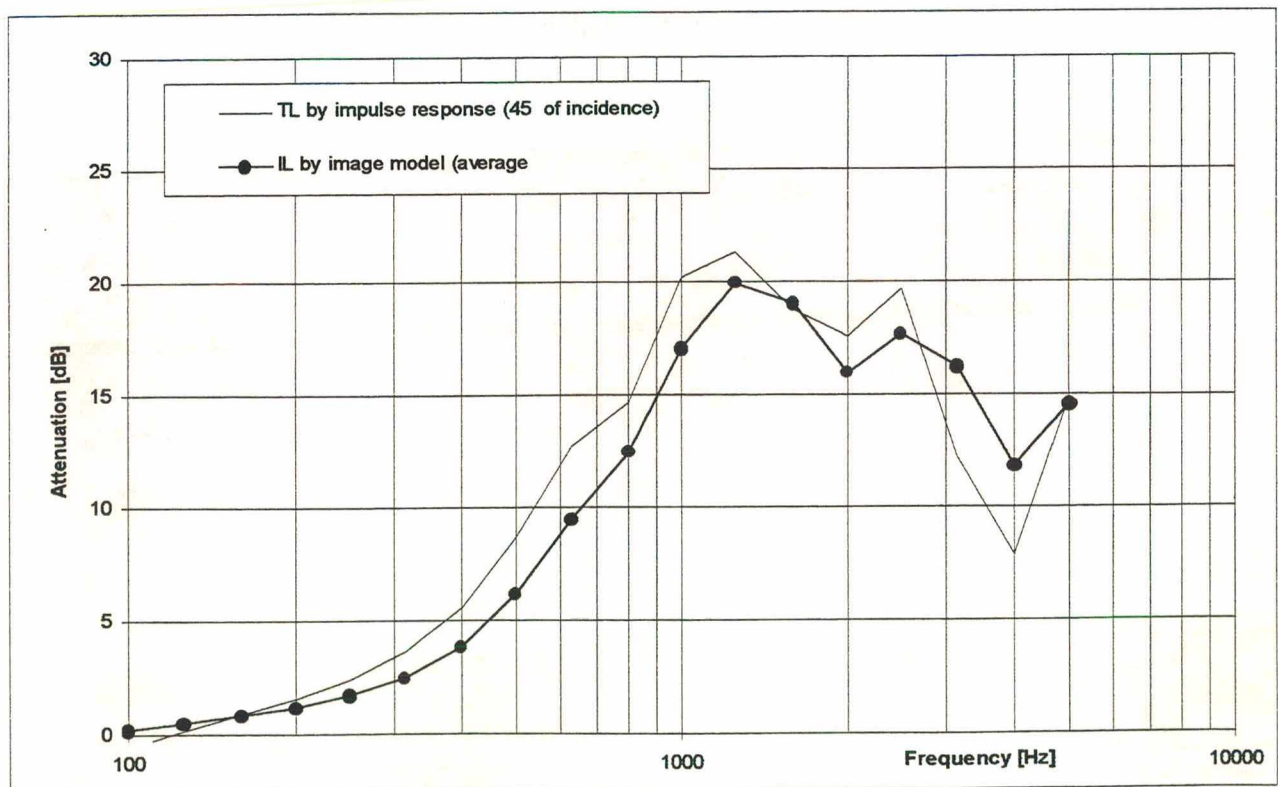


FIGURE 7.16 - Angle average insertion loss of the louvre by image model (set-up = 45°) and transmission loss measured by impulse for 45° of incidence.

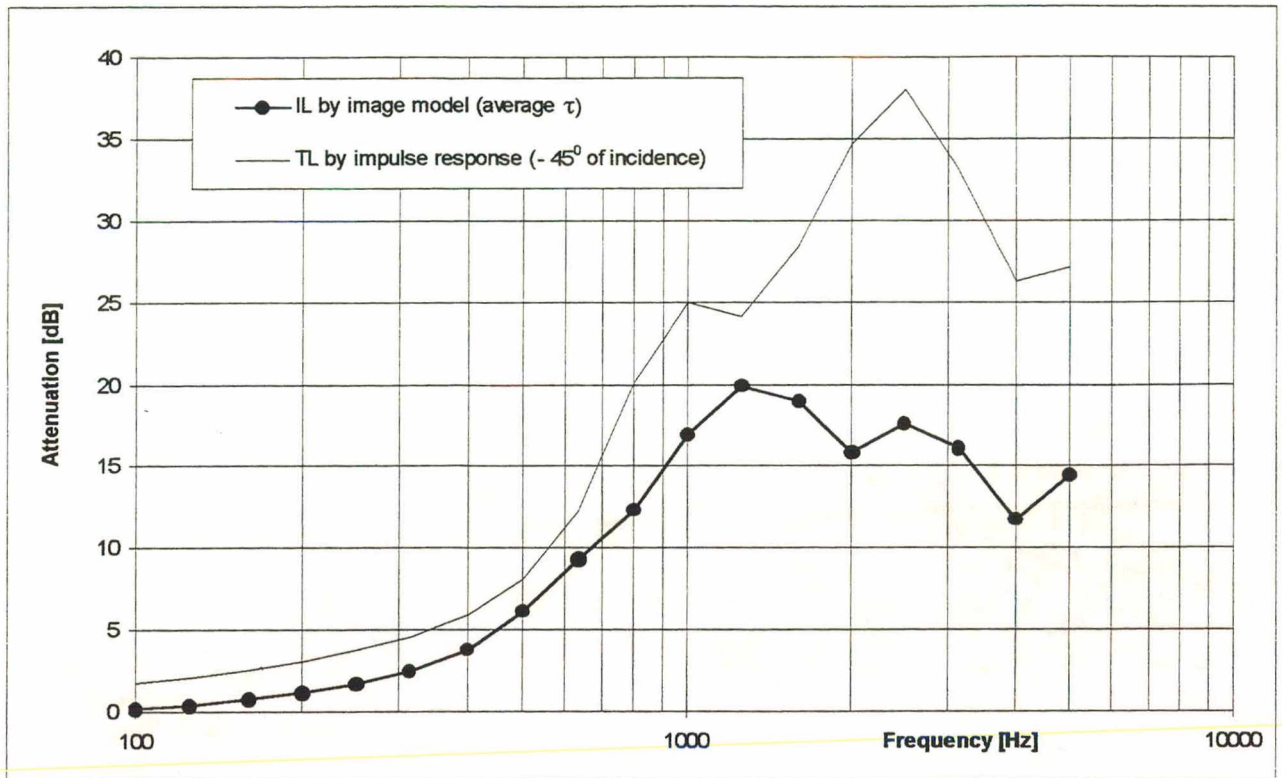


FIGURE 7.17 - Angle average insertion loss of the louvre by image model (set-up = -45°) and transmission loss measured by impulse for -45° of incidence.

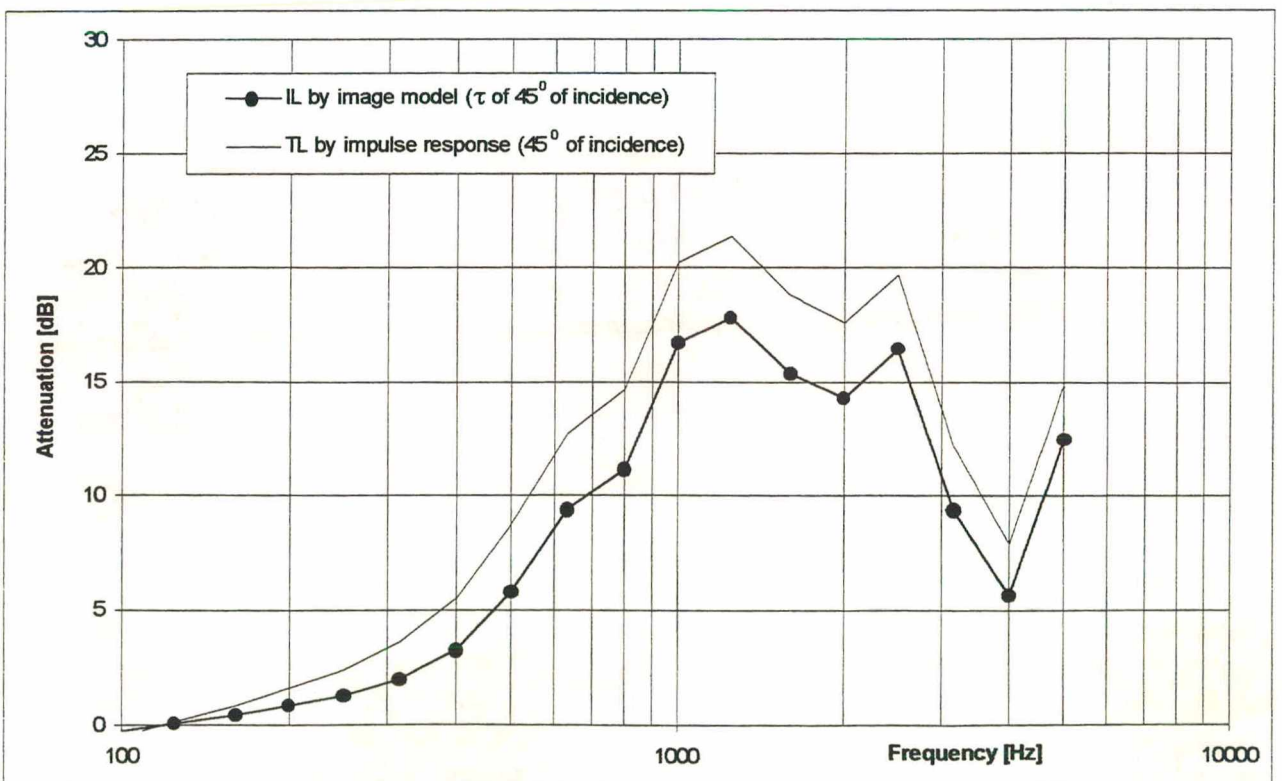


FIGURE 7.18 - Angle average insertion loss of the louvre by image model (set-up = 45°) and transmission loss measured by impulse for 45° of incidence.

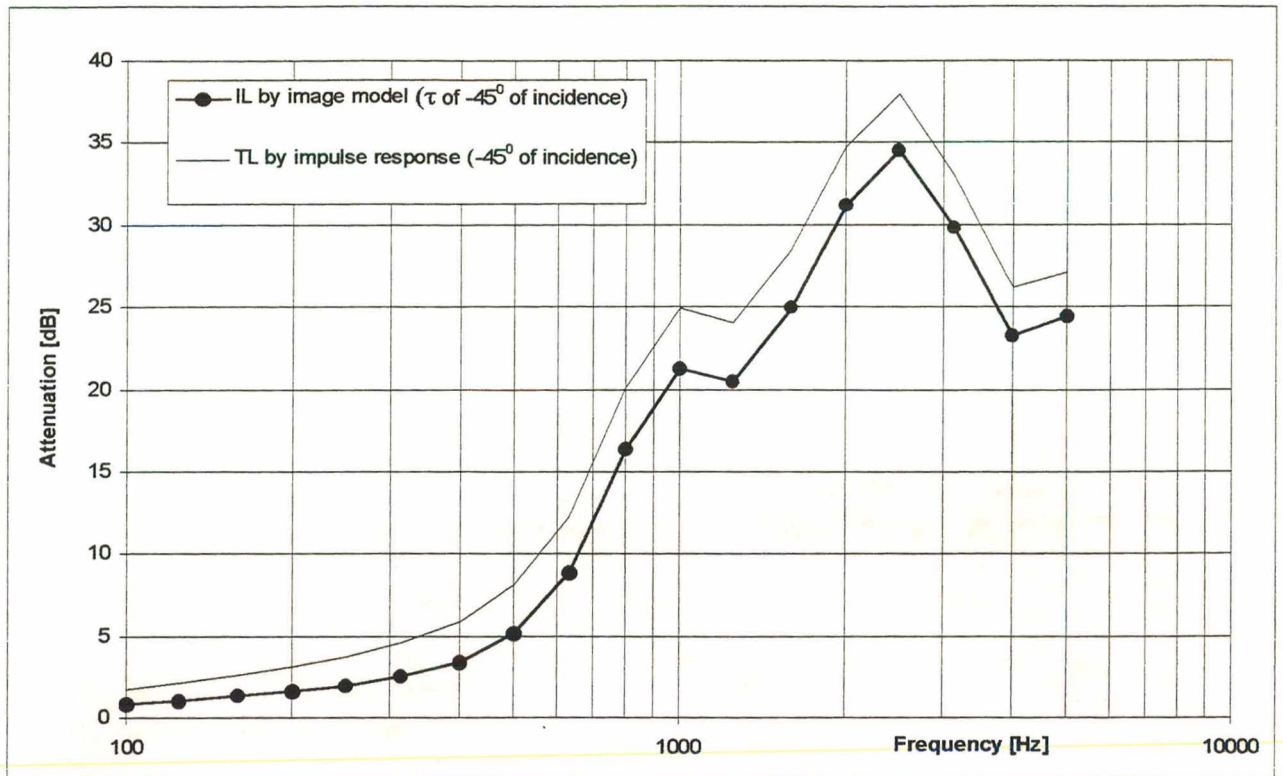


FIGURE 7.19 - Angle average insertion loss of the louvre by image model (set-up = -45°) and transmission loss measured by impulse for -45° of incidence.

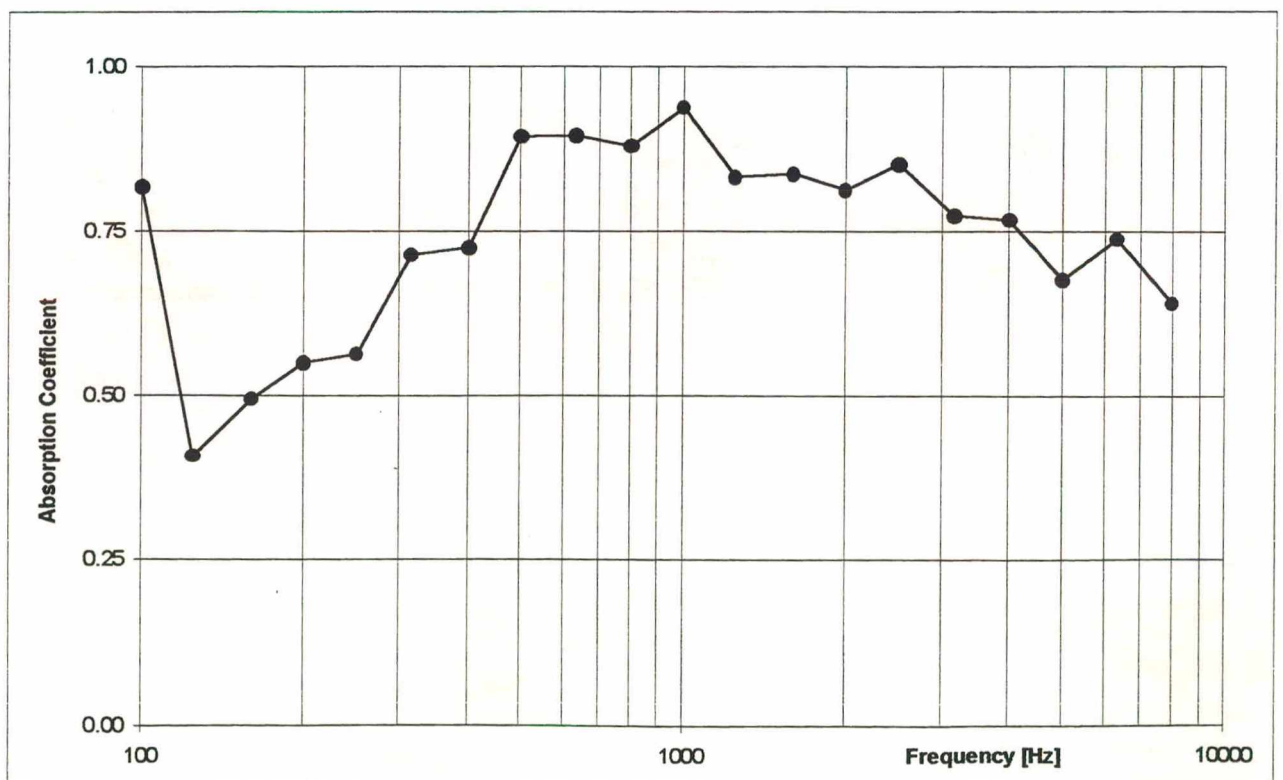


FIGURE 7.20 - Absorption coefficient of the louvre for diffuse incidence.

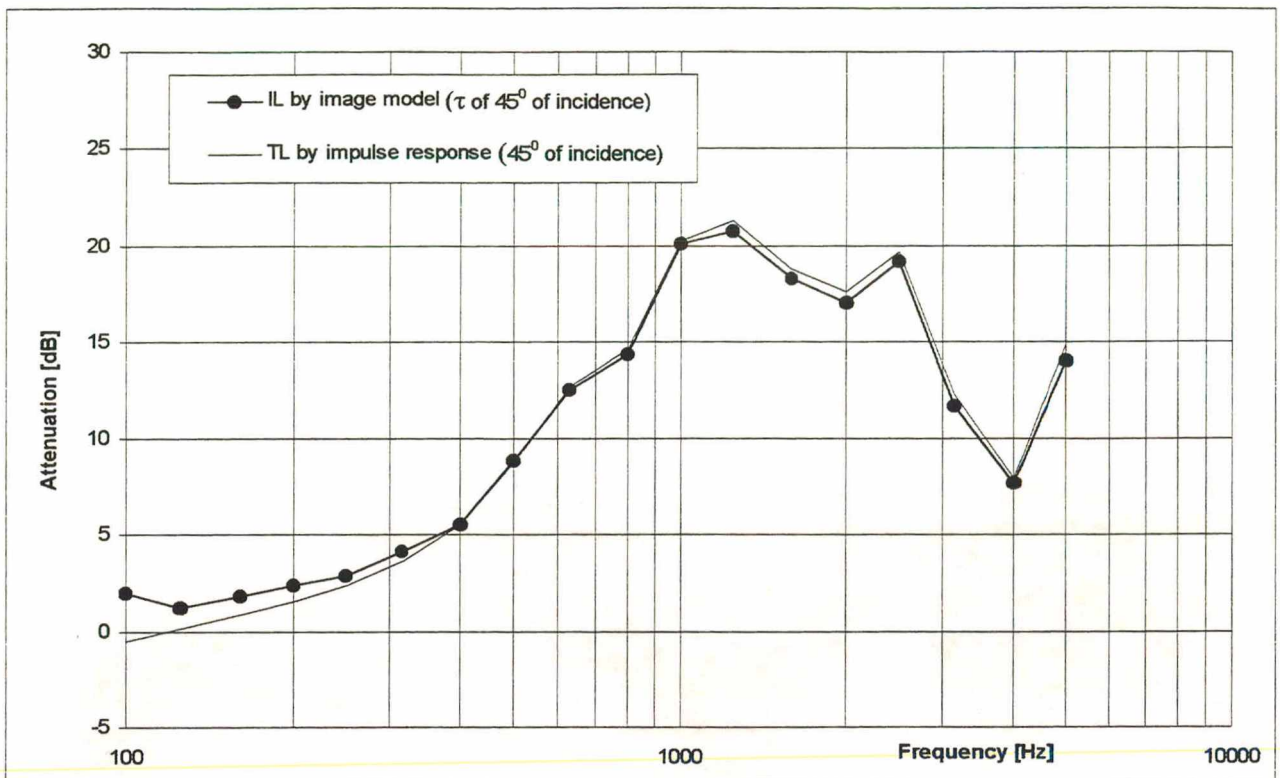


FIGURE 7.21 - Insertion loss by image model (set-up = 45°) considering the diffuse absorption of the louvre and transmission loss measured by impulse.

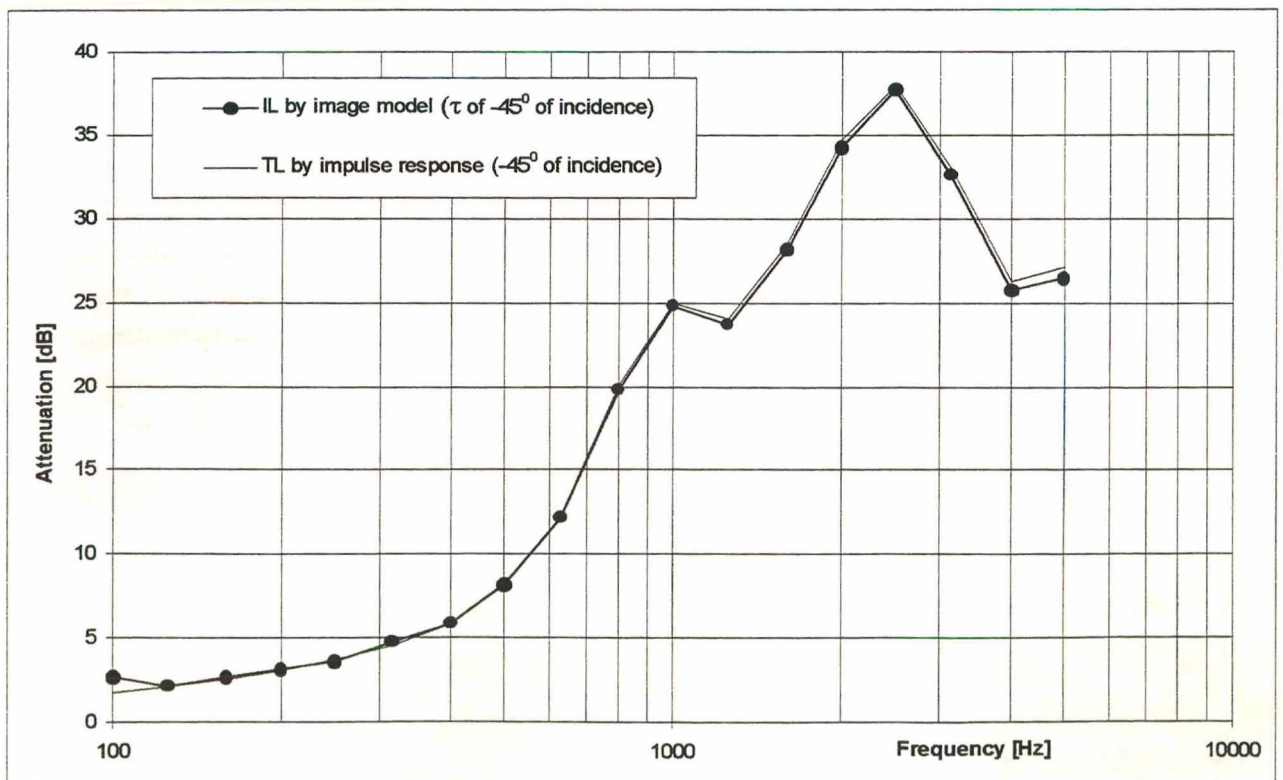


FIGURE 7.22 - Insertion loss by image model (set-up = -45°) considering diffuse absorption of the louvre and transmission loss measured by impulse.

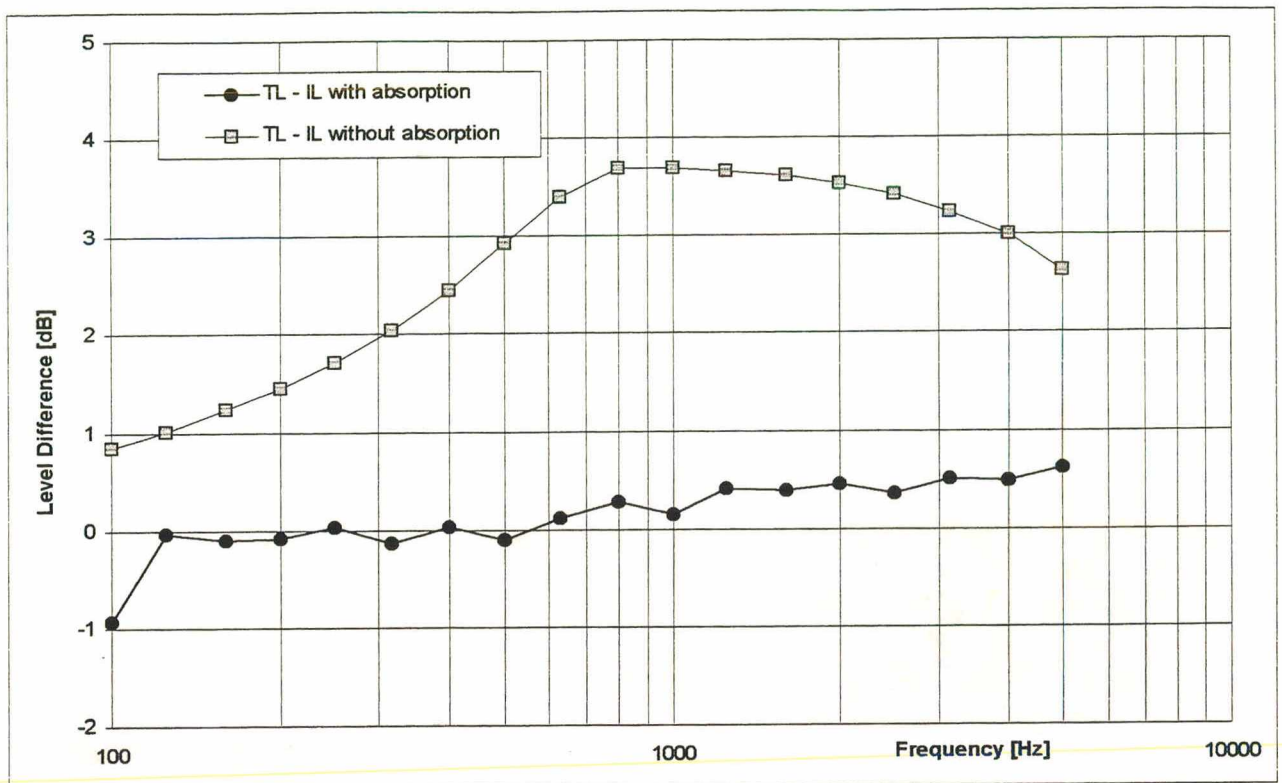


FIGURE 7.23 - Level difference between TL measured by impulse and IL predicted by image model, with and without diffuse absorption of louvre considered; set-up = -45° .

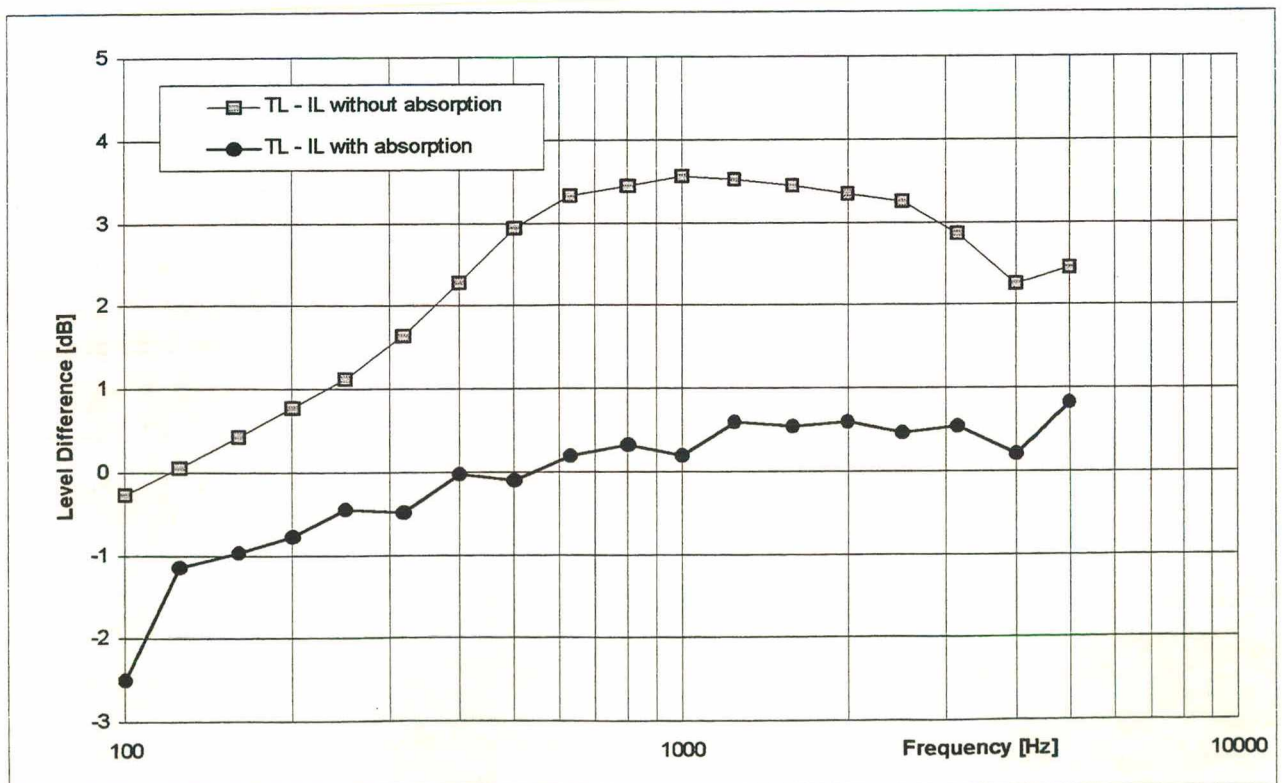


FIGURE 7.24 - Level difference between TL measured by impulse and IL predicted by image model, with and without diffuse absorption of louvre considered; set-up = 45° .

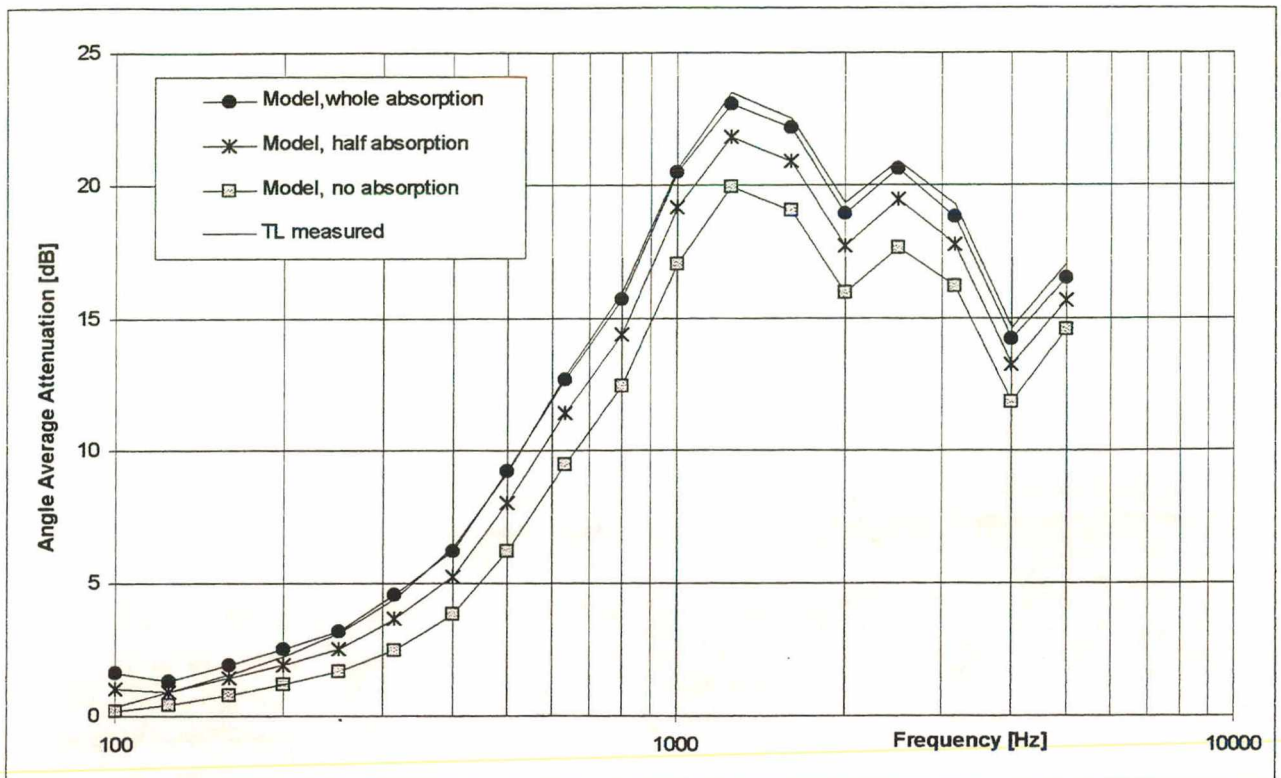


FIGURE 7.25 - Angle average insertion loss by image model considering different amounts of absorption of the louvre and transmission loss measured by impulse.

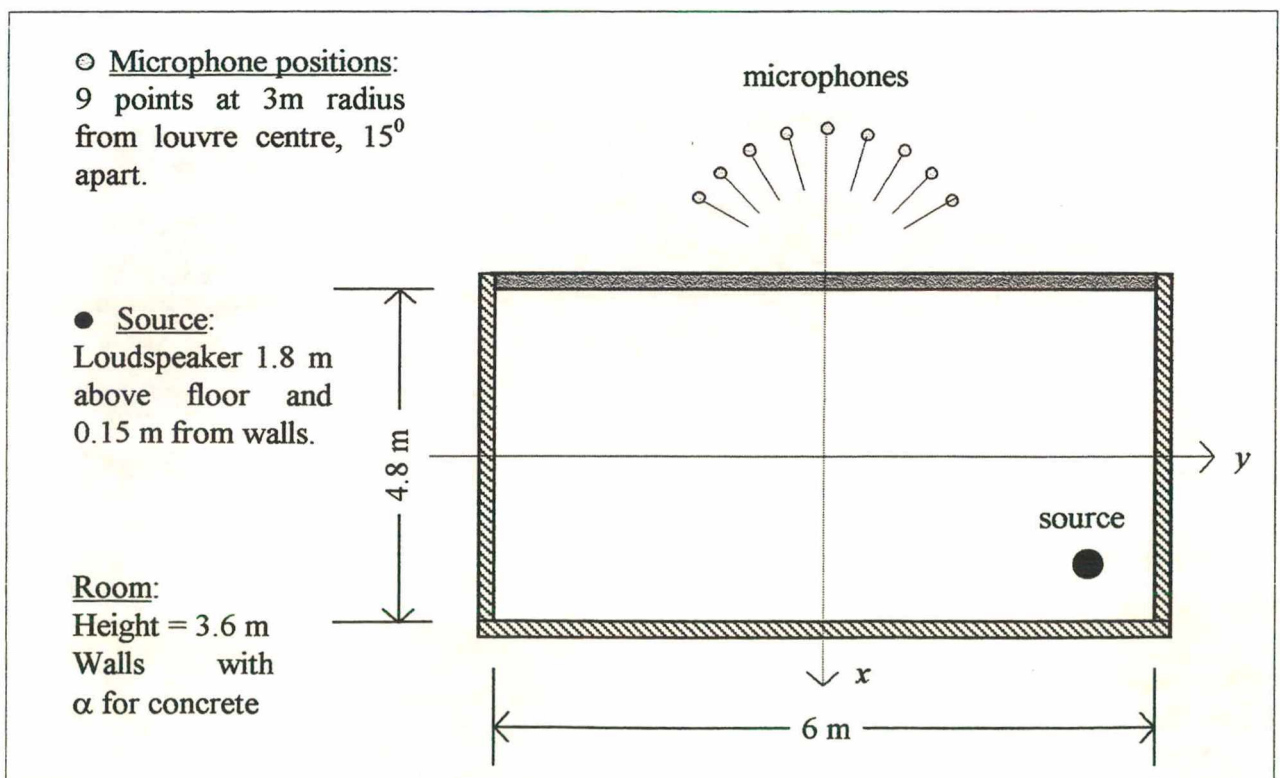


FIGURE 7.26 - Image model layout for insertion loss simulation by HEVAC method.

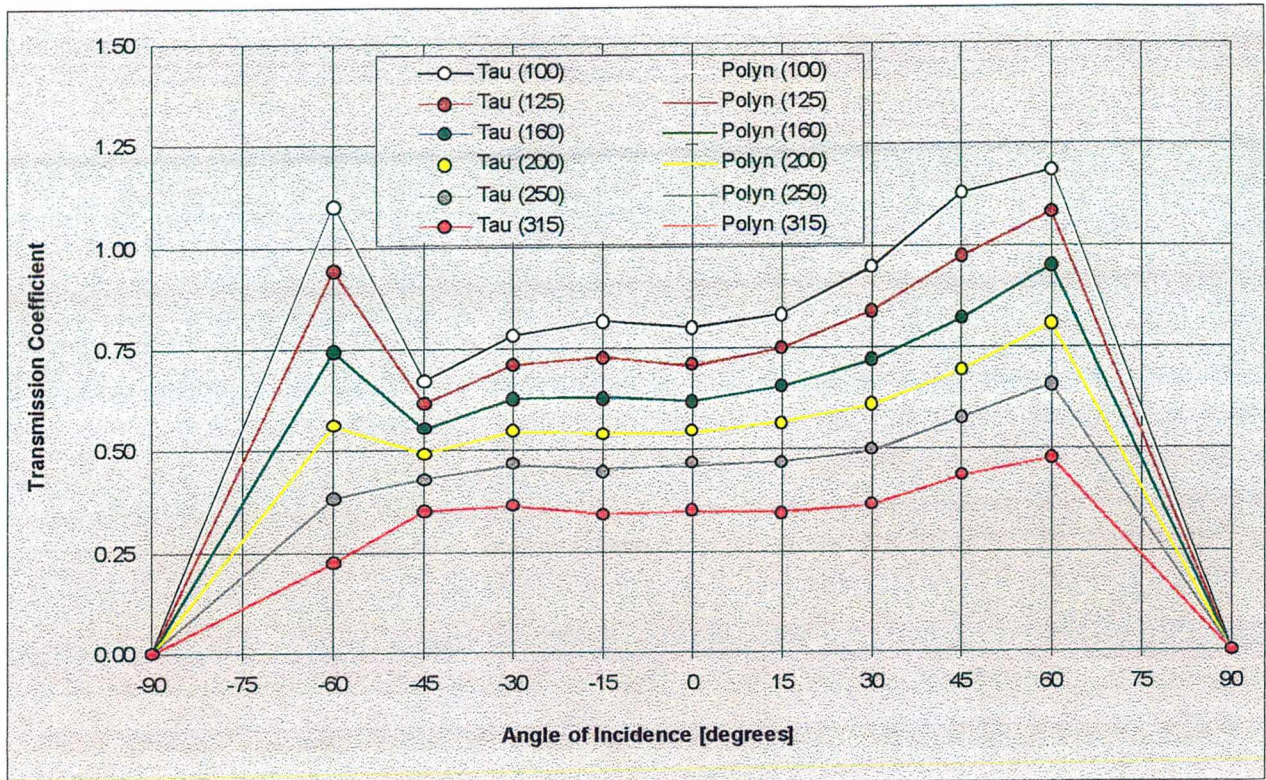


FIGURE 7.27 - Measured transmission coefficient and polynomial fit for 100-315 Hz bands.

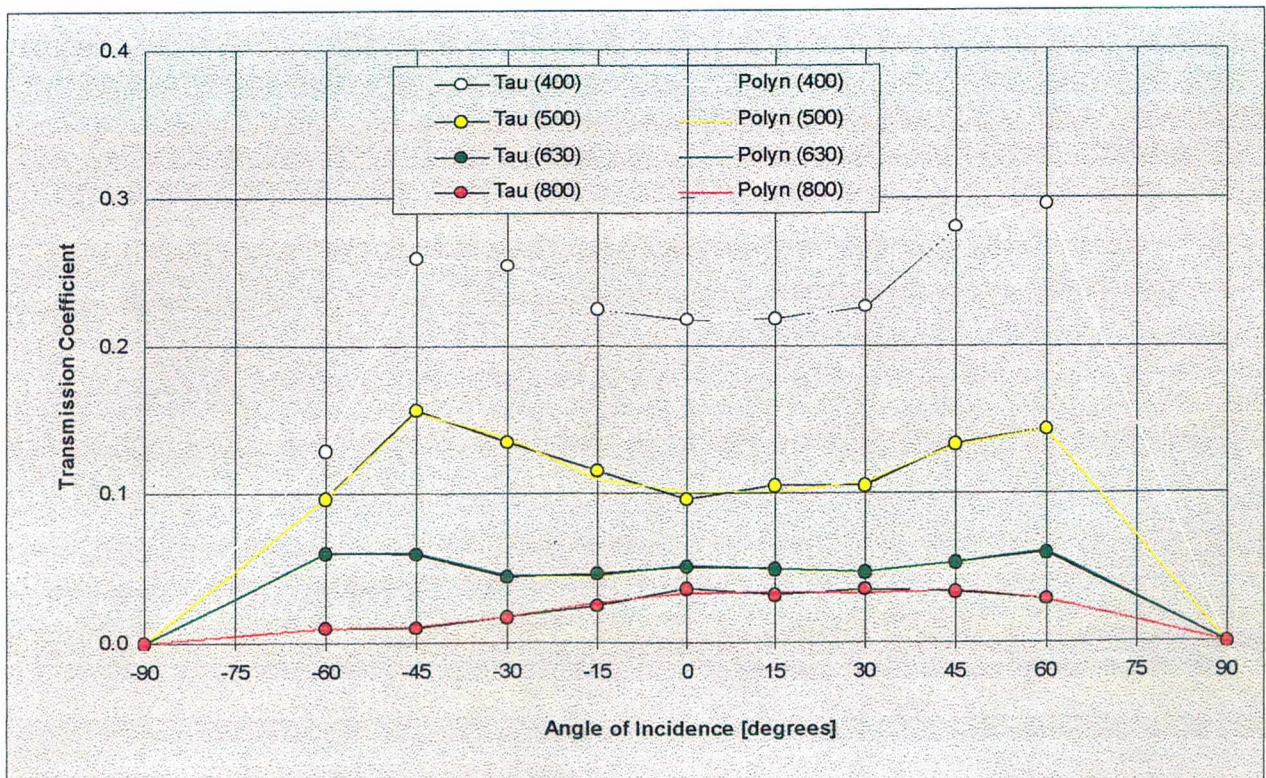


FIGURE 7.28 - Measured transmission coefficient and polynomial fit for 400-800 Hz bands.

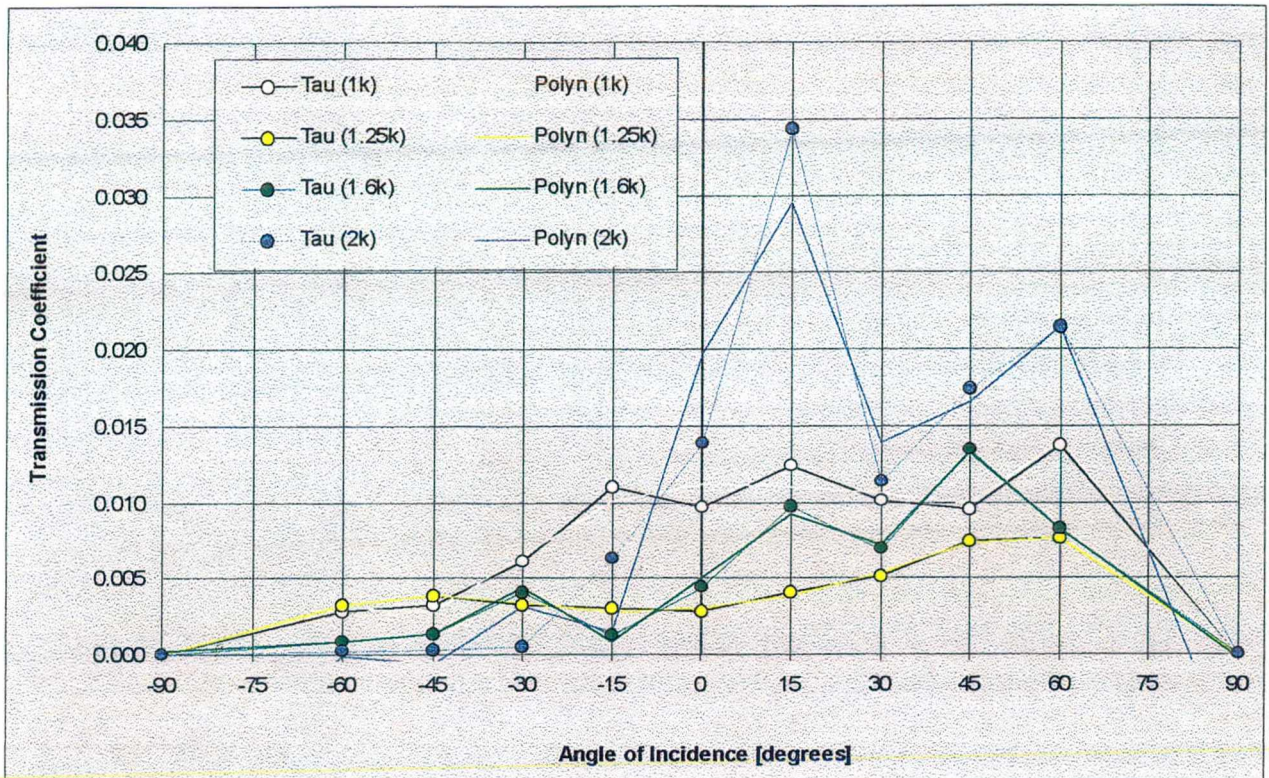


FIGURE 7.29 - Measured transmission coefficient and polynomial fit for 1k-2k Hz bands.

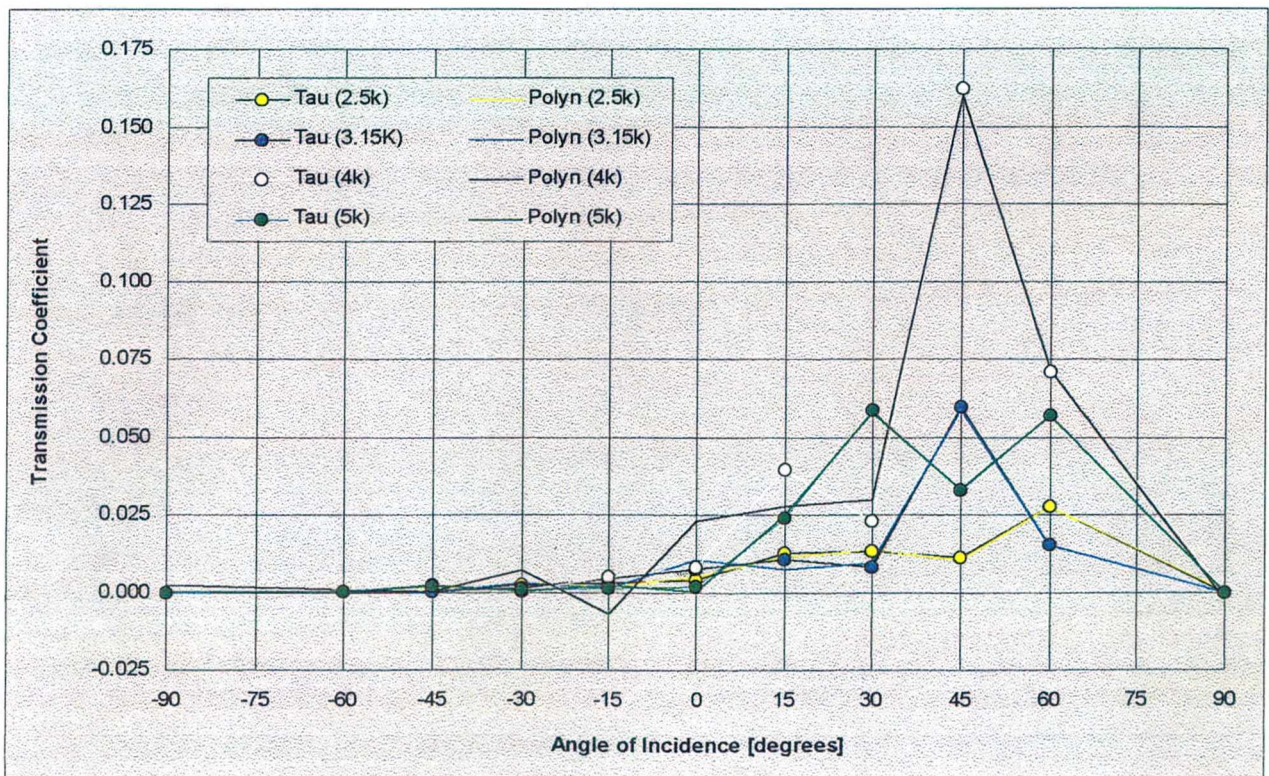


FIGURE 7.30 - Measured transmission coefficient and polynomial fit for 2.5k-5k Hz bands.

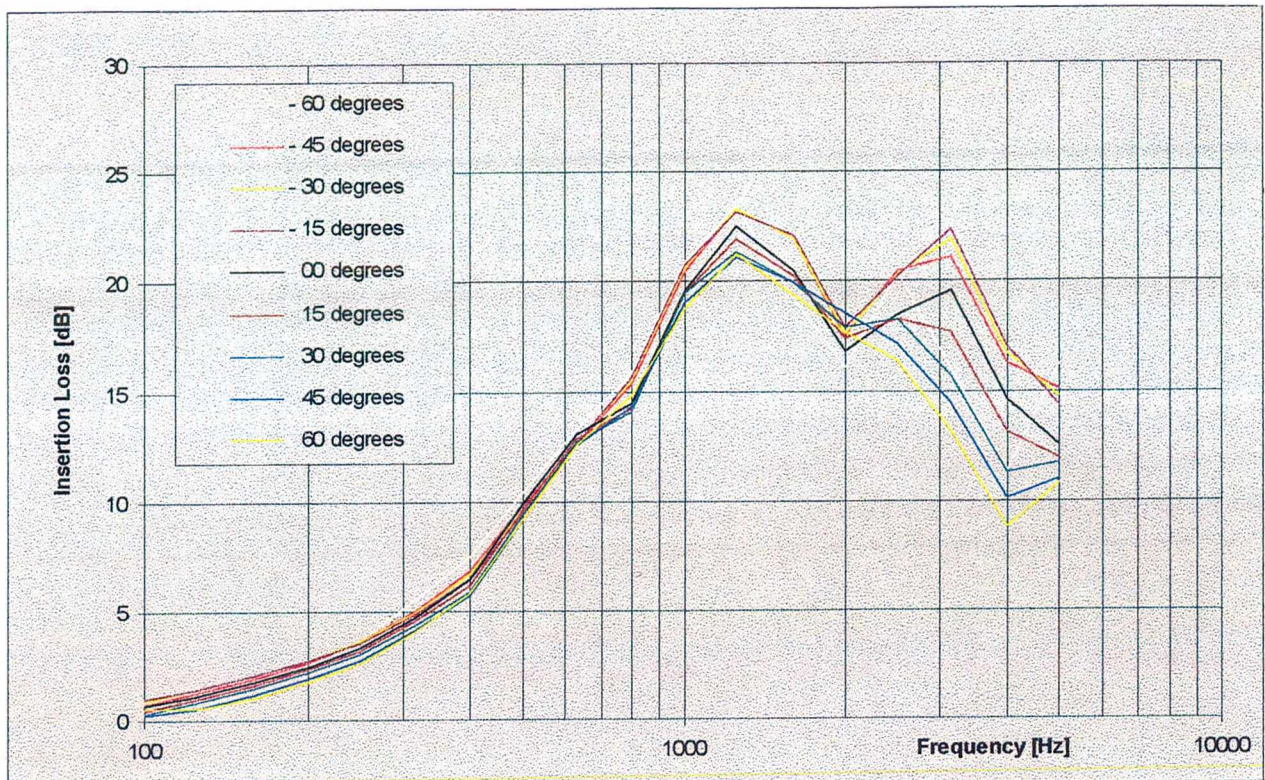


FIGURE 7.31 - Results of HEVAC test simulation of insertion loss of the louvre.

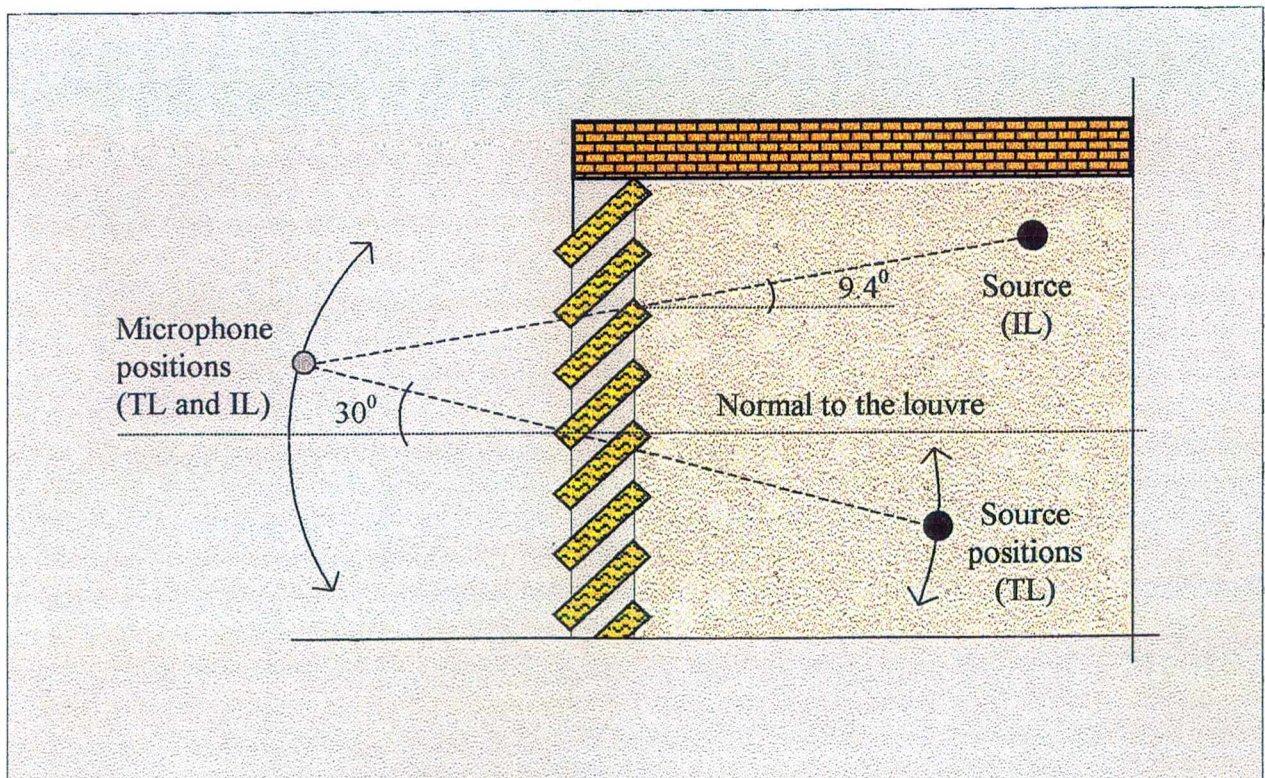


FIGURE 7.32 - Set-up for 30° of incidence for IL simulation and TL measurements.

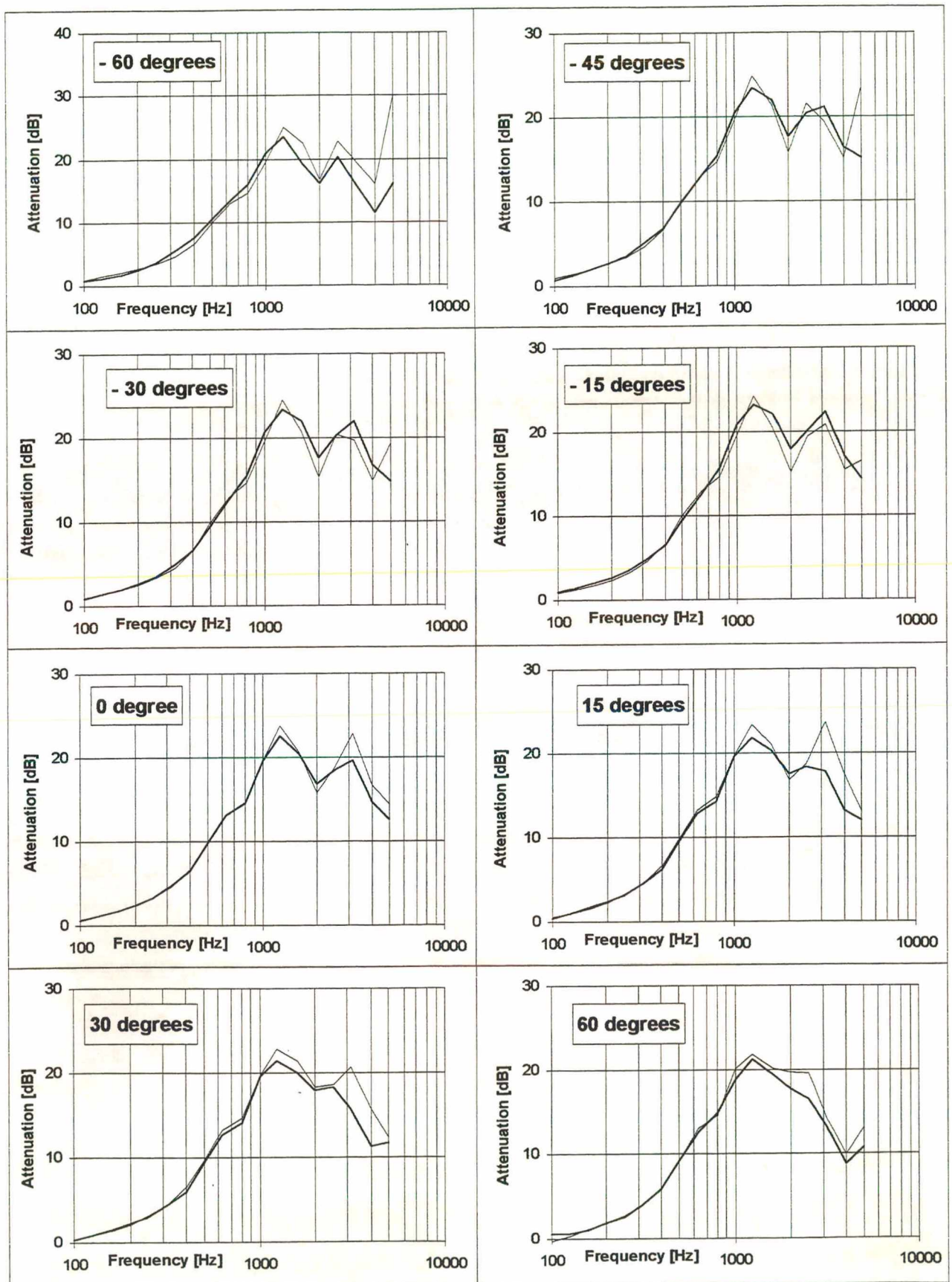


FIGURE 7.33 - Simulated insertion loss by HEVAC method and measured transmission loss;
 — IL simulations — TL measurements

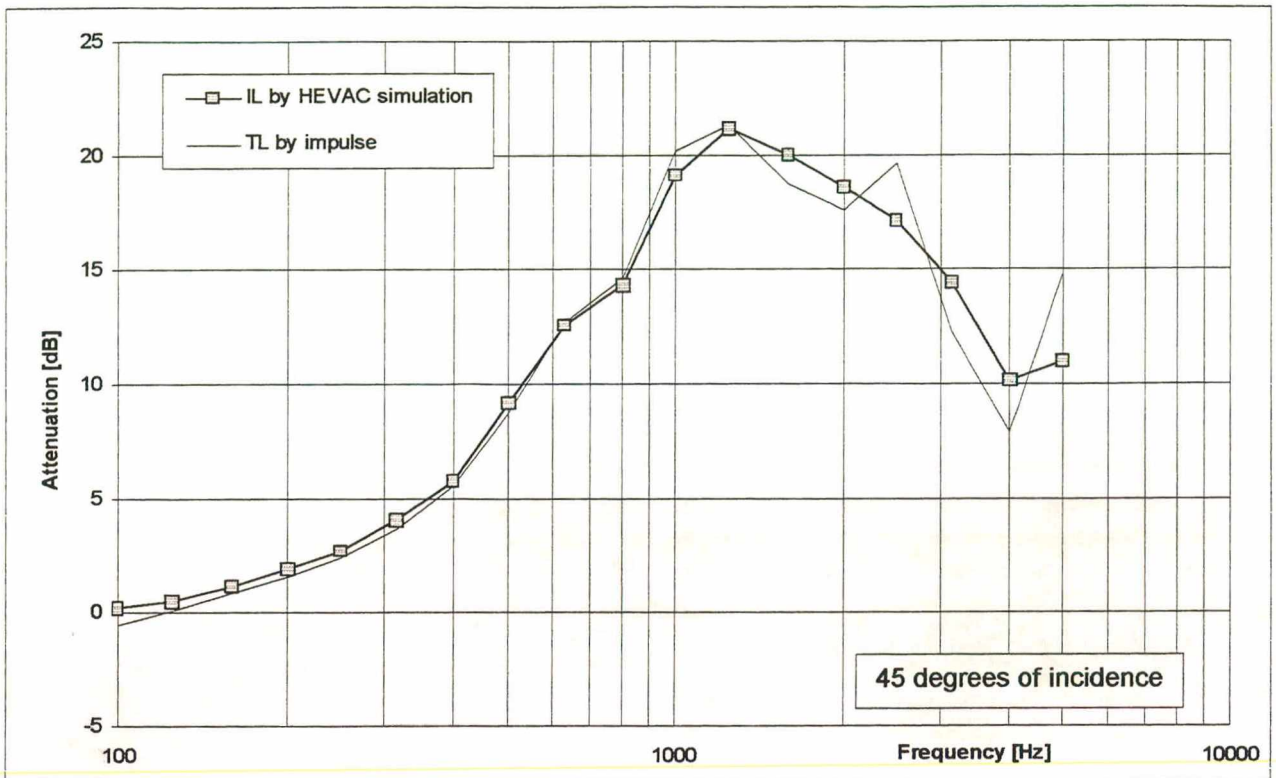


FIGURE 7.34 - HEVAC insertion loss simulation and measured transmission loss for 45°.

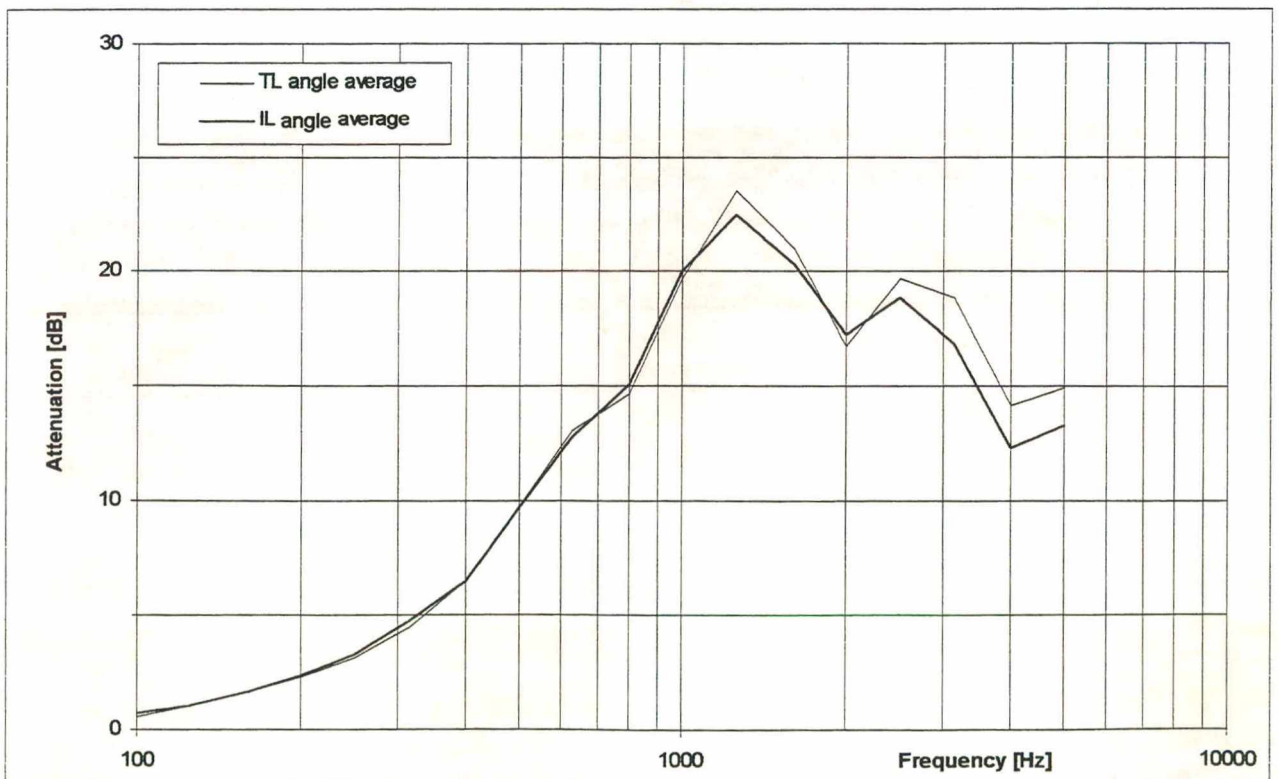


FIGURE 7.35 - Angle average attenuation of IL simulation and TL predicted by polynomials.

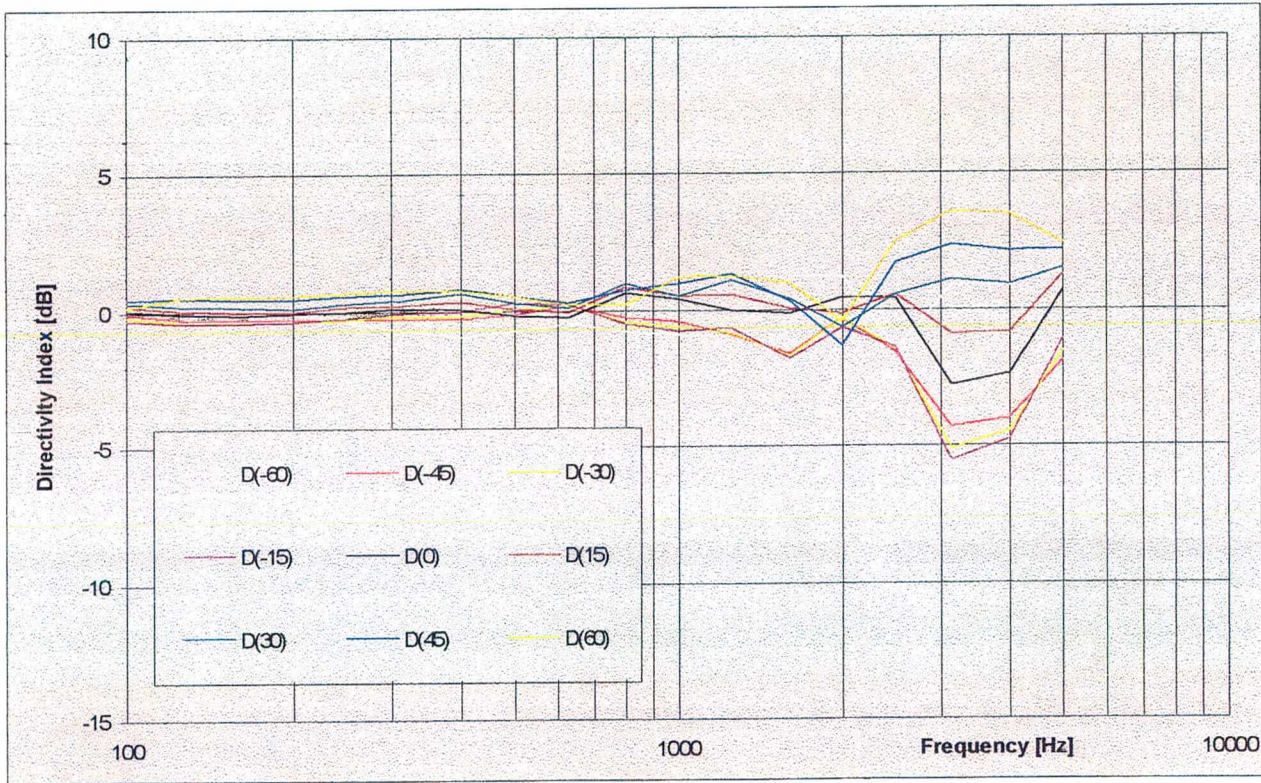


FIGURE 7.36 - Directivity index of HEVAC insertion loss simulation.

CHAPTER 8 REFLECTION FACTOR BY IMPULSE RESPONSE

- 8.1 Introduction**
- 8.2 Principle of the Method**
- 8.3 Direct Component**
- 8.4 Analysis of Time Window**
- 8.5 Absolute Error Due to Background Noise**
- 8.6 Results**
- 8.7 Application to the Image Method**
- 8.8 References**

8.1 INTRODUCTION

The previous chapter has presented the insertion loss measurement condition, simulated by an image model, so as to assess the performance of the louvre according to the HEVAC test procedure. The required input data for the simulation includes the absorption in the source room, the transmission and absorption coefficient of the louvre and the geometry of source room and set-up.

The image model has been shown to be reliable. However, although the transmission coefficient was measured by the impulse method, it was necessary to use an absorption coefficient obtained by the reverberant decay method. In order to obtain a simulation method completely independent of any technique requiring standard acoustic facilities, the acquisition of a reflection coefficient was carried out by impulse response and applied to the model.

There are three accepted methods of measuring sound absorption. The reverberant decay method [1] is still the most common despite unavoidable errors [2] due to the simplifying assumptions in the derivation of the expression for reverberation time.

The second method uses a standing wave tube [3,4,5,6]. The standard ISO 10534 [7] in part 1 deals with standing wave ratio and part 2 presents the procedure regarding transfer function methods. Some of the new techniques have drastically reduced the time involved, since broad band analysis are now available instead of time consuming pure tone measurements. There are disadvantages. It is not possible to perform in-situ measurements and the small sample may not be representative of the material when installed. Also, there is a strong dependency between the sample absorption coefficient and its mounting conditions [8]. In addition, the theoretical arguments used in converting acoustic impedance tube data to sound absorption coefficient are open to criticism. Paris' equation used to calculate α_θ from the impedance Z obtained in the standing wave tube

$$\alpha_\theta = 1 - \left| \frac{(Z / \rho c) \cos \theta - 1}{(Z / \rho c) \cos \theta + 1} \right|^2 \quad (8.1)$$

in which ρc is the air impedance, is derived on the assumption that Z is independent of the angle of incidence θ but there is some evidence that the specific acoustic impedance is a function of the angle of incidence [9].

Lastly, a reflection coefficient method, which involves measurements by impulse response methods, is currently under review for inclusion as a revision of ISO 354 [10]. The absorption coefficient, which is function of frequency and incident angle, is deduced from a measure of the complex reflection coefficient.

Ingard and Bolt [11] measured large sample using pure tones in an anechoic room. Pressure and phase at the surface of the absorption material were compared with that at the surface of a perfectly reflecting plane. The absorption coefficient was obtained from

$$\alpha = \cos^2 \psi - 4 \left[\frac{p_r}{p_h} - \frac{1}{2} \cos \psi \right]^2 \quad (8.2)$$

where p_r and p_h are the pressures at the test sample and at the hard wall, respectively, and ψ is the phase difference between the two signals.

Ando [12] proposed an “interference pattern method”, which exploited the effect generated by a point source in front of an absorbing surface. The complex reflection coefficient was found in a way similar to that applied in the standing wave tube.

A number of authors have investigated pulse techniques [13,14,15,16], which, as seen along this work, allow the free-field response to be obtained in any environment conditions as long as the set-up geometry is such that the component of interest can be separated from unwanted reflections.

Problems of repeatability, signal to noise ratio and non-linearity have been overcome with the advance in digital techniques. The use of maximum-length sequences has expanded in-situ applications of reflection methods [17,18] as well in all other areas, as described in Chapter 4.

8.2 PRINCIPLE OF THE METHOD

Absorption coefficient $\alpha(f, \theta)$ is the ratio of the absorbed energy (strictly speaking, the energy not reflected back) to the energy incident upon a surface. By means of the measurement of the complex reflection coefficient $R(f, \theta)$, the absorption coefficient can be obtained according to [14]:

$$\alpha(f, \theta) = 1 - |R(f, \theta)|^2 \quad (8.3)$$

The principle of the measurement is schematically illustrated in Figure 8.1. A source near a reflecting boundary produces a pressure at a microphone near the surface, which is the sum of direct and reflected signals. In Figure 8.2 it is seen the time history obtained at the receiver position that shows the incident component, the reflection from the surface under test and some of the parasitic reflections originated from other room boundaries.

The free-field response is obtained after windowing out the unwanted reflections, as in the procedure presented in Chapter 5 for the acquisition of the transmitted component. The Fourier transformed signal is then corrected for sphericity effect, air attenuation and equipment characteristics by means of a reference signal. The source to receiver position vector is kept constant, the effect of which is removed from the effect of the reflecting surface. The incident and reflected components are then obtained.

8.3 DIRECT COMPONENT

How far the microphone is to the surface conditions the information obtained and the corresponding signal processing required. In measurements of oblique incidence, a microphone close to the surface has the following consequences:

- i) The time window can be longer as the reflected component will have a longer time separation from parasitic reflections. The longer the window the lower the frequency limit of analysis, as demonstrated in section 4.3.2.
- ii) Lateral direct contributions are avoided (see Figure 8.3).
- iii) The incident component must be subtracted from the measured total response.

- iv) The reflected component does not require compensating for distance effects.

Figure 8.3 illustrates an oblique incidence set-up and Figure 8.4 shows the resulting response at the microphone for two conditions: microphone close to and away from the surface.

For measurement of the louvre, if the microphone is placed close to the surface, the measured reflection coefficient would not be representative of the louvre behaviour as a whole. Due to the periodic nature of the surface, with alternative gaps and solid metallic blades, and when in the frequency region where the wavelengths are of the same order as the periodicity, the measured reflection would be strongly dependent upon the position of the microphone. Hence, it was decided to carry out the measurements with the microphone away from the surface. The distance would be conditioned by the need to have the reflection signal from the louvre not overlapping with other components of the total time history.

The measurements were carried out in the receiving reverberation chamber in the laboratory of the Acoustics Research Unit of Liverpool University. This was because the louvre previously had been mounted with the perforated, internal side facing the receiver room. This was unfortunate but unavoidable and did not seriously compromise measurement. Therefore, the room characteristics, small dimensions and highly reflective surfaces, were a complication to the measurements. It was often difficult to separate, in time domain, the reflection from the louvre from direct sound and reflections from floor, side and back walls, ceiling and even diffusers. Various source-receiver geometries were proposed with the help of a simple computer program (listing in Appendix 5). Into the program, along with the geometric data, the duration of all impulses was input. In this way, optimum conditions were sort where the desired reflected impulse would not overlap with others.

However, there was no feasible geometry that allowed the proper application of the time window of the signal reflected from the louvre. Therefore, it was decided to apply the “cancelling method” proposed by Mommertz [18]. Figure 8.5 shows in a schematic way the desired time history. If the direct component only masks the reflected component, then the method permits the cancelling of the former.

The method was implemented as follows:

- i) Measurement of reflected impulse response of the louvre.
- ii) Time window is applied, separating the combined direct and reflected components, as shown in Figure 8.5.
- iii) A reference signal is measured with a source to receiver distance such that: Reference distance = [(source to louvre) + (louvre to microphone)], as measured in (i) set-up.
- iv) Reference signal is inverted, in the time domain.
- v) Addition of steps (ii) + (iv).

For complete cancellation, three characteristics of the impulse response should be unchanged: amplitude, time delay and shape. With environmental conditions unaltered during the measurements, as seen in Chapter 4, and with the same source power output, there should be no change in the first parameter. A time delay may result as a consequence of different set-ups. With a time resolution of $66.75\mu\text{sec}$, a change of about 2 cm in the set-up is enough to shift the signal in one point in the time history. When dealing with power spectra a change of that order is not important, but for temporal cancellation the signal processing is sensitive to any phase delay. The impulse shape was expected to have a good repeatability. Therefore, in order not to introduce extra error, an ideal situation was proposed: the measurement would be performed consecutively, without any change in the set-up whatsoever.

Two signals were measured within two minutes. The second signal was inverted and added to the first. The resulting spectrum should have been zero over the full frequency range. Figure 8.6 shows the second sample before and after inversion and the resultant summation in the time domain. Although the direct is apparently cancelled, the power difference between the two original signals revealed the existence of a level difference of about 2 dB in some frequencies, as seen in Figure 8.7. By visual inspection, it could be observed that the two impulses presented no time delay but the shapes varied slightly. If time delay is the source of error it can be easily overcome by digitally processing the signals. Difference in the response of the system to successive measurements can be unambiguously attributed to noise in the system [19]. Therefore, to reduce the difference in shape a second test was performed with the average increased to 160 samples and the maximum power difference was reduced to about 0.2 dB this time. The

controlled test required a large number of averages to cancel the direct component. As the real measurement would involve the removal of the set-up to a different room for the measurement of direct sound, and therefore introducing some variation in the set-up, it was considered not safe to adopt the cancellation method.

In the process of investigation of the “cancellation method”, another approach was proposed. If the direct and reflected components could be separated in time, the reference measurement that accounts for the system response and distance effects would not be necessary. As far as absorption coefficient is concerned, there was no need to apply any correction due to time delay, necessary only if a complex measurement of reflection coefficient is measured to obtain the specific impedance of the surface. Theoretically, the method is demonstrated as follows.

The spectrum of the total signal at the receiver position is

$$P_t(\omega) = P_i(\omega) + P_r(\omega) + \sum_n P_n(\omega) \quad (8.4)$$

where $P_i(\omega)$ and $P_r(\omega)$ are the spectra of the incident and reflected signals respectively and the n -terms represent the unwanted reflections from walls, ceiling and floor. The reflected sound can be written as

$$P_r(\omega) = k R(\omega) P_i(\omega) e^{-j\omega\phi} \quad (8.5)$$

where $R(\omega)$ is the complex reflection coefficient, k is a correction factor due to sphericity effects given by the distance ratio of incident to reflected, $k = d_i / d_r$, and ϕ is a time delay due to the same path difference, $r_r - r_i$ (air attenuation has been disregarded). When the direct component is extracted from the time history and compensated for distance and time delay according to

$$P_i(\omega) k e^{-j\omega\phi} \quad (8.6)$$

then the reflection coefficient is obtained from the ratio of reflected to incident component. Equation, (8.5) divided by equation (8.6), gives:

$$R(\omega) = \frac{P_r(\omega)}{P_i(\omega)} = \frac{k R(\omega) P_i(\omega) e^{-j\omega\phi}}{k P_i(\omega) e^{-j\omega\phi}} \quad (8.7)$$

The method of acquisition the reference signal is advantageous. It is more precise than performing a separate measurement, where differences in temperature, background noise, geometry, and equipment response can take place. The comparison with the incident sound will be with the real incident sound, not with another measured in the same conditions.

Therefore, the method was used throughout the measurements. The computer program was used again to process a feasible set-up that would leave direct and reflected components separated. The solution was to create a “temporal bin”: that is, to impose conditions to the set-up such that all reflections arrive within a certain time interval. This presented schematically in Figure 8.8, showing all reflections except those from the ceiling, within the same time interval.

Due to the short distances involved in the measurements it was assumed that the compensation for air attenuation could be safely disregarded. In a preliminary measurement of the louvre, the reflection coefficient was calculated in both ways, with and without compensation for air attenuation, and results are presented in Figure 8.9. The largest difference in the resulting reflection coefficient, in the high frequency, is about 2% and air attenuation was not taken into account in subsequent measurements.

8.4 ANALYSIS OF TIME WINDOW

Throughout this work, all impulse measurements were performed by means of application of rectangular windows to extract the component under analysis from the time history. As long as the whole impulse fits within the window limits, this “flat weighting” is recommended. Actually, it would be detrimental to use a smoothly shaped window in the analysis because it would give different weighting to different parts of the time history, particularly the extremities, and thus modify the result [20]. However, as stated previously, the small dimensions of the room and its acoustics characteristics gave rise to difficulties in separating the components. The time interval between reflections from louvre and from the ceiling was small and hence it proved difficult to window. In this circumstance, a different window function is required.

The half Blackman-Harris window is suggested in the literature [17,18], which is the right hand side of the whole function. Due to its nature, the initial portion of the window does not alter the impulse power and its amplitude varies smoothly along the length towards zero value and slope at the end. A four-term full Blackman-Harris window for a J -point data sample is equal to [21]:

$$w(j) = a_0 - a_1 \cos\left(\frac{2\pi j}{J}\right) + a_2 \cos\left(\frac{4\pi j}{J}\right) - a_3 \cos\left(\frac{6\pi j}{J}\right) \quad (8.8)$$

where $a_0 = 0.35875$, $a_1 = 0.48829$, $a_2 = 0.14128$, $a_3 = 0.01168$, and $j = 0, \dots, J-1$. The function is plotted in Figure 8.10 for $J = 100$.

The application of the two different types of windows was investigated in a preliminary test. An aluminium panel of dimensions 2.23 m length, 1.78 m height and 3 mm thickness was measured for normal incidence impulsive sound. Loudspeaker to microphone distance was 0.82 m, with both raised 0.89 m from the floor. The equipment used was the same as in Chapter 5.

The incident and reflected impulses were windowed using the rectangular window, Fourier transformed and the reflection coefficient calculated. The procedure was repeated with the half Blackman-Harris applied to the reflected impulse (the rectangular window remained applied to the direct component) and the result is shown in Figure 8.11. The use of half Blackman-Harris proved to be better for this case as the resulting reflector coefficient showed less fluctuations. The window was selected for the louvre measurements.

8.5 ABSOLUTE ERROR DUE TO BACKGROUND NOISE

The measurement of reflection coefficient (or absorption coefficient) by impulse response methods has been successfully applied both indoors and outdoors, such as for noise barriers. The influence of background noise on the accuracy of the absorption coefficient measured has been investigated by Vorländer [22]. He suggests that the required effective S/N should be expressed rather in terms of the absolute error of the absorption coefficient $\Delta\alpha$.

$$\Delta\alpha = 10^{-0.1(S/N)_{conv}} 10 \log \left(\frac{t_{window}}{n t_{MLS}} \right) \quad (8.9)$$

where t_{window} is time length of the window applied, n is the number of averages and t_{MLS} denotes the time elapsed during one MLS period. The relative error is simply given by $\Delta\alpha/\alpha$.

Another useful guideline given states that the absolute error caused by background noise is smaller than $\Delta\alpha < 0.001$ if

$$(S/N)_{conv} + 10 \log \left(\frac{t_{MLS} n}{t_{window}} \right) > 20 \text{ dB} \quad (8.10)$$

The measurement of background noise levels was repeated many times along the two years involved in the experimental work at the Acoustics Research Unit at Liverpool University. Using 16 averages, the lowest ratio for the conventional (S/N) was 37 dB at 100 Hz. Considering the selected parameters of the MLS measurements presented in Chapter 4, the right hand side of equations (8.10) gives 80 dB, which complies with the minimum requirement. Therefore, the uncertainty caused by S/N limits can be disregarded.

8.6 RESULTS

The reflection coefficient was measured at nine incident angles, from -60° to 60° , according to the convention used throughout this work. The four pairs of symmetric (to the normal) incident angles would present the same reflection coefficient, according to the principle of reciprocity [23]. Therefore, reflection coefficients for 0° , 15° , 30° , 45° and 60° were required. However, due to the small dimensions of the room, as described in 8.3, the measurement of reflection coefficient was feasible for normal and 45° of incidence only. For the other angles, there was no possible geometry that could avoid the overlapping of the reflected and other components.

Figure 8.12 shows the initial segment of the time history for 45° of incidence. Direct sound is within the interval indicated by the dots and it is shown again after amplitude and phase calibration. The equivalent reflection coefficient is presented in Figure 8.13 along with the result for normal

incidence.

Despite the impossibility to measure all angles, the method shows promise. Even if the analysis is carried out for random incidence, as sometimes is desirable in room acoustics, the use of the impulse method is not limited. The relation between angle dependent and diffuse absorption coefficient, as obtained in reverberation room measurements, is given by Paris [24]:

$$\alpha_{diffuse} = \int_0^{\pi/2} \alpha(\theta) \sin 2\theta d\theta \quad (8.11)$$

where θ is the incident angle.

An estimate of the diffuse absorption can be obtained from the absorption coefficient for 45° of incidence, as the term $\sin 2\theta$ in equation (8.11) is a maximum [24]. The absorption coefficient for 45° of incidence was obtained from the impulse response measurement of the reflection coefficient and is shown in Figure 8.14 along with absorption coefficient measured in reverberant conditions.

8.7 APPLICATION TO THE IMAGE METHOD

A further set of image model simulations were performed, with reflection measured by impulse used as input, rather than those calculated from diffuse decay field measurements. The transmission coefficient also was measured by the impulse response method. Presented in Figure 8.15 are the results for 45° , normal and -45° of incidence, along with the outcome of the simulations when assuming diffuse absorption. It can be observed that there is little change at high frequencies but with an averaged difference of about 3 dB in the low frequency region. Below 125 Hz, all simulations give negative values of insertion loss. It is believed that this is due to some degree of inaccuracy in the reflection coefficient measurement rather than the image model. The geometry set-up imposed by the room dimensions has induced the window to be set as short as possible, which in turn can reduce the frequency band of analysis.

8.8 REFERENCES

- [1] ISO 354:1985. Part 1, *Measurement of Sound Absorption in a Reverberation Room*.
- [2] Kosten C.W., *International Comparison Measurement in the Reverberation Room*, *Acustica*, **12**, 3-13, (1960).
- [3] Fahy F.J., *Rapid Method for the Measurement of Sample Acoustic Impedance in a Standing Wave Tube*, *J. Sound Vib.*, **97**(1), 168-170, (1984).
- [4] Seybert A.F. and Ross D.F., *Experimental Determination of Acoustic Properties Using a Two-Microphone Random-Excitation Technique*, *J. Acoust. Soc. Am.*, **61**(5), 1362-1370, (1977).
- [5] Chung J.Y and Blaser D.A., *Transfer Function Method of Measuring In-Duct Acoustic Properties. I. Theory*, *J. Acoust. Soc. Am.*, **68**(3), 907-913, (1980).
- [6] Chung J.Y and Blaser D.A., *Transfer Function Method of Measuring In-Duct Acoustic Properties. II. Experiment*, *J. Acoust. Soc. Am.*, **68**(3), 914-921, (1980).
- [7] ISO 10534:1996, *Determination of Sound Absorption Coefficient and Impedance in Impedance Tubes - Part 1: Method using Standing Wave Ratio, Part 2: Transfer Function Method*.
- [8] Cummings A., *Impedance Tube Measurements on Porous Media: The Effects of Air-Gaps Around the Sample*, *J. Sound Vib.*, **151**(1), 63-75, (1991).
- [9] London A., *The Determination of Reverberant Sound Absorption Coefficients from Acoustic Impedance Measurements*, *J. Acoust. Soc. Am.*, **22**(2), 263-269, (1950).
- [10] Goydke H., *New International Standards for Building and Room Acoustics*, *Appl. Acoust.*, **52**(3/4), 185-196, (1997).
- [11] Ingard U. and Bolt R.H., *A Free-Field Method of Measuring the Absorption Coefficients of Acoustic Materials*, *J. Acoust. Soc. Am.*, **23**, 509-516, (1951).
- [12] Ando Y., *The Interference Pattern Method of Measuring the Complex Reflection Coefficient of Acoustic Materials at Oblique Incidence*, 6th. Intern. Congress on Acoustics, paper E33, (1968).
- [13] Kintsl Z., *Investigation of the Sound Absorption of Wall Sections by a Pulse Technique*, *Sov. Phys. Acoust.*, **21**(1), 30-32, (1975).
- [14] Davies J.C. and Mulholland K.A., *An Impulse Method of Measuring Normal Impedance at Oblique Incidence*, *J. Sound and Vib.*, **67**(1), 135-149, (1979).

- [15] Cramond A.J. and Don C.G., *Reflection of Impulses as a Method of Determining Acoustics Impedance*, J. Acoust. Soc. Am., **75**(2), 382-389, (1984).
- [16] Yuzawa M., *A Method of Obtaining the Oblique Incident Sound Absorption Coefficient Through an On-The-Spot Measurement*, Appl. Acoustics, **8**, 27-41, (1975).
- [17] Garai M., *Measurement of the Sound-Absorption Coefficient In Situ: The Reflection Method Using Periodic Pseudo-Random Sequences of Maximum Length*, Appl. Acoust. **39**, 119-139, (1993).
- [18] Mommertz E., *Angle-Dependent In-situ Measurements of Reflection Coefficients Using a Subtraction Technique*, Appl. Acoust., **46**, 251-263, (1995).
- [19] Borish J. and Angell J.B., *An Efficient Algorithm for Measuring the Impulse Response Using Pseudorandom Noise*, J. Audio Eng. Soc., **31**(7), 478-488, (1983).
- [20] Broch J.T., *Mechanical Vibration and Shock Measurements*, Brüel & Kjær, (1984).
- [21] Rife D.D. and Vanderkoy J., *Transfer-Function Measurements with Maximum-Length Sequences*, J. Audio Eng. Soc., **37**(6), 419-444, (1989).
- [22] Vorländer M. and Mommertz E., *Guidelines for the Application of the MLS Technique in Building Acoustics and in Outdoor Measurements*, Proc. InterNoise, vol.III, (1997).
- [23] Kuttruff H., *Room Acoustics*, Chapter III, 2nd edition, Applied Science Publishers Ltd, London, (1979).
- [24] Kuttruff H., *Room Acoustics*, Chapter II, 2nd edition, Applied Science Publishers Ltd, London, (1979).

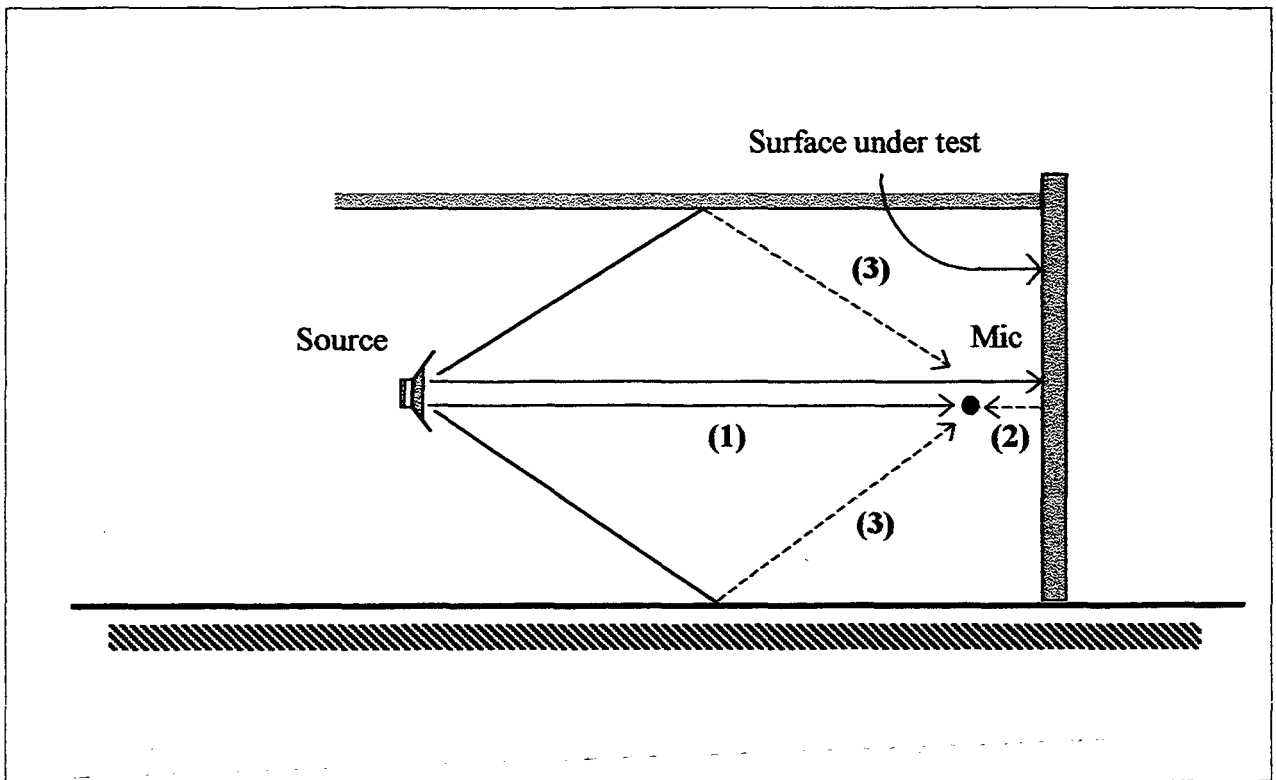


FIGURE 8.1 - Set-up of reflection method for normal incidence measurements.

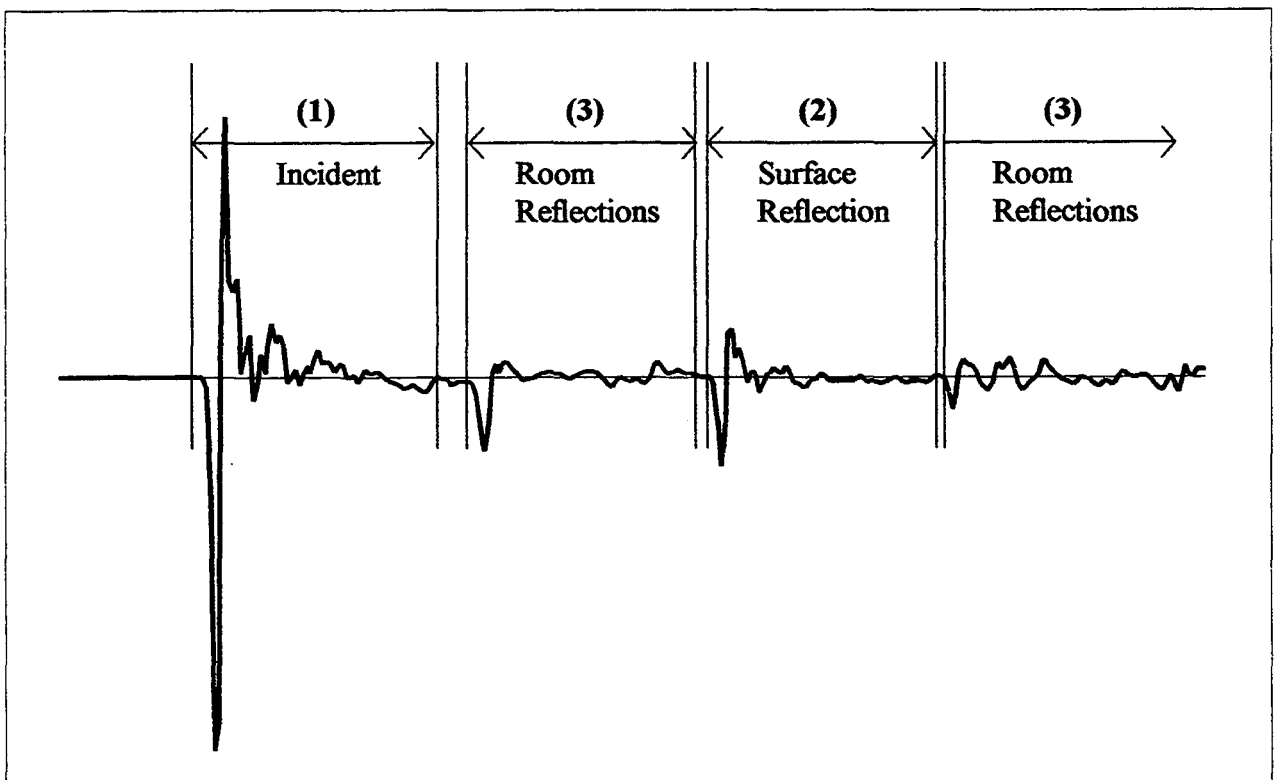


FIGURE 8.2 - Time history with incident and reflected components.

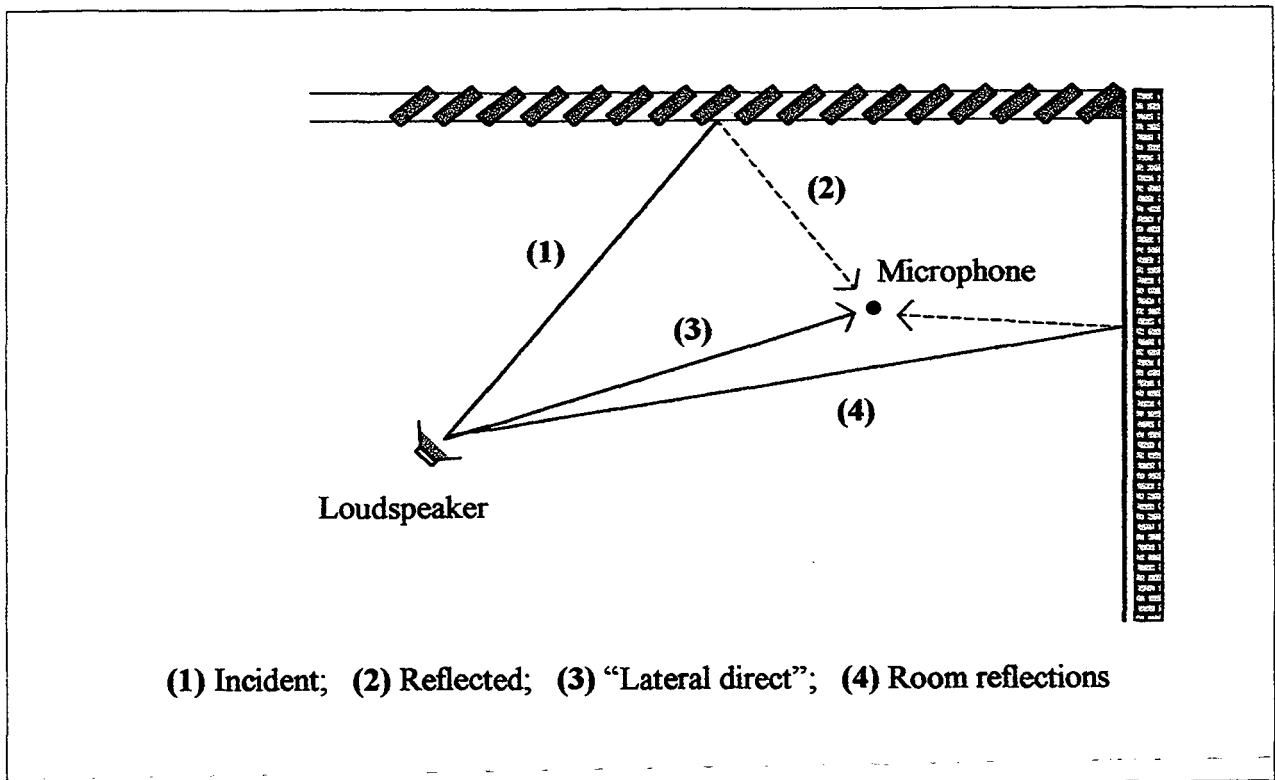


FIGURE 8.3 - Set-up of reflection method for oblique incidence measurements.

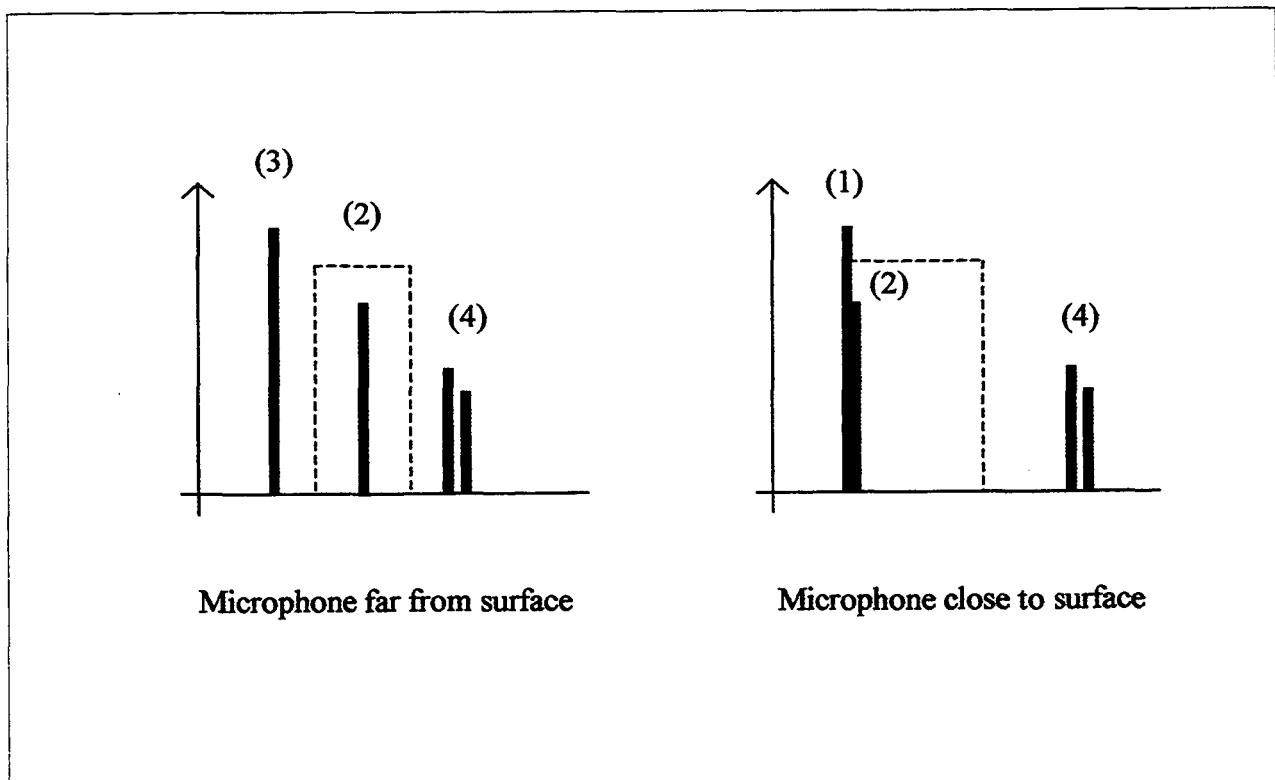


FIGURE 8.4 - Time histories for different microphone to surface distances [18].

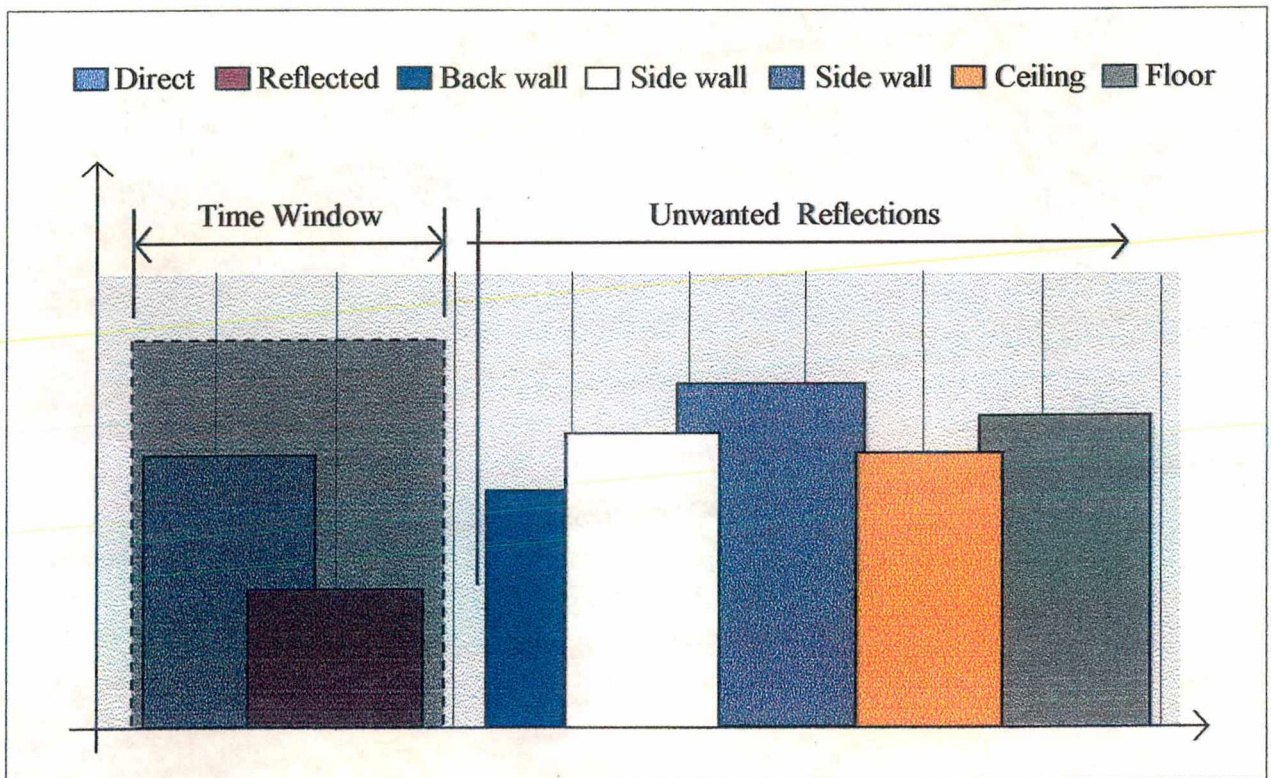


FIGURE 8.5 - Proposed time history for the use of the "cancelling method".

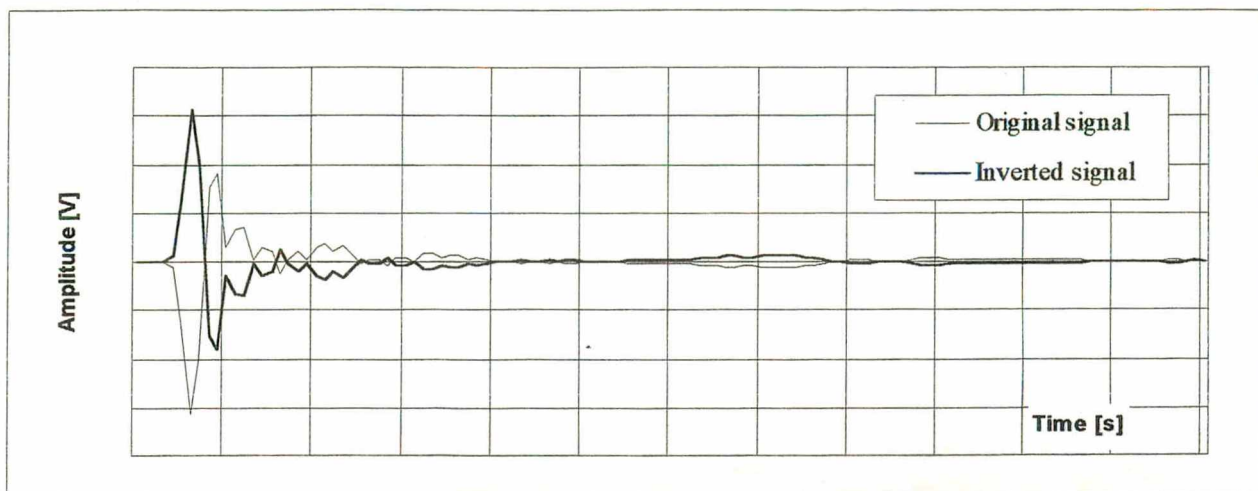


FIGURE 8.6 - Time history with original and inverted direct sound.

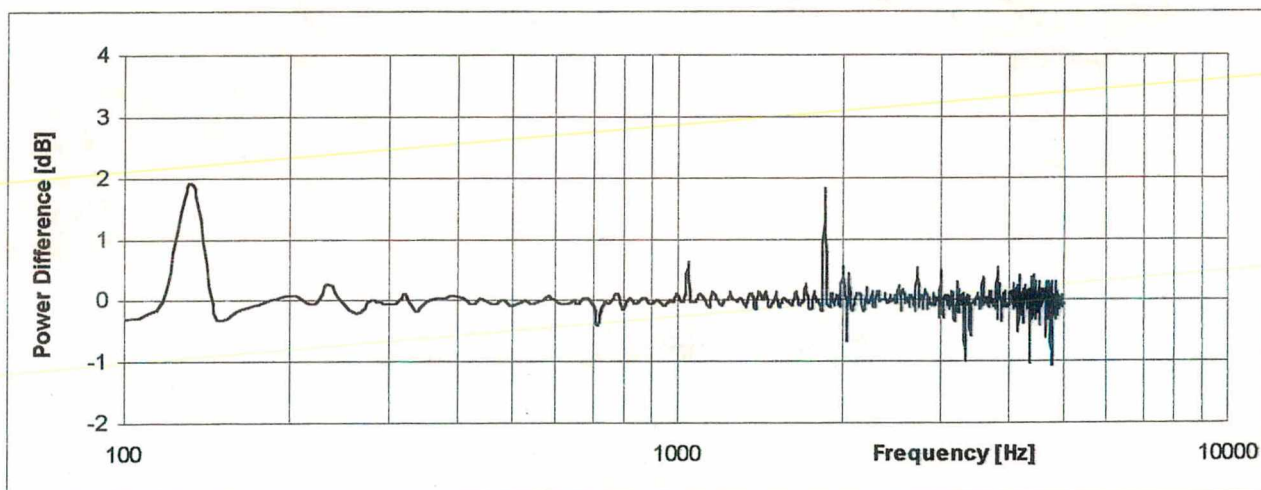


FIGURE 8.7 - Power difference of two successive impulses.

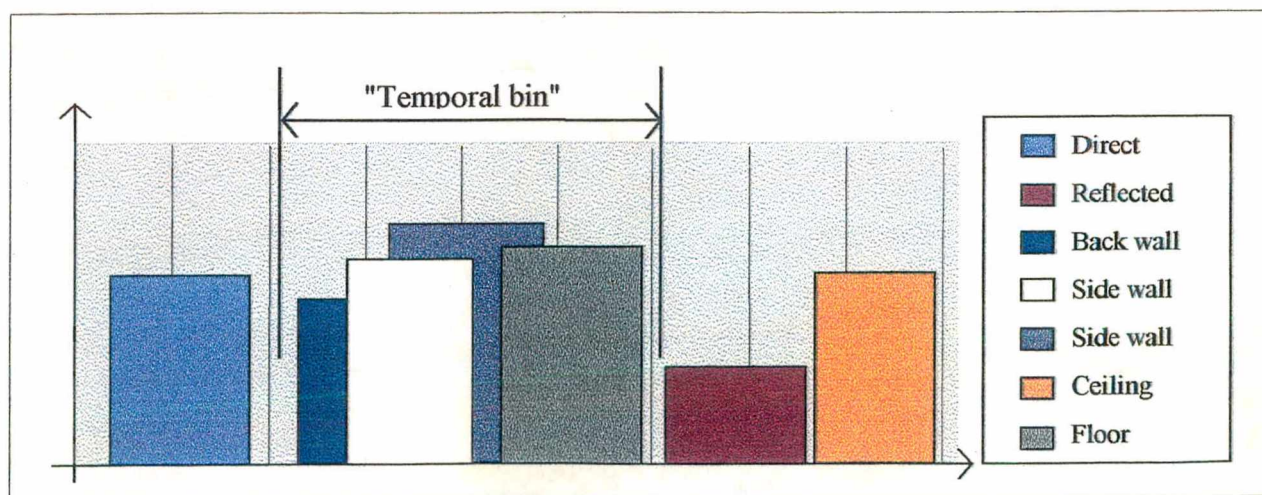


FIGURE 8.8 - Time history where all unwanted reflections are concentrated into the same time interval. The direct sound is windowed out, calibrated and used as reference signal.

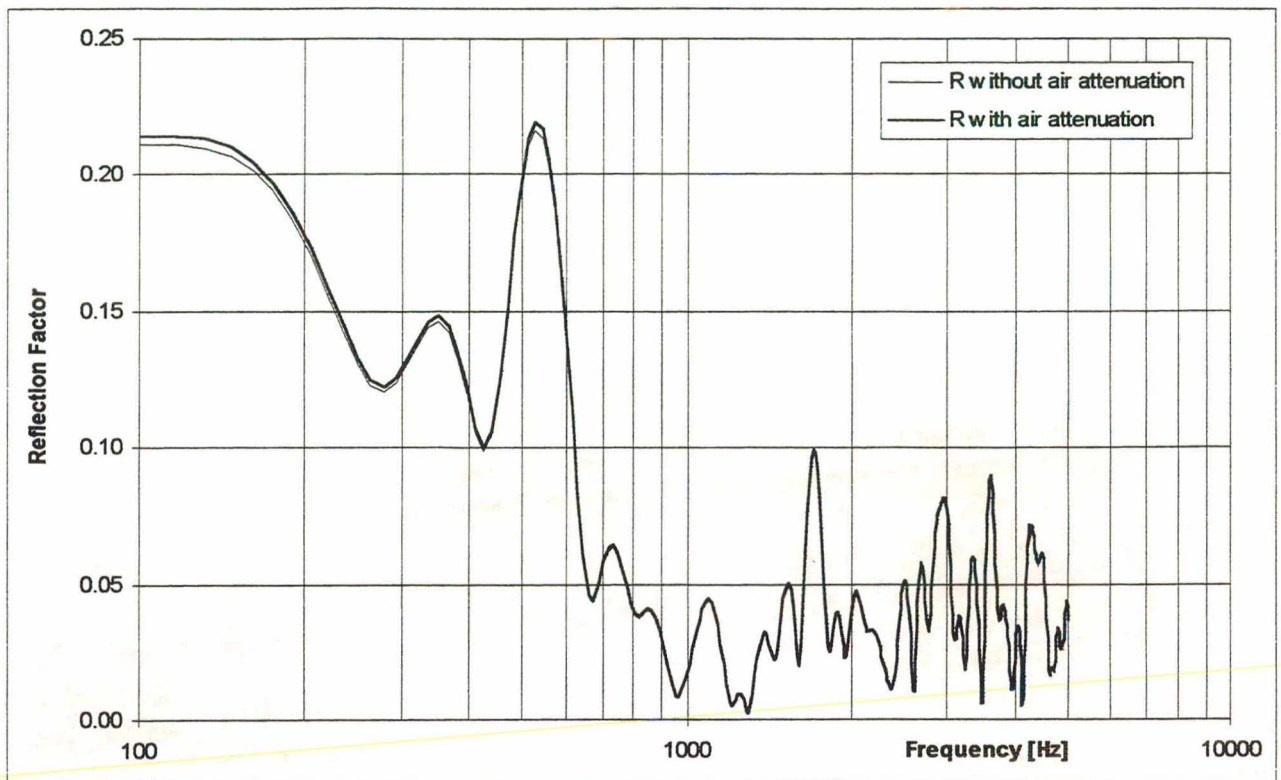


FIGURE 8.9 - Preliminary test of measurement of reflection coefficient with and without compensation for air attenuation.

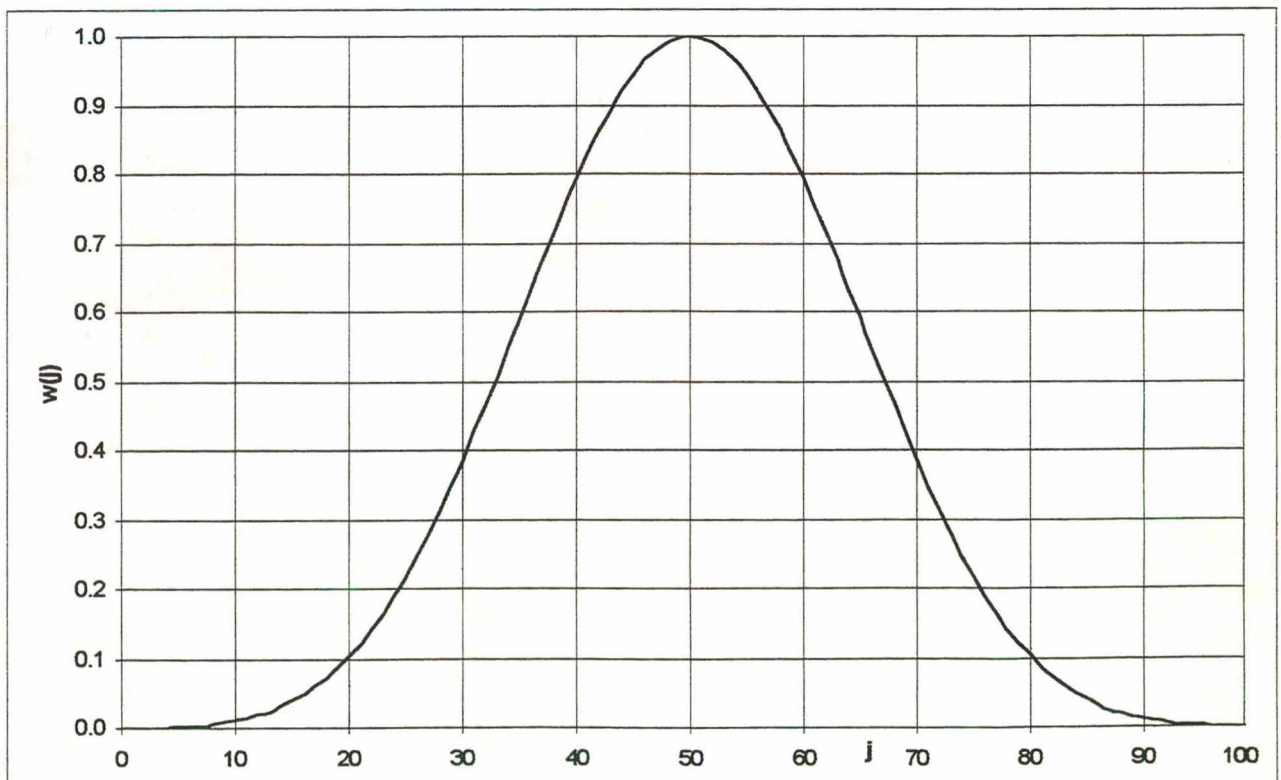


FIGURE 8.10 - Blackman-Harris window computed for $J = 100$.

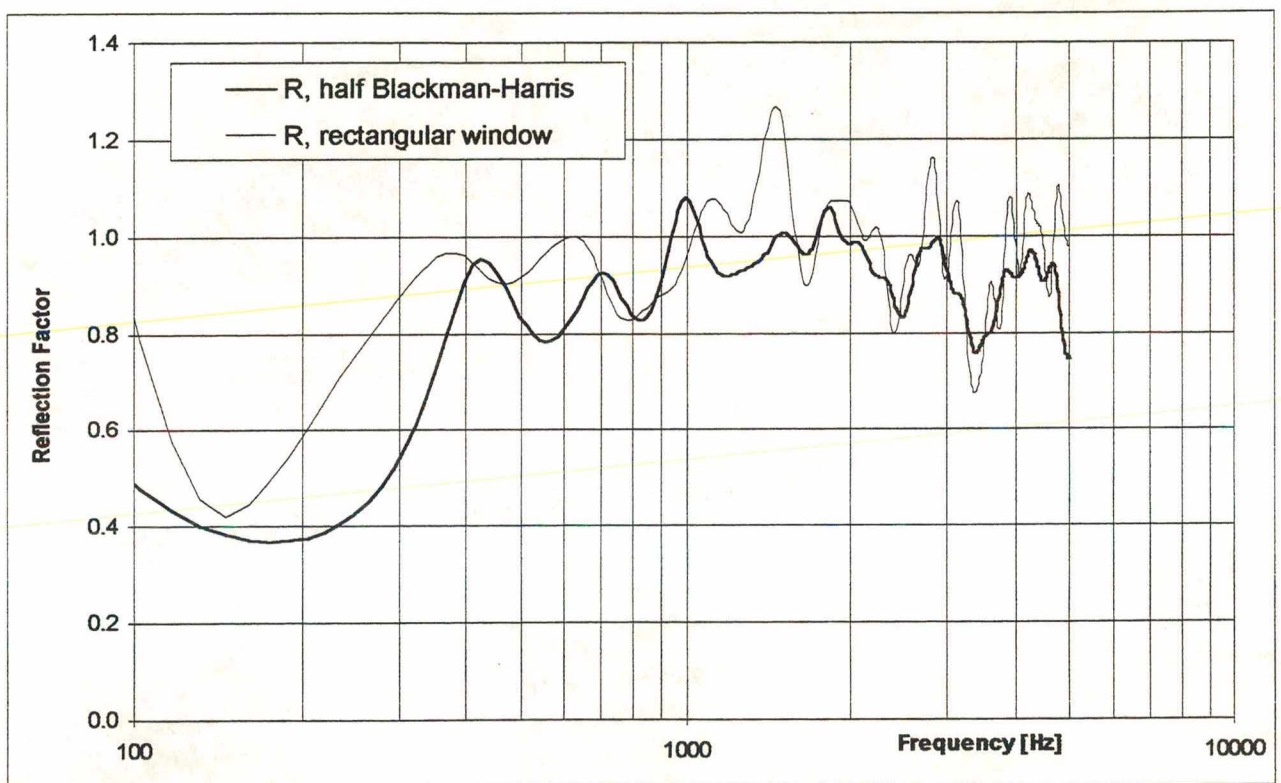


FIGURE 8.11 - Reflection coefficient of a metallic sheet using different windows.

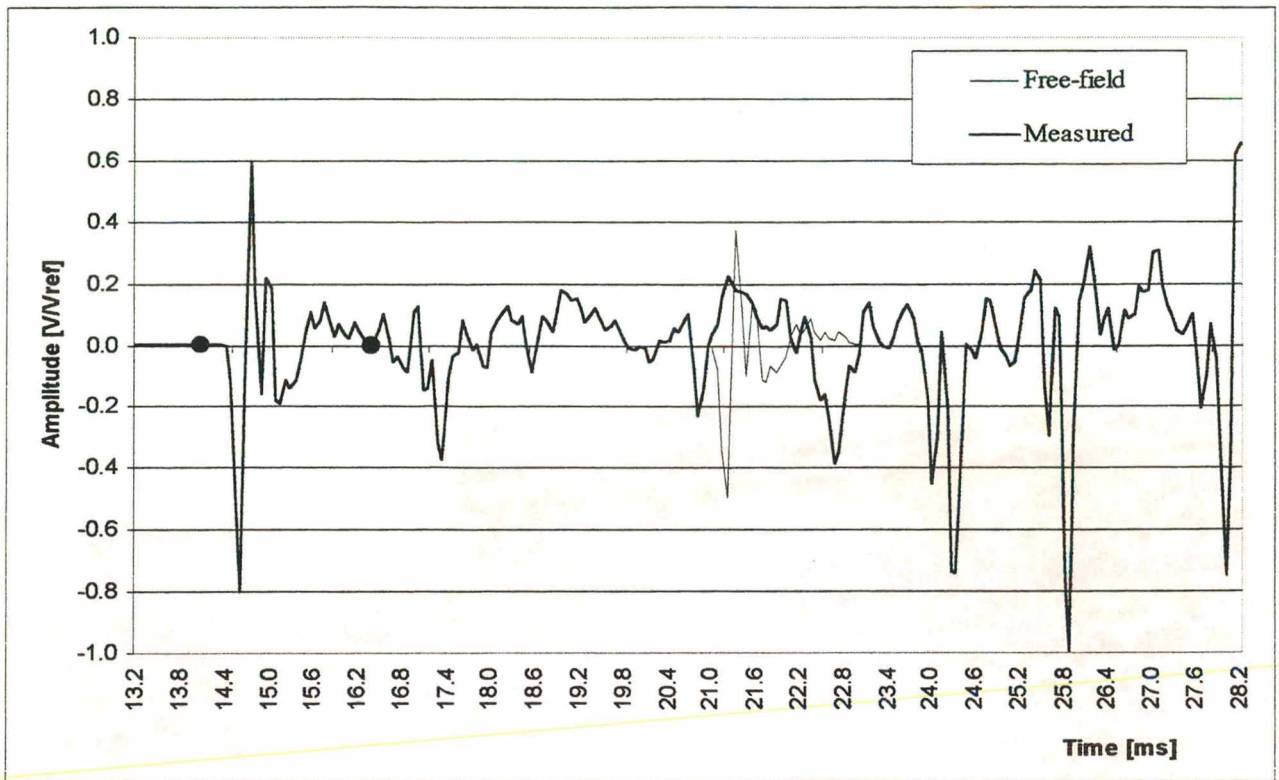


FIGURE 8.12 - Segment of measured time history and processed signal for free-field for 45° of incidence. The direct sound is within the dots.

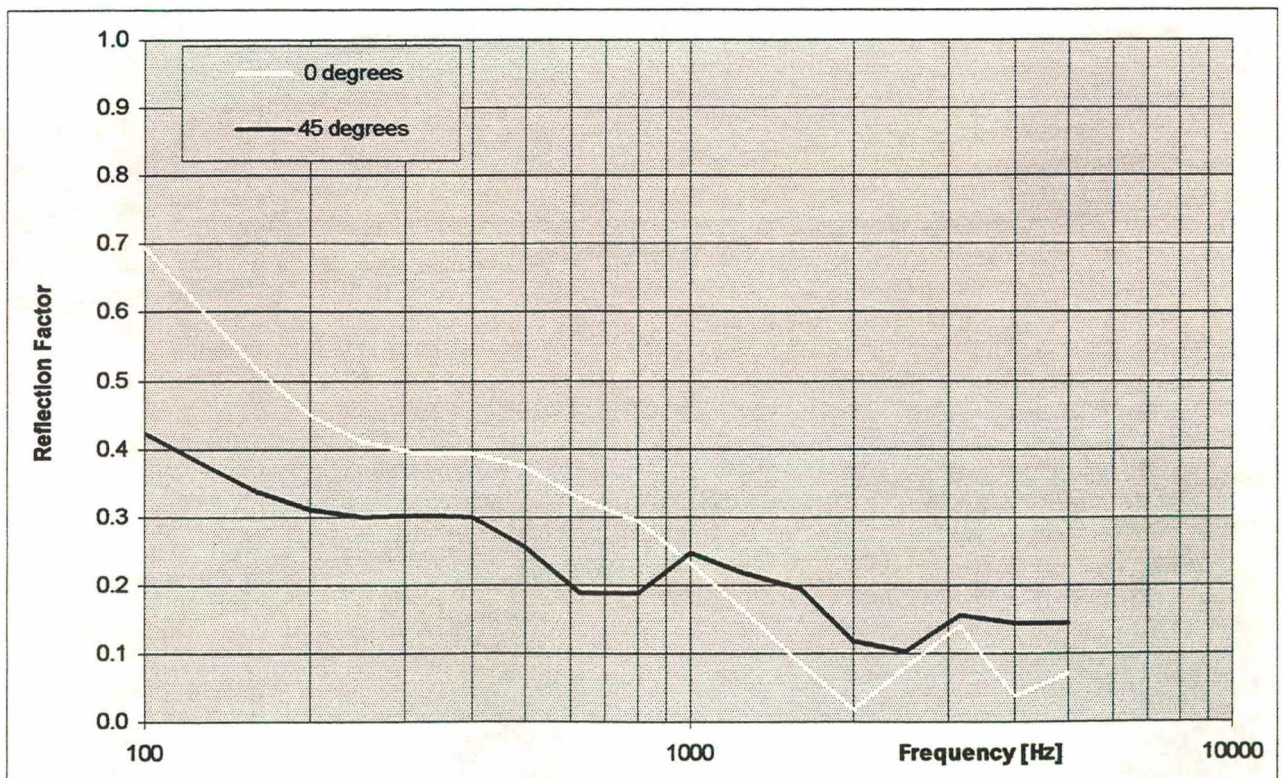


FIGURE 8.13 - Reflection coefficient measured by impulse for 2 incident angles.

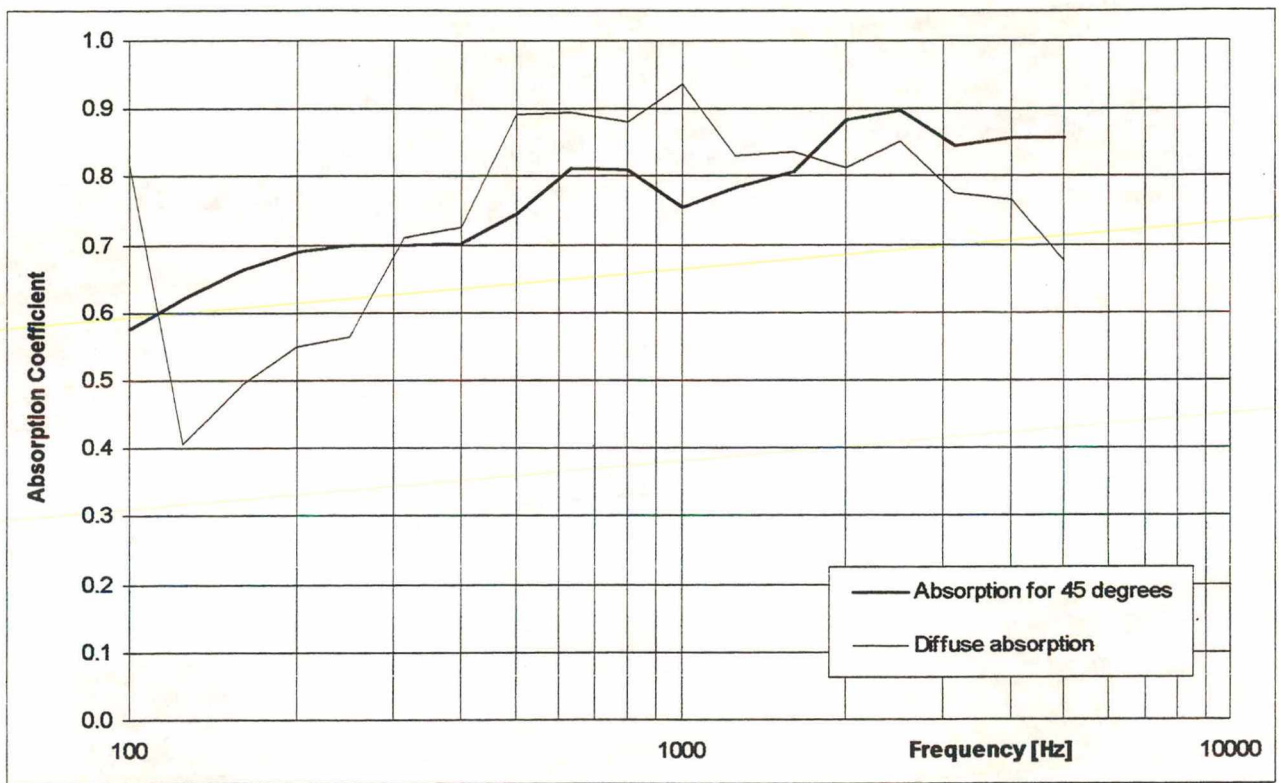


FIGURE 8.14 - Absorption coefficient measured for diffuse incidence and by impulse response for 45° of incidence.

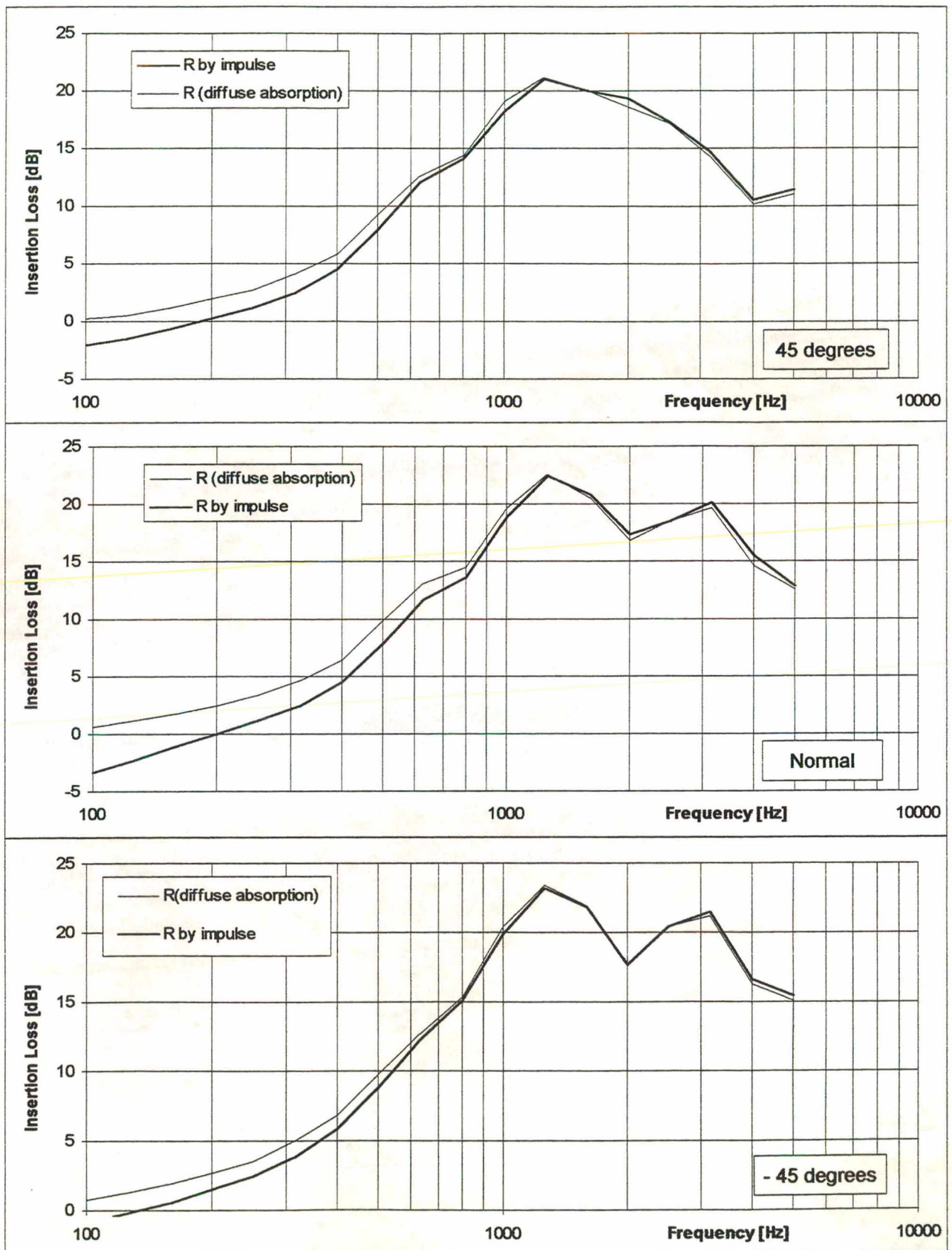


FIGURE 8.15 - Insertion loss for different incident angles simulated by image method for two different reflection factors: measured by impulse, and calculated using diffuse absorption and transmission coefficient by impulse.

CHAPTER 9

CONCLUDING REMARKS

9.1

Introduction

9.2

Conclusions

9.3

Topics for Further Research

9.1 INTRODUCTION

In this thesis, the problems of characterising and rating the sound insulation of acoustic louvres have been addressed. Acoustic louvres provide weather protection, allow natural and forced ventilation, whilst affording acoustic protection. The acoustic protection can be for the control of industrial noise breakout or noise break-in into residential and other noise sensitive areas.

In Europe and the USA, acoustic louvres are commonly used as part of the facades of industrial buildings and ventilation entry and exit areas of enclosures around noise producing plant and machinery. They are less common in Brazil and in other hot climate countries but offer the possibility of providing the designer with a low cost solution to the problem of providing natural ventilation to and low noise in internal spaces. Their use will increase world-wide if and when their acoustic performance can be simply rated and specified and where performance data can be made available for low noise design engineering.

At present, acoustic louvres differ from conventional ventilation louvres only in the addition of sound absorbent material on the underside of the louvre blades. Other devices and controlling mechanisms have been proposed but not developed, again, because there is no accepted method of measuring and rating performance. This has been confirmed by a recent survey of manufacturers and suppliers of acoustic louvres in the UK.

This thesis has shown that existing standard methods of measurement of sound insulation of louvres and other low insulation devices are inappropriate. Indeed, confusions persist in the terminology used to describe performance. It is confirmed that insertion loss in field conditions is the desired performance index and the method proposed by HEVAC is an appropriate test method but large test facilities would be required, in a low noise external environment.

Therefore, the work reported in this thesis was towards the development of a quick and accurate test method that did not involve large acoustic test facilities. The approach proposed is the impulse response analysis method and the aims of the thesis work, therefore, were to establish the practicality of the measurement method and confirm that the test data obtained properly represented field performance.

9.2 CONCLUSIONS

- 1 Impulse response analysis has been successfully implemented as a measurement system and technique for acoustic louvres and other low insulation devices. The measurement system used conventional small loudspeakers and microphones. The novelty is in the data acquisition and processing. The acquisition was successfully implemented in the form of maximum-length sequences, which gave superior signal-noise when compared with normal white noise excitation.

The processing was in the form of windowing of response time histories and then fast Fourier analysing to give the insertion loss of the louvre, independent of the room acoustic response. It has been demonstrated that careful but easily obtained source-device-receiver geometries allow the direct signal to be obtained for frequency analysis in non specialist environments. This was confirmed by comparison of measured and predicted sound transmission loss of thin solid panels. This was further confirmed by measuring the diffracted component around solid panels and comparing results with prediction according to Kirchhoff.

- 2 Impulse response analysis of acoustic louvres shows that the response signal is dominated by direct and internally diffracted components that must be included in the time window.

The resultant spectrum of the transmission loss shows two characteristic regions. At low frequencies, the transmission loss is controlled by a mass-layer effect, which depends on the porosity of the louvre. In this region, typically up to 1 kHz, the sound insulation can be increased by increasing the area/depth of contact between the solid and contained air. At frequencies, typically above 1.6 kHz, diffraction and absorption are the dominant controlling mechanisms. This was confirmed for the former by comparison of measurement with prediction according to Kirchhoff diffraction theory. Diffraction and the resultant interference are indicated as dips and peaks in the transmission loss, which are dependent on source and receiver location and angle of incidence.

- 3 The angle dependence of transmission loss was investigated over a range $-60^{\circ} < \theta < 60^{\circ}$

degrees. It was demonstrated that transmission at the angle of incidence equal to the louvre blade angle dominates the angle averaged value. The practical implication is this; that a single measurement of transmission loss approximates the more laborious angle averaged measurement, to engineering accuracy.

- 4 A relevant aspect of the simulation was to disclose that the insulation performance of open screens is dependent upon the geometry alone. Both the low and high frequency ranges, where mass layer and diffraction effects dominate, respectively can be predicted independently of the mass of the louvre. The angle of incidence parallel to the blades was shown to be dominant with respect to the overall performance. Therefore, in developing novel designs of louvres for high insulation, special attention should be made at that incident angle by the choice of the periodicity, the absorption material and ratio of perforation of its cover, and dimensions of gaps and blades.
- 5 It remained to relate measured transmission loss, obtained by the impulse response method, to insertion loss when installed, obtained by simulation of the HEVAC proposed test method.

The HEVAC facility was simulated by means of a simple acoustic image model implemented on computer. The model was validated by comparing results with impulse measurements for the same source-louvre-receiver vector.

- 6 The transmission loss also was obtained directly by near-field measurement of the transfer function across the blades of the louvre. The measured values were then incorporated into a modified diffraction model and gave good agreement with far-field impulse measurement of transmission loss.
- 7 Angular dependence was then incorporated into the model and obtained by the impulse method were compared with those predicted for HEVAC test.
- 8 It had been presumed that insertion loss would differ from transmission loss measurement because of the absorption in the HEVAC test room. This in turn would be primarily

dependent on the absorption offered by the internal face of the tested louvre.

The absorption was first modelled as an angle averaged value obtained from reverberation chamber measurement of the same absorbent material. Measured transmission loss and predicted insertion loss were compared and it was observed that the agreement was good in the frequency range controlled by the mass layer effect. The angle average results presented typically 2dB difference at high frequencies.

- 9 In order that all acoustic parameters of louvres, required for the HEVAC simulation, were obtained from impulse response measurement only, the apparatus was set up for capture of reflected rather than transmitted signals.

A temporal cancellation method, proposed by Mommertz, was tested but not found suitable due to the large amount of averages required to obtain perfectly identical successive impulses. When less number of averages was used the magnitude of the non-cancelled direct can be significant compared with rather small reflected component.

However, by careful selection of source-louvre-receiver geometry, the reflected component was isolated and the absorption coefficient spectrum obtained.

This angular dependent value was incorporated into the simulation and average insertion loss and directivity index obtained. When compared with impulse response measurement, it was observed that the louvre is less directional if insertion loss is the parameter in analysis, therefore, less directionality will be observed in real situations.

- 10 To summarise; impulse response analysis has been shown to be a practical measurement method which yields data representative of field performance of acoustic louvres when in the installed condition.

9.3 TOPICS FOR FURTHER RESEARCH

- 1 Lack of time and the unavailability of a large, apertured source room, in a low noise external

environment, prevented a full validation of the computer simulation of the HEVAC proposed measurement system. Therefore, although the agreement between impulse response measurement of transmission loss and the simulated insertion loss was promising, it remains to compare full-scale insertion loss measurement with impulse measurement.

- 2 Predicted values obtained from the simple image model must be treated with caution for low frequencies. This is because the sound field in the test enclosure will be modal and the assumption of a ray-like behaviour does not apply.

Finite element methods (FEM) would be more appropriate for low frequencies and therefore the performance of the test chamber should be modelled accordingly.

- 3 In addition, it remains to validate the transfer function measurement of louvre transmission loss by FEM modelling of the sound field between the louvre blades. This would be the initial step in design optimisation of louvres by consideration of the separate roles of geometry and absorption, the significant parameters.
- 4 The impulse method can be used to test the insulation characteristics of other and more novel perforated screens and low sound insertion loss devices in general. Such a quick test method will promote innovation in acoustic design.
- 5 Proposed design should be designed having geometry and absorption material as parameters of insulation performance. Changes could be tested by the impulse measurement method. New designed louvres, with same geometry and absorption material but different blade material, should be tested to confirm the non-significant role played by the blade material.

APPENDICES

Photography of the Louvre

- | | |
|-------------------|--|
| Appendix 1 | Transmission Loss of a Solid Screen |
| Appendix 2 | Transmission Loss of Louvre by Mass Layer Model |
| Appendix 3 | Transmission Loss of Louvre by Diffraction Model |
| Appendix 4 | Normal-Mode and Image Method Solutions for Rectangular Enclosure of Rigid Walls |
| Appendix 5 | Geometry for Reflection Coefficient Measurements |
| Appendix 6 | Insertion Loss Simulation of HEVAC Test by Image Method |
| Appendix 7 | Published papers |

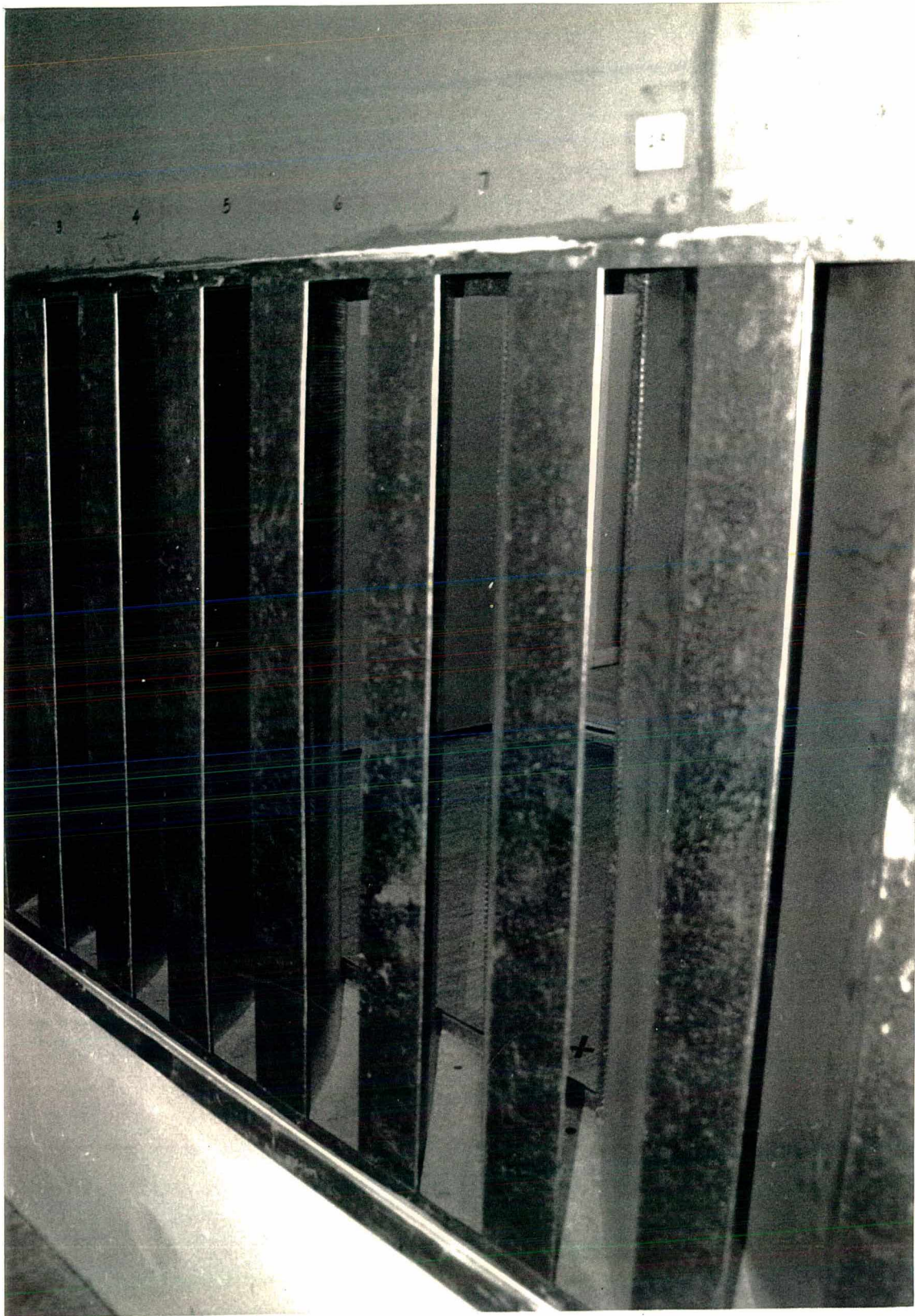


PLATE 1 - External view of the louvre: surface of the blades in solid steel.

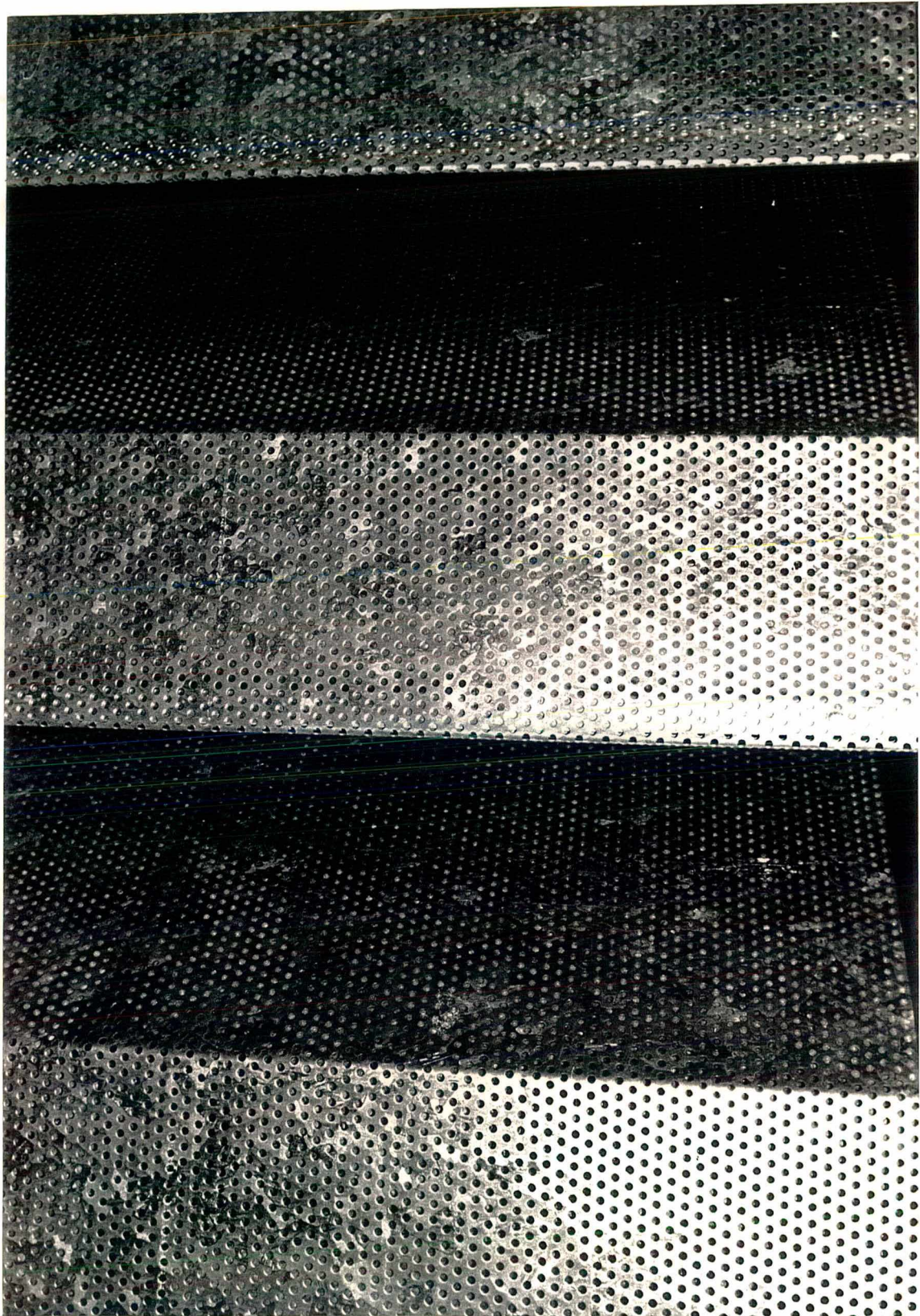


PLATE 2 - Internal view of the louvre: perforated steel sheet with mineral wool infill.

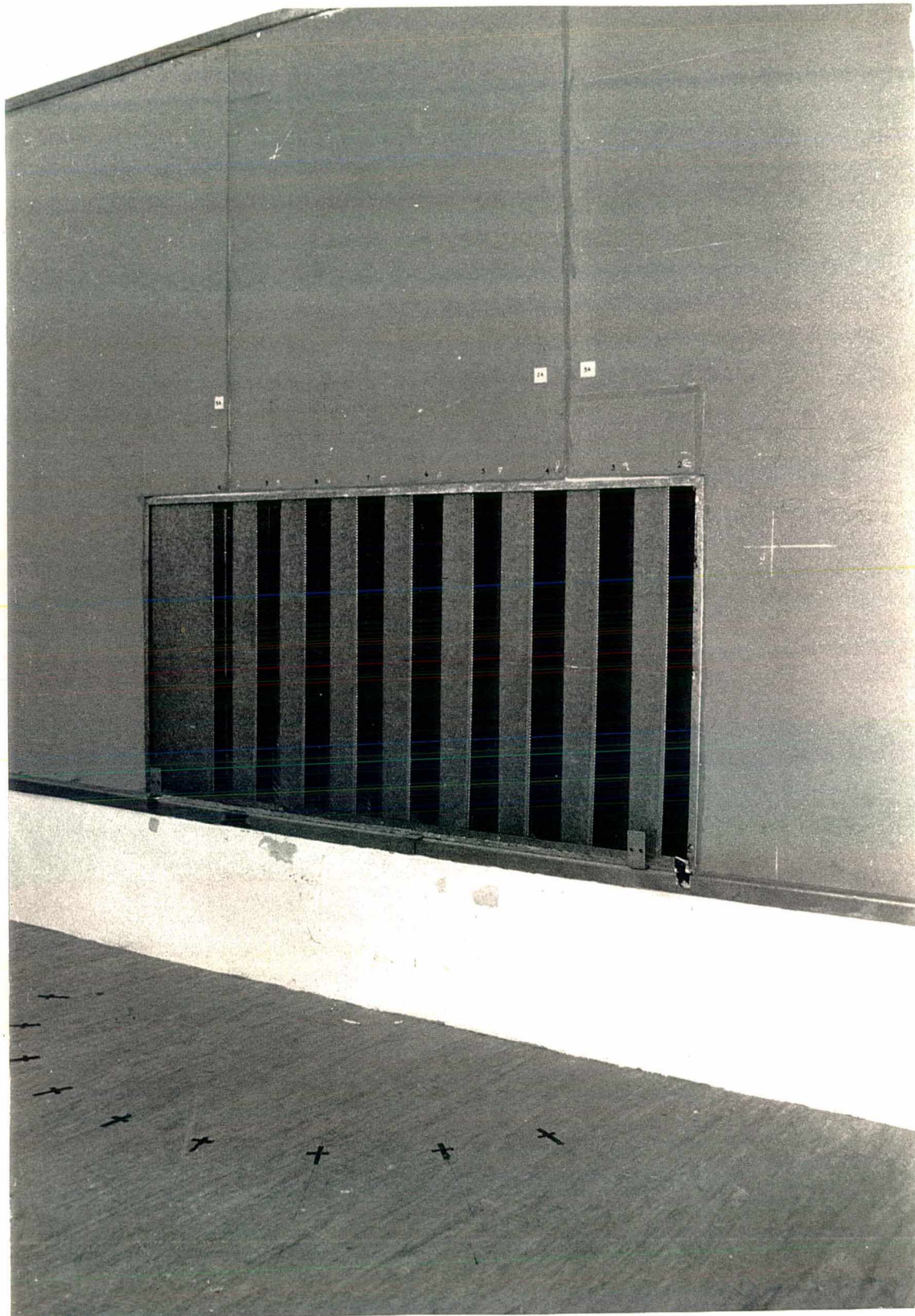


PLATE 3 - Louvre mounted in the aperture of the transmission suite.

! PROGRAM LISTING FOR SOLID SCREEN

```

! Calculates the transmission loss of a solid screen/barrier using
! Fresnel-Kirchhoff diffraction theory with term added for transmission.

! Frequency range of prediction: 43.89 Hz to 5003.51 Hz

! Output file will contain four columns:
! Freq (Hz): Resolution is 14.63 Hz
! Dir(i): Transmission loss of direct sound transmission
! Diff(i): Transmission loss of diffracted sound energy
! Tot(i): Total Transmission Loss

REAL          y(330),z(300),rs,rr,cosr,coss,mass,stepy,stepz,yNo,zNo
REAL          f(340),Dir(340),Diff(340),Tot(340),wn(340),lowfre,hifre
COMPLEX*8     ppp0(340)
COMPLEX*8     ppp(330,300),p2,p1,pppp(330,300)
CHARACTER*8   fnameo,ana,anb
DATA          c/340.0/,pi/3.14159/,pc/410/

! Input coordinates of source (xs,ys,zs), receiver (xr,yr,zr),
! screen(xb,yb1,yb2,zb1,zb2).
! The barrier is in plan view in the XY co-ordinates and Z represents the
! height.

PRINT*,'Enter output file name'
READ '(a8)',fnameo
1000 PRINT*,'Input X of the source'
READ*,xs
PRINT*,'Enter Y of the source'
READ*,ys
PRINT*,'Enter Z of the source'
READ*,zs
PRINT*,'Enter x of the receiver'
READ*,xr
PRINT*,'Enter y of the receiver'
READ*,yr
PRINT*,'Enter z of the receiver'
READ*,zr
PRINT*,'Enter x of the barrier'
READ*,xb
PRINT*,'Enter y1 of the barrier'
READ*,yb1
PRINT*,'Enter y2 of the barrier'
READ*,yb2
PRINT*,'Enter z1 of the barrier'
READ*,zb1
PRINT*,'Enter z2 of the barrier'
READ*,zb2
PRINT*,'Enter the lowest frequency (min. freq.= 43.89 Hz)'
READ*,lowfre
PRINT*,'Enter the highest frequency (max. freq.= 5003.51 Hz)'
READ*,hifre
PRINT*,'Enter the mass'
READ*,mass
PRINT*,'Would you like to check the data you entered ? (y/n)'
READ'(a4)',ana
IF (ana.eq.'y'.or.ana.eq.'Y')THEN
PRINT*,'
PRINT*,'-----'
PRINT*,'Source:  xs',xs,' ys=',ys, ' zs=',zs

```

```

PRINT*, 'Receiver:  xr=',xr, ' yr=',yr, ' zr=',zr
PRINT*, 'Barrier :  xb=',xb, 'yb1=',yb1, 'yb2=',yb2
PRINT*, '          zb1=',zb1, 'zb2=',zb2
PRINT*, 'Lowest frequency =',lowfre, 'Hz'
PRINT*, 'Highest frequency =',hifre, 'Hz'
PRINT*, 'Mass =',mass, 'kg/m2'
PRINT*, '
PRINT*, '-----'
PRINT*
PRINT*
PRINT*, 'Would you like to change the data ? (y/n)'
READ  '(a4)',anb
      IF (anb.eq.'y'.or.anb.eq.'Y') THEN
          GOTO 1000
      ENDIF
ENDIF
OPEN (UNIT=4,file=' '//fnameo//' .dat')
WRITE (4,100)
100 FORMAT(3x, 'Coordinates of the SOURCE are:')
WRITE (4,200)xs,ys,zs
200 FORMAT(3x, 'xs= ',f6.3,10x, 'ys= ',f6.3,10x, 'zs= ',f6.3)
WRITE (4,300)
300 FORMAT (3x, 'Coordinates of the RECEIVER are:')
WRITE (4,400)xr,yr,zr
400 FORMAT (3x, 'xr= ',f6.3,10x, 'yr= ',f6.3,10x, 'zr= ',f6.3)
WRITE (4,500)
500 FORMAT (3x, 'Coordinates of the SCREEN are:')
WRITE (4,600)xb,yb1,yb2,zb1,zb2
600 FORMAT(3x, 'xb= ',f6.3,10x, 'yb1= ',f6.3,9x, 'yb2= ',f6.3
          &/3x, 'zb1= ',f6.3,9x, 'zb2= ',f6.3)
WRITE (4,700)hifre,lowfre
700 FORMAT(3x, 'HIGH freq.= ',f7.2, ' Hz',5x, 'LOW freq.= ',&
          &f7.2, ' Hz')
WRITE (4,800)mass
800 FORMAT(3x, 'mass=',f6.3, ' kg/m2')
CLOSE(4)
OPEN (unit=3,file=' '//fnameo//' .out',position='append')
WRITE (3,40)
40 FORMAT(3X, 'Freq.      ',',',5x, 'IL (Dir)',',',5x, 'IL (Dif)',',',5x, 'IL (Tot)')

! Parameters: step -- The dimension of each elemental area
! ds ----- equals to 1/5th of the wavelength.
! pnumb ----- The number of the points decided by a 14.63 Hz
!              interval in the whole frequency range
! length ----- The length of the barrier
! high ----- The height of the barrier
! rr0 ----- The distance between receiver and barrier
! rs0 ----- The distance between receiver and source
! wn(i) ----- The wavenumber
!
step=c/(hifre*5.0)
pnumb=(hifre-lowfre)/14.63
length=yb2-yb1
high=zb2-zb1
rr0=sqrt((xr-xb)**2)
rs0=sqrt((xs-xb)**2)
r0=sqrt((xs-xr)**2+(ys-yr)**2+(zs-zr)**2)

! Calculation
DO 10 i=1,int(pnumb)+1
f(i)=lowfre+(i-1)*14.63
wn(i)=2*pi*f(i)/c
ppp0(i)=exp(cmplx(0.0,wn(i)*r0))/r0

```

```

yNo = int(length/step)+1
zNo = int(high/step)+1
p1=(0.0,0.0)
p2=(0.0,0.0)
DO 20 m=1,yNo
DO 30 n=1,zNo
stepy = length/yNo
stepz = high/zNo
y(m)=yb1+(1/2.0+(m-1))*stepy
z(n)=zb1+(1/2.0+(n-1))*stepz
rr=sqrt((xb-xr)**2+(y(m)-yr)**2+(z(n)-zr)**2)
rs=sqrt((xb-xs)**2+(y(m)-ys)**2+(z(n)-zs)**2)
cosr=rr0/rr
coss=rs0/rs

pppp(m,n)=(stepy*stepz)/(4*pi)*exp(cmplx(0.0,wn(i)*(rs+rr)))/(rr*rs) &
&*((cmplx(0.0,wn(i))-1/rs)*coss &
&+(cmplx(0.0,wn(i))-1/rr)*cosr) &
&*SQRT(1/(1+(2*pi*f(i)*mass*coss/(2*pc))**2)) &
&*exp(cmplx(0.0,Atan(2*pi*f(i)*mass*coss/(2*pc))))

ppp(m,n)=(stepy*stepz)/(4*pi)*exp(cmplx(0.0,wn(i)*(rr+rs))) &
&/ (rr*rs)*((cmplx(0.0,wn(i))-1/rr)*cosr &
&+(cmplx(0.0,wn(i))-1/rs)*coss)

p1=p1+pppp(m,n)
p2=p2+pppp(m,n)
30 CONTINUE
20 CONTINUE
Dir(i)=20*log10(abs(ppp0(i))/abs(-p2))
Diff(i)=20*log10(abs(ppp0(i))/abs(p1+ppp0(i)))
Tot(i)=20*log10(abs(ppp0(i))/abs(p1+ppp0(i)-p2))
WRITE(3,50)f(i),',',Dir(i),',',Diff(i),',',Tot(i)
10 CONTINUE
50 FORMAT(1x,f9.3,2x,a1,2x,f9.3,2x,a1,2x,f9.3,2x,a1,2x,f9.3)
CLOSE(3)
STOP
END

```

! PROGRAM LISTING FOR MASS MODEL

```

! Program MASS.F90
! This program runs the prediction according to mass layer effect.
! Resolution of 14.63 Hz to match MLSSA's output

! Output file will contain two columns:
! Freq (Hz): Frequency range from 43.63 Hz to 5003.51 Hz
! Mas(i): Transmission loss using mass-layer model

INTEGER      yNo, zNo, numfreq
REAL         xs, ys, zs, xr, yr, zr, xl, yll, yl2, zll, zl2, out
REAL         temp, blade, gap, thickness, lowfre, hifre, mass, length
REAL         high, meq
REAL         rr0, rs0, w, k, yy, zz
REAL         f(350), Mas(350)
COMPLEX*8    jk, P0, P1, PM, PG
CHARACTER*8  output, prg_name, ana, anb
DATA         pi/3.14159/,airdens/1.21/resol/14.63015/

100 PRINT*,'Enter ouput file name:'
    READ'(a8)',output
    PRINT*,'Enter name of program to be used:'
    READ'(a8)',prg_name
    PRINT*,'Enter air temperature:'
    READ*,temp
    PRINT*,'Input X of the source:'
    READ*,xs
    PRINT*,'Enter Y of the source:'
    READ*,ys
    PRINT*,'Enter Z of the source:'
    READ*,zs
    PRINT*,'Enter X of the receiver:'
    READ*,xr
    PRINT*,'Enter Y of the receiver:'
    READ*,yr
    PRINT*,'Enter Z of the receiver:'
    READ*,zr
    PRINT*,'Enter X of the louvre:'
    READ*,xl
    PRINT*,'Enter Y1 of the louvre:'
    READ*,yll
    PRINT*,'Enter Y2 of the louvre:'
    READ*,yl2
    PRINT*,'Enter Z1 of the louvre:'
    READ*,zll
    PRINT*,'Enter Z2 of the louvre:'
    READ*,zl2
    PRINT*,'Enter the width of blade:'
    READ*,blade
    PRINT*,'Enter the width of gap:'
    READ*,gap
    PRINT*,'Enter the thickness of louvre:'
    READ*,thickness
    PRINT*,'Enter the mass density'
    READ*,mass
    PRINT*,'Enter the lowest frequency (min. freq.= 43.89 Hz):'
    READ*,lowfre
    PRINT*,'Enter the highest frequency (max. freq.= 5003.51 Hz):'
    READ*,hifre
    PRINT*,'Would you like to check the data you entered ? (y/n)'

```

Appendix 2. Transmission Loss of Louvre by Mass Layer Model

```

READ '(a)', ana
IF (ana.EQ.'y'.or.ana.EQ.'Y') THEN
  PRINT*,'-----'
  PRINT*,'
  PRINT*,'The output filename is ',output
  PRINT*,'The program to be used is ',prg_name
  PRINT*,'Air temperature: ',temp
  PRINT*
  PRINT*,'Source:  xs =',xs,'  ys =',ys,'  zs =',zs
  PRINT*,'Receiver:  xr =',xr,'  yr =',yr,'  zr =',zr
  PRINT*,' Louvre :  x1 =',x1,'  y11 =',y11,'y12 =',y12
  PRINT*,'              z11 =',z11,'z12 =',z12
  PRINT*
  PRINT*,' Lowest frequency = ',lowfre,' Hz'
  PRINT*,' Highest frequency = ',hifre,' Hz'
  PRINT*
  PRINT*,' Width of blade = ',blade,' m'
  PRINT*,'  Width of gap = ',gap,' m'
  PRINT*,'              Mass = ',mass,' kg/m2'
  PRINT*,'-----'
  PRINT*
  PRINT*,'Would you like to change the data ? (y/n)'
READ '(a)', anb
  IF (anb.EQ.'y'.OR.anb.EQ.'Y') THEN
    GOTO 100
  ENDIF
ENDIF

OPEN (UNIT=4,file=' '//output//' .out',position='append')
  WRITE (4,200)prg_name
200  FORMAT(3x,'Program used: ',A)
  WRITE (4,300)temp
300  FORMAT (3x,'Air temperature = ',f4.1,' centigrades')
  WRITE (4,400)
400  FORMAT(3x,'Coordinates of the SOURCE are:')
  WRITE (4,500)xs,ys,zs
500  FORMAT(3x,'xs = ',f6.3,10x,'ys = ',f6.3,10x,'zs = ',f6.3)
  WRITE (4,600)
600  FORMAT (3x,'Coordinates of the RECEIVER are:')
  WRITE (4,700)xr,yr,zr
700  FORMAT (3x,'xr = ',f6.3,10x,'yr = ',f6.3,10x,'zr = ',f6.3)
  WRITE (4,800)
800  FORMAT (3x,'Coordinates of the LOUVRE are:')
  WRITE (4,900)x1,y11,y12,z11,z12
900  FORMAT(3x,'x1 = ',f6.3,10x,'y11 = ',f6.3,9x,'y12 = ',f6.3      &
          &/3x,'z11 = ',f6.3,9x,'z12 = ',f6.3)
  WRITE (4,1000)blade,gap
1000 FORMAT(3x,'Blade width = ',f5.3,' m',6x,'Gap width = ',f5.3,' m')
  WRITE (4,1100)thickness
1100 FORMAT(3x,'Thickness of the louvre = ',f5.3,' m')
  WRITE (4,1200)lowfre,hifre
1200 FORMAT(3x,'LOW freq. = ',f10.5,' Hz',5x,'HIGH freq. = ',f10.5,' Hz')
  WRITE (4,1300)mass
1300 FORMAT(3x,'Mass density = ',f6.2,' kg/m2')
  WRITE (4,1400)
1400 FORMAT(' ')
  WRITE (4,1500)
1500 FORMAT(2x,'Frequency      ',',5x,'Mas(f)')

  c=331.3+(0.6*temp)
  pc=airdens*c
  step=0.00625
  length=y12-y11

```

```

high=z12-z11
rx=(xl-xr)**2
rr0=sqrt(rx)
sx=(xl-xs)**2
rs0=sqrt(sx)
yNo=(int(length/step)+1)
zNo=(int(high/step)+1)
stepz=high/zNo
A=step*stepz/(4*pi)
numfreq=int((hifre-lowfre)/resol)+1

DO 10 i=1,numfreq
  f(i)=lowfre+(i-1)*resol
  w=2*pi*f(i)
  k=w/c
  jk=cplx(0.0,k)
  P0=(0.0,0.0)
  P1=(0.0,0.0)
  yy=0.0

  DO 20 m=1,yNo
    yy=y11+(1/2.0+(m-1))*step
    ry=(yy-yr)**2
    sy=(yy-ys)**2

    DO 30 n=1,zNo
      zz=z12-(1/2.0+(n-1))*stepz
      rr=sqrt(rx+ry+(zz-zr)**2)
      rs=sqrt(sx+sy+(zz-zs)**2)
      cosr=rr0/rr
      coss=rs0/rs

!      Diffraction through an aperture:
      PG = -A/(rr*rs)*((jk-(1/rs))*coss+(jk-(1/rr))*cosr) &
          &* exp(cplx(0.0,k*(rs+rr)))

!      Transmitted through the aperture according to mass layer effect:
      tau=gap/(gap+blade)
      meq=airdens*((thickness/tau)+((gap+blade)*0.3))
      wmeq=(w*meq)/(2*pc)
      wmeqcos=wmeq*coss
      PM=PG*sqrt(1/(1+(wmeqcos)**2))*exp(cplx(0.0,Atan(wmeqcos)))

  P0=P0+PG
  P1=P1+PM

  30 CONTINUE
  20 CONTINUE

  Mas(i)=20*log10((abs(P0))/(abs(P1)))

WRITE(4,50) f(i),',',Mas(i)

10 CONTINUE

50 FORMAT(1x,f10.5,3x,a1,2x,f9.3)
CLOSE(4)
STOP
END

```

! PROGRAM LISTING FOR OPTICAL MODEL

```

! Program Optical.F90

! Calculates the transmission loss of a louvre using Fresnel-Kirchhoff
! diffraction theory with a term added for the transfer function.
! Reference signal: free-field.

! Resolution is 14.63 Hz to match MLSSA's output.
! Frequency range from 43.89 Hz to 5003.51 Hz

INTEGER yNo, zNo, numfreq
REAL xs, ys, zs, xr, yr, zr, x11, y11, x12, y12, z11, z12
REAL temp, blade, gap, thickness, lowfre, hifre, length, high, mass
REAL*8 rs0, rr0tf, w, k, yy, zz, newyy
REAL*8 f(340), IL(340)
COMPLEX*8 jk, PS, P2, PGtf, TF(340), free(340)
CHARACTER*8 output, prg_name
CHARACTER*8 ana, anb

DATA pi/3.14159/,airdens/1.21/,resol/14.63015/

100 PRINT*, 'Enter ouput file name:'
    READ '(a8)', output
    PRINT*, 'Enter name of program to be used:'
    READ '(a8)', prg_name
    PRINT*, 'Enter air temperature:'
    READ*, temp
    PRINT*, 'Input X of the source:'
    READ*, xs
    PRINT*, 'Enter Y of the source:'
    READ*, ys
    PRINT*, 'Enter Z of the source:'
    READ*, zs
    PRINT*, 'Enter X of the receiver:'
    READ*, xr
    PRINT*, 'Enter Y of the receiver:'
    READ*, yr
    PRINT*, 'Enter Z of the receiver:'
    READ*, zr
    PRINT*, 'Enter X of the louvre:'
    READ*, x11
    PRINT*, 'Enter Y1 of the louvre:'
    READ*, y11
    PRINT*, 'Enter Y2 of the louvre:'
    READ*, y12
    PRINT*, 'Enter Z1 of the louvre:'
    READ*, z11
    PRINT*, 'Enter Z2 of the louvre:'
    READ*, z12
    PRINT*, 'Enter the width of blade:'
    READ*, blade
    PRINT*, 'Enter the width of gap:'
    READ*, gap
    PRINT*, 'Enter the thickness of louvre:'
    READ*, thickness
    PRINT*, 'Enter the mass density'
    READ*, mass
    PRINT*, 'Enter the lowest frequency:'
    READ*, lowfre
    PRINT*, 'Enter the highest frequency:'

```


Appendix 3. Transmission Loss of Louvre by Diffraction Model

```

READ*,hifre
PRINT*,'Would you like to check the data you entered ? (y/n)'
READ '(a)', ana
IF (ana.EQ.'y'.or.ana.EQ.'Y') THEN
PRINT*,'
PRINT*,'
PRINT*,'The output filename is ',output
PRINT*,'The program to be used is ',prg_name
PRINT*,'Air temperature: ',temp
PRINT*
PRINT*,' Source:  xs =',xs,' ys =',ys,' zs =',zs
PRINT*,'Receiver:  xr =',xr,' yr =',yr,' zr =',zr
PRINT*,' Louvre :  xl =',xl1,' yll =',yll1,' yll2 =',yll2
PRINT*,'              zll =',zll1,' zll2 =',zll2
PRINT*
PRINT*,' Lowest frequency = ',lowfre,' Hz'
PRINT*,' Highest frequency = ',hifre,' Hz'
PRINT*
PRINT*,' Width of blade = ',blade,' m'
PRINT*,' Width of gap = ',gap,' m'
PRINT*,'              Mass = ',mass,' kg/m2'
PRINT*,'
PRINT*,'
PRINT*,'Would you like to change the data ? (y/n)'
READ '(a)',anb
IF (anb.EQ.'y'.OR.anb.EQ.'Y') THEN
GOTO 100
ENDIF
ENDIF
OPEN (UNIT=4,file=' //output//'.out',position='append')
WRITE (4,200)prg_name
200 FORMAT(3x,'Program used: ',A)
WRITE (4,250)
250 FORMAT (3x,'Input Data File = TF.TXT')
WRITE (4,300)temp
300 FORMAT (3x,'Air temperature = ',f4.1,' centigrades')
WRITE (4,400)
400 FORMAT(3x,'Coordinates of the SOURCE are:')
WRITE (4,500)xs,ys,zs
500 FORMAT(3x,'xs = ',f6.3,10x,'ys = ',f6.3,10x,'zs = ',f6.3)
WRITE (4,600)
600 FORMAT (3x,'Coordinates of the RECEIVER are:')
WRITE (4,700)xr,yr,zr
700 FORMAT (3x,'xr = ',f6.3,10x,'yr = ',f6.3,10x,'zr = ',f6.3)
WRITE (4,800)
800 FORMAT (3x,'Coordinates of the LOUVRE are:')
WRITE (4,900)xl1,yll1,yll2,zll1,zll2
900 FORMAT(3x,'xl = ',f6.3,10x,'yll = ',f6.3,9x,'yll2 = ',f6.3 &
&/3x,'zll = ',f6.3,9x,'zll2 = ',f6.3)
WRITE (4,1000)blade,gap
1000 FORMAT(3x,'Blade width = ',f5.3,' m',6x,'Gap width = ',f5.3,' m')
WRITE (4,1100)thickness
1100 FORMAT(3x,'Thickness of the louvre = ',f5.3,' m')
WRITE (4,1200)lowfre,hifre
1200 FORMAT(3x,'LOW freq. = ',f10.5,' Hz',5x,'HIGH freq. = ',f10.5,' Hz')
WRITE (4,1300)mass
1300 FORMAT(3x,'Mass density = ',f6.2,' kg/m2')
WRITE (4,1400)
1400 FORMAT(' ')
WRITE (4,1500)
1500 FORMAT('Freq.', 'IL(f)')

```

Appendix 3. Transmission Loss of Louvre by Diffraction Model

```

c=331.3+0.6*temp
pc=airdens*c
step=0.00625
length=y12-y11
high=z12-z11

xl2=x11+thickness
rxtf=(xl2-xr)**2
rr0tf=sqrt(rxtf)

sx=(x11-xs)**2
rs0=sqrt(sx)
r0=sqrt((xs-xr)**2+(ys-yr)**2+(zs-zr)**2)
yNo=(int(length/step)+1)
zNo=(int(high/step)+1)
stepz=high/zNo
A=step*stepz/(4*pi)
numfreq=int((hifre-lowfre)/resol)+1
OPEN (UNIT=5,FILE='TF.txt')

! Calculation
DO 10 i=1,numfreq
  f(i)=lowfre+(i-1)*resol
  w=2*pi*f(i)
  k=w/c
  jk=cmplx(0.0,k)
  free(i)=exp(cmplx(0.0,k*r0))/r0
  READ (UNIT=5,FMT='(F9.6,F9.6)',END=3000)TF(i)
  3000 P2=(0.0,0.0)
  yy=0.0
  newyy=0.0
  PS=(0.0,0.0)

  DO 20 m=1,yNo
    yy=y11+(1/2.0+(m-1))*step
    sy=(yy-ys)**2
    rytf=(yy+0.30-yr)**2

    DO 30 n=1,zNo
      zz=z12-(1/2.0+(n-1))*stepz
      rs=sqrt(sx+sy+(zz-zs)**2)
      coss=rs0/rs
      rrtf=sqrt(rxtf+rytf+(zz-zr)**2)
      cosrxtf=rr0tf/rrtf

! Diffraction model plus Transfer Function:
      PGtf=-A*exp(cmplx(0.0,k*(rs+rrtf)))/(rrtf*rs) &
        &*((jk-(1/rs))*coss+(jk-(1/rrtf))*cosrxtf)*TF(i)

! Decide where louvre opens and closes using if statement
      EXCEPTION: IF (m.LE.7) THEN
        PS=(0.0,0.0)
      ELSEIF (m.GE.8.AND.m.LE.20) THEN
        PS=PGtf
      ELSEIF (m.GE.21.AND.m.LE.276) THEN
        newyy=(y11-0.125)+(1/2.0+(m-1))*step
        yif=newyy/(blade+gap)-int(newyy/(blade+gap))
        ROUTINE: IF (yif.GT.blade/(blade+gap).and.yif.LE.1)THEN
          PS=PGtf
        ELSEIF(yif.GE.0.and.yif.LE.blade/(blade+gap))THEN
          PS=(0.0,0.0)
        END IF ROUTINE
      ELSE

```

Appendix 3. Transmission Loss of Louvre by Diffraction Model

```
                PS=(0.0,0.0)
END IF EXCEPTION
P2=P2+PS

    30 CONTINUE
    20 CONTINUE

IL(i)=20*log10((abs(free(i)))/(abs(P2)))

WRITE(4,50) f(i),',',IL(i)
10 CONTINUE
50 FORMAT(1x,f10.5,3x,a1,3x,f9.3)
CLOSE(4)
STOP
END
```

NORMAL-MODE SOLUTION

The frequency response function (Green's function) for the pressure $P(\omega)$ in an enclosure is given by solving the Helmholtz equation driven by a single frequency point acceleration source, according to [1]:

$$\nabla^2 P[(\omega/c), X, X'] + \frac{\omega^2}{c^2} P[(\omega/c), X, X'] = -\delta(X - X') \quad (\text{A4.1})$$

where ω is the frequency and c is the sound speed.

The solution to this equation, assuming rigid boundaries, is given by:

$$P(k, X, X') = \frac{1}{V} \sum_{r=-\infty}^{\infty} \frac{\psi_r(X) \psi_r(X')}{(k_r^2 - k^2)} \quad (\text{A4.2})$$

where $k = \omega/c$, $r = (n, l, m)$ indicates a three dimensional sum, V is the room volume and

$$\mathbf{k}_r = \left(\frac{n\pi}{L_x}, \frac{l\pi}{L_y}, \frac{m\pi}{L_z} \right),$$

$$k_r^2 = |\mathbf{k}_r|^2 \quad (\text{A4.3})$$

and

$$\psi_r(X) = \cos\left(\frac{n\pi x}{L_x}\right) \cos\left(\frac{l\pi y}{L_y}\right) \cos\left(\frac{m\pi z}{L_z}\right) \quad (\text{A4.4})$$

where L_i is the room dimension in the x , y and z directions.

Using the exponential expansion for cosine, multiplying the terms of equation (A4.2) together and gathering, is obtained:

$$P(k, X, X') = \frac{1}{8V} \sum_{r=-\infty}^{\infty} \sum_{p=1}^8 \frac{e^{(jk_r \cdot R_p)}}{(k_r^2 - k^2)} \quad (\text{A4.5})$$

where R_p represents the eight vectors given by the eight permutations over \pm of:

$$R_p = (x \pm x', y \pm y', z \pm z') \quad (\text{A4.6})$$

where x, y, z and x', y', z' are the source and receiver co-ordinates position, respectively.

Using the property of the delta function on k_x, k_y and k_z , which states that:

$$\int_{-\infty}^{\infty} \delta(x-a)F(x)dx = F(a) \quad (\text{A4.7})$$

equation (A4.5) may be rewritten in integral form as:

$$P(k, X, X') = \frac{1}{8V} \sum_{p=1}^8 \int_{-\infty}^{\infty} \int_{-\infty}^{\infty} \int_{-\infty}^{\infty} \frac{e^{(j\xi \cdot R_p)}}{(|\xi|^2 - k^2)} \sum_{r=-\infty}^{\infty} \delta(\xi - k_r) d^3 \xi \quad (\text{A4.8})$$

By Fourier series analysis it may be shown that:

$$\sum_{n=-\infty}^{\infty} \delta\left(\xi_x - \frac{n\pi}{L_x}\right) = \frac{L_x}{\pi} \sum_{n=-\infty}^{\infty} e^{(j2L_x n \xi_x)} \quad (\text{A4.9})$$

Thus (with analogous equations to (A4.9) for y and z):

$$P(k, X, X') = \frac{1}{(2\pi)^3} \sum_{p=1}^8 \int_{-\infty}^{\infty} \int_{-\infty}^{\infty} \int_{-\infty}^{\infty} \sum_{r=-\infty}^{\infty} \frac{e^{[j\xi \cdot (R_p + R_r)]}}{(|\xi|^2 - k^2)} d^3 \xi \quad (\text{A4.10})$$

where R_r is the vector,

$$R_r = \lambda(nL_x, mL_y, mL_z) \quad (\text{A4.11})$$

Each triple integral is just a plane wave expansion for a point source in free space since

$$\frac{e^{(jk|R|)}}{4\pi|R|} = \frac{1}{8\pi^3} \int \int \int_{-\infty}^{\infty} \frac{e^{(j\xi \cdot R)}}{(|\xi|^2 - k^2)} d^3\xi \quad (\text{A4.12})$$

Finally, using equation (A4.12), equation (A4.10) becomes,

$$P\left(\frac{\omega}{c}, \mathbf{X}, \mathbf{X}'\right) = \sum_{p=1}^8 \sum_{r=-\infty}^{\infty} \frac{e^{[j(\omega/c)|R_p + R_r|]}}{4\pi|R_p + R_r|} \quad (\text{A4.13})$$

Taking the inverse Fourier transform of equation (A4.13), the echo structure becomes explicit

$$p(t, \mathbf{X}, \mathbf{X}') = \sum_{p=1}^8 \sum_{r=-\infty}^{\infty} \frac{\delta\left[t - \left(|R_p + R_r|/c\right)\right]}{4\pi|R_p + R_r|} \quad (\text{A4.14})$$

IMAGE METHOD SOLUTION

A single frequency point source of acceleration in free space emits a pressure wave of the form

$$P(\omega, \mathbf{X}, \mathbf{X}') = \frac{e^{[j\omega(R/c-t)]}}{4\pi R} \quad (\text{A4.15})$$

Where,

$$\omega = 2\pi f$$

$$R = |\mathbf{X} - \mathbf{X}'|$$

\mathbf{X} = source vector location (x, y, z)

\mathbf{X}' = receiver vector location (x', y', z')

c = speed of sound

When a rigid wall is present, the rigid wall (zero normal velocity) boundary condition may be satisfied by placing an image symmetrically on the far side of the wall. Thus,

$$P(\omega, X, X') = \left\{ \frac{e^{[j(\omega/c)R_+]} }{4\pi R_+} + \frac{e^{[j(\omega/c)R_-]} }{4\pi R_-} \right\} e^{(-j\omega t)} \quad (\text{A4.16})$$

where the two distances from the microphone to the source R_- and to the image R_+ are defined by:

$$\begin{aligned} R_-^2 &= (x-x')^2 + (y-y')^2 + (z-z')^2, \\ R_+^2 &= (x+x')^2 + (y-y')^2 + (z-z')^2 \end{aligned} \quad (\text{A4.17})$$

The wall has been placed at $x=0$.

In the general case of six walls the situation becomes more complicated because each image is itself imaged. The pressure may be written as (as shown in equation (A4.13)):

$$P(\omega, X, X') = \sum_{p=1}^8 \sum_{r=-\infty}^{\infty} \frac{e^{[j(\omega/c)|R_p + R_r|]} }{4\pi |R_p + R_r|} e^{(-j\omega t)} \quad (\text{A4.18})$$

where R_p is the same as defined in equation (A4.6), r as in equation (A4.2) and

$$R_r = \lambda(nL_x, lL_y, mL_z) \quad (\text{A4.19})$$

where (L_x, L_y, L_z) are the room dimensions. Equation (A4.18) is the pressure frequency response assuming rigid walls for a point source at $X = (x, y, z)$ and receiver at $X' = (x', y', z')$. If equation (A4.18) is Fourier transformed, the room impulse response function (time domain Green's function) is obtained:

$$p(t, X, X') = \sum_{p=1}^8 \sum_{r=-\infty}^{\infty} \frac{\delta[t - |R_p + R_r|/c]}{4\pi |R_p + R_r|} \quad (\text{A4.20})$$

which is the same as equation (A4.14) as desired.

REFERENCES

- [1] Allen J.B. and Berkely D.A., *Image Method for Efficiently Simulating Small-Room Acoustics*, J. Acoust. Soc. Am., **65**(4), 943-950, (1979).

! PROGRAM LISTING FOR REFLECTION COEFFICIENT

! Calculates the beginning and the end of each component, in the
! time domain, for Reflection coefficient measurements.

PROGRAM geometry
IMPLICIT NONE

REAL :: a, b, c, d, f, g, h, k, l, m, n, p, q, r, s, t, u, x, y, &
ang, sound, Direct, Floor, Back_Wall, Right_Wall, &
Left_Wall, Ceiling, Reflected, Time_Direct, Time_Floor, &
Time_Back, Time_Right, Time_Left, Time_Ceiling, Time_Reflected, &
End_Direct, End_Floor, End_Back, End_Right, End_Left, End_Ceiling, &
End_Reflected

CHARACTER(LEN=12), PARAMETER :: output='geometry.dat'
REAL, PARAMETER :: pi = 3.14159
INTEGER, PARAMETER :: temp = 22
sound = 331.4 + 0.607 * temp

OPEN (UNIT=4, FILE=output, STATUS='new', POSITION='append')
WRITE (4,100)temp
100 FORMAT ('Temp = ', I2, ' degrees')
WRITE (4,200)sound
200 FORMAT ('Sound Speed = ', F7.3, ' m/s')

ang = 45*pi/180

a = 3.29
b = a * sin(ang)
x = 0.37
c = x * sin(ang)
d = x * cos(ang)
Direct = sqrt((2*b + c)**2 + d**2)
f = 3.02 - d - a*cos(ang)
g = d + f
n = (2*b+c)/(g/f+1)
m = ((2*b+c)/(g/f+1))*(g/f)
h = sqrt(g**2 + m**2)
k = sqrt(n**2+f**2)
p = d * ((1+ (2.79+b+c)/(2.79-b))**(-1))
q = d - p
l = sqrt((2.79-b)**2 + p**2)
y = sqrt((2.79+b+c)**2 + q**2)
s = d * (((3.01-b-c)/(3.01+b))+1)**(-1))
r = d - s
t = sqrt((3.01+b)**2 + s**2)
u = sqrt((3.01-b-c)**2 + r**2)

Reflected = 2*a + x
Time_Reflected = Reflected/sound
End_Reflected = Time_Reflected + 4e-03

Time_Direct = Direct/sound
End_Direct = Time_Direct + 4e-03

Floor = (sqrt((Direct/2)**2 + 1.06**2)) * 2
Time_Floor = Floor/sound
End_Floor = Time_Floor + 3e-03

Right_Wall = t + u

Appendix 5. Geometry for Reflection Coefficient Measurements

```

Time_Right = Right_Wall/sound
End_Right = Time_Right + 3e-03

Left_Wall = l + y
Time_Left = Left_Wall/sound
End_Left = Time_Left + 3e-03

Back_Wall = k + h
Time_Back = Back_Wall/sound
End_Back = Time_Back + 3e-03

Ceiling = (sqrt((Direct/2)**2 + 3.20**2)) * 2
Time_Ceiling = Ceiling/sound
End_Ceiling = Time_Ceiling + 4e-03

WRITE (4,400)Time_Direct,End_Direct
400 FORMAT ('Time_Direct = ',E11.4,' End_Direct = ',E11.4)

WRITE (4,500)Time_Floor,End_Floor
500 FORMAT ('Time_Floor = ',E11.4,' End_Floor = ',E11.4)

WRITE (4,600)Time_Right,End_Right
600 FORMAT ('Time_Right = ',E11.4,' End_Right = ',E11.4)

WRITE (4,700)Time_Left,End_Left
700 FORMAT ('Time_Left = ',E11.4,' End_Left = ',E11.4)

WRITE (4,800)Time_Back,End_Back
800 FORMAT ('Time_Back = ',E11.4,' End_Back = ',E11.4)

WRITE (4,900)Time_Ceiling,End_Ceiling
900 FORMAT ('Time_Ceiling = ',E11.4,' End_Ceiling = ',E11.4)

WRITE (4,1000)Time_Reflected,End_Reflected
1000 FORMAT ('Time_Reflected = ',E11.4,' End_Reflected = ',E11.4)

CLOSE(4)
STOP

END PROGRAM geometry

```

! PROGRAM LISTING FOR HEVAC SIMULATION

```

! Program image.F90

! The program calculates the insertion loss of the louvre using IMAGE METHOD.
! It predicts the SPL with and without the louvre placed in an aperture that
! connects a reverberant source room to the exterior. The proposed approach
! simulates HEVAC method of measuring open screens.

! Frequency range of prediction: 100 Hz to 5 kHz, in 1/3 octave bands.
! Origin of co-ordinates at CENTRE OF ROOM.
! Microphone is situated outside the room.

! Output file contains the data input and two columns:
! Freq (i), 100 to 5kHz in 1/3 octave bands
! IL(i): Insertion Loss of louvre

PROGRAM image
IMPLICIT NONE

INTEGER          :: i, l, m, n, L_cells, M_cells, N_cells, xupp_lim, &
                 xlow_lim, yupp_lim, ylow_lim, zupp_lim, zlow_lim, &
                 refl_surf, tt_ref, angle_setup, lou_opp

INTEGER, DIMENSION(18)  :: Freq

REAL             :: xr, yr, PL, PA, d, dx, dy, dz, k_lou, k_ap, &
                 teta_pos_xy, teta_neg_xy, teta_max_xy, &
                 teta_min_xy, teta_pos_xz, teta_neg_xz, &
                 teta_max_xz, teta_min_xz, &
                 side, SPLap, SPLlou, angle_setup_rd, angle_ray_x, &
                 angle_ray_z, sin_z, A, B, C, E, F, G, H, K, Q, R, &
                 tau_lou, tau_lou_opp, m_real

REAL, DIMENSION(18)    :: m_air, alfa_room, refl_00, IL

CHARACTER(LEN=7)      :: xkind_cell, ykind_cell, zkind_cell

REAL, PARAMETER :: xs = 2.25, ys = 2.75, zs = 0.00, zr = 0.00
REAL, PARAMETER :: width = 4.80, length = 6.00, height = 3.60
REAL, PARAMETER :: r_setup = 3.00 ! Microphones positions at 3m radius
REAL, PARAMETER :: radius = 50.00
REAL, PARAMETER :: pi = 3.14159
CHARACTER(LEN=12), PARAMETER :: prg_name = 'image.F90', output = 'image.out'
OPEN (UNIT=4, FILE='image.out', STATUS='new', POSITION='append')

```

Appendix 6. Insertion Loss Simulation of HEVAC Test by Image Method

```

WRITE (4,100)prg_name
100 FORMAT('Program used: ',A)
WRITE (4,200)radius
200 FORMAT('Radius of accuracy : ',F5.2,' m')

! NUMBER OF CELLS in each direction according to radius of accuracy
L_cells = Num_cells(radius,width) !invoke FUNCTION
M_cells = Num_cells(radius,length) !invoke FUNCTION
N_cells = Num_cells(radius,height) !invoke FUNCTION

! Source and Receiver COORDINATES:
angle_setup = 0
angle_setup_rd = angle_setup*pi/180
xr = (width/2 + 0.30 + r_setup*cos(angle_setup_rd)) * (-1)
yr = r_setup*sin(angle_setup_rd) * (-1)

OPEN (UNIT=5,FILE='m1_3.txt') ! m_air(i) = Air Attenuation
OPEN (UNIT=7,FILE='absch1_3.txt') ! alfa_room(i) = Room Absorption
OPEN (UNIT=11,FILE='refl_00.txt') ! refl_00(i) = Louvre's Reflection Factor
OPEN (UNIT=13,FILE='freq.txt') ! freq(i) = Frequencies in 1/3

! TETA MAX and TETA MIN
side = -xr - width/2 - 0.30
teta_max_xy = ATAN((length/2 - yr) / side)
teta_min_xy = ATAN((-length/2 - yr) / side)
teta_max_xz = ATAN(height/2 / side)
teta_min_xz = ATAN(-height/2 / side)

WRITE (4,300)angle_setup
300 FORMAT('Incident Angle = ',I3,' degrees')
WRITE (4,350)xs,ys,zs
350 FORMAT('xs = ',F6.3,7x,'ys = ',F6.3,7x,'zs = ',F6.3)
WRITE (4,400)xr,yr,zr
400 FORMAT('xr = ',F6.3,7x,'yr = ',F6.3,7x,'zr = ',F6.3)
WRITE (4,500)
500 FORMAT(' ')
WRITE (4,600)angle_setup
600 FORMAT('Freq,', 'IL(',I3,')')

DO 10 i=1,18 ! For each frequency:
    READ (UNIT=5,FMT='(E8.2)')m_air(i)
    READ (UNIT=7,FMT='(F8.6)')alfa_room(i)

```

Appendix 6. Insertion Loss Simulation of HEVAC Test by Image Method

```

READ (UNIT=11,FMT='(F8.5)') refl_00(i)
READ (UNIT=13,FMT='(I4)') freq(i)

PL = 0.0
PA = 0.0

! ----- ALONG x-direction -----
xupp_lim = up_cell(L_cells)    !invoke FUNCTION
xlow_lim = 0
DO 20 l=xlow_lim,xupp_lim
  lou_opp = (l+2)/4    ! number of reflections upon louvre in opposite
                      ! direction
  xkind_cell = kind_cell(l)    !invoke FUNCTION
  IF (xkind_cell.EQ.'cel_zer') THEN
    refl_surf = (l+1)
    dx = ( xs - xr )
  ELSEIF (xkind_cell.EQ.'pos_odd') THEN
    refl_surf = (l+1)/2
    dx = (l * width) - xs - xr
  ELSE !pos_evn
    refl_surf = (l/2)+1
    dx = (l * width) + xs - xr
  END IF

! ----- ALONG y-direction -----
yupp_lim = up_cell(M_cells)    !invoke FUNCTION
ylow_lim = low_cell(yupp_lim)  !invoke FUNCTION

DO 30 m=ylow_lim,yupp_lim
  ykind_cell = kind_cell(m)    !invoke FUNCTION
  IF (ykind_cell.EQ.'neg_odd') THEN
    dy = (-m * length) + ys + yr
  ELSEIF (ykind_cell.EQ.'neg_evn') THEN
    dy = (-m * length) - ys + yr
  ELSEIF (ykind_cell.EQ.'cel_zer') THEN
    dy = (ys - yr)
  ELSEIF (ykind_cell.EQ.'pos_odd') THEN
    dy = (m * length) - ys - yr
  ELSE !pos_evn
    dy = (m * length) + ys - yr
  END IF

! ----- ALONG z-direction -----
zupp_lim = up_cell(N_cells)    !invoke FUNCTION
zlow_lim = low_cell(zupp_lim)  !invoke FUNCTION

```

Appendix 6. Insertion Loss Simulation of HEVAC Test by Image Method

```

DO 40 n=zlow_lim,zupp_lim
  zkind_cell = kind_cell(n)  !invoke FUNCTION
  IF (zkind_cell.EQ.'neg_odd') THEN
    dz = (-n * height) - zs + zr
  ELSEIF (zkind_cell.EQ.'neg_evn') THEN
    dz = (-n * height) + zs + zr
  ELSEIF (zkind_cell.EQ.'cel_zer') THEN
    dz = zs - zr
  ELSEIF (zkind_cell.EQ.'pos_odd') THEN
    dz = (n * height) - zs - zr
  ELSE !pos_evn
    dz = (n * height) + zs - zr
  END IF

! --- DISTANCE 'd' and TOTAL NUMBER OF REFLECTIONS -----
  d = SQRT ((dx**2) + (dy**2) + (dz**2))
  tt_ref = abs(l) + abs(m) + abs(n) + 1

! --- ANGLE BETWEEN PROJECTED RAY AND PLANES XY AND XZ -----
  IF (m.GE.0) THEN
    teta_pos_xy = ATAN(dy/dx)
    teta_neg_xy = 0.0
  ELSE ! (m.LT.0)
    teta_pos_xy = 0.0
    teta_neg_xy = ATAN(-dy/dx)
  ENDIF

  IF (n.GE.0) THEN
    teta_pos_xz = ATAN(dz/dx)
    teta_neg_xz = 0.0
  ELSE ! (n.LT.0)
    teta_pos_xz = 0.0
    teta_neg_xz = ATAN(-dz/dx)
  ENDIF

! --- ANGLE BETWEEN RAY-LOUVRE and RAY-AZIMUTE LOUVRE -----
  m_real=REAL(m)
  angle_ray_x = SIGN(ACOS(dx/d)*180/pi,m_real)
  angle_ray_z = ACOS(dz/d)

! --- AZIMUTE CORRECTION -----
  sin_z = SIN(angle_ray_z)

SELECT CASE (freq(i))  ! Polynomial express for tau(angle)
  CASE(100)

```

Appendix 6. Insertion Loss Simulation of HEVAC Test by Image Method

A=8.2754e-17; B=-4.1794e-15; C=-9.0e-13; E=4.5528e-11
F=1.5717e-9; G=-1.251e-7; H=2.3431e-6; K=1.5385e-4
Q=-3.0058e-5; R=7.911e-1

CASE(125)
A=6.4418e-17; B=-4.2579e-15; C=-7.2978e-13; E=4.7839e-11
F=1.5396e-9; G=-1.3925e-7; H=1.1296e-6; K=1.6458e-4
Q=3.7605e-4; R=7.0835e-1

CASE(160)
A=4.911e-17; B=-3.4138e-15; C=-6.0207e-13; E=3.8518e-11
F=1.6792e-9; G=-1.1402e-7; H=-3.0891e-7; K=1.3426e-4
Q=8.9123e-4; R=6.1860e-1

CASE(200)
A=3.8938e-17; B=-1.8693e-15; C=-5.1947e-13; E=2.0234e-11
F=1.7910e-9; G=-5.9196e-8; H=-1.2534e-6; K=7.8029e-5
Q=1.0972e-3; R=5.4091e-1

CASE(250)
A=2.9010e-17; B=-1.4873e-16; C=-4.1820e-13; E=-1.5335e-13
F=1.6556e-9; G=1.3848e-9; H=-1.4954e-6; K=2.1420e-5
Q=8.5735e-4; R=4.5738e-1

CASE(315)
A=2.0229e-17; B=1.0496e-15; C=-3.1828e-13; E=-1.3737e-11
F=1.4282e-9; G=3.7837e-8; H=-1.4854e-6; K=-5.7368e-6
Q=3.9883e-4; R=3.4626e-1

CASE(400)
A=1.3308e-17; B=1.1665e-15; C=-2.2570e-13; E=-1.4139e-11
F=1.1222e-9; G=3.4147e-8; H=-1.3564e-6; K=4.2054e-6
Q=1.7582e-5; R=2.1809e-1

CASE(500)
A=6.0285e-18; B=5.5555e-16; C=-1.0805e-13; E=-6.6160e-12
F=5.8629e-10; G=1.3628e-8; H=-8.4684e-7; K=1.5901e-5
Q=-1.3793e-4; R=1.0165e-1

CASE(630)
A=-1.6989e-18; B=3.5593e-16; C=1.6693e-14; E=-5.1859e-12
F=-7.0187e-12; G=2.0356e-8; H=-1.5635e-7; K=-2.0121e-5
Q=1.6868e-4; R=5.1304e-2

CASE(800)
A=-8.2435e-20; B=1.0907e-16; C=5.7821e-15; E=-1.6444e-12
F=-6.1496e-11; G=7.4380e-9; H=1.3719e-7; K=-1.4453e-5
Q=2.0551e-4; R=3.3473e-2

CASE(1000)
A=-8.8887e-19; B=-5.6748e-17; C=1.2387e-14; E=5.8179e-13

Appendix 6. Insertion Loss Simulation of HEVAC Test by Image Method

```

F=-5.4351e-11;G=-8.3717e-10;H=9.8220e-8; K=-2.6105e-6
Q=1.3847e-5; R=1.1165e-2
CASE(1250)
A=3.4781e-19; B=1.7608e-17; C=-4.9007e-15; E=-2.1641e-13
F=1.8987e-11; G=4.0610e-10;H=-2.2102e-8; K=1.1723e-6
Q=4.0500e-5; R=3.0727e-3
CASE(1600)
A=1.1345e-17; B=6.6922e-17; C=-1.5901e-13; E=-8.0603e-13
F=6.4995e-10; G=2.1103e-9;H=-9.1761e-7; K=-3.9120e-7
Q=4.5526e-4; R=4.9971e-3
CASE(2000)
A=2.3682e-17; B=1.4229e-16; C=-3.4627e-13; E=-2.3328e-12
F=1.5380e-9; G=1.1746e-8;H=-2.499e-6; K=-2.1204e-5
Q=1.4215e-3; R=1.9708e-2
CASE(2500)
A=3.92e-19; B=-2.7877e-16; C=-1.4755e-14; E=3.4834e-12
F=1.2995e-10; G=-1.1411e-8;H=-3.4153e-7; K=1.1451e-5
Q=3.9438e-4; R=4.7492e-3
CASE(3150)
A=3.0715e-17; B=1.1295e-15; C=-3.9985e-13; E=-1.4459e-11
F=1.3766e-9; G=4.7371e-8;H=-1.2929e-6; K=-3.6651e-5
Q=4.3404e-4; R=1.0586e-2
CASE(4000)
A=9.2184e-17; B=2.6471e-15; C=-1.2317e-12; E=-3.4004e-11
F=4.5136e-9; G=1.1123e-7;H=-4.9961e-6; K=-7.9543e-5
Q=2.0602e-3; R=2.2833e-2
CASE DEFAULT !(5000)
A=-3.1021e-17; B=-1.0836e-15; C=4.1694e-13; E=1.4657e-11
F=-1.5492e-9; G=-5.6503e-8;H=1.6204e-6; K=7.1911e-5
Q=4.7356e-4; R=1.822e-4
END SELECT

tau_lou = polyn(A,B,C,E,F,G,H,K,Q,R,angle_ray_x)
tau_lou_opp = polyn(A,B,C,E,F,G,H,K,Q,R,angle_ray_x+90)

! --- TRUNCATE HIGHEST TAU AS 1.00 AND LOWEST AS 0.00 -----
IF (tau_lou.GE.1.00) THEN
    tau_lou = 1.00
ELSEIF (tau_lou.LE.0.00) THEN
    tau_lou = 0.00
ELSE

```


Appendix 6. Insertion Loss Simulation of HEVAC Test by Image Method

```

    tau_lou = tau_lou
ENDIF

IF (tau_lou_opp.GE.1.00) THEN
    tau_lou_opp = 1.00
ELSEIF (tau_lou_opp.LE.0.00) THEN
    tau_lou_opp = 0.00
ELSE
    tau_lou_opp = tau_lou_opp
ENDIF

! ----- Calculation -----
IF (teta_pos_xy.GT.teta_max_xy.OR.teta_neg_xy.LT.teta_min_xy) &
&THEN

    k_lou = 0.0
    k_ap = 0.0

ELSEIF (teta_pos_xz.GT.teta_max_xz.OR.teta_neg_xz.&
&LT.teta_min_xz) THEN

    k_lou = 0.0
    k_ap = 0.0

ELSEIF (refl_surf.EQ.1) THEN
    k_ap = d**(-2) * (1 - alfa_room(i))**(tt_ref - refl_surf) &
& * sin_z * exp(m_air(i)*(1-d))
    k_lou = d**(-2) * (1 - alfa_room(i))**(tt_ref - refl_surf) &
& * tau_lou * sin_z * exp(m_air(i)*(1-d))
ELSE
    k_ap = 0.0
    k_lou = d**(-2) * (1 - alfa_room(i))**(tt_ref - refl_surf) &
& * (refl_00(i))**(refl_surf - lou_opp - 1) &
& * (refl_00(i))**lou_opp * tau_lou &
& * exp(m_air(i)*(1-d)) * sin_z**3
ENDIF

PL = PL + k_lou
PA = PA + k_ap

    40 CONTINUE      ! next z-cell(n)
    30 CONTINUE      ! next y-cell(m)
    20 CONTINUE      ! next z-cell(1)

SPLap = 10*LOG10(PA)

```

Appendix 6. Insertion Loss Simulation of HEVAC Test by Image Method

```

SPLlou = 10*LOG10(PL)

IL(i) = SPLap - SPLlou

PRINT*, 'IL (' ,i, ') = ', IL(i)

WRITE (4,700) Freq(i), ', ', IL(i)
10 CONTINUE ! next freq(i)
700 FORMAT(I4,A1,F6.2)
CLOSE(5); CLOSE(7); CLOSE(11); CLOSE(13)
CLOSE(4)
STOP
CONTAINS !Internal Procedures

! --- COUNTS NUMBER OF CELLS (in each x, y and z directions) -----
FUNCTION Num_cells(a,r_dimens)
INTEGER Num_cells
REAL a
REAL r_dimens
Num_cells = CEILING((a-r_dimens/2)/r_dimens)*2+1
END FUNCTION Num_cells

! --- SORT KIND OF CELLS (neg, pos, zero, odd or even) -----
FUNCTION kind_cell(b)
INTEGER b, remainder
CHARACTER*7 kind_cell
remainder = MOD(b,2)
IF (b.LT.0.AND.remainder.EQ.1) THEN
kind_cell = 'neg_odd'
ELSEIF (b.LT.0.AND.remainder.EQ.0) THEN
kind_cell = 'neg_evn'
ELSEIF (b.EQ.0) THEN
kind_cell = 'cel_zer'
ELSEIF (b.GT.0.AND. remainder.EQ.1) THEN
kind_cell = 'pos_odd'
ELSE
kind_cell = 'pos_evn'
ENDIF
END FUNCTION kind_cell

! --- SETS UPPER LIMIT CELLS (in each x, y and z directions) -----
FUNCTION up_cell(c)

```

Appendix 6. Insertion Loss Simulation of HEVAC Test by Image Method

```
INTEGER up_cell, c
up_cell = (c-1)/2
END FUNCTION up_cell

! --- SETS LOWER LIMIT CELLS (in each x, y and z directions) -----
FUNCTION low_cell(upp)
  INTEGER low_cell, upp
  low_cell = upp * (-1)
END FUNCTION low_cell

! --- CALCULATES TAU ACCORDING TO INCIDENT ANGLE -----
FUNCTION polyn(A,B,C,E,F,G,H,K,Q,R,angle_ray_x)
  REAL polyn, A, B, C, E, F, G, H, K, Q, R, angle_ray_x
  polyn = A*angle_ray_x**9 + B*angle_ray_x**8 + C*angle_ray_x**7 &
    & + E*angle_ray_x**6 + F*angle_ray_x**5 + G*angle_ray_x**4 &
    & + H*angle_ray_x**3 + K*angle_ray_x**2 + Q*angle_ray_x + R
END FUNCTION polyn
! -----
END PROGRAM image
```

APPENDIX 7 PUBLISHED PAPERS

- **Measurement of the Sound Insertion Loss of Ventilation Louvres**
Viveiros E.B and Gibbs B.M. **Internoise 96**

- **Sound Insulation of Acoustic Louvres**
Viveiros E.B., Gibbs B.M. and Gerges S.N.Y. **Internoise 97**

MEASUREMENT OF THE SOUND INSERTION LOSS OF VENTILATION LOUVRES

E B Viveiros (1) & B M Gibbs (2)

(1) Dept of Architecture and Urbanism, Fed Univ of Santa Catarina, Brazil, (2) Acoustics Research Unit, University of Liverpool, Liverpool, UK

1. INTRODUCTION

In industrial plantrooms it is often necessary to provide openings, the function of which is to allow air flow to equipment. This link with the outside is likely to cause noise breakout. To avoid such a problem to the environment a louvre that can also provide a reduction in the sound transmission is desirable. Although a wide variety of louvres is available on the market, their acoustic performance cannot be compared meaningfully, as there is no agreed method to characterise their insulation [1]. In this study, a proposed method of measuring the sound insertion loss of ventilation louvres, by an impulse response method, is described which does not require a large scale acoustic installation.

2. MEASURING SOUND INSULATION

The acoustical performance of ventilation louvres is presented by manufacturers using different indices, such as transmission loss, noise reduction index or insertion loss. The diversity of parameters demonstrates the need for standardisation in the method of measuring low insertion loss devices. Briefly, the existing methods can be described as follows:

Standard Method

The majority of data, evaluating louvres, is presented in the form of transmission loss, TL, also known as sound reduction index, which is measured according to ISO 140 [2]. This approach, although appropriate for solid partitions, is not so for low transmission loss devices, as the rooms are acoustically occupied in such circumstances. The lower limit of applicability is a TL of 15 dB which is seldom achieved by open screens such as louvres at low frequencies.

Non-Standard Method

The Acoustic Group of the Heating Ventilating and Air Conditioning Manufacturers Association of the UK (HEVAC) propose a test procedure where outside sound pressure levels are measured with and without the louvre fitted in the aperture of a test building. Again, this method requires the provision of a reverberant volume with aperture, ideally, located on an open site [3].

3. IMPULSE RESPONSE METHOD

Unlike the methods described above, impulse response methods do not require special facilities. Instead, the direct, reflected and diffracted components of the transmitted signal are time windowed and the influence of room reflections removed.

Its use to determine the transmission loss of panels was first reported in 1955 [4]. Since then, it has been used to validate theory [5] and in in-situ measurements [6,7].

Excitation Signal

Single impulses give low S/N ratio. Replacing them by a digitally generated sequence of impulses results in an increase in the effective signal intensity. Among the stationary sequences of binary impulses, the maximum-length sequence is widely used [8].

Signal Processing

On obtaining the impulse response of the system, time-of-flight methods are used to window the direct component. The FFT of the anechoic response is then compared with that obtained with the panel between the sound source and the microphone and the insertion loss of the partition thus obtained. The use of a Maximum-Length Sequence System Analyzer/MLSSA permitted a high frequency resolution and the whole process is performed in a single channel system.

4. RESULTS

Acoustic louvres provide acoustic attenuation by a combination of transmission and diffraction mechanisms and these were investigated separately as a prelude to the measurement of acoustic louvres (see Figure 1).

In Figure 2 is the time history and in Figure 3 the resultant insertion loss of a thin solid panel. The latter was obtained from windowing the direct component of the former and a mass law characteristic is clearly seen for normal incidence. In addition, a coincidence plateau is indicated for oblique incidence.

The top edge diffracted component was windowed (see Figure 2) to provide the acoustic screening of a long (4.8m x 1.2m) barrier shown in Figure 4. Results are compared with theory according to Maekawa [9].

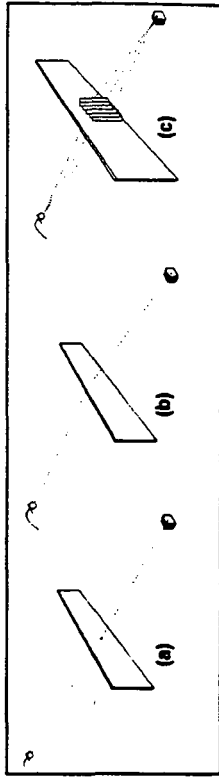


Figure 1 - Time analysis: (a) direct path (b) edge diffraction and (c) internal diffractions.

In Figure 5 are shown the insertion loss, IL, of an acoustic louvre at different angles of incidence. The louvre consisted of five metal blades (200mm x 100mm) with absorbent exposed on one side. At low frequencies the IL increases monotonically with frequency due to the mass layer effect. Here, the IL is independent of angle of incidence. Between 500 Hz - 2 kHz, there is strong angular dependence; the maximum value being for sound incidence parallel to the blades of the louvre. The same trend is also observed above 2 kHz. The angular variation of IL is complicated and is not symmetric. Therefore, a proposed test method, involving impulse response analysis, requires that measurements are repeated for different angles of incidence. In Figure 6 is shown the angle averaged insertion loss of the same louvre, again displaying the mass layer gradient at low frequency and a plateau region at higher frequencies.

Concluding Remarks

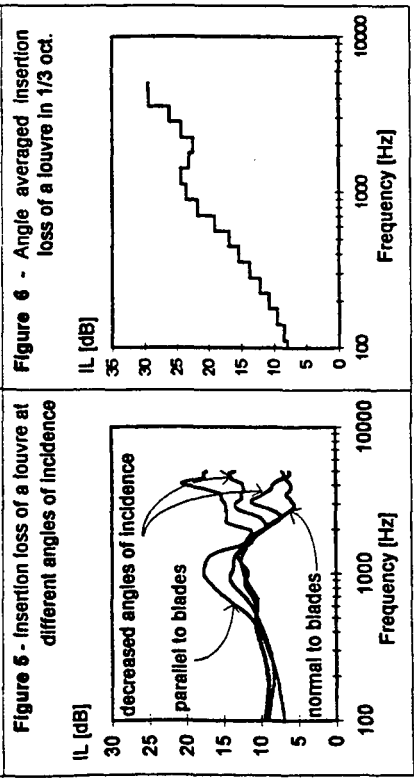
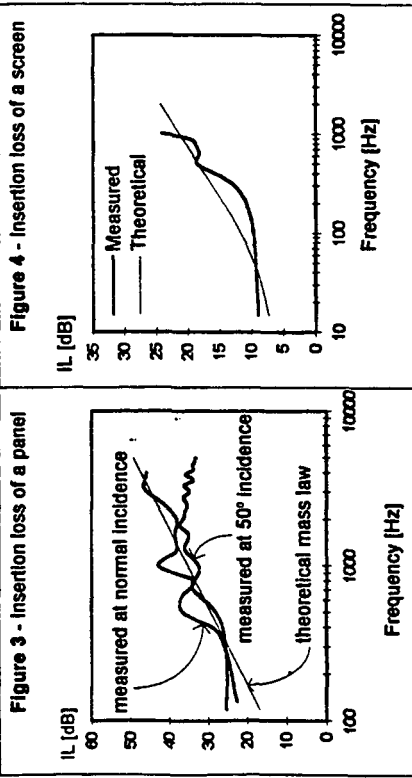
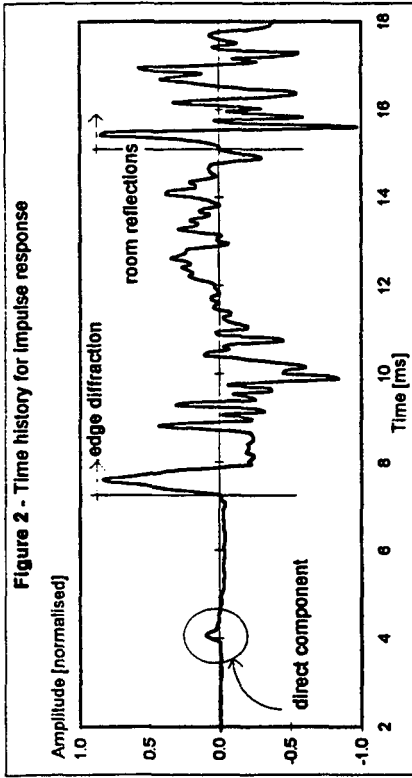
Impulse response analysis promises a quick method of test of acoustic louvres without recourse to large scale acoustics facilities. It remains to explore the relationship between the angle average insertion loss with that obtained by ISO 140 and the method proposed by HEVAC.

5. REFERENCES

- [1] R. Lyons - Building elements of low sound insertion loss. Ph.D. thesis, University of Liverpool, UK (1993).
- [2] ISO 146 - Part 1-3 (1978).
- [3] HEVAC Guide - Test procedure for acoustic louvres, Issue 11 (1990).
- [4] A.C. Raes - JASA, 27(1), 98-102(1955).
- [5] M.M. Loudon - Acustica, 25, 167-172(1971).
- [6] J. Roland - Noise Control Engng, 19(1), 6-14(1981).
- [7] Y.A. Baillat and B.M. Gibbs - JSV, 123(2), 228-245(1988).
- [8] M. Voriänder - Impulse measurement technique for headphones. 9th Fase Symposium and 10th Hungarian Conference on Acoustics (1991).
- [9] Z. Maekawa - Applied Acoustics, 1(3), 157-173(1968).

ACKNOWLEDGEMENTS

The authors would like to thank CAPES - Fundação Coordenação de Aperfeiçoamento de Pessoal de Nível Superior in Brazil, for funding the Ph.D. research, on which this paper is based.



inter·noise 97

Budapest – Hungary, August 25-27

SOUND INSULATION OF ACOUSTIC LOUVRES

E.B. Viveiros (1,2), B.M. Gibbs (2) and S.N.Y. Geroges (3)

- (1) Dept. Architecture and Urbanism, Federal University of Santa Catarina / BR
- (2) Acoustics Research Unit, Liverpool University / UK
- (3) Dept. Mechanical Engineering, Federal University of Santa Catarina / BR

1. INTRODUCTION

Machinery such as compressors, boilers and generators require adequate ventilation and extract. In such cases, the buildings in which they are installed have to provide apertures in their envelope for air exchange. To avoid excessive noise breakout, an acoustic louvre is designed to give the required open area while providing a certain amount of sound reduction. A problem remains in that there is not yet an agreed method of test of acoustic louvres and the standard ISO 140 [1] has been demonstrated to be inappropriate in certain conditions [2].

The insulation performance of an acoustic louvre has been investigated by an impulse response technique. The advantage of the method over others is that there are no special acoustics requirements to be achieved for the measurements, even regarding the background noise level. The results for different angles of incidence are presented and the comparison with standard methods analysed.

2. TRANSMISSION LOSS BY IMPULSE RESPONSE

2.1. Signal processing

The maximum-length sequence, normally known as m-sequence, enables the impulse response of a system to be obtained by means of cross correlation [3]. Measuring sound insulation with this sort of excitation has great advantages. The signal to noise ratio is improved and, due to its stationary characteristics, further increase can be achieved by averaging the signal response. The excitation and the signal processing were performed using the software MLSSA, which is based on the Hadamard Transformation.

The attenuation is calculated by windowing out the room characteristics from the responses obtained with and without the device in the transmission path and applying the FFT to these 'anechoic' responses. The spectrum level of the

windwed impulse response is subtracted from that of the reference to give the partition transmission loss directly, independent of the environment where the measurements are performed. Figure 1 shows a typical impulse response for a solid free-standing partition and the reference signal.

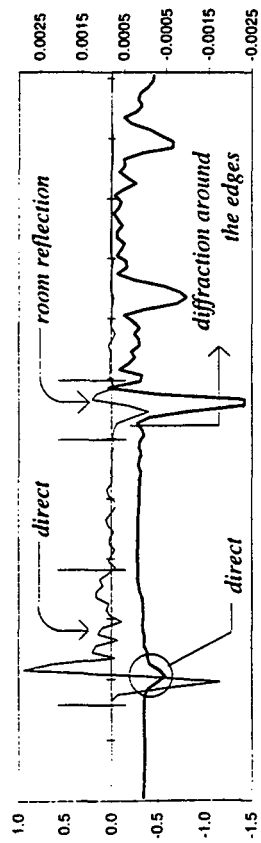


Fig. 1 - Impulse response for a partition, thin line, and the reference signal with an unobstructed transmission path.

2.2. Louvre

Acoustic louvres provide sound attenuation by a combination of transmission, absorption and diffraction. The commercial louvre investigated is shown in Figure 2. The louvre was placed in the aperture of the transmission suit of the Acoustics Research Unit, Liverpool University and the impulse response results compared to the transmission loss obtained by ISO 140.

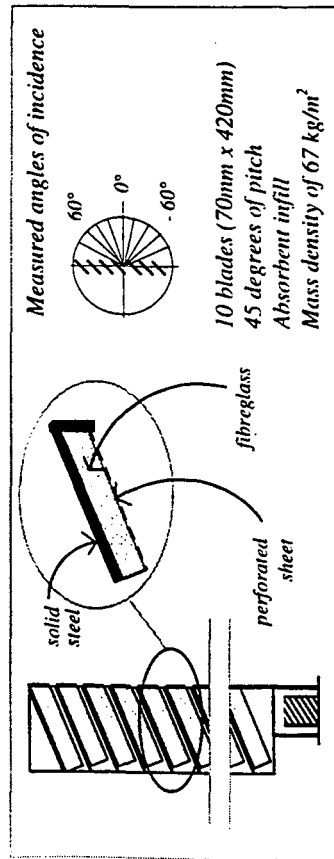


Fig. 2 - Details of the acoustic louvre and measured incident angles.

3. RESULTS

Unlike a solid screen, the direct component that passes through the louvre is represented as a spread of the time signal, as shown in Figure 3.

The transmission loss was obtained for 9 different angles of incidence in 15 degree increments (see Figure 2) and is shown in Figure 4.

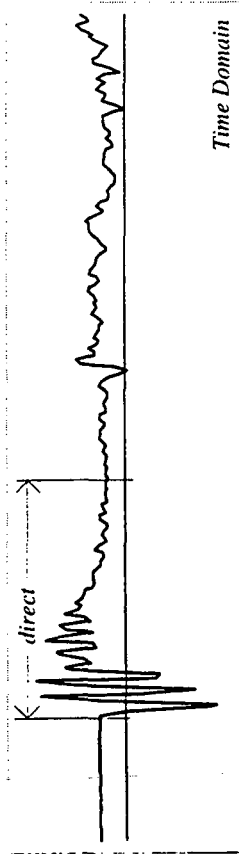


Fig. 3 - Typical impulse response of the louvre.

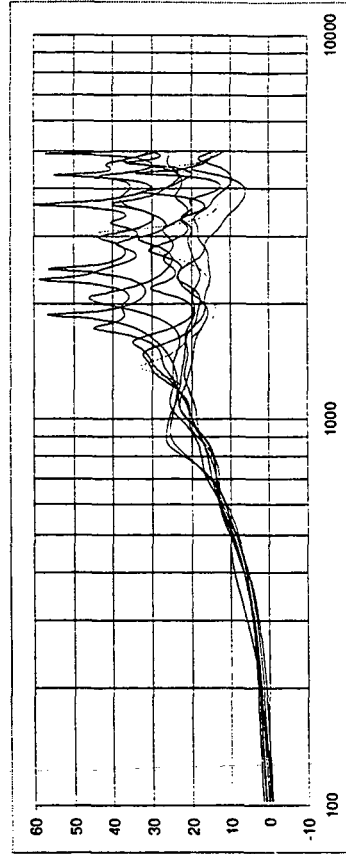


Fig. 4 - Angle dependent transmission loss for the acoustic louvre.

At low frequency the louvre performance is nearly independent of the incident angle and a mass effect can be identified [4]. Above 1 kHz, the performance is characterised by fluctuations about a plateau due to destructive and constructive interference from the different transmission paths through the separate slits. Although dependent of the incident angle, Figure 5 shows that the path parallel to the blade pitch (in this case at 45°) strongly influences the overall performance.

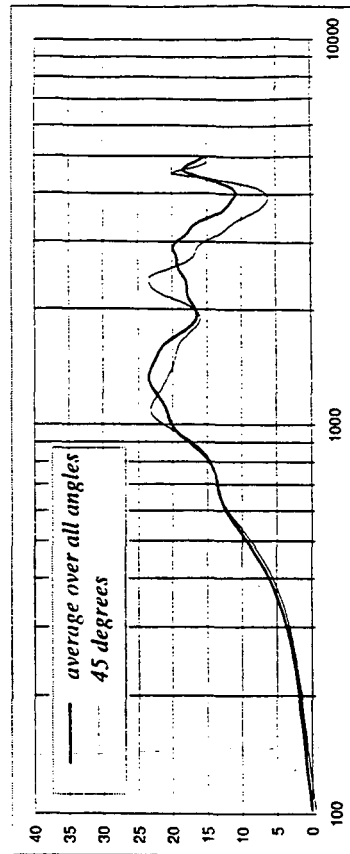


Fig. 5 - TL averaged over all angles and for sound incident parallel to the pitch.

Figure 6 shows the comparison between the transmission loss measured by ISO 140 and impulse response obtained by angle averaging for all incidences. The curves show good agreement, particularly for values greater than 15 dB. The discrepancy at low frequency is believed to be caused by an overestimation of the standard method as the aperture itself is likely to give a certain amount of attenuation due to mass layer effect of the air in the open aperture [4].

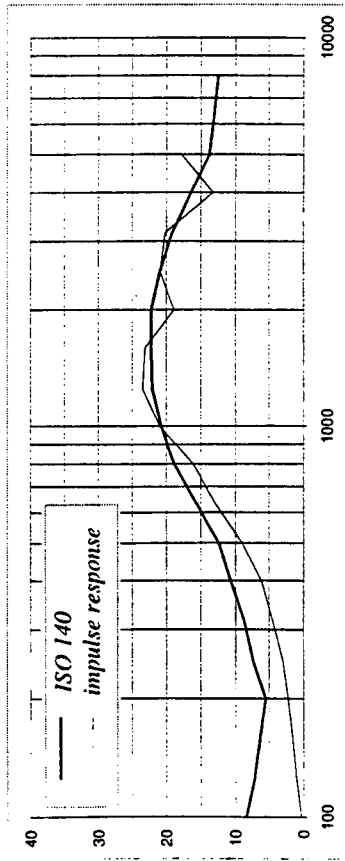


Fig. 6 - TL by ISO 140 and by impulse response averaged over all angles of incidence.

4. CONCLUDING REMARKS

The impulse response method is practical and easy to implement, particularly when employing MLSSA. No special facilities are required and even the presence of high background noise can be overcome by means of averages.

As might be expected for the louvre geometry, an average over different angles of incident must be required although sound incidence parallel to the pitch is a good approximation to the overall performance.

When compared to the standard method the results obtained indicate good agreement. Discrepancies exist in low frequencies, and it is believed that ISO 140 overestimates the louvre performance in this region.

5. REFERENCES

- [1] ISO 140 - *Methods of measurement of sound insulation in buildings and of buildings elements*, parts I-III (1978).
- [2] E. B. Viveiros and B.M. Gibbs - Measurement of the Sound Insertion Loss of Ventilation Louvre, *Proceedings of InterNoise 96*, vol.3, 733-736, 1996.
- [3] M. Voriänder - Applications of Maximum Length Sequences in Acoustics, *Proceedings of I Simpósio Brasileiro de Metrologia em Acústica e Vibrações, 17º Encontro da Sociedade Brasileira de Acústica*, 35-44, 1996.
- [4] L. Cremer and H. Müller, *Principles and Applications of Room Acoustics*, vol.2, Applied Science Publishers, Essex, 1978.

ACKNOWLEDGEMENTS - The authors would like to thank CAPES, in Brazil, for funding the Ph.D. research, on which this paper is based.